



Provided by the author(s) and University of Galway in accordance with publisher policies. Please cite the published version when available.

Title	Development of non-metallic and adhesive-free timber-timber moment connections using compressed wood connectors
Author(s)	Mehra, Sameer
Publication Date	2020-09-30
Publisher	NUI Galway
Item record	http://hdl.handle.net/10379/16580

Downloaded 2024-04-25T15:01:11Z

Some rights reserved. For more information, please see the item record link above.



Development of Non-metallic and Adhesive-free Timber-timber Moment Connections using Compressed Wood Connectors

Sameer Mehra

Supervisor: Prof. Annette M. Harte

Co-supervisor: Dr Conan O'Ceallaigh

Civil Engineering, College of Science and Engineering,
National University of Ireland Galway



NATIONAL UNIVERSITY OF IRELAND GALWAY

Civil Engineering

College of Science and Engineering

Thesis submitted to the National University of Ireland in partial fulfilment of the
requirements for the Degree of Doctor of Philosophy

September 2020

Abstract

Increasing the sustainability credentials of building materials is one of the main challenges in the built environment. Over the last few decades, there has been a renewed interest in the use of timber in construction in response to the challenges of global warming and climate change. The ongoing transition towards a bio-based and circular economy has contributed to significant developments in the mass timber products market and associated novel connection typologies. These advancements have resulted in the use of traditional carpentry type connections being replaced by fast, efficient, and cost-effective modern connections using mechanical fasteners and synthetic adhesives. However, metallic fasteners have high embodied energy and synthetic adhesives have negative implications for end-of-life disposal of such products. Therefore, it is favourable to replace these materials with sustainable wood-based connectors.

Today, robotic fabrication is a key enabler of innovation in mass timber construction with advanced production technologies using computer numerically controlled (CNC) tools. This has facilitated the development of cost-competitive dowel-laminated timber (DLT) products using low-cost precision machining and assembly thereby eliminating the need for synthetic adhesives. By replacing metallic connection systems with wood-based alternatives, all-wood high-performance building systems, with enhanced environmental and health benefits, are then possible.

Enhancement of the properties of wood using modification techniques, such as thermo-mechanical compression, is an emerging field. Thermo-mechanically compressed wood (CW) has increased density, decreased porosity and significantly improved material strength, stiffness and dimensional stability when compared to uncompressed wood. Despite several studies focusing on the manufacturing and basic material properties of CW, only a few studies have examined the suitability of CW connectors in an all-wood timber connection for a mass timber structure.

The objective of this research is to develop a novel approach to produce non-metallic and adhesive-free timber moment connections incorporating thermo-mechanically CW connectors. To achieve this objective, an extensive experimental programme was undertaken, which included material characterisation tests on CW connectors, tests on the long-term swelling and shrinkage-behaviour of CW and the development and experimental testing of timber-CW dowel moment connections, namely beam-beam and beam-column connections.

The material characterisation tests demonstrated that CW offers superior mechanical properties when compared to uncompressed softwoods and hardwoods when comparing

embedment strength, yield moment capacity, cross-grain shear capacity and bending strength and could be used as an ideal wood-based connector material in the form CW dowels and CW plates to connect glulam, DLT and CWDLT elements in mass timber structures. A key finding from the long-term swelling and shrinkage-behaviour of CW has shown that “springback”, which is the expansion of CW in response to external climate conditions, is a beneficial characteristic of CW in connections as it facilitates form and friction fit with the timber substrate and yields a higher pull-out strength of the dowel.

The experimental characterisation of timber-CW dowel connections has enabled the evaluation of the load-carrying capacity, moment capacity, rotational stiffness, ductility ratio and failure modes of a range of semi-rigid type timber-CW connection design, which have been developed to connect both glued-laminated members and adhesive-free CWDLT members. Furthermore, the developed timber-CW connection systems were successfully implemented within portal frames manufactured using both glued-laminated and CWDLT members. The test results have shown that the lateral load-carrying capacity and moment capacity of the frames with timber-CW connections and CWDLT members are comparable to frames with timber-CW connections and glued structural members. This indicates that an all-wood connection concept would be a suitable choice in heavy timber structures with CWDLT members as well as with solid timber and glulam members.

Also, the suitability of current design rules in Eurocode 5, which is the European standard governing the design of timber structures, supplemented by design rules from other research studies was assessed for designing and predicting the moment capacity and rotational stiffness of the novel timber-CW connections.

It is anticipated that the current study will provide an improved understanding of the structural behaviour of CW connectors and timber-CW connections that may widen the knowledge base and help structural engineers to design timber-CW connections. It is also anticipated that the material characterisation tests performed will provide the necessary input data for numerical models to further examine the connection designs developed in this study and contribute to the optimised design of such connections with increased reliability. The findings are important to develop safe, sustainable, recyclable, and energy-efficient timber connection systems and mass timber products using CW connectors.

Acknowledgements

Embarking on this PhD programme, I have come across some incredible people who have made lasting impressions on me and my life. And writing this dissertation report has made me realise and appreciate what an incredible support system I have around me. I would like to take this opportunity to express my deepest gratitude to all the people without whom I would have not realised this dream!

I would like to convey my heartfelt thanks to my supervisor at NUI Galway, Prof. Annette M. Harte for guiding my PhD research at the Timber Engineering Research Group (TERG) for the past 3.5 years and for (virtually) sitting long hours with me to make my thesis what it is today! She has patiently mentored me while being kind, and kept me on track with her extensive knowledge, experience, and insights.

I deeply appreciate the constant efforts of my co-supervisor Dr. Conan O’Ceallaigh. He has helped me from the first day till the last in designing setups, doing calculations, and has provided corrections at short notices. He has been a great support in helping me get settled in the university and to life in Galway. I would like to thank my Graduate Research Committee members Prof. Padraic O’Donoghue, Prof. Xinmin Zhan and Dr. Eoghan Clifford for their inputs and guidance regarding the progress of my research throughout my time at NUI Galway.

I would like to sincerely acknowledge the funding provided by the European Regional Development Fund (ERDF) via Interreg NWE grant 348 ‘‘Towards Adhesive Free Timber Buildings’’, AFTB and the National University of Ireland Galway for my study and research here in Ireland, and for all the opportunities and experiences that came with it. This dissertation report would not have been possible without the extensive mentoring and worldwide exposure I received through the AFTB project partners.

A large amount experimental work presented in thesis was completed in the Heavy Structures Laboratory, at NUI Galway, and I would like to thank to all of the technical staff particularly Mr. Peter Fahy and Mr. Colm Walsh. This research work on timber connection would not have been possible without our carpenter, Mattie O’Malley who handcrafted the test specimens with a high precision.

I am extremely thankful for the constant support from my colleagues- Daniel, Luka, David, Des, Cairtriona, Goshia, Karlo, Cathal and Sukanya. My life in Galway became much more amusing because of these people right here. They have been that circle of friends that I could always count on, if I was stuck at any point on any day!

I am forever grateful for the everlasting support of my family and friends. I would not be able to come this far if not for the relentless efforts of my dearest Dadi Smt. Kailash Bai, and my Bade Papa. Their hard work and sacrifices are the reasons that I stand tall and strong today. I appreciate the support from my mother, father, and badi mummy. I cannot thank my Appa and Amma enough, who have been my sound boards, for taking my calls at all odd hours, for loving me as I am, and for always being there. Big kudos to my extended family Pankaj, Nitin, Namita, Kalpana, Poorvi, Vishwanath and my dearest energy pill Yakshita! Cheers to Sujay anna and Meghana akka who have constantly been my welcome escape as my only Irish family.

Last, but not least, I would like to thank my better half Ramya for being there with me through it all. Ramya is the only person who can appreciate my ups and downs as they come and go. There are no words to convey how much I love her. Ramya has been my true cheerleader and has unconditionally loved me during my good and bad times. She has had faith in me and my intellect even when I lost faith in myself and felt like digging hole and crawling into it. The past decade has not been an easy ride, both academically and personally. I truly thank Ramya for being there in my corner and sticking by my side. I truly believe that we both have learnt a lot about life, only to strengthen our respect, commitment, and determination towards each other and to live life to the fullest. It's truly commendable that we marked this milestone, all while social distancing in the COVID-19 related lockdown and working from home to write my thesis on the dining table for the past 6 months!

In these trying times, I remain eternally grateful that I was able to make the best of this opportunity with all the blessings that I was bestowed with!

Table of contents

ABSTRACT	I
ACKNOWLEDGEMENTS	III
TABLE OF CONTENTS	V
LIST OF FIGURES	X
LIST OF TABLES	XIX
NOMENCLATURE	XXII
CHAPTER 1 INTRODUCTION	1
1.1 BACKGROUND AND MOTIVATION	1
1.2 MODERN MASS TIMBER FRAME SYSTEMS	1
1.3 RESEARCH OBJECTIVES	5
1.4 RESEARCH METHODOLOGY	6
1.5 LAYOUT OF THE THESIS	9
CHAPTER 2 LITERATURE REVIEW	11
2.1 INTRODUCTION	11
2.2 WOOD AS A STRUCTURAL MATERIAL	11
2.2.1 <i>Introduction</i>	11
2.2.2 <i>Cellular structure and function of wood</i>	12
2.2.3 <i>Microstructure and chemical composition of wood</i>	15
2.2.4 <i>Wood density</i>	16
2.2.5 <i>Mechanical properties of wood</i>	17
2.2.6 <i>Wood and moisture</i>	18
2.2.7 <i>Shrinkage and swelling in wood due to moisture</i>	20
2.3 WOOD MODIFICATION	21
2.3.1 <i>Introduction</i>	21
2.3.2 <i>Wood densification and compressed wood</i>	22
2.3.3 <i>Types and mechanism of wood densification</i>	26
2.3.4 <i>Springback of compressed wood</i>	29
2.3.5 <i>Mechanical properties of compressed wood</i>	30
2.4 TIMBER CONNECTIONS IN FRAME CONSTRUCTION	36
2.4.1 <i>Introduction</i>	36
2.4.2 <i>Carpentry connections</i>	38

2.4.3 <i>Metallic timber connections</i>	49
2.4.4 <i>Timber connections using thermo-mechanically compressed wood</i>	57
2.5 CONCLUSION	58
CHAPTER 3 MATERIAL CHARACTERISATION OF CW AND UNCOMPRESSED WOOD	61
3.1 INTRODUCTION	61
3.2 SELECTION OF MATERIAL CHARACTERISATION TESTS	61
3.3 MATERIALS	62
3.3.1 <i>Compressed wood</i>	63
3.3.2 <i>Hardwood</i>	67
3.3.3 <i>Softwood</i>	67
3.4 TEST PROCEDURES	68
3.4.1 <i>Embedment test</i>	68
3.4.2 <i>Yield moment of dowels test</i>	71
3.4.3 <i>Cross-grain shear test</i>	73
3.4.4 <i>Three-point bending test</i>	75
3.5 TEST RESULTS AND DISCUSSION	76
3.5.1 <i>Embedment test results</i>	76
3.5.2 <i>Yield moment of dowels test results</i>	86
3.5.3 <i>Cross grain-shear test results</i>	94
3.5.4 <i>Bending test results</i>	98
3.6 CONCLUSION	104
CHAPTER 4 SWELLING/SHRINKAGE BEHAVIOUR OF CW AND TIMBER-CW CONNECTIONS	107
4.1 INTRODUCTION	107
4.2 MATERIALS	109
4.2.1 <i>Compressed wood</i>	109
4.2.2 <i>Hardwood dowels</i>	109
4.2.3 <i>Softwood</i>	109
4.3 TEST PROCEDURES	110
4.3.1 <i>Unconstrained swelling/shrinkage of CW</i>	110
4.3.2 <i>Accelerated ageing tests on timber-CW and timber-hardwood connections</i>	113
4.4 TEST RESULTS AND DISCUSSIONS	120
4.4.1 <i>Results of unconstrained swelling/shrinkage of CW plates</i>	120
4.4.2 <i>Results of accelerated ageing test</i>	131
4.5 CONCLUSION	151
CHAPTER 5 DEVELOPMENT OF SEMI-RIGID TIMBER CONNECTIONS USING CW CONNECTORS	

5.1 INTRODUCTION.....	154
5.2 SELECTION OF CONNECTION DESIGNS	155
5.3 MATERIAL	156
5.3.1 <i>Compressed wood</i>	156
5.3.2 <i>Compressed laminated wood</i>	158
5.3.3 <i>Steel connectors</i>	158
5.3.4 <i>Structural members (softwood)</i>	158
5.4 BEAM-BEAM CONNECTIONS USING FULL-DEPTH CW/STEEL PLATES AND GLUED STRUCTURAL MEMBERS (PHASE-I)	160
5.4.1 <i>Connection configuration, fabrication and assembly</i>	160
5.4.2 <i>Test set-up and procedure</i>	162
5.4.3 <i>Test results and discussion</i>	164
5.4.4 <i>Results summary and discussion</i>	168
5.5 BEAM-BEAM CONNECTIONS USING NARROW-DEPTH CW PLATES AND GLUED STRUCTURAL MEMBERS (PHASE-II)	169
5.5.1 <i>Connection configuration, fabrication and assembly</i>	170
5.5.2 <i>Test set-up and procedure</i>	172
5.5.3 <i>Test results and discussion</i>	173
5.5.4 <i>Results summary and discussion</i>	178
5.6 BEAM-COLUMN CONNECTIONS USING GLUED STRUCTURAL MEMBERS (PHASE-III).....	179
5.6.1 <i>Connection configuration, fabrication and assembly</i>	181
5.6.2 <i>Test procedure</i>	183
5.6.3 <i>Test results and discussion</i>	184
5.6.4 <i>Results summary and selection of optimum design</i>	193
5.7 BEAM-COLUMN CONNECTIONS USING CW DOWEL LAMINATED STRUCTURAL MEMBERS (PHASE-IV).....	195
5.7.1 <i>Connection configuration, fabrication and assembly</i>	195
5.7.2 <i>Test procedure</i>	199
5.7.3 <i>Test results and discussion</i>	200
5.7.4 <i>Results summary and discussion</i>	204
5.8 CONCLUSION.....	205
CHAPTER 6 EXPERIMENTAL INVESTIGATION OF LATERALLY LOADED LAMINATED TIMBER PORTAL FRAMES WITH CW CONNECTIONS	210
6.1 INTRODUCTION.....	210
6.2 MATERIAL AND MANUFACTURING OF FRAMES.....	210
6.3 TEST-PROCEDURE.....	213
6.4 TEST RESULTS AND DISCUSSION	218
6.4.1 <i>Load-lateral displacement</i>	218

6.4.2 Load-frame base rotation	219
6.4.3 Moment- rotation behaviour	221
6.4.4 Failure modes.....	222
6.5 SUMMARY AND CONCLUSIONS	226
CHAPTER 7 DESIGN CALCULATIONS FOR TIMBER-CW CONNECTIONS	228
7.1 INTRODUCTION	228
7.2 CONNECTION DESIGN MOMENT CAPACITY.....	228
7.2.1 Material properties used for design calculations.....	231
7.2.2 Beam-beam connections with full-depth steel plates.....	233
7.2.3 Beam-beam connections with full-depth CW plates.....	236
7.2.4 Beam-beam connections with narrow-depth CW plates	239
7.2.5 Beam-column connections with CWDLT members (Design-IV-2).....	242
7.2.6 Results summary	246
7.3 CONNECTION DESIGN ROTATIONAL STIFFNESS.....	247
7.3.1 Beam-beam connections with full-depth steel plates	248
7.3.2 Beam-beam connections with full-depth CW plates.....	249
7.3.3 Beam-beam connections with narrow-depth CW plates	250
7.3.4 Beam-column connections with CWDLT members (Design-IV-2).....	251
7.3.5 Result summary	252
7.4 CONCLUSIONS.....	253
CHAPTER 8 CONCLUSIONS AND RECOMMENDATIONS.....	256
8.1 INTRODUCTION	256
8.2 MATERIAL CHARACTERISATION TESTS CONCLUSIONS	256
8.3 SWELLING/SHRINKAGE BEHAVIOUR OF CW AND TIMBER-CW CONNECTIONS TESTS CONCLUSIONS.....	257
8.4 DEVELOPMENT OF NOVEL SEMI-RIGID TIMBER CONNECTIONS USING CW CONNECTORS	258
8.5 EXPERIMENTAL INVESTIGATION OF LATERALLY LOADED LAMINATED TIMBER PORTAL FRAMES WITH CW CONNECTIONS	259
8.6 DESIGN OF TIMBER-CW CONNECTIONS.....	259
8.7 OVERALL CONCLUSION.....	260
8.8 APPLICATION OF THE PROPOSED TIMBER-CW CONNECTIONS FOR STRUCTURAL PURPOSES.....	261
8.9 RECOMMENDATIONS FOR FUTURE WORK	263
REFERENCES.....	265
APPENDIX-A.....	285
DESIGN-III-1.....	285
DESIGN-III-2.....	286
DESIGN-III-3.....	287

DESIGN-III-4	288
DESIGN-III-5	289
DESIGN-III-6	290
DESIGN-III-7	291
APPENDIX-B	292
DESIGN-IV-1	292
DESIGN-IV-2	293
APPENDIX-C	294
PORTAL FRAME USING GLUED STRUCTURAL MEMBERS	294
PORTAL FRAME USING CWDLT MEMBERS	296
APPENDIX-D	298

List of figures

Figure 1.1- Mjøstårnet, Norway, (a) building, (b) skeleton of the building, (c) slotted-in steel plate and dowel connection [15,16]	3
Figure 1.2- Dowel laminated timber (DLT), Structurecraft [17]	4
Figure 1.3- Research methodology	8
Figure 2.1- Three-dimensional section of a tree bole [28].....	12
Figure 2.2- Microscopic cross-section of <i>Abies alba</i> showing earlywood and latewood [36]	14
Figure 2.3- Microscopic structure of softwood and hardwood [38]	14
Figure 2.4- Microstructure of the wood cell wall [40].....	15
Figure 2.5- Chemical composition of a cell in cross-section and longitudinal direction [38]	16
Figure 2.6- Orthotropic axes of wood [48]	17
Figure 2.7- Schematic picture of glass transition temperature for lignin, hemicellulose and amorphous cellulose as a function of moisture content [91].....	27
Figure 2.8- Radially compressed Douglas Fir (<i>Pseudotsuga menziesii</i>), (a) microscopic structure before densification, (b) microscopic structure after densification, (c) macroscopic structure before densification, (d) macroscopic structure after densification [14].....	28
Figure 2.9- Efficiency of connections between 100 mm by 200 mm timber members transmitting a tensile axial force [13].....	37
Figure 2.10- Moment-rotation behaviour.....	37
Figure 2.11- Scheme of review on the timber-timber connections	38
Figure 2.12- Splayed scarf joint with locating keys and dowels [130].....	39
Figure 2.13- Scarf joints, (a) halved scarf with two pegs, (b) side-halved & bridled with two pegs, (c) stop-splayed & tabled scarf with key and four pegs, and (d) face-halved and bladed scarf with four pegs [131]	40
Figure 2.14- Lapped Scarf Joint -Four dowel and two dowel joints [132]	40
Figure 2.15- Scarf joint, (a) halved joint with pins, and (b) oblique scarf joint with pins[134]	41
Figure 2.16- Standard geometry of mortise and tenon joint [138].....	42
Figure 2.17- Failure modes in mortise and tenon joints, (a) mortise failure, (b) tenon relish failure, (c) peg deformation [138].....	43
Figure 2.18- Joint configuration for the shear test, (a) housed joint, (b) open mortise joint, (c) tenon splitting, (d) tenon rolling shear failure.....	44

Figure 2.19- Various forms mortise and tenon joints, (a) with shouldered mortise and without shouldered tenon/Type-1 (b) with shouldered mortise and tenon/Type-2, (c) shouldered mortise and tenon with knee brace/Type-3, (d) unshouldered mortise and tenon fork and tongue/Type-4 [53]	44
Figure 2.20- Failure mode of pegs[53]	45
Figure 2.21- Three-plank mortise and tenon joint test by Shanks [141].....	46
Figure 2.22- Mortise and tenon joint tested by Shanks et al. [142]	47
Figure 2.23-Traditional dovetailed mortise and tenon joint tested by Pang et al.[143]	47
Figure 2.24 Nuki joint, (a) with wedges [124], (b) without wedges and with shorter and longer reinforcement [147]	48
Figure 2.25- Wood-wood/wood-steel beam-beam connections (dimensions in mm), (a) half symmetry of the connected specimens, (b) horizontal bolt arrangement, (c) circular bolt arrangement, (d) vertical bolt arrangement [157]	50
Figure 2.26- Bolted beam-beam connections (dimensions in mm), (a)half symmetry of the connection, (b)test set up, (c) failure mechanism of the connection [158]	51
Figure 2.27- Assembled beam-beam connection and it's assembling scheme: 1 – timber element; 2 – steel detail; 3 – mounting bolts; 4 – structural bolts; contact between timber and steel zone filled with filler [165]	51
Figure 2.28- Timber-steel moment connection using DVW reinforcement and tube fasteners, (a) connection configuration, and (b) four-bending test set up (dimension in mm) [120]	52
Figure 2.29- Beam-column connections with or without knee braces [171]	53
Figure 2.30- Beam-column test set up[172].....	54
Figure 2.31- Geometry of bending test set up (dimension in mm)	54
Figure 2.32- Beam-column connection, (a) frame test set up, (b) failure mode of beam-column connection in frame, (c) splitting within the beam member of small-scale specimens, and (d)bending of the bolts within small-scale specimen s[173].....	55
Figure 2.33- Beam-column connection, (a) bearing failure, (b) shear failure, (c) splitting along the row of bolts [174].....	56
Figure 2.34- Beam-column connections, (a) simplified test geometry, (b) splitting failure [176]	57
Figure 2.35- Slotted-in CW plates using CW dowels, (a) column-sill connection, (b)beam-column connection [80]	58
Figure 3.1- Hydraulic press used for production of CW dowels and plates, University of Liverpool, Liverpool, United Kingdom	63

Figure 3.2- Compressed wood plates, (a) direction of compression, (b) flowchart of manufacturing process, (c) radially compressed specimens before and after compression (University of Liverpool).....	65
Figure 3.3- Flow chart of production of 54% radially compressed Scots pine dowels (University of Liverpool), (a) cross-section of the radially uncompressed specimen, (b) dimensioning and filleting of specimens, (c) arrangement of specimens on aluminium mould, (d) radial compression of specimens, (e) finished product – 54% radially compressed dowels, (f) drawing of mould.....	66
Figure 3.4- Embedment test set up, (a) parallel to the grain, (b) perpendicular to the grain and, (c) dimensions of the test rig (mm).....	68
Figure 3.5- Deformation of S275 grade steel dowel.....	70
Figure 3.6- Yield moment tests, (a) test set up, (b) geometry of the test set up, and (c) load direction	73
Figure 3.7- Shear test set up, (a) testing rig, (b) rig dimensions, and (c) loading direction (in mm).....	75
Figure 3.8- Bending test set up and specimen geometry	76
Figure 3.9- Uncompressed Douglas fir – parallel to the grain, (a) embedment stress-displacement graph, and (b) failure modes of the tested specimens with a close-up view showing typical failure.....	77
Figure 3.10- Uncompressed Douglas fir – perpendicular to the grain, (a) Embedment stress-displacement graph, and (b) failure modes of the tested specimens with a close-up view showing typical failure.....	79
Figure 3.11- Compressed Western hemlock (CWH68) – parallel to the grain, (a) embedment stress-displacement graph, and (b) failure modes of the specimens (specimens 1 to 5 are shown in sequence).....	81
Figure 3.12- Compressed Western hemlock (CWH68) – perpendicular to the grain, (a) embedment stress-displacement graph, and (b) failure modes of the tested specimens with a close-up view showing typical failure.....	83
Figure 3.13- Embedment strength comparison of CW between mean values of experimental results and existing literature (TM – Thermo-mechanically densified wood, DVW- Densified Veneer Wood)	86
Figure 3.14- Load-displacement behaviour of CW and beech wood dowels (CW_R = CW dowels tested at 0° angle to load; CW_T = CW dowels tested at 90° angle to load; CW_F = CW dowels tested at 45° angle to load; HW_R = beech wood dowel tested at 0° angle to load; HW_T= beech wood dowel tested at 90° angle to load; HW_F = beech wood dowel tested at 45° angle to load)	87
Figure 3.15- Interlaminar shear failure of CW dowels	88

Figure 3.16- Formation of plastic hinges at midspan and over the supports	88
Figure 3.17- Tensile failure at the midspan	89
Figure 3.18- Failure modes of the tested specimens	89
Figure 3.19- Comparison between mean experimental yield moment capacity of CW dowels and literature (0 – radial and 90- tangential direction).....	93
Figure 3.20- Load-displacement behaviour of CW and beech wood dowels tested in shear (SCW_R denotes CW dowels tested at 0° angle to load; SCW_T denotes CW dowels tested at 90° angle to load; SHW_R denotes beech wood dowel tested at 0° angle to load; SHW_T denotes beech wood dowel tested at 90° angle to load).....	94
Figure 3.21- Failure modes of the tested specimens in shear	95
Figure 3.22- Comparison of mean values of experimental cross-grain shear strength with the literature	98
Figure 3.23- Load-displacement behaviour of specimens tested in bending	99
Figure 3.24- Bending failure of the specimens	99
Figure 3.25- Internal damage along with the growth rings in the longitudinal direction of compressed Douglas fir.....	101
Figure 3.26- Bending strength comparison between mean values of experimental results and literature (TM – Thermo-mechanically densified wood, THM- Thermo-Hydro-Mechanically densified wood, MD – Mechanically Densified wood).....	102
Figure 3.27- Modulus of Elasticity (GPa) comparison between mean values of experimental results and literature (TM – Thermo-mechanically densified wood, THM- Thermo-Hydro-Mechanically densified wood)	103
Figure 4.1- Scheme of the experiment	110
Figure 4.2- Test measurement, (a) direction of the measurement, (b) positions of measurement, (c) thickness measurement using vernier calliper	111
Figure 4.3- Scheme of accelerated ageing test.....	114
Figure 4.4- Specimen preparation of accelerated ageing test, (a) process , (b) geometry of specimens, (c) assembly process, (d) position of measurement of dowel diameter.....	116
Figure 4.5- Swelling/shrinkage measurement in the radial direction at measurement points indicated by red circles	117
Figure 4.6- Accelerated ageing test equipment, (a) pressure vessel, (b) treatment station, (c) drying treatment	119
Figure 4.7- Testing rig, (a) test set up, (b) plan view of the test specimen showing edge distances of steel plate from the centre of the dowel	120
Figure 4.8- Change in the thickness of CW plates over a period of 510 days during conditioning phase (specimen number 5 and 8 were taken out for shrinkage study after 190 days).....	121

Figure 4.9- Mean rate of thickness change vs. number of days during the conditioning phase	122
Figure 4.10- Change in the mass of CW plates over a period of 510 days during the conditioning phase (Specimen number 5 and 8 were taken out for shrinkage study after 190 days).....	124
Figure 4.11- Mean rate of mass change vs. number of days during the conditioning phase	125
Figure 4.12- Relationship between change in the thickness vs. mass change of CW during the conditioning phase	127
Figure 4.13- Thickness change during oven-drying, (a) overall change in thickness, (b) thickness change during the first 24 hours	129
Figure 4.14- Mass change during oven-drying	130
Figure 4.15- Typical behaviour of CW when subjected to moisture and heat.....	130
Figure 4.16- Mean percentage radial swelling/shrinkage results of beech wood dowels (denoted as HW) and CW dowels during the conditioning phase at 20 ± 2 °C temperature and 65 ± 5 % RH for 45 days (Series B, C and D)	131
Figure 4.17- Change in dowel diameters of CW and beech wood dowels for series B	132
Figure 4.18- Shape of the dowels of Series B after 45 days of the conditioning phase	133
Figure 4.19- Change in dowel diameters of CW and beech wood dowels for series C	134
Figure 4.20- Shape of the dowels of series C, (a) after water soaking and pressure treatment (b) after oven drying	135
Figure 4.21- Change in dowel diameters of CW and beech wood dowels for series D.....	136
Figure 4.22- Shape of the dowels of series D after 3 rd cycle, (a) after water soaking and pressure treatment (b) after final drying treatment, (c) splitting in one of the beech wood dowels	137
Figure 4.23- Cracks on the surface of specimens after 3 rd pressure cycle	138
Figure 4.24- Pull-out load vs. ram displacement graph for Series A	139
Figure 4.25- Failure of CW dowels and beech wood dowels of series A	139
Figure 4.26- Pull-out load vs. ram displacement graph for Series B	140
Figure 4.27- Pull-out load vs. ram displacement graph of Series C.....	141
Figure 4.28- Failure of CW and beech wood dowels of Series C	142
Figure 4.29- Pull-out load vs. ram displacement graph of Series D	143
Figure 4.30- Failure of CW and beech wood dowels of series D	143
Figure 4.31- Development of cracks due to ageing treatments, (a) timber substrate of Series D, (b) timber substrate of Series C.....	149
Figure 4.32- Typical swelling/shrinkage mechanism of CW dowel during ageing cycles..	150
Figure 5.1- Scheme of small scale-structural testing	155
Figure 5.2- Full-depth CW plates	157

Figure 5.3- Narrow-depth CW plates.....	157
Figure 5.4- Threaded beechwood dowels	158
Figure 5.5- Manufacturing of CW dowel laminated timber beams, (a) staggered arrangement of dowels with dowel spacing (mm), (b) insertion of dowels.....	160
Figure 5.6- Beam-beam connection using full-depth CW/steel plates (all dimension are in mm) (a) connection configuration, (b) edge spacing, end distances and cross section	162
Figure 5.7- Four-point bending test, (a) test set up, (b) geometry in mm.....	163
Figure 5.8- Load-midspan displacement of beam-beam connections using full-depth CW and steel plates.....	165
Figure 5.9- Moment-rotation behaviour of connections with CW connectors and steel connectors	166
Figure 5.10- Failure mode of connection with full-depth CW plates	166
Figure 5.11- Cross-grain shear failure of dowels.....	167
Figure 5.12-Failure mode of connection with full-depth steel plates(a) splitting along the row of dowels in tension zone, (b) red circles shows partial plastic hinges in dowels	168
Figure 5.13- Test program of Phase-II.....	169
Figure 5.14- 3D design configuration, (a) 6-dowel arrangement, (b) 8-dowel arrangement	170
Figure 5.15- Edge spacing and end distance (all dimensions are in mm) (a) 6-dowel arrangement, (b) 8-dowel arrangement, (c) cross-section of the connection using 10 mm thick CW plates, (d) cross-section of the connection using 20 mm thick CW plates ..	171
Figure 5.16- Four-point bending test, (a) test set up, (b) geometry in mm.....	172
Figure 5.17- Load-midspan displacement behaviour of timber-CW connections of Phase-II, (a) 6-dowel arrangement using 10/20 mm thickness narrow-depth CW plates, and (b) 8-dowel arrangement using 10/20 mm thick narrow-depth CW plates.....	174
Figure 5.18- Moment-rotation behaviour of timber-CW connections of Phase-II, (a) 6-dowel arrangement using 10 and 20 mm thickness narrow-depth CW plates, and (b) 8-dowel arrangement using 10/20 mm thick narrow-depth CW plates	175
Figure 5.19- 6-dowels connection using 10 mm CW plates, (a) gap opening at the bottom of the connection and (b)splitting of CW plates along the row of dowels in the tension zone	176
Figure 5.20- 6 dowels connection using 20 mm CW plates, (a) tension failure perpendicular to the grain in timber and splitting in the CW plates, (b) interlaminar shear failure of CW dowels, (c) cross-grain shear failure of the CW dowels	177
Figure 5.21- 8 dowel connection using 20 mm CW plates, (a)splitting in the timber in tension zone and compression zone, (b) interlaminar shear failure of CW dowels.....	178
Figure 5.22- Classification of connections designs for beam-column connections	180
Figure 5.23- 3D models of beam-column connection designs.....	181

Figure 5.24- Assembly of the connection, (a) modern connection design, (b) carpentry mortise and tenon, (c) drilling of holes, (d) chamfered end of CW dowels.....	183
Figure 5.25- Test set up, (a) orientation of the test specimen under load, (b) position of the LVDTs	184
Figure 5.26- Load-ram displacement behaviour of beam-column connections using glued structural members and CW connectors	185
Figure 5.27- Moment-rotation behaviour of beam-column connections using glued structural members and CW connectors	186
Figure 5.28- Failure mechanism, (a) Splitting in CW plates in the tension and compression zone, (b) tension perpendicular to grain failure in the column, (c) formation of partial plastic hinges in the dowel of tension zone, (d) formation of partial plastic hinges in the dowel 2 of the tension zone.....	187
Figure 5.29- Failure mechanism, (a) tension perpendicular to grain failure in the column, (b) formation of partial plastic hinges in dowel 1 of tension zone, (c) formation of partial plastic hinges in dowel 2 of tension zone, (d) splitting in CW plate of the compression zone.....	188
Figure 5.30- Failure mechanism, (a) splitting of CW plates in the compression zone, (b) splitting in the beam, (c) deformations of dowel 2 of the beam, (d) deformation of dowel 3 of the beam.....	189
Figure 5.31- Failure mechanism, (a) typical failure mechanism of the CW dowels with the formation of partial plastic hinges, (b) tenon relish failure.....	190
Figure 5.32- Failure mechanism, (a) typical failure mode of CW dowels, (b) tenon relish failure, and (c) mortise failure.....	191
Figure 5.33- Failure mechanism, (a) deformation of CW dowels, (b) embedment of beam-column, (c) uplifting of column	192
Figure 5.34- Failure mechanism, (a) deformation of CW dowels, (b) tenon relish failure..	193
Figure 5.35- Showing constraints in manufacturing of carpentry connection types using CWDLT structural members.....	195
Figure 5.36- Test program of Phase-IV	195
Figure 5.37- 3D design of beam-column connection for CWDLT members, (a) exploded view, (b) assembled connection.....	196
Figure 5.38- Plan view of column, (a) Design-IV-1 (initial design), (b) Design-IV-2 with optimised configuration (all dimensions in mm). Red colour circles indicate compressed threaded beechwood dowels	197
Figure 5.39- Compressed threaded beech wood dowels in the connection area (outer two laminates were removed to show the position of threaded dowels).....	198

Figure 5.40- Assembled beam-column connections using CWDLT beam-column connections	199
Figure 5.41- Test set up for beam-column connections using CWDLT members	200
Figure 5.42- Load-ram displacement graph showing a comparison between beam-column connections using CWDLT members and glued members.....	201
Figure 5.43- Moment-rotation graph showing a comparison between beam-column connections using CWDLT members and glued members.....	202
Figure 5.44- Failure mechanism of beam-column connection with 20 mm thick CW plates and CWDLT structural members.....	203
Figure 5.45- Failure mechanism of beam-column connection with 15 mm thick CW plates and larger dowel spacing, (a) opening of the connection in tension zone, (b) no failure in the CWDLT members.....	204
Figure 6.1- Frame geometry (a) 3D conceptualisation, (b) dimensions (in mm).....	212
Figure 6.2- Configuration of the connections for frames (a) with glued members (b) CWDLT members.....	213
Figure 6.3- Frame test set up, (a) testing rig, (b) slotted steel plate mounted on loaded side, and (c) rolling load head.....	214
Figure 6.4- Instrumentation, (a) arrangement of LVDTs, and (b) arrangement of potentiometers.....	215
Figure 6.5- Determination of F_{max} , F_y and F_u in accordance with EN 12512 [187]	217
Figure 6.6- Load-lateral displacement graph	219
Figure 6.7- Load-base rotation behaviour of glued and CWDLT structural members.....	220
Figure 6.8- Typical deformation of frames, (a) glued frame, and (b) CWDLT frame.....	220
Figure 6.9- Moment rotation behaviour of localised connections of loaded and unloaded sides within both frame types.....	221
Figure 6.10- Typical failure mechanism in the connection area of the glued frame (a) loaded side, (b) unloaded side, (c) loaded end, (d) unloaded end.....	224
Figure 6.11- Typical failure mechanism in the connection area of frame with CWDLT members (a) loaded side, (b) unloaded side, (c) loaded end, (d) unloaded end.....	226
Figure 7.1- Possible failure modes of a double shear timber-timber connection [55]	229
Figure 7.2- Possible failure modes for slotted-in steel plate timber connections [55].....	230
Figure 7.3- Connection configuration of beam-beam connections with full-depth steel plates	233
Figure 7.4- The rotation of steel dowels (all dimensions are in mm)	234
Figure 7.5- The rotation of CW dowels (all dimensions are in mm)	237

Figure 7.6- Transfer of the bending moment among the connection components, (a) connections with 6-dowel arrangement, and (b) connections with 8-dowel arrangement (all dimensions are in mm).....	239
Figure 7.7- Transfer of internal forces through the contact surfaces of loaded ends of the beams in the compression zone.....	242
Figure 7.8- Beam-column connection configuration (Design-IV-2)	243
Figure 7.9- Embedment between beam-column around bearing point	245
Figure 8.1- Timber building using CWDLT members and designed timber-CW connection systems at Ness Botanical Garden, Liverpool, United Kingdom - Towards Adhesive Free Timber Building (a) demonstrator structure, (b) during construction, (c) internal space and location of timber-CW connections, (d) close up view of narrow-depth timber-CW connections	262

List of tables

Table 2.1- Development of wood densification processes in chronological order	25
Table 2.2- Summary of mechanical properties of compressed wood from literature	34
Table 3.1- List of material characterisation tests included in this chapter	62
Table 3.2- Specification of the CW material	67
Table 3.3- Dimensions of embedment test specimens	69
Table 3.4- Results of individual specimens of the uncompressed Douglas fir tested in parallel to the grain direction	78
Table 3.5- Results of individual specimens of the uncompressed Douglas fir tested in perpendicular to the grain direction	80
Table 3.6- Results of individual specimens of the CHW68 tested in parallel to the grain direction	82
Table 3.7- Result of individual specimens of the CWH68 tested in perpendicular to the grain direction	84
Table 3.8- Comparison between characteristic embedment strength of uncompressed Douglas fir and compressed Western hemlock (CWH68) from experiments and EC 5 values (MPa)	85
Table 3.9- Yield moment test results for CW dowels	90
Table 3.10- Yield moment test results for beech wood dowels	91
Table 3.11- Cross-grain shear test results of CW dowels	96
Table 3.12- Cross-grain shear test results of beech wood dowels	97
Table 3.13- Results of three-point bending test	100
Table 4.1- Mean hole clearance for each series	117
Table 4.2- Change in the thickness of individual CW plates over a period of 510 days during the conditioning phase.	123
Table 4.3- Change in the mass of individual CW plates over a period of 510 days during the conditioning phase	126
Table 4.4- Results of pull-out tests	144
Table 4.5- Radial and tangential swelling of CW dowels for Series C and Series D after corresponding ageing treatment	147
Table 4.6- Radial and tangential swelling of beech wood dowels for Series C and Series D after corresponding ageing treatment.....	148
Table 5.1- Test programme of Phase-I.....	161
Table 5.2- Test results of Phase-I.....	169
Table 5.3- Test scheme of Phase-II.....	171

Table 5.4- Test results of beam-beam connections with narrow-depth CW plates (Phase-II)	179
Table 5.5- Results summary of beam-column connections using glued structural members and CW dowels.....	194
Table 5.6- Result summary showing a comparison between beam-column connections using CWDLT members and reference design using glued structural members (Design-III-3)	205
Table 6.1- Instruments used in frame testing	215
Table 6.2- System characteristic of tested frames.....	219
Table 6.3- Characteristics of localised connections.....	222
Table 7.1- Timber properties	231
Table 7.2- Material properties of CW material	232
Table 7.3- Properties of steel connectors	232
Table 7.4- Dowel distribution and lever arm distances (beam-beam connections with full-depth steel plates).....	235
Table 7.5- Experimental mean moment capacity and characteristic moment capacity of the beam-beam connections with full-depth steel plates	235
Table 7.6- Dowel distribution and lever arm distances (beam-beam connections with full-depth CW plates).....	238
Table 7.7- Experimental mean moment capacity and characteristic moment capacity of the beam-beam connections with full-depth CW plates	239
Table 7.8- Connection parameters for specimens with 6-dowel arrangement and 8-dowel arrangement.....	240
Table 7.9- Characteristic load-carrying capacity per shear plane per CW dowel for beam-beam connections with narrow-depth CW plates for each failure modes	241
Table 7.10- Experimental moment capacities and calculated characteristic moment capacities of beam-beam connections with narrow-depth CW plates	242
Table 7.11- Experimental mean moment capacity and characteristic moment capacity of the beam-column connections with narrow-depth CW plates and CWDLT members.....	245
Table 7.12- Results summary of the experimental mean moment capacities and calculated characteristic moment capacities	246
Table 7.13- Comparison between experimental mean rotational stiffness and calculated rotational stiffness of beam-beam connections with full-depth steel plates.....	249
Table 7.14- Comparison between experimental mean rotational stiffness and calculated rotational stiffness of beam-beam connections with full-depth CW plates.....	250
Table 7.15- Comparison between experimental mean rotational stiffness and calculated rotational stiffness of beam-beam connections with narrow-depth CW plates.....	251

Table 7.16- Comparison between experimental mean rotational stiffness and calculated rotational stiffness of beam-column connections with CWDLT members	252
Table 7.17- Results summary of the experimental mean rotational stiffness and calculated rotational stiffness	253

Nomenclature

a_1	(mm)	Spacing, parallel to the grain, of dowels within one row
a_2	(mm)	Spacing, perpendicular to the grain, of dowels between rows
$a_{3,c}$	(mm)	Distance between dowels at the unloaded end
$a_{3,t}$	(mm)	Distance between dowels at the loaded end
$a_{4,c}$	(mm)	Distance between dowels at the unloaded edge
$a_{4,t}$	(mm)	Distance between dowels at the loaded end
b	(mm)	Width of the specimen
CR	(%)	Compression ratio of compressed wood
D	(-)	Ductility ratio
d_i	(mm)	Initial dowel diameter
d_t	(mm)	Dowel diameter after ageing treatment
E	(GPa)	Modulus of elasticity
F	(N or kN)	Force
F_{20}	(N or kN)	20% of the maximum force
F_{40}	(N or kN)	40% of the maximum force
f_h	(MPa)	Embedment strength
$f_{h,0,k}$	(MPa)	Characteristic embedment strength parallel to the grain
$f_{h,90,k}$	(MPa)	Characteristic embedment strength perpendicular to the grain
$f_{h,\alpha,k}$	(MPa)	Characteristic embedment strength at an angle to the grain
f_m	(MPa)	Bending strength
F_{max}	(N or kN)	Maximum force

f_{sp}	(MPa)	Cross-grain shear strength of compressed or hardwood dowel
$F_{v,Rk}$ (<i>cross-grain shear</i>)	(N)	Characteristic load-carrying capacity per dowel per shear plane calculated using characteristic cross-grain shear strength of the compressed wood dowel
$F_{v,Rk}$	(N)	Characteristic load-carrying capacity per dowel per shear plane
h	(mm)	Depth of the beam
h_{CW}	(mm)	Depth of the compressed wood plates
h_{steel}	(mm)	Depth of the steel plates
k_{def}	(-)	Deformation factor
k_{exp}	(kN/rad)	Experimental rotational stiffness
K_{ser}	(kN/mm)	Slip modulus at Serviceability Limit State (SLS)
$k_{ser,con}$	(kN/rad)	Design rotational stiffness of connection
k_{sys}	(kN/m)	Lateral stiffness of the portal frame
l	(mm)	Lever arm distance
L	(mm)	Span of the test specimen
l_{CW}	(mm)	Length of compressed wood plates
l_{steel}	(mm)	Length of steel plates
m_d	(%)	Percentage decrease in the mass of compressed wood plates
M_{exp}	(kN.m)	Experimental moment capacity
m_i	(g)	Initial mass of the compressed wood plate
m_m	(g)	Mass of the compressed wood plate on the day of measurement
M_{Rk}	(kN.m)	Characteristic moment capacity

$M_{y,eff}$	(N.mm)	Effective yield moment capacity of compressed wood dowel or hardwood dowel
$M_{y,Rk}$	(N.mm)	Characteristic yield moment capacity of steel dowel
n	(-)	Number of dowels
n_{eff}	(-)	Effective number of dowels
n_{sp}	(-)	Number of shear planes
r_{max}	(mm)	Lever arm distance of dowel which is at a maximum distance from the centroid of fastener group
t_1	(mm)	Thickness of side member
t_2	(mm)	Thickness of middle member
t_b	(mm)	Thickness of compressed wood plate at the start of the experiment
t_d	(%)	Percentage decrease in thickness of the compressed wood plate
t_{MDS}	(%)	Moisture dependent swelling of the compressed wood plate
t_o	(mm)	Oven-dried thickness of the compressed wood plate
t_s	(%)	Springback of the compressed wood plate
V_{10}	(mm)	Displacement of connection at F_{10}
V_{40}	(mm)	Displacement of connection at F_{40}
V_u	(mm)	Ultimate displacement at a load level of $0.8F_{max}$
V_y	(mm)	Displacement at yield load
w	(mm)	Width of the beam
α	(°)	Angle between the force and the grain direction
β	(-)	Friction effect
Δ_{10}	(mm)	Displacement at F_{10}
Δ_{40}	(mm)	Displacement at F_{40}

Δd	(mm)	Change in dowel diameter
Δm	(g)	Change in the mass of the compressed wood plate
$\Delta m\%$	(%)	Percentage change in the mass of the compressed wood plate
Δt	(mm)	Change in the thickness of the compressed wood plate
$\Delta t\%$	(%)	Percentage change in the thickness of the compressed wood plate
θ	(°)	Rotation angle of the connection
θ_u	(°)	Rotation angle of the connection at $0.8M_{\max}$
θ_y	(°)	Rotation angle of the connection at yield load
ρ	(kg/m ³)	Timber density
ρ_{CW}	(kg/m ³)	Mean density of compressed wood
ρ_m	(kg/m ³)	Mean density of timber
ω	(%)	Moisture content of timber

Chapter 1 Introduction

1.1 Background and motivation

Increasing the sustainability credentials of building materials is one of the most widely researched and discussed topics in the construction sector today. This is driven by tightening environmental regulations and customer pressure to decrease the environmental impact of building materials to tackle the adverse effects of climate change. According to 2019 Global Status Report for Buildings and Construction [1], the buildings and construction sector accounted for 36% of global final energy use and 39% of energy and process-related carbon dioxide (CO₂) emissions in 2018. The report highlights that 11% of the CO₂ emissions out of 39% was related to the manufacturing of building materials and products such as steel, concrete and glass. The construction industry uses steel and concrete as predominant materials for building construction globally which have significant environmental impacts at various life cycle stages directly from material extraction to their end of life disposal [2–4]. Particularly, the production processes of cement and steel are major sources of energy use and CO₂ emissions. The current production technologies of these materials involve usages of inputs from non-renewable energy resources which originate from fossil fuel-based feedstock [5,6]. To reduce the emissions from construction and also from other sectors (aviation, agriculture etc), the Paris agreement requires greenhouse gas emissions to be net-zero by 2050-2070 [3,7].

However, these targets are further coupled with other foreseeable issues such as urbanisation and growing global population. According to the Global Building Stock Database [8], approximately 2.4 billion square meters of new building stock (dwellings, offices, factories, shops, educational establishments, agricultural buildings etc) is required every year between 2020 and 2029. The OECD report Global Material Resources Outlook to 2060 [9] forecasted an increase of approximately 110% in global material use by 2060. The worldwide trend in the construction sector is to reduce the energy usage and emissions from the manufacturing of conventional building materials (steel and concrete) and increase the use of renewable materials like timber [10,11].

1.2 Modern mass timber frame systems

Recent advancements in timber engineering have led to the development of high-performance engineered wood products (EWPs) which are allowing the construction of taller, safer and more economical timber buildings. In the last two decades, the EWPs which are garnering attraction across the globe are massive or mass timber products. Mass timber products are

EWPs with larger section sizes, typically with the smallest dimension greater than 75 mm [11]. They are layered products comprising sawn timber boards (laminates) that are adhesively bonded/mechanically connected together to produce thick panels or linear elements [11–13]. These products are becoming increasingly used in building construction as they offer excellent load carrying capacity, fire performance, durability, reduced effect of natural defects and are easily customisable making them very suitable for construction purposes [11,13]. On the sustainability side, they offer lower embodied carbon solutions and provide excellent potential for recycling at the end of life of the buildings [2,5,10,11,13,14]. Due to their structural performance, environmental properties and cost-competitiveness, several studies [5,6,11,12] have shown their significant potential as an environmentally alternative to steel and concrete in construction.

Glued laminated timber (glulam) members have been used for decades as load-bearing elements in mass timber buildings. They are used as vertical columns or horizontal beams to provide resistance to the structure against external loads. Generally, in these buildings, glulam members are connected together with highly engineered and customisable metallic connectors to transmit the heavier loads. One impressive example of mass timber building is the Mjøstårnet (Norway) (see Figure 1.1). This is the world's tallest timber building with a height of 85.4 m and comprises a total of 18 floors and over 11300 square meters of floor space. The structural framework of this building consists of glulam columns, beams and diagonals. All glulam members in the structure are connected using slotted-in steel plates and steel dowels (Figure 1.1c) [15]. With recent changes in building design codes and a quest to develop more sustainable ways to construct taller buildings, there has been a significant rise in the number of taller and structurally efficient mass timber buildings across the globe. Although mass timber products are bio-based and sustainable, however, there is scope to improve their environmental and health benefits by minimising the use of energy-intensive synthetic adhesives and metallic connectors during the manufacturing and assembly processes of these products.

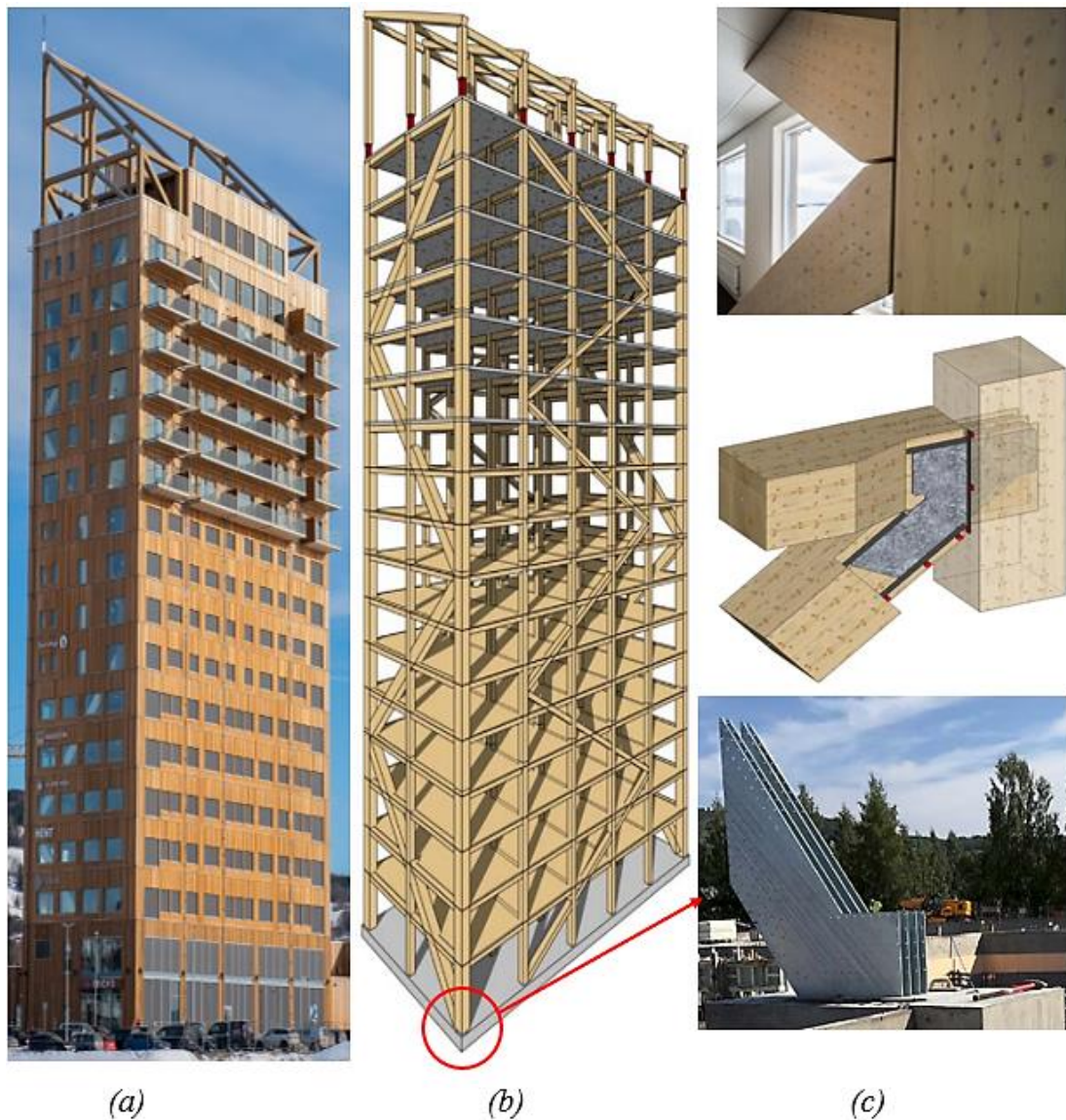


Figure 1.1- Mjøstårnet, Norway, (a) building, (b) skeleton of the building, (c) slotted-in steel plate and dowel connection [15,16]

Today, robotic fabrication is a key enabler of innovation in mass timber construction with advanced production technologies using computer numerically controlled (CNC) tools. This has facilitated the development of cost-competitive dowel-laminated timber (DLT) products using low cost precision machining and assembly thereby eliminating the need for synthetic adhesives (see Figure 1.2). By replacing metallic connection systems with wood-based alternatives, all-wood high-performance building systems, with enhanced environmental and health benefits, are then possible.



Figure 1.2- Dowel laminated timber (DLT), Structurecraft [17]

Currently, the use of synthetic adhesives and mechanical fasteners cannot be eliminated in timber construction until new bio-based solutions emerge with equivalent structural performance and cost. In the last two decades, there is a great interest in the development of modified wood and bio-based composites [18–23]. Going one step further, this study focuses on the use of a specialised form of modified wood known as compressed wood (CW) as a connector material within timber-timber connections and timber products. When compared to uncompressed timber, CW offers superior material properties such as increased density, strength, stiffness, and hardness, and could be an ideal choice for manufacturing of wood-based connectors for structural applications [24,25]. These connectors may be used for connection between load-bearing elements (beam/column) or in the lamination of wood products.

The research presented in this thesis is associated with a larger European project “Towards Adhesive Free Timber Buildings (AFTB)”. The project was conducted by six European partner institutions aimed at the development of timber building systems made entirely out of natural renewable raw material. The project addresses the wasteful and harmful use of synthetic adhesives in the manufacturing of Engineered Wood Products (EWPs) by the construction industry. This research project involves:

- (a) Investigation on the mechanical performance of one- and two-dimensional building elements in the form of DLT beams/columns and panels using local timber species and high-performance CW dowel connectors,
- (b) Evaluation of the structural performance of CW dowel fastened timber-timber moment connections between load-bearing DLT beam/columns,
- (c) Optimisation of design and structural performance of CWDLT members and timber-CW connections using CW connectors through computer models,
- (d) Development of demonstration structures using CWDLT members and timber-CW connections.

This thesis mainly focuses on the use of CW connectors within beam-beam or beam-column connections using glulam and compressed wood dowel laminated timber (CWDLT) members. However, this requires extensive research to generate data on the mechanical properties and structural feasibility of CW connectors in high-end timber connections. The ongoing transition towards a bio-based circular economy is the motivation behind this study and it aims to develop a novel approach to produce non-metallic and adhesive-free timber-timber moment connections using CW connectors.

1.3 Research objectives

The primary objective of this research is to investigate the feasibility of CW connectors in semi-rigid type timber-timber moment connections. The following sub-objectives have been defined to achieve the primary objective:

- Characterise the mechanical behaviour of CW and CW connectors
 - Evaluate the mechanical properties of CW and CW as a connector material
 - Compare the mechanical properties of CW with uncompressed hardwood and softwood.
 - Create a database on mechanical properties of CW connectors based on the experimental test results and the available literature.
- Investigate the moisture dependent behaviour of CW and timber-CW connections
 - Quantify the moisture dependent swelling/shrinkage behaviour of CW
 - Determine the effect of ageing on the structural performance of timber-CW dowel/ timber-hardwood dowel connections
- Characterise the structural performance of semi-rigid timber-CW connections
 - Beam-beam connections
 - Compare the structural performance of timber-CW and timber-steel connections
 - Develop a range of designs for beam-beam connections and compare their structural performances
 - Investigate the moment-rotation behaviour of the beam-beam connections using CW connectors
 - Beam-column connections
 - Design, develop and structurally characterise the beam-column connection systems fastened using CW connectors
 - Evaluate the moment-rotation behaviour of timber-CW beam-column connections produced using CWDLT members
 - Application of timber-CW connections in portal frames

- Design, develop and structurally characterise the timber-CW connections within structural frames produced using glued/CWDLT structural components
- Evaluate design approaches to determine the moment capacity and stiffness of timber-CW connections
 - Compare experimental test results of beam-beam and beam-column connections with current design guidelines in Eurocode 5 (EC 5) and research studies
 - Calculate design moment capacity and design rotational stiffness of timber-CW connections.

1.4 Research methodology

To realise the objectives of this study, research was carried out based on the research methodology shown in Figure 1.3. The methodology used is as follows:

- Firstly, small scale laboratory experiments were carried out to determine the mechanical properties of CW as a connector material using embedment, yield moment, shear and bending tests. The mechanical performance of CW connectors was also compared with hardwood and softwood materials.
- A long-term study was carried out to characterise the swelling/shrinkage behaviour (springback) of thermo-mechanically densified CW. Also, to develop a better understanding of the long-term behaviour of timber-CW dowel connections, accelerated ageing tests were conducted to evaluate the mechanical behaviour of these connections through dowel pull-out tests. Prior to carrying out pull-out tests, specimens were subjected to different environmental conditioning including constant temperature and relative humidity (RH), and pressure wetting and rapid drying cycles. Finally, the test results of timber-CW connections were compared with the timber-hardwood dowel connections.
- Based on the material properties of CW connectors, connection designs of semi-rigid type beam-beam timber moment connection were developed using CW plates and CW dowels. Specimens were tested under pure bending and their load-carrying capacity, moment-rotation behaviour, ductility and failure modes were compared with a similar design of timber-steel connection of approximately equal capacity. Further, to improve the structural performance of beam-beam connections, the connection designs were optimised by

varying the geometrical parameters of the structural members and CW connectors.

- Two series of semi-rigid type beam-column timber-CW connections were developed for small-scale testing, one using glued and another using CWDLT structural members. The load-carrying capacity, moment-rotation behaviour, ductility ratio and failure modes of the developed connections were evaluated experimentally. Finally, the structural performance developed connections were evaluated.
- Based on the test results of small-scale beam-column timber-CW connections, four portal frames comprising two frames using conventional glued members and two frames using CWDLT members were manufactured and subjected to lateral load (racking) tests. The load-carrying capacity, moment-rotation behaviour, ductility ratio and failure modes of both frame types were compared.
- Finally, a study was carried out to assess the suitability of current design rules in EC 5 and in research studies for designing and predicting the moment capacity and rotational stiffness of the developed timber-CW connections.

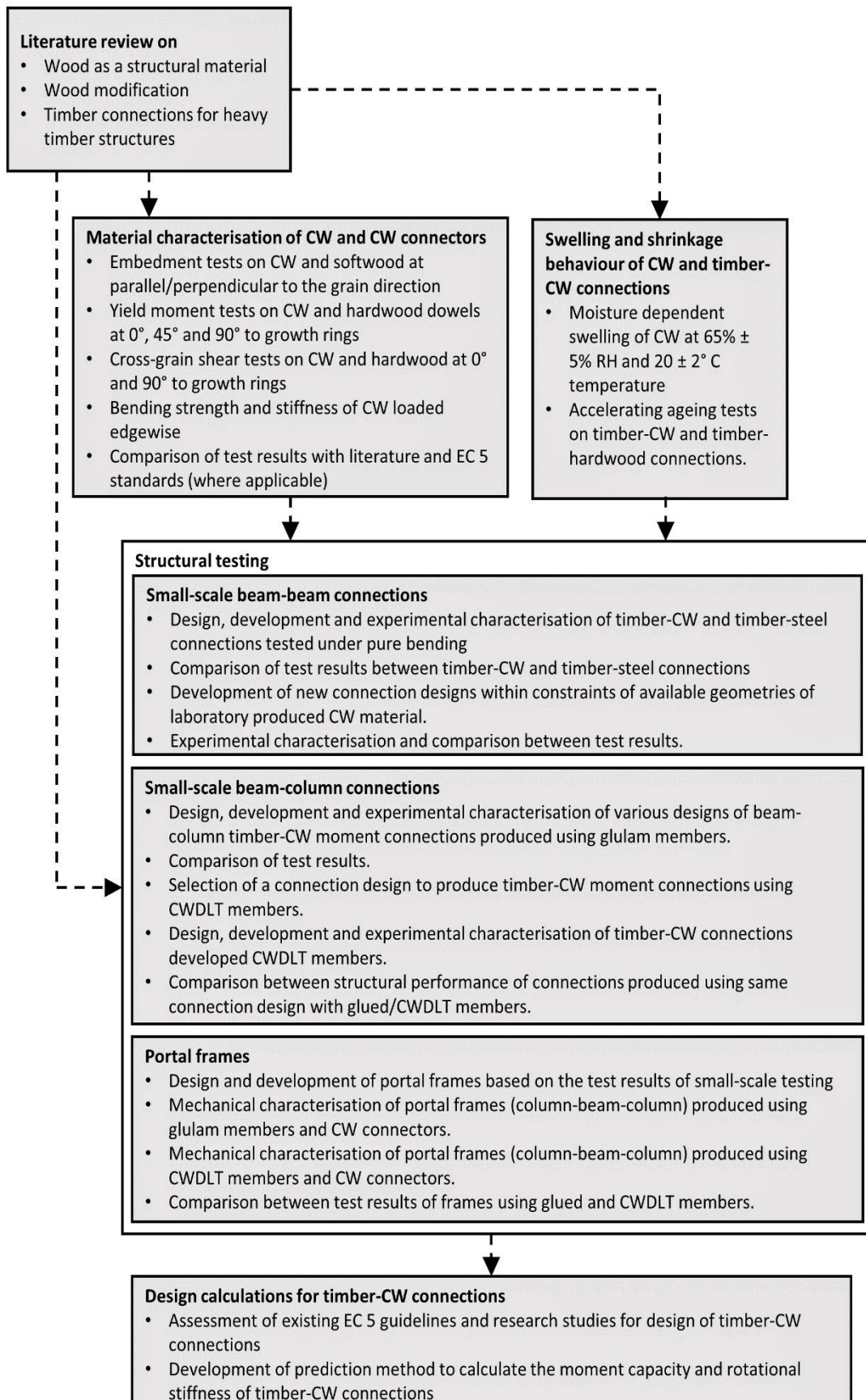


Figure 1.3- Research methodology

1.5 Layout of the thesis

The thesis is comprised of eight chapters. In Chapter 2, the thesis begins with a literature review. This chapter is divided into three sections covering up to date research on wood as a structural material, wood modification techniques, and carpentry and metallic timber connections suitable for heavy timber structures. Chapter 3 presents the material characterisation test results of CW and CW as a connector material. This section also discusses the suitability of existing test procedures for CW connectors. Chapter 4 details the moisture dependent swelling/shrinkage behaviour of CW and timber-CW connections. This chapter is split into two sections. The first section includes the results of long-term unconstrained swelling/shrinkage behaviour of CW plates. The second section presents the comparative results of accelerated ageing tests on timber-CW dowel and timber-hardwood dowel connections that were subjected to cyclic treatments using varying parameters such as temperature, RH and pressure. Chapter 5 details the manufacturing procedures, assembly and experimental test results of semi-rigid type timber-CW connections fabricated using CW connectors and glued/CWDLT structural members. This chapter is divided into four sections. The first section details the experimental test results of timber-CW and timber-steel beam-beam connections. Further, this section also compares the structural performance of timber-CW and timber-steel connections. The second section covers the experimental test results of various designs of semi-rigid type beam-beam connections developed using varying parameters such as the geometry of the glued structural members, number of CW dowels, depth and thickness of the CW plates. The third section covers various designs of semi-rigid type beam-column connections fabricated using glued structural members and CW connectors. And the final section presents the design and test results of beam-column connections developed using CW connectors and CWDLT members. Chapter 6 details the structural performance of timber-CW connections in portal frames produced using glued/CWDLT members. Chapter 7 details the design calculation for timber-CW connections. Finally, Chapter 8 concludes the thesis and outlines the recommendation for future work. Further information is given in the appendices.

Chapter 1 – Introduction

Chapter 2 – Literature review

Chapter 3 – Material characterisation of CW and uncompressed wood

Chapter 4 – Swelling/shrinkage behaviour of CW and timber-CW connections

Chapter 5 – Development of semi-rigid timber connections using CW connectors

Chapter 6 – Experimental investigation of laterally loaded laminated timber portal frames with CW connections

Chapter 7 – Design calculations for timber-CW connections

Chapter 8 – Conclusion and recommendation

Appendix A – AutoCAD drawings of beam-column connections using CW connectors and glued structural members

Appendix B – AutoCAD drawings of beam-column connections using CW connectors and CWDLT structural members

Appendix C – AutoCAD drawings of portal frames using timber-CW connections and glued/CWDLT structural members

Appendix D – Suitability of EC 5 design rules and research studies to determine the rotational stiffness of the timber-CW connections

Chapter 2 Literature review

2.1 Introduction

This chapter is divided into three sections to cover current research to date on wood as a structural material, modified wood, and timber connections for heavy timber structures. The chapter begins with the review of wood as a material and discusses various aspects of wood required for its structural applications and design of timber connections. This section comprises details of its macroscopic and microscopic structures, chemical composition, mechanical properties, moisture effect and swelling/shrinkage behaviour. The particular focus is on its intrinsic properties related to wood modification techniques and the performance of timber connections. There is a brief introduction to wood modification and, in particular, densification techniques that do not involve the use of synthetic chemicals. In this section, the focus is on type, manufacturing process and mechanical properties of CW. This section also discusses challenges and opportunities for the use of CW in timber connections and in the manufacture of timber products. This is followed by a review of existing and recent timber-timber connection technologies, with particular focus on the beam-beam and beam-column connection typologies for mass timber structures. This section comprises of both carpentry and metallic connection types.

2.2 Wood as a structural material

2.2.1 Introduction

Wood is a natural biopolymer obtained from tree stem/trunk/bole/branches. Trees are classified into two categories, namely, softwoods and hardwoods. Softwood trees are characterised by needle-like leaves. They are commonly known as evergreen trees because they retain the needles throughout the year, annually losing only a portion of them. Softwood trees also bear scaly cones (seeds are produced within) and are therefore often referred to as conifers. Some of the examples of softwood species are spruces, pines, firs (SPF). In contrast to softwoods, hardwoods are characterised by broad leaves. Most of them are deciduous and they shed leaves in the autumn [26].

Generally, softwoods grow much more quickly and are less dense compared to hardwoods. However, the term softwood and hardwood are misnomers because hardwood is not always harder and dense than softwoods. For example, Balsa wood is a hardwood that is relatively less dense and softer compared to softwoods whereas yew is a softwood which is relatively harder than hardwoods. Both hardwood and softwoods are used in structural applications. However, softwoods make up approximately 60% of industrial roundwood production and are largely used in construction due to greater availability and lower costs [27].

2.2.2 Cellular structure and function of wood

Wood is a porous cellular material. It is located inside the tree bark and forms the interior bulk of the tree stem. It essentially acts as a conductive and supportive tissue which facilitates translocation of water and dissolved minerals (sap) from the root to active growth regions of the tree during its life cycle. Figure 2.1 shows a three-dimensional section of a tree trunk. The tree trunk is multi-layered, which going from the outer layer to the centre in both softwood and hardwood consists of bark, intervacular or vascular cambium, sapwood, heartwood and pith.

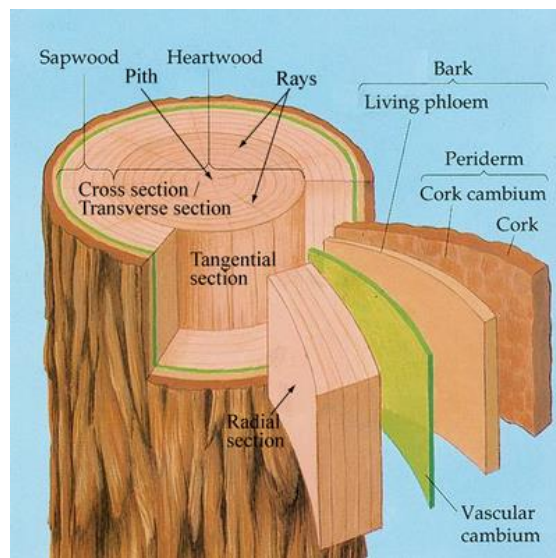


Figure 2.1- Three-dimensional section of a tree bole [28]

The part inside the vascular cambium towards the centre of the trunk is known as secondary xylem or wood. The young secondary xylem is commonly known as sapwood and can be differentiated by its light colour on the cross-section of a tree trunk. The main function of sapwood is upward/axial transport of water/sap. Similarly, young secondary phloem (living phloem) is responsible for the downward transport of photosynthates and hormones from the leaves and buds to growth regions. Secondary xylem and secondary phloem also have secondary xylem and secondary phloem rays, respectively. They are responsible for the radial transport of sap and photosynthates. As the tree grows secondary xylem keeps on accumulating toward the pith and secondary phloem towards the perimeter of the trunk. Ultimately, this results in an increase in the tree diameter. Towards the maturation stage, the wood cells of secondary xylem which are located close to pith become unfunctional and die. These cells are essentially composed of only cell walls and voids (lumen). They are long and slender, aligned with the longitudinal axis of the tree trunk. They are commonly known as fibres. With growth, dead cells start accumulating extractives such as oils, resins, gums and polyphenols. Generally, this results in a darker colour portion in the centre of a tree trunk which is commonly known as heartwood. However, there are exceptions. Heartwood of

hemlock, aspen, cotton wood and beech are lighter in colour and difficult to differentiate [29]. The main function of heartwood is to provide mechanical support to the tree. Formation of heartwood is a continuous process during the tree growth as sapwood keeps on ageing and adding into the heartwood. Generally, the heartwood is drier than the sapwood. From the construction point of view, there is no difference between the mechanical properties of sapwood and heartwood [30]. However, the durability of heartwood is higher than the sapwood. This is because of the presence of polyphenols and other secondary metabolites in heartwood which act as a barrier against insect and fungal infestation [31].

Another interesting feature in the cross-section of wood is the circular rings which are commonly known as annual growth rings or growth rings. Growth rings indicate the amount of wood formed in one growing season. They consist of cells which originate from the vascular cambium. The rate of cell production is mainly dependent on climatic conditions. It is faster during the summer months and relatively slower in the winter months. For this reason, the wood that is produced in summer months has numerous larger cells with thin cell walls. In contrast to this, the wood which is produced in winter months has smaller cells with thick walls. The wood produced during the summer months is commonly known as earlywood, whereas wood produced during winter months is known as latewood. Earlywood is relatively lighter in colour compared to latewood, which is usually darker in colour. One growth ring consists of earlywood and latewood. Figure 2.2 shows earlywood and latewood in a microscopic cross-section of European silver fir. Due to the nature of the cells, latewood has a relatively high density compared to earlywood. From the structural point of view, the mechanical properties of latewood are superior to those of earlywood [32–34]. Usually, fast-growing plantation wood species have wider growth rings compared to slow-growing wood species and have lower density. This is one of the important reasons which is responsible for the lower mechanical performance of plantations woods compared to slow-growing wood species. The proportion of earlywood and latewood also has an effect on the strength properties of modified wood and the effectiveness of wood modification [35] (discussed in detail in Section 2.3).

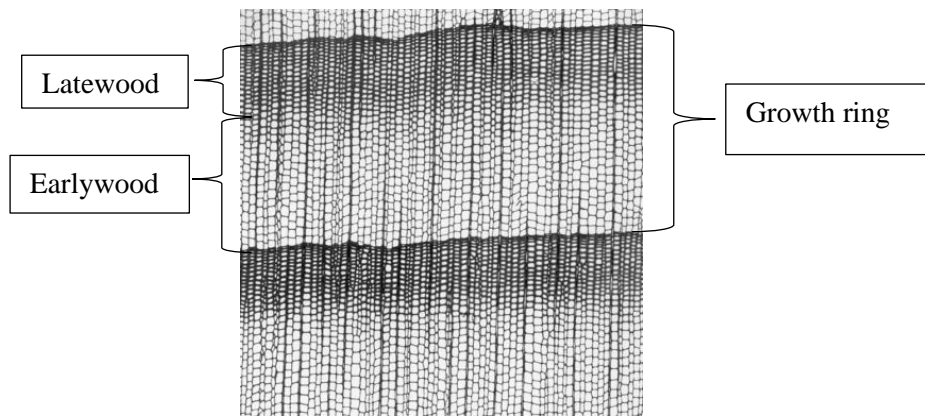


Figure 2.2- Microscopic cross-section of *Abies alba* showing earlywood and latewood [36]

From an anatomical point of view, both softwoods and hardwoods are quite different. Softwoods have a relatively simple structure and are more uniform in microscopic structure compared to hardwoods. This is because they largely (90-95%) consist of similar type of cells which are known as tracheids. Tracheids are elongated cells which are often more than 100 times longer (1 to 10 mm) than their width. Tracheids are responsible for both structural support and conduction of sap. In contrast to softwoods, hardwoods have several different cell types including highly specialised sap conducting cells known as vessels or pores. Vessels diameter typically ranges from 50 to 200 μm . They are shorter than tracheids and ranges from 0.1 mm to 1.2 mm [26]. In hardwoods, structural support is mainly provided by the fibres. Figure 2.3 shows the microscopic structure of softwood and hardwood. The size of tracheids, vessels and fibres vary from species to species and is affected by the growth conditions. The microstructure imparts anisotropy in the mechanical properties of wood [37].

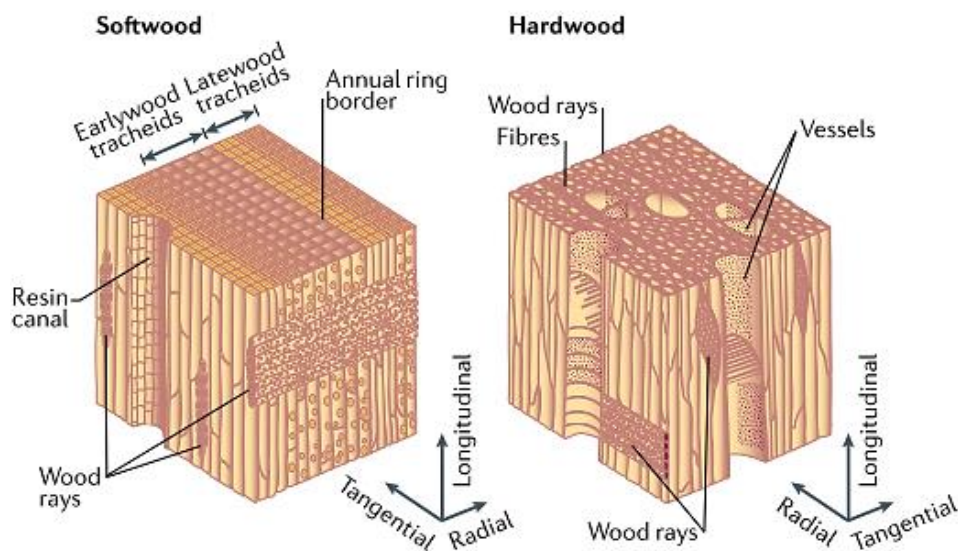


Figure 2.3- Microscopic structure of softwood and hardwood [38]

2.2.3 Microstructure and chemical composition of wood

The cell wall of each wood cell is comprised of four layers known as middle lamella (ML), primary wall (P), secondary wall (S) and the tertiary wall (T). Figure 2.4 shows the microstructure of a wood cell. The thickness, chemical composition and orientation of microfibrils vary in each layer. These variations affect the mechanical properties of the wood [39]. The secondary wall forms approximately 90% of the cell wall and is largely composed of S2 layer. Microfibrils of the S2 layer arranged roughly parallel (10° to 30°) to the fibre and the main reason for the high strength and stiffness in parallel to the grain direction. From the engineering point of view, the middle lamella has high compressive strength, the primary wall ensure dimensional stability of the cells, the microfibril angle of the S2 layer affects the tensile strength of the wood and the S1 and S3 layers provide buckling resistance against compression [37].

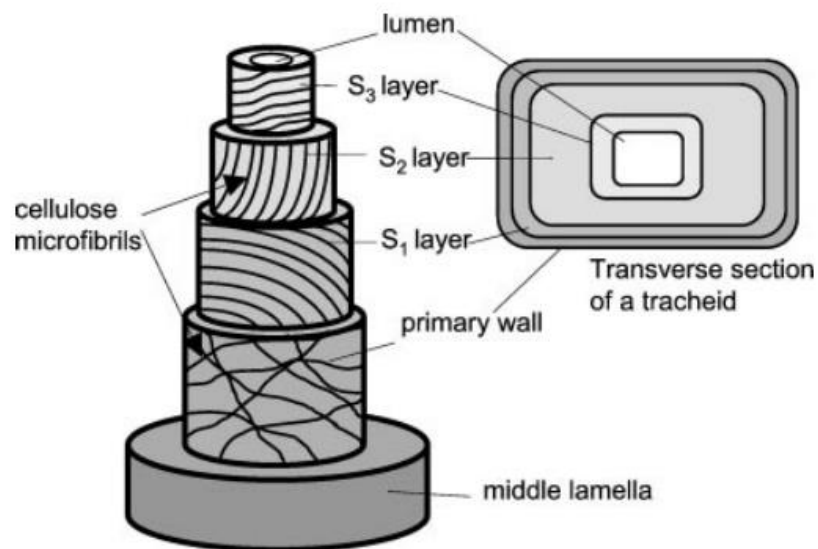


Figure 2.4- Microstructure of the wood cell wall [40]

Wood is an organic biocomposite. Each wood cell is mainly composed of cellulose, hemicellulose and lignin. Figure 2.5 shows the chemical composition of the cell. The cellulose content in most wood remains constant (approximately 40-45%) irrespective of the wood types (softwood and hardwoods) [41]. Cellulose is a polymer comprising a crystalline region (about 65%) and amorphous region. The microfibrils of the cell wall are composed of cellulose which provides axial strength to the cells. Cellulose is hydrophilic and it affects the moisture sorption capacity of the wood fibres since amorphous regions can absorb more moisture. Hemicellulose is closely associated with cellulose and provides support to cellulose microfibrils. Compared to cellulose, hemicellulose has a large number of free hydrophilic groups (hydroxyl groups). It is an amorphous polymer with high sorptive capacity and affects the moisture absorption capacity of wood. Compared to cellulose and hemicellulose, lignin is

hydrophobic. It imparts moisture repellent properties to the cell wall. It acts as a cementing material in the cell wall and glues together the cellulose and hemicellulose. From the engineering perspective, it provides hardness and strength to the wood cells. It is pressure-resistant and provides compressive strength to the cell wall. Generally, softwoods contain a higher amount of lignin and the lower amount of hemicellulose compared to hardwoods [41]. Due to their lower lignin content, hardwoods show less resistance to dimensional changes compared to softwoods [42–44].

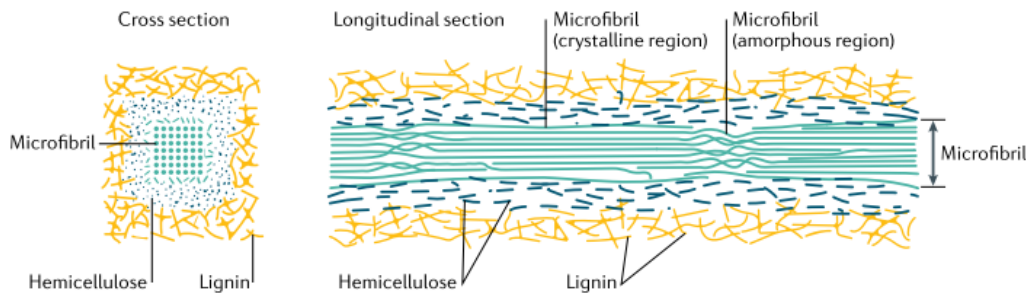


Figure 2.5- Chemical composition of a cell in cross-section and longitudinal direction [38]

2.2.4 Wood density

Wood density is defined as the mass of the wood divided by its volume at a given moisture content. It can be calculated using the following expression:

$$\rho = \frac{m}{V} \quad \text{Eq. 2.1}$$

where ρ is the wood density, m is the mass and V is the volume.

Although the density of wood cell wall remains constant at approximately 1500 kg/m^3 , the wood density varies with species and within species [37,45]. Since wood is porous, its density is mainly affected by cellular structure (earlywood and latewood proportion, size of the tracheids/vessels etc) and moisture content. As the moisture content of the surrounding environment changes, it leads to an increase or decrease in the mass and volume and ultimately affects the wood density. Therefore, in timber engineering, oven-dry density or density at 12% moisture content are used. Density is the most important physical characteristic of wood because most of the mechanical properties are positively correlated to the wood density including the strength and stiffness of wood and the load-carrying capacity of the connections [46]. For this reason, increasing the density of wood is one of the important parameters in wood modification research [47]. Usually, the mean densities of the softwood and hardwoods range from approximately 400 to 650 kg/m^3 and 500 to 1200 kg/m^3 , respectively [30]. In general, wood with high density shrinks and swells more with moisture variations compared to low-density wood.

2.2.5 Mechanical properties of wood

Wood is a heterogeneous and fibrous material. The mechanical properties of wood in its three mutually perpendicular axes, namely longitudinal, radial and tangential directions, are unique. For this reason, wood is described as an orthotropic material. Figure 2.6 shows the three orthotropic axes of wood. The longitudinal direction (L) is parallel to the grain (fibres), the radial direction (R) is along the growth rings or radius of tree cross-section, and the tangential direction (T) is perpendicular to the fibres but tangential to the growth rings. However, in timber engineering for practical purposes, only two directions of the wood, parallel (longitudinal) and perpendicular (radial and tangential) to the grain, are taken into consideration. The mechanical properties of the wood are determined from laboratory tests on either small clear or defect-free (e.g. without knots) or structural timber specimens. The mechanical properties of small clear specimens are significantly higher than those of the structural timber because of the absence of natural defects (knots, sloppy grain, shakes, check etc) [30,39]. For this reason, in timber engineering, structural timber is graded by testing full-size or ‘in-grade’ specimens.

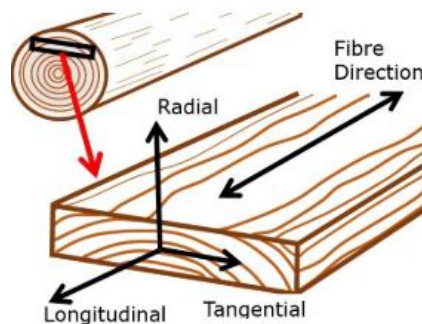


Figure 2.6- Orthotropic axes of wood [48]

2.2.5.1 Parallel to grain properties

Due to the alignment of fibres along the longitudinal axis of the tree trunk, much higher stiffness and strength values are found when testing parallel to the grain compared to the perpendicular to the grain direction. When compression load is applied in the parallel to grain direction, it shortens the wood cells in the longitudinal direction. Each cell acts as a hollow column which has lateral support from the neighbouring cells. At failure, large deformation occurs due to the crushing of internal cellular structure. When wood is in tension in the parallel to the grain direction, failure occurs due to relative slippage of cells and cell wall failure. The compression failure is ductile while tension failure is usually brittle. When loaded in shear, the cells tend to separate from each other and slide longitudinally, which ultimately results in a brittle failure [49]. In the case of bending, wood is in tension parallel to grain on one side of the neutral axis, whereas it is in compression on the other side. The bending failure is dominated by brittle tension failure. At 12% moisture content, the tensile strength parallel to

the grain of the clear specimens of softwoods varies from 70 MPa to 140 MPa, whereas compressive strength is within 30 MPa to 60 MPa [30]. For in-grade timber, the tensile strength parallel to the grain of softwoods varies from 7 MPa to 33 MPa, whereas compressive strength is within 16 MPa to 30 MPa [50]. These values for hardwoods are generally higher because of their relatively higher density compared to softwoods. The modulus of elasticity (E) values in parallel to the grain direction for both softwoods and hardwood are generally within the range of 7 to 16 GPa at 12% moisture content [30].

2.2.5.2 Perpendicular to grain properties

The mechanical properties in the perpendicular to the grain direction (radial and tangential) are much lower than the parallel to the grain direction. When a compression load is applied in the perpendicular to grain direction, it compresses the hollow cell cavities (lumen). Once the cell cavities are completely collapsed (no voids present), wood strength is greatly increased. Wood generally deforms by half of its initial thickness before cell cavities are completely collapsed [51]. In wood densification research, wood is generally compressed in the perpendicular to the grain direction (usually radially) to increase the density of the wood [52]. Compression failure perpendicular to the grain is usually ductile. Compressive strength perpendicular to the grain is about 10 % to 20% of that in the parallel to the grain direction. When wood is in tension in the perpendicular to the grain direction, splitting along the grain is commonly observed. This is because tensile stress acts perpendicular to the cell length and tends to tear out the fibres. The tensile strength in the radial and tangential direction is 5% to 8% and 3% to 5% of that in the parallel to grain direction, respectively [30]. Tension failure is usually brittle. Therefore, timber structures are designed in such a way that tension perpendicular to the grain is avoided or minimised in structural members. This situation usually occurs within the timber connections, in tapered or curved members and notched beams. Shear failure perpendicular to the grain rarely occurs because other failures such as compression perpendicular to the grain almost always occur first. However, in the case of wooden dowel type connections, wooden dowels tend to deform due to shear perpendicular to grain which is usually known as cross-grain failure [53].

2.2.6 Wood and moisture

Wood is a hygroscopic material due to its chemical composition. It exchanges moisture from the surrounding environment. The moisture exchange between the wood and surrounding environment depends on the wood moisture content, and on the RH and temperature of the surrounding air [26]. Wood moisture content is defined as the ratio of the mass of the removable water to the mass of the dry wood and is expressed as a percentage. Water is a natural constituent of all parts of a living tree. It makes up over half of the total mass of the tree. In the green condition, it is highly variable and ranges from approximately 30% to 200%.

Moisture exists in wood in two forms namely free water and bound water. Moisture present in the cell lumens is known as free water, while moisture present in the cell wall is known as bound water (held by intermolecular attraction within the cell walls). Higher moisture content in the wood negatively affects the strength, stiffness and decay resistance properties. For this reason, wood is seasoned or dried to achieve moisture content lower than the fibre saturation point (FSP). FSP is the moisture content at which free water is completely removed from the cell lumens and the cell wall is completely saturated with the bound water. For most of the species, it varies from 25% to 35% moisture content. At a moisture content above FSP, the physical and mechanical properties of the wood remain constant. In contrast to this, below FSP, these properties increase significantly with decreasing moisture content. In Europe, wood used for construction purposes has a moisture content of 12% to 18% [54]. During its service life, wood tends to maintain a moisture equilibrium with the surrounding environment. This is known as equilibrium moisture content (EMC) of the wood. It is the moisture content at which wood is neither absorbing nor losing moisture. It is an ideal situation which is usually preferred for material characterisation of wood in laboratory conditions globally.

Since moisture affects the mechanical properties of the wood and wood-based products, this must be taken into consideration when designing timber structures. The moisture content of structural members depends on the environmental conditions to which they will be subjected. In Eurocode 5 [55], this is done by defining three service classes and relevant load factors for design of timber structures. The highest strength values are obtained when the structures function in Service Class 1 (at 20° C temperature and 65% RH), and the values are least in Service Class 3 (> 20° C temperature and >85% RH).

The moisture content of wood can be determined using the oven-dry method, electrical resistance method and capacitance method. The oven-dry method is commonly used for laboratory testing due to its accuracy compared to the other two methods. It can be used for measurement of wood at any moisture content. The oven-dry method involves drying of wood at 103 ± 2 °C until it attains constant mass in accordance with EN 13183-1 [56]. The oven-dry mass of the wood specimen is calculated using the following expression:

$$\omega = \frac{m_1 - m_0}{m_0} \times 100 \quad \text{Eq. 2.2}$$

where ω is the moisture content of specimen (%), m_1 is the mass of the specimen before drying and m_0 is the mass of the oven-dried specimen.

The oven-dry method is relatively time consuming and requires small slices of timber specimens for moisture measurement. This method cannot be used for wood in service. Therefore, handheld moisture meters are commonly used at construction sites and in industry.

Handheld moisture meters work on the principles of electrical resistance and capacitance. They can measure the moisture content of wood below FSP. EN 13183-2 [57] and EN 13182-3 [58] provide the guidelines for the use and calibration settings of the electrical and capacitance-based moisture meters, respectively.

2.2.7 Shrinkage and swelling in wood due to moisture

Another influence of moisture on wood is dimensional change due to absorption/desorption of moisture. Shrinkage and swelling in the wood are linked to its dimensional stability. Wood is dimensionally stable above FSP. However, below FSP, moisture absorption leads to swelling and moisture loss or desorption causes shrinkage. In relation to swelling and shrinkage, wood is highly anisotropic. It shrinks/swells least in the longitudinal direction, whereas swelling/shrinkage is highest in the tangential direction and is about half that of the tangential direction in the radial direction. Generally, the extent of longitudinal swelling for European woods is approximately 0.4%, radial swelling is 4.3% and tangential swelling is 8.3% [37]. Swelling and shrinkage generally vary linearly with moisture content within the range 5% to 20% [46]. The swelling and shrinkage vary with wood species, wood density, latewood proportion, microscopic structure and lignin content. Wood with high lignin content shows high restraint to dimensional changes due to its hydrophobic nature of it compared to cellulose and hemicellulose (both hydrophilic) [37,42–44]. From the perspective of wood cell volume and cell wall thickness, high-density woods have proportionately less lumen volume and more cell wall volume than softwood. Thus, they tend to shrink and swell more compared to the low-density woods [45]. The swelling/shrinkage in wood is reversible due to the hygroscopic nature of wood [59]. However, wood composites (fibreboards, particle boards) and modified wood products, which are subjected to high compressive force during manufacturing, show irreversible thickness swelling, known as “springback” [37,45,46,60]. The swelling/shrinkage may result in warping, checking, splitting, which may limit its structural use. In mechanical connections, restrained swelling of wood generates internal stresses in the connected members and may lead to splitting around the connectors. In some cases, due to viscoelastic-plastic behaviour of the wood such stresses decline over time, resulting in irreversible dimensional changes. Thus, when wood returns to its original moisture content, the dimensions have shrunk, meaning the connection will no longer fit properly and has lost some of its capacity [37,46,61]. This means regular tightening of connections is required in such situations. Similarly, hardwood dowels, which are generally used in timber connections, are susceptible to high volumetric shrinkage leading to loosening of the connection and require regular maintenance [62,63]. But there is limited information available on moisture dependent swelling and shrinkage of the timber-hardwood dowel connections.

2.3 Wood modification

2.3.1 Introduction

As discussed in the previous section, wood is a biological material with several advantageous characteristics which makes it suitable for structural applications in construction. These include high strength-to-weight ratio, ease of workability, low cost and ready availability. However, it has certain undesirable characteristics such as dimensional instability, poor resistance to biological degradation (insects and fungi) and fire, low hardness and wear resistance and low resistance to ultraviolet (UV) irradiation. Thus, to increase its functionality in construction, the effect of these characteristics needs to be minimised or eliminated.

Wood modification is defined as a process to improve the physical, mechanical, or aesthetic properties of sawn timber, veneer or wood particles [64]. This process involves the action of chemical, biological, physical, or mechanical agents/parameters on the wood substrate applied individually or in combination. The finished product is usually referred to as “modified wood”. The modified wood should not release any toxic substances (such as VOCs) during its service life or at the end of disposal or during the recycling process. In short, the final product should not present any environmental hazards greater than those associated with the disposal of unmodified or normal wood [64–66]. Also, if the aim of wood modification is to increase the resistance of wood against biological attack, the mode of action should not be biocidal [66].

Wood modification can be classified into four categories based on the processes used for the production of modified wood. These processes are (1) Chemical processes, (2) Biological processes, (3) Physical processes, (4) Thermo-Hydro-Mechanical (THM) processes including Thermo-mechanical (TM) process [67].

1. **Chemical processes** – These involve two types of modifications: (1) active modification and (2) passive modification. In active modification, the hydroxyl groups (highly reactive sites) of the wood cell wall polymers (cellulose, hemicellulose and lignin) are substituted with stable and less hydrophilic groups to increase the dimensional stability of the wood. In the case of passive modification, the wood cell lumen or cell wall is impregnated with the chemicals without changing the cell wall chemistry. Although chemical modification improves durability and the dimensional stability of wood, the use of additional chemicals raises a question on the sustainability aspect of these products at the end-of-life disposal [13].
2. **Biological processes** – These involve wood modification using biological agents/metabolites. Some examples are microbial treatments using aerobic spore-forming bacteria and fungi antagonists, metabolite treatments using microbial metabolites, enzymatic grafting of functional molecules and biomimicry process [67].

These processes are mainly limited to laboratory research and may be useful in the future.

3. **Physical processes** – These involve wood modification using physical parameters such as electromagnetic radiations (UV, infrared light, microwaves), laser (CO₂ laser, UV-laser ablation) and plasma (cold and hot). These do not use any chemicals or biological agents [67–69]. These processes are still at the research and development stage and are not common in the wood industry.
4. **THM and TM processes** – These involve combined action of temperature and/or moisture and mechanical forces to produce modified wood. These processes do not involve chemicals and are based on the fact that when the wood is wet or in a thermally softened state, it can be shaped under the action of mechanical loads [64,70,71]. On the technical side, these processes are linked to softening (plasticisation) of lignin which results in the dissipation of internal stresses from the wood. Once these stresses are released, wood can be shaped into desirable forms and geometries. THM processes include a large range of modification techniques including TM modification of wood. The difference between these processes lies between conditions of modifications. The THM modified is produced by using heat, steam and mechanical compression.

TM modified wood is produced by densifying the wood under combined action of high temperature and pressure. It is relatively simple process compared to other wood modification techniques. For example, THM compression involves three different processes which are relatively time-consuming and complex, whereas chemically modified wood involves chemicals that may be costly and compromise the environmental advantages of using wood. TM modified wood has superior physical and mechanical properties than uncompressed wood and offers high potential of improving structural performance of low-density fast grown plantation wood species [72]. The following section discusses THM/TM densification processes, CW and its mechanical properties in detail.

2.3.2 Wood densification and compressed wood

Most of the mechanical properties of wood are correlated with its density. Generally, high-density woods have superior mechanical performance compared to low-density woods. The density of wood can be increased using the wood densification process. Wood densification can be defined as a process of compressing (pressing) the wood by THM/TM processes or filling (impregnation) the cell lumen and cell wall with the chemicals such as polymers/resins, or by a combination of both chemical impregnation and THM/TM processes [35,73]. The final product of wood densification is commonly known as densified wood or CW. The primary aim of the wood densification process is to decrease the void (cell wall lumen) in the wood

and improve its mechanical properties. From an engineering perspective, CW has increased density, decreased porosity and superior mechanical properties such as strength, stiffness, dimensional stability, abrasion and wear resistance compared to uncompressed wood [24]. This allows the use CW in more diverse and advanced structural applications.

The concept of wood densification is not new. Wood densification technology originally emerged at the beginning of the 20th century. The first patent for compressed wood was filed in the USA by Sears in 1900, followed by Walch and Watts in 1923, and Olesheimer in 1929, Brossman in 1931, Esselen in 1934 and Olson in 1934 [73]. However, these developments were based on the mechanical compression of the wood and did not consider the plasticization (softening) behaviour of the wood. The developed products were unstable in nature due to “shape memory effect” of CW which resulted in complete recovery of the product into its original shape (discussed in Section 2.3.4) [70]. For this reason, these products have not been adopted by the industry. The historical development of CW shows that the focus of many studies was mainly towards the elimination of the shape memory effect [35,52,74]. The solution to minimising the shape memory effect was first addressed in Europe through a German patent issued in 1923. The patent was for the complete elimination of the shape memory effect by a combined chemical treatment and thermo-mechanical process. In Europe, compressed wood was first produced and marketed under the trade name of *Lignostone* in the 1930s, and it is still in production by Rochling Group, Germany and by Lignostone®, Netherlands. *Lignostone* was produced by compressing the solid wood (at 10-15% moisture content) in the radial direction at a temperature around 140°C and pressure of up to 25 MPa for 2 hours. The described process resulted in a compressed wood with a high density (1450 kg/m³), more than twice the density of original wood (650 kg/m³). Another similar product named *Lignofol* was produced and marketed in Europe during that time. *Lignofol* was a compressed laminated wood produced by compressing resin-impregnated thin veneers under high pressure and heat. Today *Lignostone* is manufactured in a similar way to *Lignofol* using compressed laminated wood. In the USA, the USDA Forest Products Laboratory developed various products to increase the dimensional stability of densified wood materials between 1930 to 1960. A few well-known examples are *Impreg*, *Compreg* and *Staypak*. *Impreg* was an initial product developed by Seborg et al. [75]. It was produced by impregnating thin veneers with an aqueous solution of thermosetting type PF resins without any compression load. Although *Impreg* resulted in a product with high dimensional stability, the density of the product was just 10-15% higher than the wood and the product was not suitable for tooling and moulding work. *Compreg* involves densification of resin (mainly PF) impregnated veneers/solid wood before the resin is cured at a temperature and pressure of about 150°C and 6.5 MPa, respectively. *Compreg* usually has high density varying from 1000 kg/m³ to 1400

kg/m³ with a low level of shape memory effect. It has superior mechanical properties to normal wood and *Impreg*. It can be used in the manufacturing of connector plates, drilling jigs, fan blades, bobbins, tool handles, nuts and bolts, musical cases, electrical insulators and various novelties [26,76]. Some companies producing *Compreg* products in Europe are Permali Deho, Dehonit and Segliwa GmbH. *Staypak* was another product developed by Seborg et al. [76]. It was produced by compressing the untreated solid timber/veneer at a temperature above 150°C and pressure between 10 to 18 MPa. The density of *Staypak* varies from 1250 to 1400 kg/m³. Although the *Staypak* product has higher tensile and bending strength compared to *Compreg*, it exhibits a high level of shape memory effect. It can be used in applications where high strength is required but not suitable for applications where high dimensional stability is needed [26].

Kutnar et al. [35,52] described the historical development of wood densification techniques up to 2014. They pointed out that the shape memory effect is one of the main challenges associated with densified wood. The permanent fixation of compressive deformation is still a topic of research efforts. They also highlighted that the durability, strength and load-bearing capacity of the densified wood can be further improved using varying combinations of processing parameters such as temperature, pressure and steam. More recently (2018), Song et al. [74] developed densified wood by means of a chemical process followed by thermo-mechanical densification. The chemical process involved partial removal of lignin/hemicellulose by immersing the wood specimens in a boiling aqueous solution of sodium hydroxide (NaOH) and sodium sulfite (Na₂SO₃), followed by immersion in deionized water to remove the chemicals. Specimens were then compressed at 100 °C temperature under a pressure of approximately 5 MPa for a period of 1 day. The density of the final product was approximately 1300 kg/m³, which was about 200% higher than the uncompressed wood (430 kg/m³). The wood modified in this way had significantly superior mechanical properties to uncompressed wood, even exceeding those of many commonly used structural materials such as plastic, alloy and steel. The tensile strength of the densified wood was about 587 MPa, which is about 11.5 times higher than the uncompressed wood. The compressive strength was about 5.5 times and 33-52 times higher than the uncompressed wood in the parallel to the grain and perpendicular the grain directions, respectively. It should be noted here that previous studies [35,52] showed the use of relatively high temperature (120°C - 160°C) in the densification process compared to this process (100 °C). This may be due to the partial removal of lignin (gives stiffness of cell wall) which lowers the plasticization (softening) temperature of the wood.

Table 2.1 summarises the development of wood densification processes in chronological order.

Table 2.1- Development of wood densification processes in chronological order

Year	Researcher/ Company/ Institution	Temperature range (°C)	Pressure (MPa)	Final product/ type of wood densification process
1900	Sears	-	-	Mechanically densified wood
1923	Walch and Watts	-	-	
1929	Olesheimer	-	-	
1931	Brossmen	-	-	
1934	Esselen	-	-	
1934	Olson	-	-	
1923	Deutsche Holzveredelung Schmeing GmbH & Co. KG			TM compressed laminated wood
1930s	Rochling Group Germany and Lignostone® the Netherlands	Up to 140	Up to 25 MPa	TM compressed resin impregnated solid wood (Lignostone) and laminated wood (Lignofol)
	Jicwood Division, Airscrew Company Limited, England			TM compressed resin impregnated laminated wood (Jicwood)
	F. Hills and Sons Limited and Jablo Propellers Limited, England			TM compressed resin impregnated laminated wood (Jablo)
	Hordern Richmond, England			TM compressed laminated wood (Hydulignum)
1954	Permal Deho Limited, England			TM compressed resin impregnated laminated wood (Permatred)
1941	Stamm and Seborg	150	7-8 MPa	TM compressed resin impregnated solid wood/laminated wood (Compreg)
1945	Seborg et al.	150-180	10-17 MPa	TM compressed wood (Staypak)
1990s	Kyoto and Gifu University and Swiss Federal Institute of Technology	Up to 200	Up to 13 MPa	THM densified wood
2004	Blomberg and Persson	No heating	up to 140 MPa	Semi-static compression (Calignum)
2005	Kamke and Sizemore	160-225	0.65-4 MPa	Viscoelastic-thermal- compression (VTC) wood
2018	Song et al.	100	5 MPa	Chemical-thermal- mechanical densification of wood

2.3.3 Types and mechanism of wood densification

Wood can be densified or compressed using surface and bulk densification techniques. Surface densification is used to compress/densify the wood up to a few millimetres beneath the surface, whereas bulk densification is used to compress the whole volume of the wood specimen. From a utility perspective, surface densified wood has high abrasion resistance and hardness and can be used in applications where the surface is exposed such as tabletops and flooring [77]. In contrary to this, bulk densified wood not only includes properties of surface densified wood but also offers superior strength and stiffness properties compared to normal wood. Studies [62,78–80] have shown that bulk densified wood can be used as a connector material in timber connections because of its superior mechanical performance. Therefore, in this study, the focus is given on the bulk densification of wood without using any chemicals.

Today, bulk densification using THM/TM processes is an emerging area of research due to its ability to increase the density and mechanical of properties of wood without posing any additional risk on the end of life disposal of the product [71,81]. Blomberg [82] used another method of bulk densification using semi-isostatic pressure technique. However, this technique is not as common as THM/TM processes in wood science and technology field, and it is not discussed in the current study.

Wood can be compressed using an open, closed system or semi-open system. In the case of an open system, densification is carried out at atmospheric pressure at about 130 °C temperature and moisture content of wood specimen is up to 13% [83,84]. TM densification is usually carried out in an open system. In a closed system, densification is carried out in a closed multi-chamber device. This system offers precise control of densification parameters such as temperature, pressure, and moisture. Navi et al. [70,71] presented a detailed specification of the closed system. The semi-open system is a combination of an open and closed system. The process is carried out in an integrated pressure vessel. In this system, the temperature varies from 175 °C to 200 °C. The pressure in the chamber is applied through a combination of pressurised gas and atmospheric pressure. From a utility perspective, closed system can only be used for small wood specimens up to 150 mm x 40 mm x 40 mm [71]. However, an open system and semi-open system can be used for manufacturing of larger specimens compared to a closed system. Densified wood developed through closed and semi-open systems shows a relatively lower level of springback compared to one produced using an open system [71,83]. This is because closed and semi-open systems offer exact control of process parameters when compared to open system [71]. In the last decade, several research programmes were focused on the optimisation of the manufacturing process of CW by means of varying process parameters (temperature, pressure level, steam and heat) to improve its physical and mechanical properties [85–89].

Irrespective of densification device/system, the mechanism of wood densification can be broken down into four steps; (a) softening or plasticization of the cell wall, (b) compression in the softened state, (c) setting and cooling in the dry state, (d) fixation in the deformed state. Softening is a primary process in the THM/TM densification of wood. The softening mechanism of wood can be understood by considering the behaviour of its cell wall constituents. Due to the viscoelastic nature of wood, its mechanical properties are dependent on time, temperature and moisture. Wood has glassy behaviour at low moisture content and temperature, whereas it exhibits rubbery behaviour at high temperature and high moisture content. The temperature at which transition from glassy behaviour to rubbery behaviour occurs is known as the glass transition temperature (T_g). The T_g of lignin is an important factor in the wood densification process. Figure 2.7 shows the T_g of the wood constituent as a function of moisture content. Temperatures higher than T_g promote polymer mobility and permit rearrangement of the molecules. During the densification process, when the temperature of lignin is above T_g , it causes softening of amorphous regions of the cell wall. The densification processes temperature usually ranges between 120°C - 160°C to avoid the microscopic fractures [35]. Temperature beyond this range negatively affects the mechanical properties due to thermal degradation of cell wall constituents [90]. In some cases, wood is soaked in boiling water to soften the cell wall constituents [18].

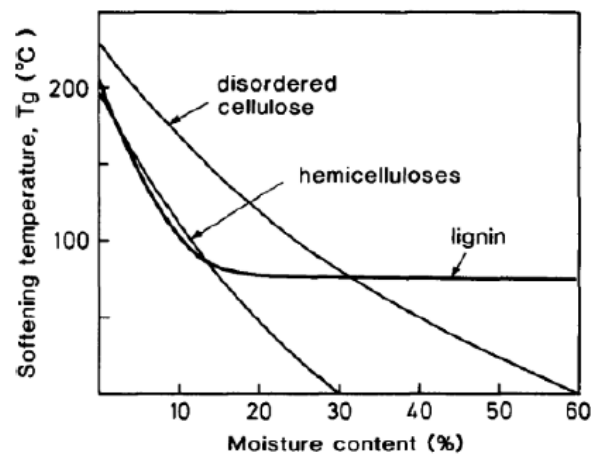


Figure 2.7- Schematic picture of glass transition temperature for lignin, hemicellulose and amorphous cellulose as a function of moisture content [91]

Once the wood is softened, it can be compressed by mechanical load without causing any significant damage to the cell wall up to a certain limit (maximum of approximately 1500 kg/m³). Wood can be compressed in one or more directions. However, it is mainly carried out along one of the orthotropic axes. Compression in the longitudinal direction results in buckling deformation which leads to severe damage with very low or no densification [92]. Therefore, wood is usually compressed in the perpendicular to the grain or transverse directions.

Densifying along the tangential direction, the latewood of the annual rings spread into the earlywood and forms waves or a zigzag pattern [52]. In contrast to this, compression in the radial direction flattens the cells without any noticeable damage at the macroscopic level [35,52,81]. For this reason, densification is usually carried out in a radial direction. Figure 2.8 shows the micro and macroscopic structure of radially compressed Douglas fir (*Pseudotsuga menziesii*). The level of compression achieved due to the densification process is quantified in terms of percentage reduction in the compressed dimension and is commonly referred to as the compression ratio (CR) or compression set. It can be calculated using Eq. 2.3. The level of densification depends on various parameters such as the initial density of wood, percentage of latewood material, ray volume and loading direction [93].

$$CR (\%) = \frac{t_0 - t_1}{t_0} \times 100 \quad \text{Eq. 2.3}$$

where t_0 and t_1 are the thicknesses in the direction of compression at ambient conditions before and after the densification process, respectively.

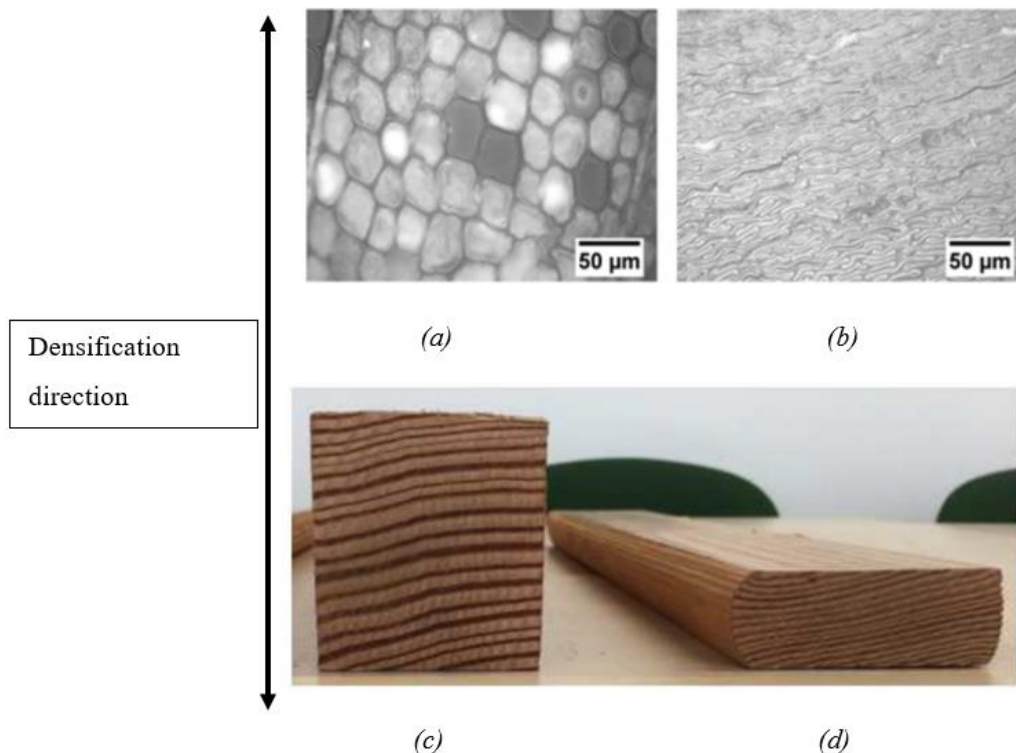


Figure 2.8- Radially compressed Douglas Fir (*Pseudotsuga menziesii*), (a) microscopic structure before densification, (b) microscopic structure after densification, (c) macroscopic structure before densification, (d) macroscopic structure after densification [14]

Once compressed, the specimen is cooled while under pressure to avoid immediate springback. Immediate springback occurs because lignin remains in a softened condition at

high temperature and is less constrained to dimensional changes. The final stage of the densification process is a post-treatment/fixation treatment. This is required to fix the deformation by means of thermomechanical parameters such as moisture, steam, heat, high pressure and temperature [35]. In applications where springback is desirable, post-treatment is not required. Some successful examples of CW without post-treatment are strengthening of glulam beams and maintaining tightness within timber-timber connections [23,79,94–96].

2.3.4 Springback of compressed wood

CW has a rheological memory. The effect of this rheological memory causes swelling in the direction of densification when compressed wood is subjected to moisture/heat or a combination of both [90]. This rheological memory of compressed wood is often referred to as the “springback” or “shape memory effect” or “compression set recovery” [52,71,77,83,97–99]. Springback (R) can be quantified in terms of percentage using the following expression [100]:

$$R = \frac{t_R - t_c}{t_o - t_c} \times 100 \quad \text{Eq. 2.4}$$

where t_o and t_c are the oven-dry thickness before and after compression, respectively. t_R is the thickness after the recovery test.

During service life, CW can exhibit both reversible and irreversible swelling [14,18,35,82]. Reversible swelling occurs due to the hygroscopic nature of the wood and irreversible swelling occurs due to springback behaviour which causes a partial or full return of the CW to its original dimensions. Inoue et al. [101] reported that CW recovers 90% of its original shape at the temperature which was used during the compression process. Studies have also reported that continuous moisture absorption results in an increase in the thickness of CW [60,102,103]. This is because moisture acts as a plasticizing agent and helps in relieving the stresses that were developed during the compression process. Generally, wood with the highest CR exhibits higher springback compared to that with lower CR [82,104]. The type of process used for densification also affects the springback. TM compressed wood has a higher amount of springback (approximately 4.5-5 times higher) compared to THM densified wood [84].

In several studies, springback has been reported as an undesirable characteristic because it causes the compressed material to go back to its original shape when exposed to weathering (moisture/heat) [52,76,77,100,105–112]. Only a few wood densification techniques have been used at an industrial scale and one of the reasons for this is the unstable nature of compressed wood material due to springback behaviour [113]. There have been several studies on methods to minimise the springback behaviour of compressed wood [71,83,97,99,104]. However, the

springback behaviour of compressed wood could be utilised as a beneficial trait in applications such as dowel-type timber connections where the increased tightness in the connection caused by springback is desirable.

2.3.5 Mechanical properties of compressed wood

The literature shows that the focus of CW research has been on improving not only the dimensional stability but also the physical and mechanical properties of wood. Navi and Girardet [84] radially densified small specimens (40 mm x 30 mm x 30 mm) of Beech (*Fagus sylvatica*), Spruce (*Picea abies*) and Maritime Pine (*Pinus pinaster*) using a THM process. The densification process resulted in mean density increases of approximately 90%, 210% and 164% for Beech, Spruce and Maritime pine compared to uncompressed wood specimens of the corresponding species. This shows that the density increment is a species-dependent property, and different species respond differently to the densification process. They also demonstrated significant improvements in some mechanical properties by evaluating the hardness and shear strength of the densified specimens. The mean Brinell surface hardness values in a radial plane for compressed Beech, Spruce and Maritime pine were approximately 4, 7.5 and 5.3 times higher than the corresponding uncompressed wood specimens, respectively. The mean Brinell hardness values in the tangential plane for Beech, Spruce and Maritime pine were approximately 5.3, 7.0 and 4.3 times higher than the corresponding uncompressed wood specimens. The shear strength values on longitudinal-radial (LR) plane for Spruce and Maritime pine were 13.8 and 11 times higher than the corresponding uncompressed wood specimens.

The degree of densification or the CR is also a very important factor. Yoshihara and Tsunematsu [114] compared the Young's modulus, bending and shear properties of THM compressed Sitka Spruce (*Picea sitchensis* Carr.) with uncompressed specimens. The specimens were radially compressed to four different levels of CRs: 33%, 50 %, 60% and 67%. They found a continuous increase in the density as the CR increased up to 60%. However, the density of specimens with 67% CR was almost the same as the specimen with 60% CR. This was probably due to closing of all the voids (cell lumens) at approximately 60% CR. The densities of specimens with 33%, 50%, 60% and 67% were 25%, 46%, 67% and 67% higher, respectively, than the uncompressed specimen (480 kg/m³). Young's modulus (E_L) was also shown to increase with increasing CRs irrespective of the orientation of specimens (radial or tangential) relative to the loading direction. The E_L values of CW with CRs of 33%, 50%, 60% and 67% were approximately 1.8, 1.9, 2.1 and 2.3 times higher than the uncompressed wood specimens, respectively. Interestingly, the bending strength was highest for 33% CR compared to specimens with greater CRs. It was 1.3 times higher than the uncompressed wood specimens while specimens with 50 %, 60% and 67% CRs showed lower

bending strength despite higher density compared to the specimens with a CR of 33%. The study did not comment on this difference. However, it should be noted that this study used a higher temperature (180°C) compared to the typical temperature range (120-160°C) used in THM densification. A study from Navi and Heger [97] highlighted processing timber at a temperature of 180°C or higher could lead to macroscopic cracks and a reduction in mechanical properties. Further, Yoshihara and Tsunematsu [114] indicated that CR has little influence on the shear strength properties in both longitudinal-tangential (LT) and longitudinal-radial (LR) planes. While this study did not show any direct correlation between the CR and the bending/shear strength properties of the specimens, other studies have shown positive correlations between mechanical properties and CR.

Kamke [115] and Kutnar et al. [116] investigated the performance of densified timber produced from a viscoelastic thermal compression (VTC) method which is an example of semi-open system [117] discussed previously. Kamke [115] demonstrated that the VTC process performed on densified Radiata Pine (*Pinus radiata*) resulted in density increases of 78%, 159% and 170% for 3 mm veneer and 4 mm and 8 mm sawn wood specimens, respectively, compared to uncompressed specimens. This resulted in an increase in Young's modulus (E_L) values of densified 3 mm veneer and 4 mm and 8 mm sawn wood specimens of 116%, 174% and 152%, respectively. Kutnar et al. [116] carried out study on VTC densified Hybrid Poplar. They prepared specimens of three different degrees of densifications: 63%, 98% and 132% and the results showed that bending strength and Young's modulus of VTC densified specimens were approximately proportional to the increase in the density. The bending strength of specimens with 63%, 98% and 132% densification levels showed increases of approximately 32%, 66% and 102% when compared to control specimens, respectively. Similarly, the Young's modulus of specimens with 63%, 98% and 132% densification levels showed increases of approximately 37%, 84% and 129%, respectively, when compared to control specimens.

Anshari et al. [102] evaluated the mechanical properties of TM compressed Japanese Cedar (*Cryptomeria japonica*) based on the results of compression and shear tests. Specimens were compressed to four CRs of 33%, 50%, 67% and 70% and the densification process resulted in mean density increases of approximately 25%, 75%, 175% and 261%, respectively. Both Young's and shear moduli values in all three directions (L , R and T) were shown to increase significantly with increasing CRs. It should be noted that Yoshihara and Tsunematsu [114] found an insignificant difference in the density and mechanical properties of specimens with 60% and 67% CR. However, Yoshihara and Tsunematsu [114] did not observe a significant increase in density between the 60% and 67% CR, whereas in this study by Anshari et al. [102], the density of specimens with 70% CR was approximately 44% higher than the

specimens with 67% CR. The highlights that the level of compression and improvement in material properties can be species dependent and is often influenced by various factors such as the initial density, percentage of latewood and ray volume etc. [35,93].

It has also been shown that the temperature at which densification takes place can be a significant factor on the final material properties. Tanaka et al. [118] investigated the bending strength properties of TM compressed Japanese Cedar (Sugi) wood which was radially compressed to three different levels of CRs: 33%, 50 % and 70%. For this particular study, the bending test results show a continuous increase in the bending strength and Young's modulus with increasing CRs. The bending strength results of specimens in this study were found to contradict the findings of Yoshihara and Tsunematsu [114], where specimens with 33% CR had the highest bending strength. It should be noted that the densification techniques and species of this study are different than those used by Yoshihara and Tsunematsu [114], however, the temperature used in this study was 130°C, which is significantly lower than the temperature (180°C) used by Yoshihara and Tsunematsu [114]. This indicates that densification temperature may be important parameter that affects strength properties of the CW. Higher temperature and moisture content with long processing time significantly damages wood constituents and results in a material with lower mechanical properties [71].

While there has been many studies examining the material properties of CW manufactured from different species and produced under many different wood modification methods and CRs, it is important to examine and compare the current industry standard hardwood materials available. This is particularly relevant for the potential use of CW material as connector materials in timber connections. Jung et al. [25] compared mechanical properties of TM radially compressed Japanese Cedar with high-density Maple wood in terms of bending strength, Young's modulus and shear strength. The bending strength of CW specimens with 70% CR was approximately 1.6 and 1.4 times higher than the Maple specimens in flatwise and edgewise loading directions, respectively. The Young's modulus of CW specimens with 70% CR was approximately 1.9 times higher than the Maple specimens irrespective of the loading directions. The shear strength of the CW on the LR plane was 1.3 times higher than the corresponding value for Maple wood, whereas it was 2.3 times lower in LT plane. Furthermore, Jung et al. [25] also compared the embedment strength of CW with uncompressed specimens. The embedment strength was shown to increase with increasing CRs and density. The embedment strength of CW specimen with 66% CR was 1.8 and 3.1 times higher than the specimens with 50% CR and uncompressed wood, respectively. Finally, they compared the ductility ratio of CW specimens with steel pins and Maple dowels in a double shear timber-timber connection. The ductility ratio of the CW was greater than that of the Maple dowels and relatively close to the steel pin. This indicated the potential of CW

connectors as an alternative to hardwood dowels and steel pins in timber connections. The study also highlighted that the insertion of CW dowels with the annual rings of the dowel perpendicular to the loading direction results in higher ductility compared to insertion parallel to the loading direction.

All the above studies were carried out on small clear specimens of CW and there are technical difficulties that must be overcome to manufacture large scale CW elements. Adlam [72] investigated the mechanical properties of TM radially compressed Slash Pine (*Pinus elliotti*) of structural size timber. They produced CW specimens with nominal CRs of 13% and 22%. The compressed specimens were 1240 mm long with a final thickness of 35 mm. The mean Young's modulus of specimens with 13% and 22% CRs were similar to the uncompressed wood specimens irrespective of loading directions (flatwise or edgewise). On the other hand, the bending strength of specimens with 13% CR was only 8.2% higher than the uncompressed wood specimens. In the case of specimens with 22% CR, the bending strength was 3.1% lower than the uncompressed wood specimens. The difference in Young's modulus and bending strength values were relatively insignificant when compared to the uncompressed wood specimens. The study indicated that achieving a high level of CR with structural size timber is a complex process due to larger variations within the specimens compared to small clear specimens. Also, optimisation of process parameters such as pressure and temperature for structural size specimens is relatively difficult compared to small clear specimens.

A range of wood densification techniques is available that can be used to improve physical and mechanical properties. Today, the wood industry caters its demand from plantation grown timber. Such timbers have relatively lower timber quality and mechanical performance compared to slow-grown timbers. Wood densification is a promising solution to enhance the functionality of such timbers for high-end structural usage. Among all reviewed wood densification techniques, TM densification/compression in a radial direction is a relatively simple and non-chemical way of increasing the density, strength, and stiffness of the wood. The TM compression significantly improves the density (up to 1500 kg/m³) of the wood. A large amount of information is available on basic mechanical properties (Young's modulus, bending strength and shear strength) of CW. However, only a limited number of studies looked at possibilities of using CW as a connector material in timber connections. The literature is relatively scarce on mechanical properties of CW connectors such as embedment strength, yield moment capacity and cross-grain shear strength.

Table 2.2 summarises strength and stiffness properties of uncompressed wood and CW extracted from literature.

Table 2.2- Summary of mechanical properties of compressed wood from literature

Reference	Densification process	Species	CR (%)	Density (kg/m ³)	Shear strength (MPa)							
					S_{LR}							
Navi and Girardet 2000 [84]	THM	Beech	0	670	-							
			-	1270	-							
		Spruce	0	420	8							
			68	1300	110							
		Maritime Pine	0	500	10							
			67	1320	110							
Yoshihara and Tsunematsu 2007 [114]	THM	Sitka Spruce	CR (%)	Density (kg/m ³)	Young's modulus (GPa) – bending test		Bending strength (MPa)		Shear modulus (GPa)		Shear strength (MPa)	
					(E_L) (Flatwise)	(E_L) (Edgewise)	Flatwise	Edgewise	G_{LT}	G_{LR}	S_{LT}	S_{LR}
			0	458	14	16	90	90	1	1.1	23	18
			60	817	30	28	96	80	0.6	0.6	25	18
			67	800	31	30	115	98	0.6	0.6	24	17
Kamke 2006 [115]	VTC	Radiata Pine	CR (%)	Density (kg/m ³)	Young's modulus (GPa) (bending- loading direction not known)							
					(E_L)							
			0	390	7.7							
			63	1010	21.2							
			0	385	5.7							
64	1040	14.4										

Kutnar et al. 2008 [116]	VTC	Hybrid Poplar	CR (%)	Density (kg/m ³)	Young's modulus (GPa) (bending- loading direction not known)			Bending strength (MPa)				
					<i>E_L</i>							
					0	331	8.7			76		
					63	552	12			101		
			98	676	16			126				
Anshari et al. 2011 [102]	TM	Japanese cedar	CR (%)	Density (kg/m ³)	Young's modulus (MPa)- compression test			Shear modulus (MPa)				
					<i>E_L</i>	<i>E_R</i>	<i>E_T</i>	G _{LR}	G _{LT}	G _{TR}		
					0	322	8017	753	275	972	784	31
					67	886	28415	523	2347	208	1208	256
			70	1162	32858	3111	5061	1590	5717	878		
Tanaka et al. 2010 [118]	TM	Japanese cedar	CR (%)	Density (kg/m ³)	Young's modulus (GPa) – bending test		Bending strength (MPa)		Shear strength (MPa)			
					<i>E_L</i> (Flatwise)	<i>E_L</i> (Edgewise)	Flatwise	Edgewise	<i>S_{LT}</i>	<i>S_{LR}</i>		
					0	370	5	5.5	55	60	7	7
					33	460	7.5	8	85	90	8	12
					70	1200	14	16.5	175	170	10	26
Jung et al. 2008 [25]	TM	Japanese cedar	CR (%)	Density (kg/m ³)	Bending strength (MPa)		Shear strength (MPa)		Embedment strength (MPa)			
					Flatwise	Edgewise	<i>S_{LT}</i>	<i>S_{LR}</i>	<i>f_h</i>			
					0	330	85.9	87.9	6.9	7.7	28.6	
					66	990	-	-	-	-	125.8	
					70	1000	244.6	209.1	9.5	25.5	-	

2.4 Timber connections in frame construction

2.4.1 Introduction

Connections are arguably one of the most important components of any timber structure and at the same time, the weakest link in the whole structure [119,120]. The main function of a connection is to transfer the load from one member to another and maintain the integrity of the system in the event of overloading [121]. Connections have to be designed to resist at least the design capacity of the members and elements that they join. They provide a continuous load path and transfer gravity, wind and seismic loads to the foundation. In timber structures, the cross-sectional area of timber members is often determined by the strength of the section remaining after notches, drilling holes for dowels or bolts, or by the spacing requirement of the connectors rather than load carrying capacity of the timber. Therefore, they are considered a critical aspect of the design.

Timber connections have been developed from ancient times to the modern era in parallel with design developments, improvements in processing and fabrication technology [122]. They are generally classified as carpentry timber connections, metallic connections and glued connections. Each connection type has merits and demerits when it comes to its structural performance and industrial application. Figure 2.9 shows connection efficiency (ratio of connection strength/member strength) of glued, metallic and carpentry connections. A high connection efficiency can be achieved using glues or synthetic adhesives, but it compromises the sustainability aspect of using timber. From the utility perspective, connections with glues must be performed in a controlled environment due to machinery requirement and associated health and safety measures [13,123]. This largely limits their usage for on-site assembly such as heavy frame construction. On the other hand, mechanical connections have 20-30% connection efficiency [13], but they can be easily used on-site without handheld tools and machine. The mechanical connections are largely used in modern mass timber structures. When it comes to carpentry connection types, they have lower connection efficiency but better adaptability to swelling and shrinkage movement. In the last century, the use of these had been curtailed in favour of quicker, efficient and profitable connection designs using mechanical fasteners [124]. Another issue that impeded the mass application of these techniques was complex geometries and lack of codified design guidelines of using these connections in modern timber buildings. However, in the last two decades, there has been revived interest in the use of these connections due to increasing adoption of computer-aided manufacturing (CAM), CNC (Computerised Numerical Control) and robotic fabrication technologies in the wood industry. Almost any imaginary shape and geometry can be transformed into reality with high precision, customisation and faster mass production [10,125].

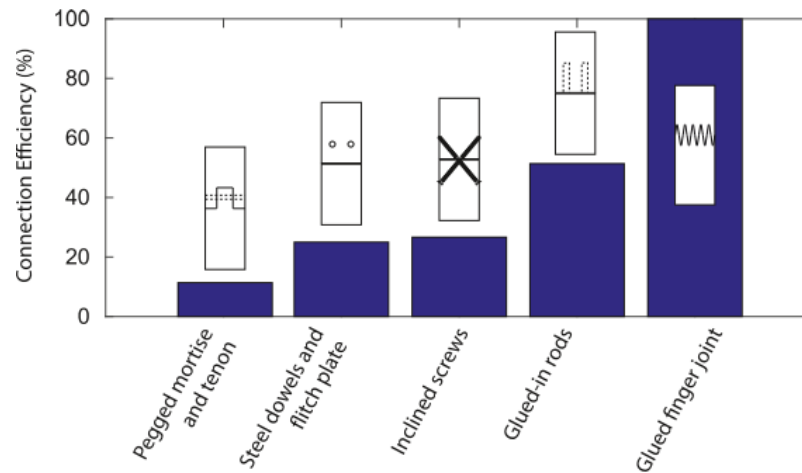


Figure 2.9- Efficiency of connections between 100 mm by 200 mm timber members transmitting a tensile axial force [13]

Generally, structural timber connections are categorised as pinned connections, moment connections or semi-rigid connections. Pinned connections are free to rotate under load and are assumed to resist shear forces. These connections can be seen in traditional carpentry timber joinery. In contrast to this, moment connections are restrained against rotation and are capable of resisting both shear forces and moments. They are also referred to as fixed or rigid connections. Moment connections are common in steel and concrete structures. Semi-rigid connections are categorised somewhere in between pinned and moment connections. They are capable of resisting a modest moment. When it comes to timber moment connections, they are often semi-rigid type.

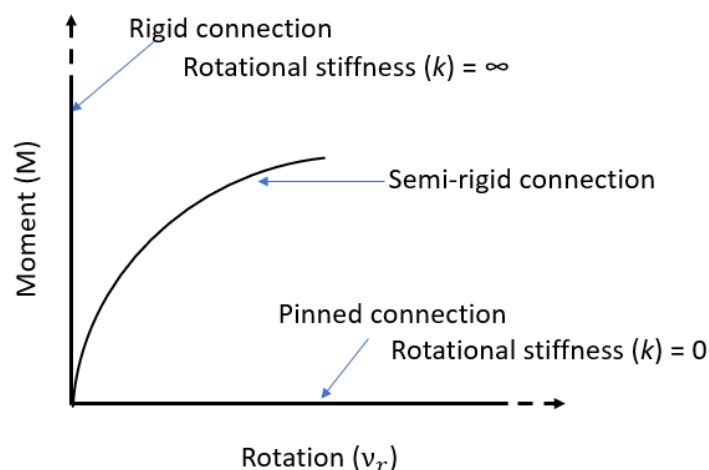


Figure 2.10- Moment-rotation behaviour

Connections using synthetic adhesives is a vast area of research and beyond the scope of this current thesis. In this section, the focus is on carpentry and metallic timber connections suitable for heavy timber framing. Heavy timber framing refers to the structural use of large timber sections within which structural members are relatively stiffer compared to the

connections [126]. This framing technique is often used in braced column and beam structures. It differs from the more common stick framing where many timber members with smaller sections are joined together frequently. Figure 2.11 shows the scheme of the literature search for this section. In both carpentry and mechanical connection types, past and recent developments are discussed for fundamental connection types; (a) beam-beam connections and (b) beam-column connections.

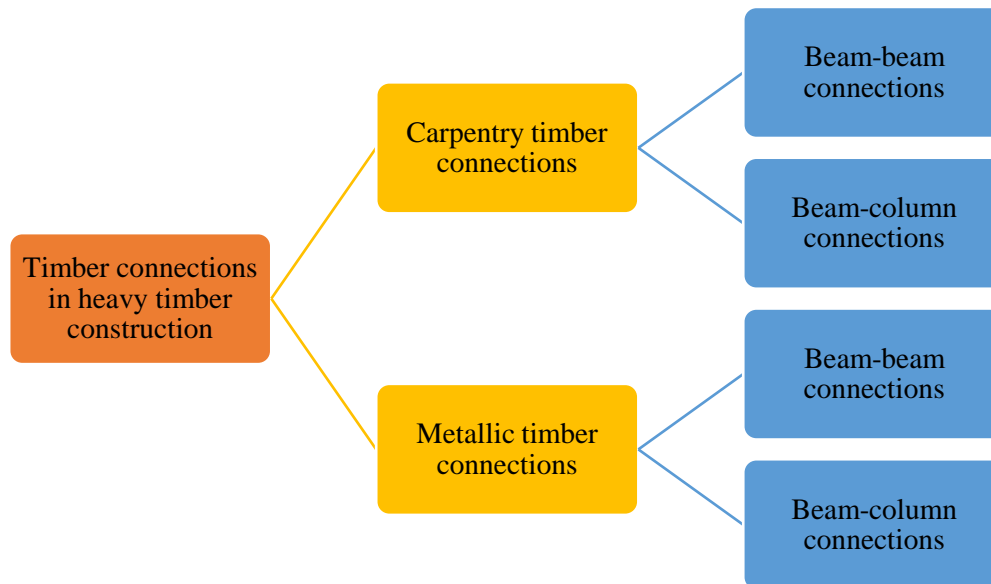


Figure 2.11- Scheme of review on the timber-timber connections

2.4.2 Carpentry connections

Traditional timber connections are often referred to as carpentry type joints. These joints are contact type where forces are transferred in compression/bearing by contact and/or friction between connected members [127]. These connections have evolved based on experiences of carpenters and artisans over generations through trial and error processes. The design configuration and assembly of these connections involve a high level of craftsmanship and a good understanding of the structural behaviour of wood elements. These joints are usually adhesive-free, non-metallic, sustainable, relying on contact only and can be easily disassembled and reconfigured for replacement or repair. Some of these connections have simple geometries such as lap joints or butt joints and some are complex such as interlocking joints. Numerous examples of carpentry connections can be seen in historic buildings that are standing for multiple centuries and have endured severe loading situations. The production methods, designs and choice of the materials (wood species) in these connections are based on the culture of local area and varies with one country to another. Erman [128] reported more than 1000 configurations and variation of carpentry connection types. He presented extensive information on the geometry of historical connections. In another study, Karel et al. [129] presented a taxonomical classification of these connections based on shape, geometry, layout

and load transfer mechanism of these connections. Despite the several configurations of carpentry joints, they can all be classified based on the basic forms of joints such as lap joint, scarf joint, spline joint, step joint, mortise and tenon joint [37].

2.4.2.1 Carpentry type beam-beam connections

Carpentry type beam-beam connections can be commonly seen in historical timber structures. They were used to increase the length of sawn solid timber to meet the structural requirement. Currently, the use of such connections is limited to repairing/ retrofitting of damaged/decayed parts in old structures. Among other carpentry type connections, scarf and spline joints are suitable for heavy timber structures. Figure 2.12 presents an example of the splayed scarf joint with locating keys and dowels.



Figure 2.12- Splayed scarf joint with locating keys and dowels [130]

Hirst et al. [131] analysed the structural performance of four types of carpentry type scarf joints (Figure 2.13) in bending. All the joints were tested in both pure vertical bending (edgewise) and pure lateral bending (flatwise) using a four-point bending setup, and the results were compared with solid timber beam. The laterally loaded configuration of the side halved & bridled joint (Figure 2.13b) showed the highest joint stiffness among all connection types irrespective of the loading direction. This was attributed to a greater lever arm distance between the peg and centroid of the joint. The superior performance of this joint can be attributed to the contribution of pegs in the load transfer mechanism. All the joints displayed considerable ductility. Connection efficiency vary from 0.05 to 0.28 when compared to a solid timber beam. Due to lower efficiency of these connections, they may not be suitable for mass timber structures.

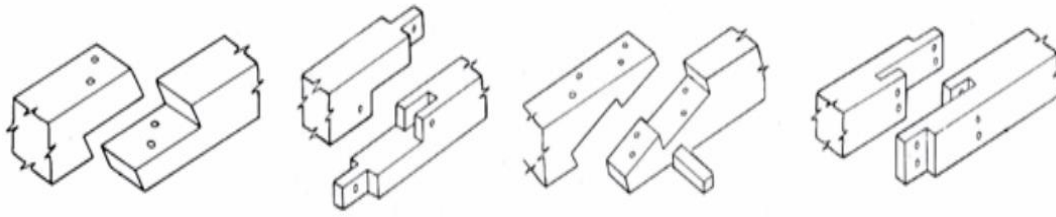


Figure 2.13- Scarf joints, (a) halved scarf with two pegs, (b) side-halved & bridled with two pegs, (c) stop-splayed & tabled scarf with key and four pegs, and (d) face-halved and bladed scarf with four pegs [131]

Arciszewska-Kdezior et al. [132,133] compared the mechanical behaviour of lapped scarf joints with a solid beam tested using a three-point bending test set up. These joints were designed with inclined contact faces, varying number of wooden dowels (2 or 4) and lap width (half or 3/8 of beam width) (see Figure 2.14). Results showed that a lapped scarf joint with oblique contact faces and wooden dowels attains between 65% and 75% strength of the solid beam. However, the linear stiffnesses of the jointed beam were not significantly affected by the joint configuration and were between 91% to 94% of the stiffness of the solid beam. All joints showed a brittle response once the maximum load was attained. Furthermore, lap width does not influence the performance of the joints, thus manufacturing a half lap configuration is relatively easier compared to one with 3/8 width of the beam.

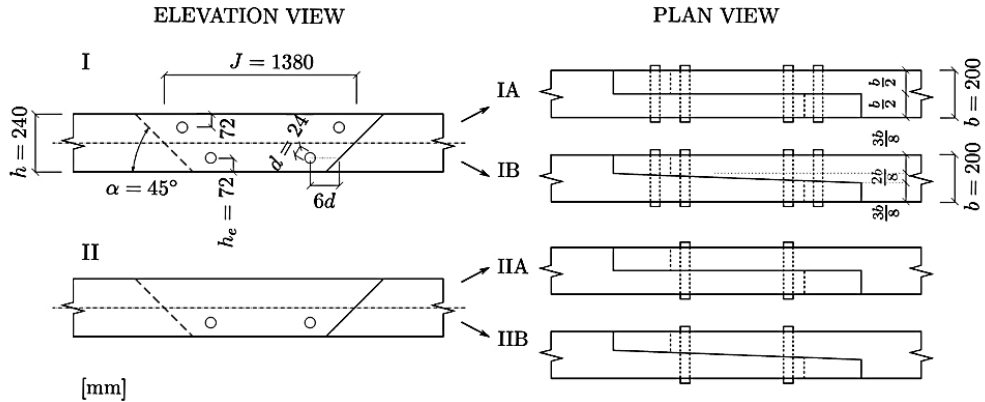


Figure 2.14- Lapped Scarf Joint -Four dowel and two dowel joints [132]

Fajman et al. [134] investigated the effect of inclination of face angle on the load-carrying capacity of the beam-beam scarf joint. The joints were manufactured using two types of face inclination angles (45° and 90°) and a constant number of dowels (4) as shown in Figure 2.15. Results showed that the joint with inclined faces (45°) increases the load-bearing capacity up to 50% against a joint with perpendicular faces (90°).

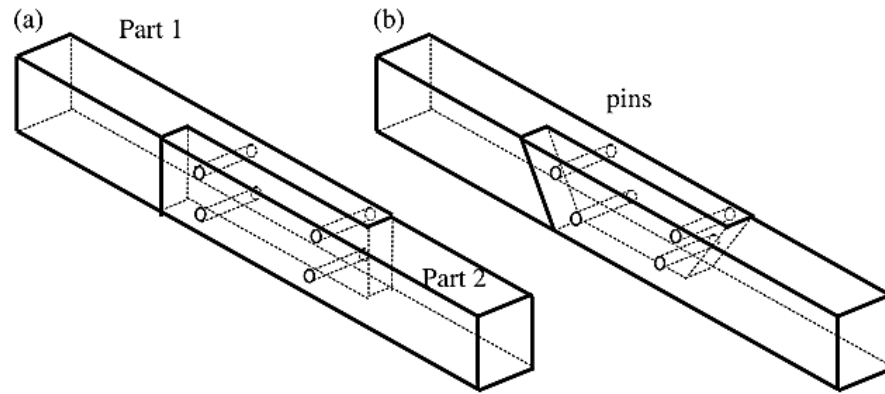


Figure 2.15- Scarf joint, (a) halved joint with pins, and (b) oblique scarf joint with pins[134]

Despite various forms of carpentry connections, the literature only shows a limited number of research articles on beam-beam connections suitable for heavy timber structures. Several configurations of scarf joint with pegs are found to be one of the most commonly used connection types. However, these connections are usually designed with solid timber members and may not be suitable with mass timber structures due to their poor moment resistance and limited strength capacities of the pegs. Further, investigation may be needed to check the suitability of these connections with mass timber products.

2.4.2.2 Carpentry type beam-column connections

The mortise and tenon joint is one of the most common beam-column connections in traditional timber frame structures (e.g. portal frames). Usually, a frame comprises of two columns (mortises) and one beam (tenon) with diagonal braces. A mortise and tenon joint typically transfers compressive load within a frame but also have tensile capacity provided by pegs. The tension capacity of these joints is limited by the double shear strength of the pegs if the proper detailing of the joint is ensured. Configurations of these joints vary from one country to another but all connections include a tenon, a mortise and a number of pegs driven through both the mortise and tenon [135]. Pegs are generally made from high-density hardwood species such as oak, maple, locust and red oak [135,136]. Brungraber et al.[137] studied the structural performance of mortise and tenon joints as an individual joint and in a full-scale frame. He reported that the mortises and dowels failed prior to the tenon and also highlighted that increasing the diameter of dowels is the most effective way to increase the strength and stiffness of the joint. Schmidt and Mackay [138] carried out material tests on pegs made of various species such as Red Oak, White Oak, Locus, Birch, Maple and Ash. They concluded that the peg bending and shear strength are positively affected the density of the wood material. A negative correlation was found between average peg shear strength and diameter, and also between peg shear strength and shear span. Further, they have also carried out a full-scale tension test on pegged mortise and tenon joint using Douglas fir as a structural

material and White Oak pegs. Pull out load was applied on the tenon to estimate the tensile capacity of the joint. The objective of this test was to evaluate the effect of peg shear strength on the joint capacity and estimate the minimum end (l_v) and edge distances (l_e) for designing of such joints. Figure 2.16 indicates l_v and l_e within a standard mortise and tenon joint.

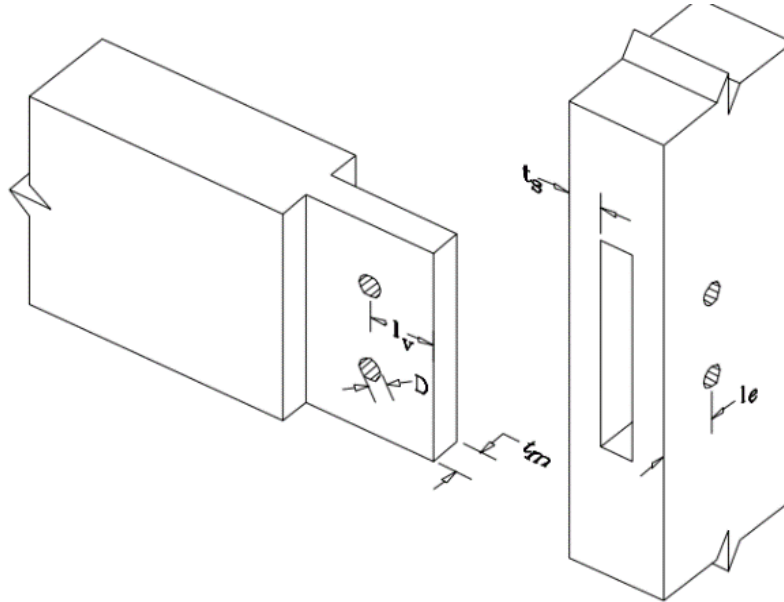


Figure 2.16- Standard geometry of mortise and tenon joint [138]

Further, this study highlighted the possible failure modes in mortise and tenon joints as shown in Figure 2.17. Mortise failure was due to tension splitting perpendicular to the grain. This initiates from the peg hole and propagates outward (Figure 2.17a). Tenon relish failure was identified as a single split that developed on the end of the tenon behind the peg hole or a block shear failure of the material behind the peg hole (Figure 2.17b). Peg failure was either bending type with a flexural hinge or shearing type failure. Both failures in the members were brittle, whereas peg failure was ductile. The study concluded that tenon relish failure can be prevented if the end distance of the peg hole is greater than or equal to three times of peg diameter. While mortise splitting can be prevented if the edge distance between the mortise and peg hole should be equal or greater than four times the peg diameter. However, this study was carried out using Douglas fir as a structural material and White Oak as a peg material. The study indicated the requirement for further investigation using different species of peg and structural members.

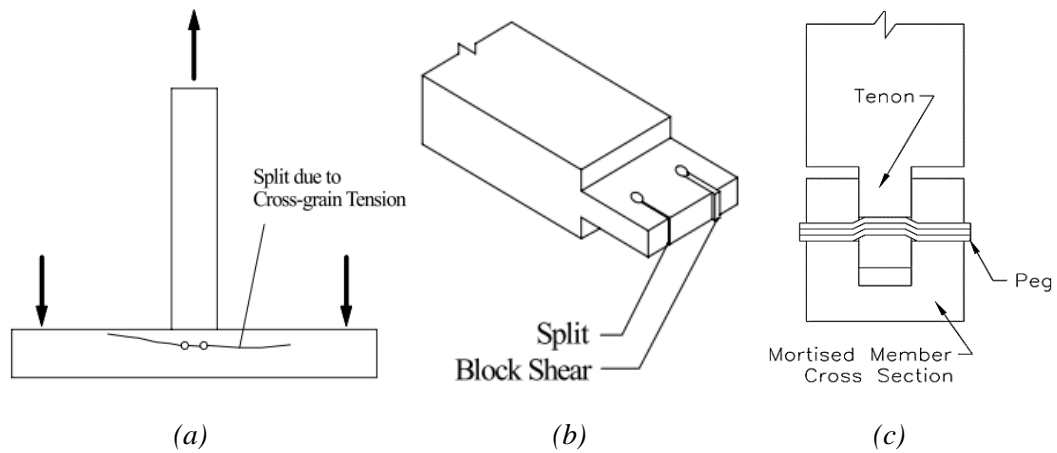


Figure 2.17- Failure modes in mortise and tenon joints, (a) mortise failure, (b) tenon relish failure, (c) peg deformation [138]

As an extension to their previous work, Schmidt and Daniel [136] further investigated the strength, stiffness and detailing requirements for mortise and tenon joints tested under tension. Tests were carried out using three different species, southern yellow pine, recycled coastal Douglas fir and red oak as material types for mortise and tenon, whereas pegs were made of White Oak. The study recommended end distances, edge distances and peg spacing for the joint design was $2d$, $2d$ and $3d$ for southern yellow pine, $2d$, $2.5d$ and $2.5d$ for recycled coastal Douglas fir, and $2d$, $2d$ and $2.5d$ for Red Oak joints to ensure peg deformation. This study also highlighted that the joints in timber with high embedment strength are more likely to fail by peg shear.

Miller and Schmidt [139] also investigated the structural performance of a full-scale mortise and tenon joint using a shear and tension test set up. This study chose yellow poplar as a structural member and a range of peg materials previously used by Schmidt et al. [138]. Joint failures from tension tests included mortise splitting, tenon relish failures, peg bending with one flexural hinge, and peg shear at two interfaces between the tenon and mortise. The peg bending failure was more common than peg shear failure which was found to be attributed due to low embedment strength of the yellow poplar. These findings validate previous research findings from Schmidt et al. [136,138]. The shear test included two different joint configurations as shown in Figure 2.18. In the case of the housed joint, the shear load was transferred through direct bearing between the tenon and mortise, and pegs served to assemble the joint during fabrication and to resist tension loading. In contrary to this, in an open mortise and tenon joint, the oversized slot was cut to ensure that there was no bearing contact between the tenon and mortise and that the load was transferred solely through pegs. Tenon splitting was the common failure type due to tension perpendicular to the grain through the bottom peg hole. In some cases, tenon rolling shear was also observed (see Figure 2.18). Thus, to avoid

these brittle failure modes, long through tenons were used which resulted in bending failure of the peg.

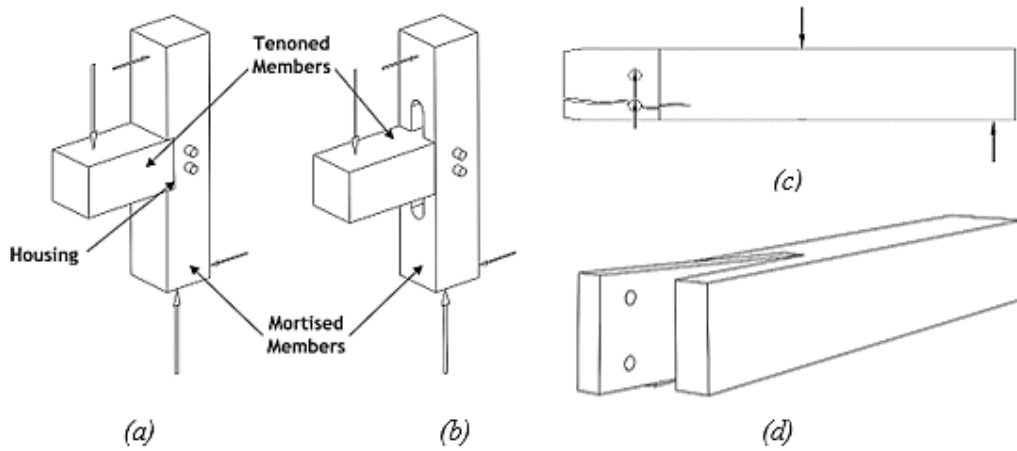


Figure 2.18- Joint configuration for the shear test, (a) housed joint, (b) open mortise joint, (c) tenon splitting, (d) tenon rolling shear failure

Bulleit et al. [53] examined the mechanical behaviour of four types of mortise and tenon joints fastened using wooden dowels. The joint types were, (1) mortise and tenon joint with shouldered mortise and unshouldered tenon, (2) with a shouldered mortise and tenon, (3) shouldered mortise and tenon with a knee brace, and (4) unshouldered mortise and tenon or fork and tongue joint, as shown in the Figure 2.19.

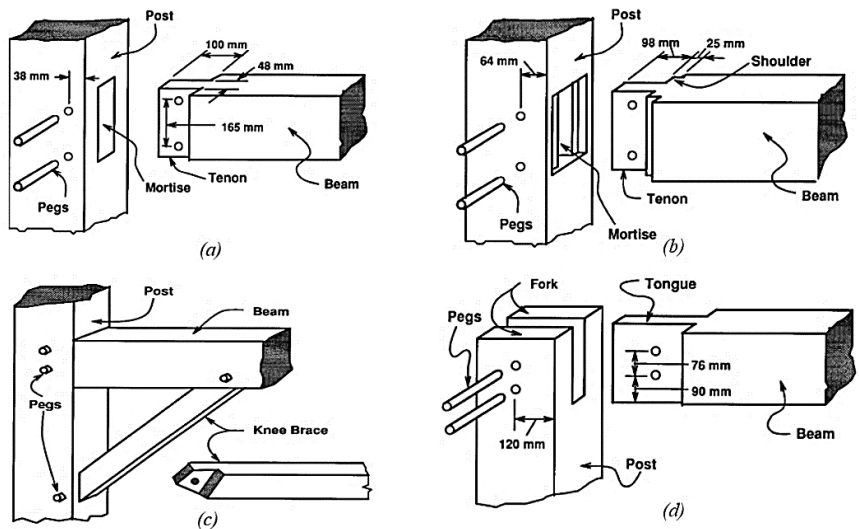


Figure 2.19- Various forms mortise and tenon joints, (a) with shouldered mortise and without shouldered tenon/Type-1 (b) with shouldered mortise and tenon/Type-2, (c) shouldered mortise and tenon with knee brace/Type-3, (d) unshouldered mortise and tenon fork and tongue/Type-4 [53]

From a utility perspective, Type-1 joint is used in non-loading bearing situations; Type-2 joint is favourable for the load-bearing beam to column connections; Type-3 joint is also used in the load-bearing beam to column connections but the joint behaviour is different than that of

Type-2, and Type-4 is commonly used as a ridge joint that joins two rafters. All connections were tested using a similar test setup under gravity load. Test results showed a linear response up to about 1/3 of the ultimate load irrespective of joint configuration. Test results showed that the Type-1, Type-2 and Type-4 joints behave as hinged joints and transmit very little moment compared to Type-3. This study also reported that the assembly tolerances affect the deformation of the pegs. The peg deformation of tightly fitted joints is relatively lower than a loose joint. The failure of pegs was through a combination of bearing, shear and bending failure as shown in Figure 2.20. A mortise and tenon joint with a shouldered mortise and tenon (Type-2) performed better than a mortise and tenon or a fork and tongue.

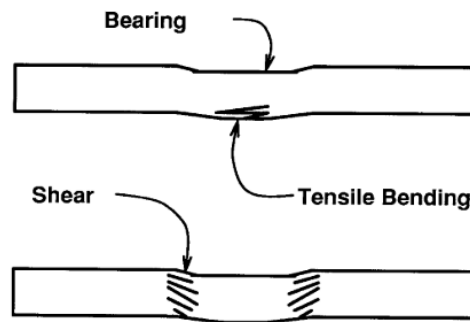


Figure 2.20- Failure mode of pegs[53]

Shanks and Walker [140] carried out tension, shear and bending tests on pegged mortise and tenon joints. Tension test results showed joint failure by the withdrawal of the tenon followed by peg deformation (four plastic hinges) without any mortise failure or tenon relish failure as indicated by Schmidt and Mackay [138]. Shear test results showed a rolling shear failure of the tenon as reported by Miller and Schmidt [139]. Bending test results showed that if the connection is not a perfect fit, the peg will carry the initial connection moment in a mode similar to the tensile tests. Finding from the test indicated that the fit of the tenon the mortise has a very important influence on both the joint strength and stiffness for all three test types. In the case of the bending test, joint behaviour can be directly related to joint performance in tension. Shanks [141] studied the effect of peg orientation, joint fit and peg failure mechanism within an oak pegged mortise and tenon joint using a three-plank test (see Figure 2.21). The study reported that peg orientation did not affect the connection strength, but the stiffness was found to be approximately 10-50% higher in when loaded radially (loading perpendicular to the growth ring) compared to tangentially (loading parallel to the growth ring). Shanks [141] also concluded that the average pull-out strength and stiffness of a poorly fitted joint, with a 12 mm gap, was within a range of 40% lower than for a perfect fit joint. This is because, in the case of a poorly fitted joint, the shear span of the peg is longer which results in bending failure of the peg, but in the case of perfect fit joints cross-grain shear (between the interface of tenon and mortise) failure is dominant. Shanks and Walker [135] concluded that stiffness

of the joint decreases as the apparent shear span of the peg increases. They also highlighted that the moment resistance of a pegged joint is related to the pull-out strength. If the pull-out strength is known, moment capacity of the joint can be predicted and finally the frame strength can be predicted based upon energy equilibrium and collapse analysis.

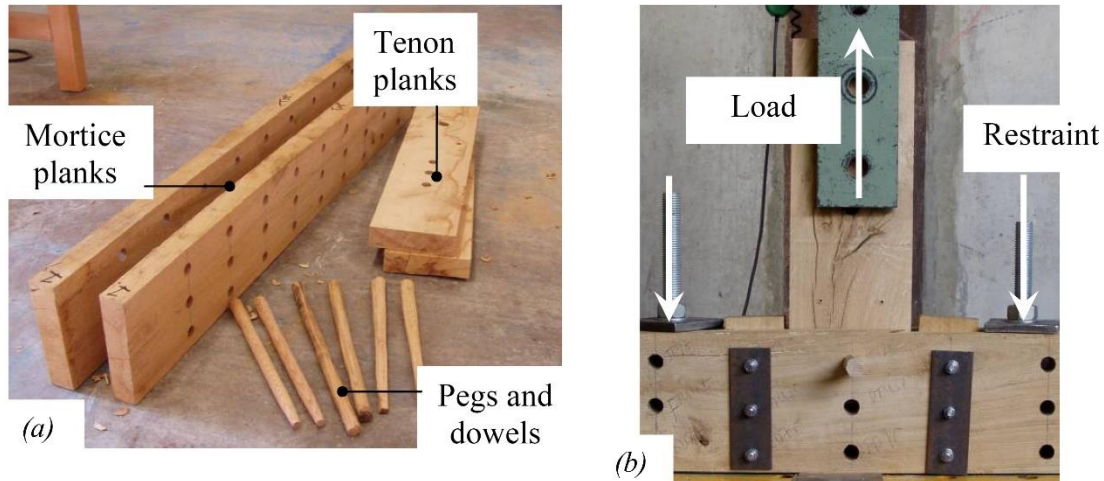


Figure 2.21- Three-plank mortise and tenon joint test by Shanks [141]

Further, Shanks et al. [142] carried out a series of pull out tests (168) to analyse the failure mode, effects of the end distance within the tenon, edge distance within the mortise, peg diameter and cross-section (square/circular shape) on the mechanical performance of all-softwood pegged mortise and tenon joint. The connections were fabricated using Sugi planks and hinoki pegs (Figure 2.22). Results showed that the relative stiffness of the peg and connection material influences the failure mode and end distance requirements of the connection. A minimum $2d$ edge distance should be given to prevent wall failure in the mortise and to perform at full capacity. The squared shaped pegs cause splitting of the mortise wall due to stress concentrations along the top face of the square peg. The study also highlighted that a square-shaped peg can lead to higher perpendicular to the grain tension strains/stresses within the mortise wall compared to circular shaped peg which is a consequence of the cross-sectional shape.

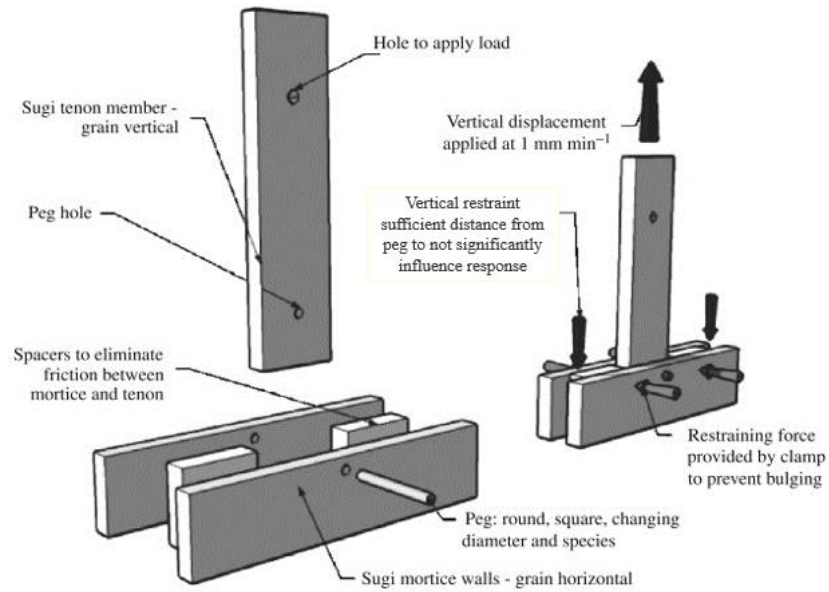


Figure 2.22- Mortise and tenon joint tested by Shanks et al. [142]

Research on moment-resisting type carpentry joints is limited. Pang et al. [143] investigated the effect on beam shoulder length on moment-rotation behaviour of mortise and tenon joints fabricated using dovetailed tenons as shown in Figure 2.23. These joints did not involve pegs and relied on the interlocking of the beam and column members. The result showed that the presence of a shoulder significantly affects the moment capacity of the joint. The moment-resisting capacity of the joint without a shoulder was just 42% of the joint with the shoulder. Hence, the presence and size of the shoulder should be considered while designing such connections.

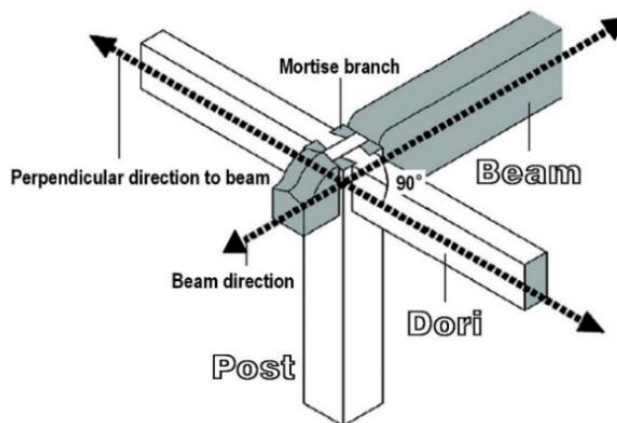


Figure 2.23-Traditional dovetailed mortise and tenon joint tested by Pang et al.[143]

One of the examples of beam-column moment connections that are widely researched is a *Nuki Joint* [124,144–146]. It is an oriental carpentry connection within which a beam member (*Nuki*) passes through a column (see Figure 2.24a). In some cases, wedges are used to tighten the connection. The stiffness and strength of this joint are largely dependent on the embedding resistance in the contact surfaces between the beam and column, between the beam and the

wedge and also between the column and the wedge. Guan et al. [144] highlighted that these joint show excellent energy absorption and seismic performance due to compressive deformation perpendicular to the grain. These wedges allow continuous contact between the column and the beam and ensure the tightness of the connection. This study also indicated the importance of assembly tolerances in these connections from the point of view of rotational stiffness. More recently, Suesada et al. [147] highlighted that the rotational stiffness and moment capacity of the joint can be further increased by suppressing the compressive deformation during loading. They evaluated the performance of hardwood reinforced *Nuki Joint*. Specimens were categorised as control (N), specimens with short hardwood reinforcement (Rs) and specimens with longer reinforcement (RI) (see Figure 2.24b). Results showed that the moment capacity and rotational stiffness of the joints can be increased by using high-density hardwood species.

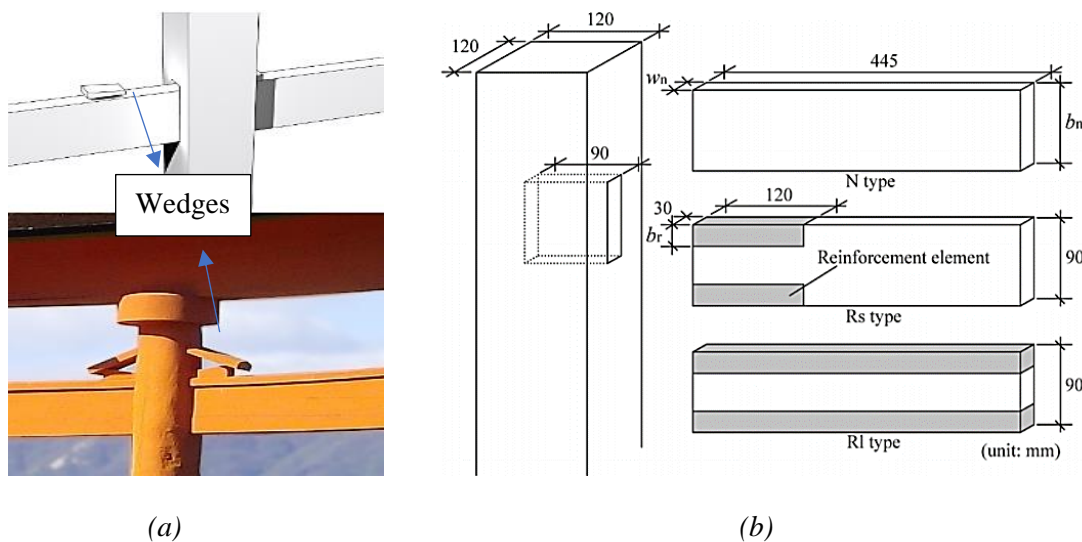


Figure 2.24 Nuki joint, (a) with wedges [124], (b) without wedges and with shorter and longer reinforcement [147]

The literature showed various forms of carpentry type beam-column connections. Mortise and tenon joints with pegs are one of the most studied connection types because of its simple geometry and structural performance suitable for heavy timber structures. Several studies are available on the strength, stiffness and failure mechanism of mortise and tenon joints. These studies also investigated the effect of various parameters such as peg diameter, end and edge distances of the peg, the orientation of the peg, bending and shear strength of pegs and the bearing strength of pegs on the different base materials. In general, the reviewed literature indicates that the strength and stiffness of the joints can be increased by using high-density material within the connections. For example, using high-density pegs may increase the strength and stiffness of the connections, whereas the use of high-density material may further increase the structural performance of the joint by local reinforcement.

2.4.3 Metallic timber connections

In modern timber construction, mechanical fasteners are the rule for connecting timber members due to manufacturing and on-site ease of assembly. These fasteners can be categorised into three major classes, dowel-type connectors, metal connector plates with integral plates teeth and shear connectors. There are also several connection configurations that combine these fasteners. Among all other fastener types, dowel-type connectors are most commonly used in timber construction. These connectors involve nails, bolts, staples, screws and dowels. They transfer either lateral or withdrawal load. The lateral load is transferred between connected members through dowel bearing and bending of the dowel, whereas withdrawal loads are parallel to the connectors axis and transferred through friction or bearing to the connected members. The plate type connectors only transfer lateral load through bearing on the connected members. In heavy timber construction, mechanical connections are often produced with metal plates (external or concealed) and laterally loaded dowel-type connectors due to the ease of assembly and structural performance [119,148–156]. In the following section, beam-beam and beam-column connection using dowel-type connectors are discussed with particular focus on connection configuration, structural performance and failure modes of slotted-in plate timber moment connections.

2.4.3.1 Metallic beam-beam connections

Awaludin et al. [157] investigated the flexural behaviour of a multi-bolt connections subjected to pure bending using a four-point bending test set up. Figure 2.25a shows a test set up with half symmetry of the connected beam. They compared the moment capacity, joint rotation, connection ductility and failure modes of wood-wood connections with wood-steel connections. There were three configurations of each connection type consisting of horizontal, circular and vertical bolt arrangements as shown in Figure 2.25b, Figure 2.25c and Figure 2.25d, respectively. Test results show that the fastener arrangement is one of the most important factors that influences the ductility and rotation stiffness of the connections. The results showed that specimens with a vertical bolt arrangement had the highest moment capacity among all the bolt configurations. This was because the vertical arrangement had a greater distance between the bolts compared to the other two arrangements. Also, the rotational stiffness, ductility and ultimate rotation were highest for the vertical bolt configuration. Comparisons between wood-wood and wood-steel types showed that the moment capacity of the wood-wood connections was about two times higher than the wood-steel connections. This may be due to a relatively larger difference between the thicknesses of wood and steel members. The ultimate rotation of the wood-wood connection was higher than the wood-steel connections. This was because wooden plates as side members in wood-wood connections are less stiff than steel plate and allow more load redistribution among bolts

during the plastic phase. However, these conclusions are made based on one replication of each configuration and may weaken the conclusion due to high variations in wood material properties.

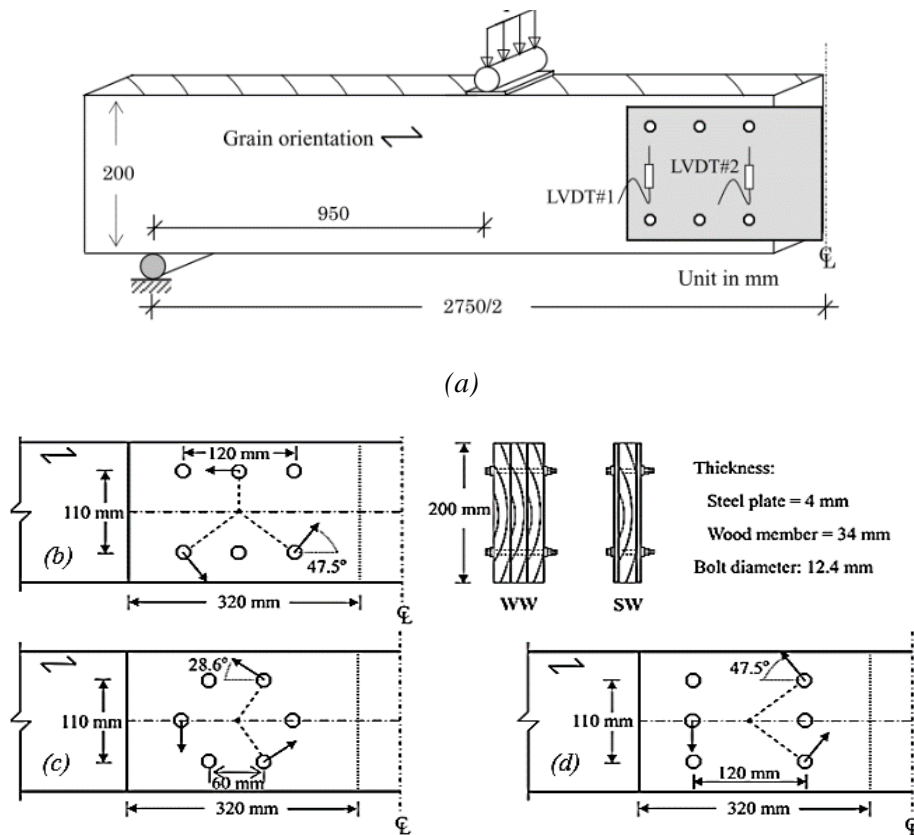


Figure 2.25- Wood-wood/wood-steel beam-beam connections (dimensions in mm), (a) half symmetry of the connected specimens, (b) horizontal bolt arrangement, (c) circular bolt arrangement, (d) vertical bolt arrangement [157]

Wang et al. [158,159] investigated the mechanical behaviour of bolted glulam beam-beam connections tested under pure bending using a four-point bending set up. Connected ends of the beams were slotted to accommodate a steel plate. Figure 2.26a and Figure 2.26b show the geometry and test set up of the connected specimen. Test results showed a brittle splitting failure of these specimens due to tension perpendicular to the grain at the bottom side of the specimen (tension zone). The splitting took place around the bolts and propagated between the rows (Figure 2.26c). This kind of failure is commonly seen in these types of connections which was discussed in detail by Jorissen et al. [160]. Therefore, to avoid premature splitting of the timber members, localised reinforcement in the vicinity of connectors has been suggested by several studies [49,161–163].

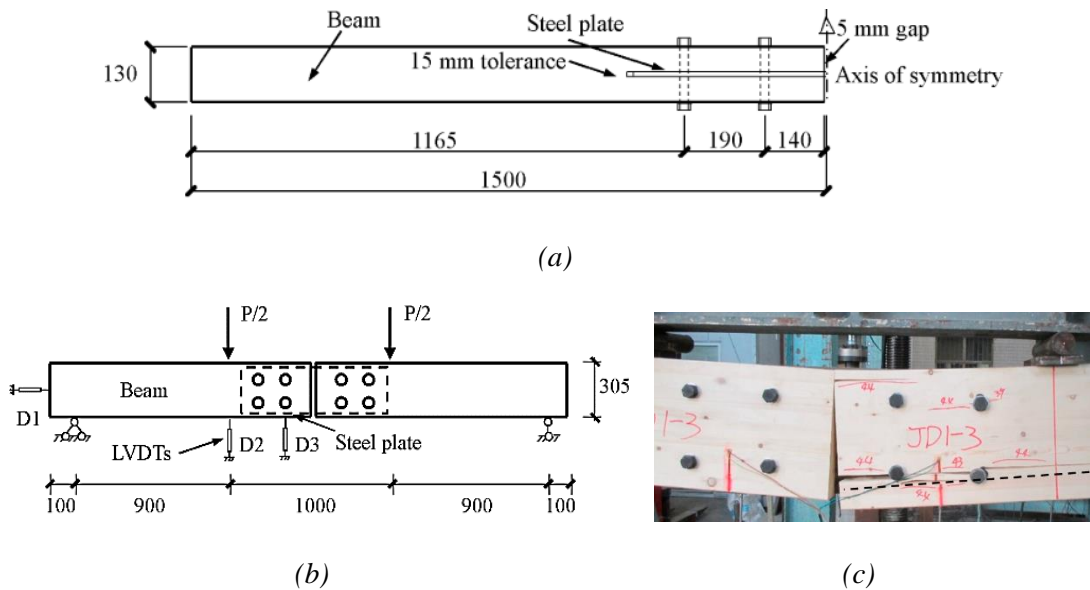


Figure 2.26- Bolted beam-beam connections (dimensions in mm), (a) half symmetry of the connection, (b) test set up, (c) failure mechanism of the connection [158]

Tomas et al. [164–166] highlighted that slotted-in steel plate connections with dowels have limited bending stiffness due to the relative deformation of the adjacent members during load transfer. They designed a steel-timber connection with steel parts embedded into the timber beam. To improve the rotation stiffness of the connections, the gaps between the timber beams and steel connectors (dowel/plates) were filled with a cement-based filler with polymer fibres. Figure 2.27 shows an assembled connection and its assembling scheme. The study suggested that the use of filler ensures a tight fit between steel parts and avoids initial movement between the joint elements. The four bending test results showed that these connections have high rotational stiffness which is compared with the glued-in steel rod connections.

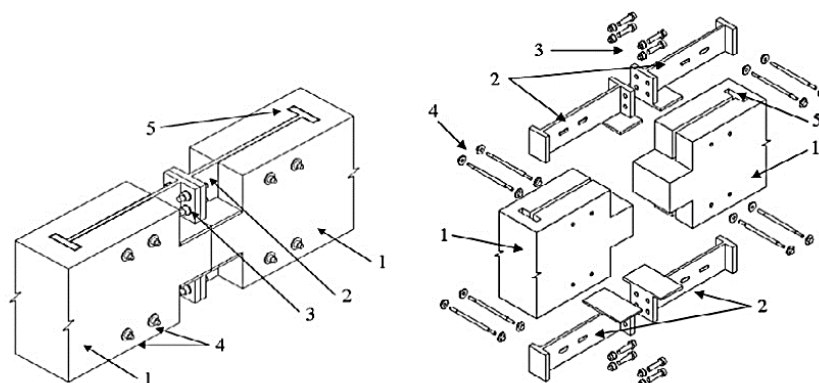


Figure 2.27- Assembled beam-beam connection and its assembling scheme: 1 – timber element; 2 – steel detail; 3 – mounting bolts; 4 – structural bolts; contact between timber and steel zone filled with filler [165]

Leijten and Brandon [120,167–169] used an innovative way to prevent premature splitting and improve the structural performance of timber-steel moment connections by using reinforcement material and tube fasteners within the connection area. They used a type of

compressed laminated wood commonly known as densified veneer wood (DVW) as a reinforcement material. These studies highlighted that the embedment strength of DVW is very high (5-6 times higher) compared to uncompressed wood. Leijten and Brandon [120] glued DVW within a timber-steel spliced beam-beam connection assembled using expanded tube fasteners. In these connections, DVW prevents the premature wood splitting and increase the localised capacity of connected timber material by allowing an increased number of connectors per unit area (reduced spacing), while expanded tube fasteners maintain the tightness of the connection and improve connection stiffness. A study from Rodd and Leijten [170] showed that such reinforcement techniques significantly improves the moment capacity and stiffness of the connections compared to unreinforced specimens. However, the procedure to assemble such connections involves using a hydraulic jack to expand the tube fastener to fit and attaching the DVW reinforcement is time-consuming and complex [161].

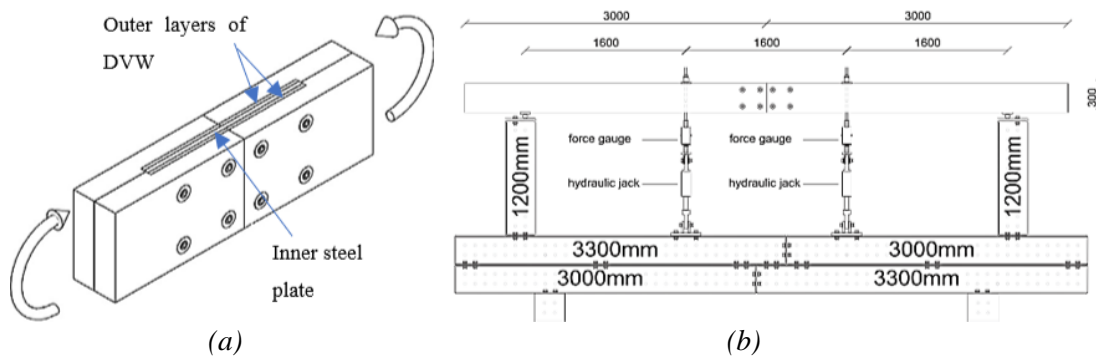


Figure 2.28- Timber-steel moment connection using DVW reinforcement and tube fasteners, (a) connection configuration, and (b) four-bending test set up (dimension in mm) [120]

Literature showed that timber connections with slotted-in steel plates and steel dowels are commonly used connection types to connect beam elements in heavy timber structures. These connections are suitable for transmitting larger force one member to another and easy to assemble. The common failure mode in these connections is tension perpendicular to the grain splitting of the timber members around the vicinity of dowel. Thus, using reinforcement material around the dowel area is recommended to improve the load-carrying capacity and overall structural performance of the connections.

2.4.3.2 Metallic beam-column connections

He et al. [171] investigated the moment-rotation behaviour of slotted-in steel plate beam-column connections with and without a knee brace. Figure 2.29 shows the configurations of the connections which were subjected to lateral monotonic and reversed cyclic loading tests. Test results showed that the specimens with knee braces had about 6 times higher rotational stiffness compared to specimens without a brace. Similarly, the moment capacity of specimens with knee braces showed about 7 times higher moment capacity when compared to the

specimen without a brace. Results also highlighted that specimens with knee braces exhibit more ductile behaviour compared to specimens without braces. Commonly observed failure modes were plug shear failure and splitting of glulam members along the row of bolts. Although beam-column connections reinforced by braces is a common practice in heavy timber construction to improve the lateral resistance capacity and overall stiffness of the structure, it decreases the flexibility of the building layout and often impacts on the architectural space.

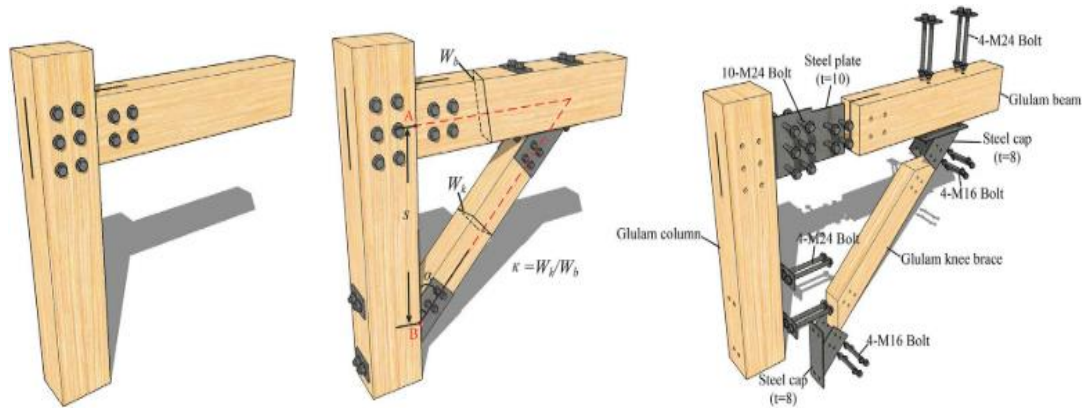


Figure 2.29- Beam-column connections with or without knee braces [171]

Solarino et al. [172] designed a semi-rigid type beam-column connection using slotted-in steel plate and dowels. For the experimental characterisation, specimens were loaded in compression to induce a bending moment in the connection (see Figure 2.30). The test results highlighted a lower stiffness of such connections during the initial loading phase. The reason for this behaviour was found to be a result of geometric roughness and imperfections of the contact surfaces between connected members and dowels. Tested specimens showed tension perpendicular to the grain splitting within the column members. The study also compared experimental rotational stiffness of the connections with the theoretical design calculation of EC 5 [55]. Results showed that experimental rotational stiffness values were two times higher than the EC 5 calculations. However, these findings were based on only a single experiment and may require further investigation to give a statistically valid conclusion. Nevertheless, the study highlighted the need for revision of design guidelines for such connections.

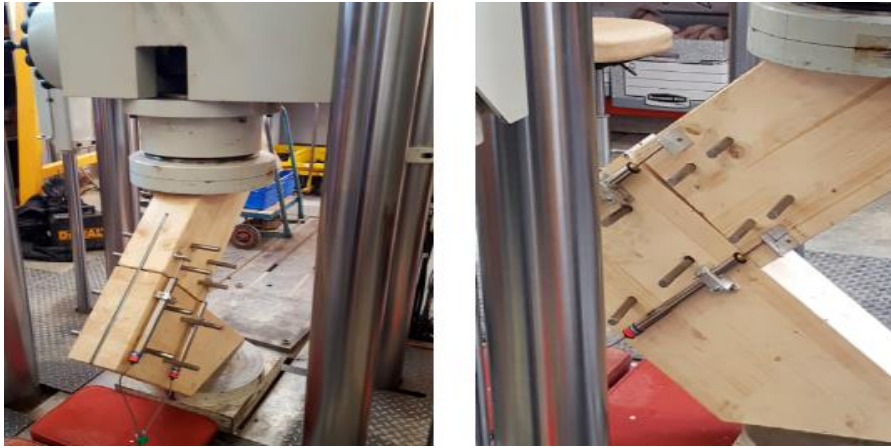


Figure 2.30- Beam-column test set up[172]

Wang et al. [159] evaluated the mechanical performance of slotted-in steel plate bolted beam-column connections. Assembled specimens were subjected to shear force and bending moment and the effect of shear-to-moment ratio was analysed on the overall resistance of the connections. Figure 2.31 shows the geometry of bending set up. Test results showed that the moment capacity of the connection decreased with the increase of shear-to-bending ratio by up to 31% compared to specimens tested under pure bending (see Section 2.4.3.1). The shear resistance decreased with the decrease of the shear to bending ratio up to 46% of the pure shear resistance test. The study highlighted that the interaction between the shear and moment resistances plays an important role in the overall structural performances of the connection under combined loading. Tested specimens exhibited perpendicular to the grain tensile splitting and parallel to grain shear splitting as dominant failure modes.

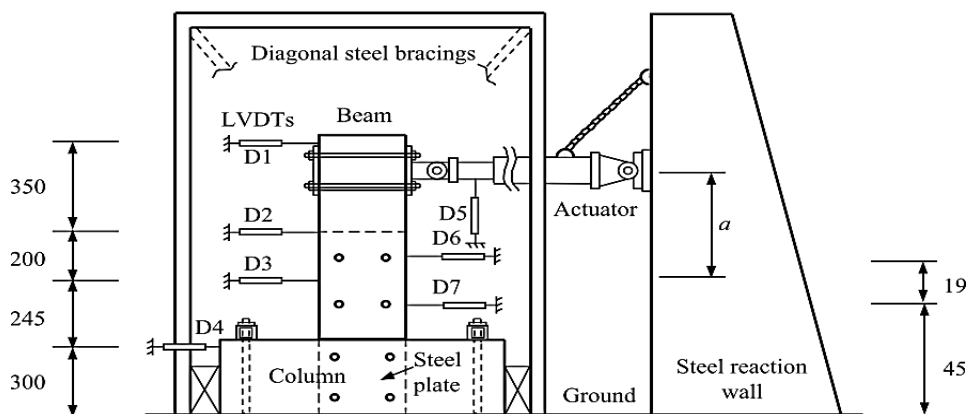


Figure 2.31- Geometry of bending test set up (dimension in mm)

Li and Xiong [173] investigated the structural performance of semi-rigid type bolted timber connections in full-scale portal frames and in small-scale beam-column connections. Connections in frames and small-scale specimens were designed by inserting a slotted-in steel plate between beam-column. One frame consisted of two types of connections, (a) column-base and (b) beam-column. Both frame specimens and small-scale specimens were subjected

to monotonic and cyclic lateral loading. The test set up for small scale specimens was similar to Figure 2.31. Figure 2.32a shows the test-set up for the framed specimen. Test results showed that the connections were weak and the members were strong. Failure was observed within the connection area due to tension perpendicular to grain and shear splitting along the row of dowels. Small scale tests showed similar failure modes. The dowels within the beams showed larger deformation compared to dowels within the column (see Figure 2.32c and Figure 2.32d). This is presumably due to the higher load per bolt within the beam due to the lesser number of bolts compared to the column. Crushing of timber was also found around the bolt holes. The study highlighted that slotted-in steel plates connections are suitable for carrying the lateral load.

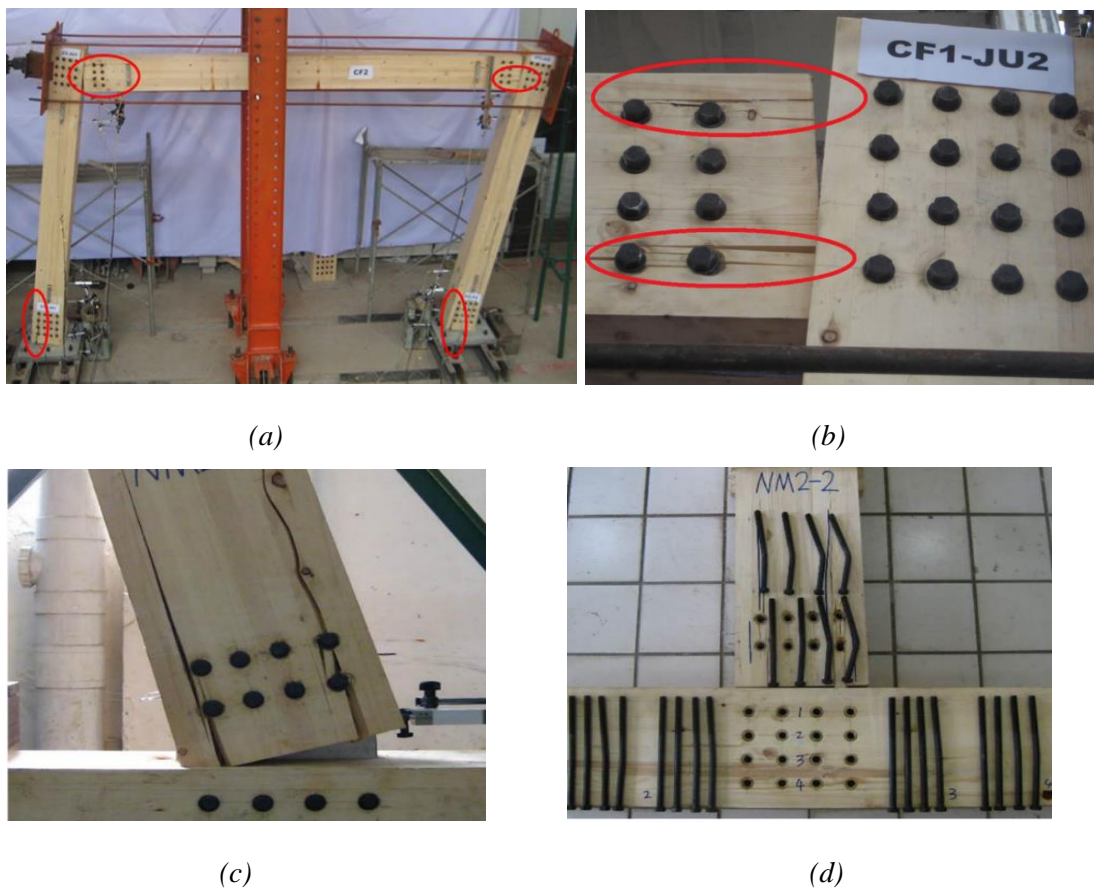


Figure 2.32- Beam-column connection, (a) frame test set up, (b) failure mode of beam-column connection in frame, (c) splitting within the beam member of small-scale specimens, and (d) bending of the bolts within small-scale specimens [173]

Lam et al. [174] and Gehloff et al. [175] evaluated the structural performance of moment-resisting slotted-in steel plate bolted timber connections using a cycling loading protocol. Beam-column members were connected and tested in a similar fashion to that shown in Figure 2.31. In these connections, self-tapping wood screws were used to reinforce the connected members in the perpendicular to the grain direction to avoid brittle failure. Test results showed

that unreinforced specimens experienced brittle behaviour and little moment resistance due to early crack formation which was attributed to the high perpendicular to the grain and longitudinal shear stresses. Contrary to this, reinforced specimens showed a large increase in moment capacity and ductility. The overall increases in the moment capacity of the reinforced specimens were more than 70% compared to unreinforced specimens. This study also highlighted the various failure modes of the test specimens (see Figure 2.33).

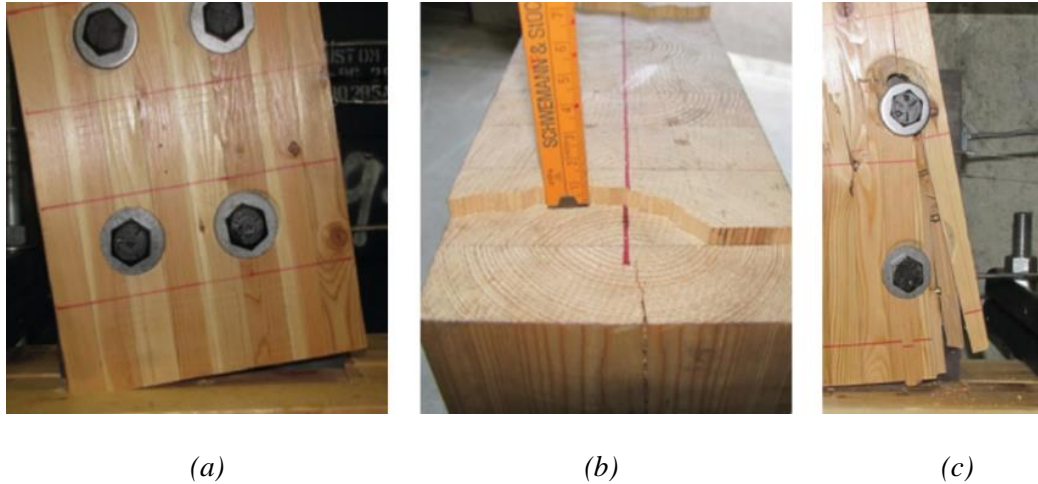


Figure 2.33- Beam-column connection, (a) bearing failure, (b) shear failure, (c) splitting along the row of bolts [174]

In another similar study, Zhang et al.[161] researched the effect of screw reinforcement on the mechanical performance of dowel-type timber connections within a portal frame. The study compared the moment-rotation behaviour between unreinforced and reinforced frames. Each frame consisted of two beam-column connections connected using slotted in steel plates and dowels. Both frame types were subjected to lateral load (racking) to induce bending moment in the connection areas. Self-taping screws were used for perpendicular to the grain reinforcement. They were placed at $1d$ from the central axis of the dowels to prevent premature splitting of timber and provide bearing support to the dowel. Test results showed that the reinforced frames achieved a 31% and 51% increase in moment-resisting capacity and ultimate rotation compared to unreinforced specimens, respectively.

Awaludin et al. [176] investigated the cyclic behaviour of moment-resisting of beam-column connections assembled using high strength bolts and with/without reinforcement in the vicinity of bolts. The study utilised plywood, high-density plybamboo and DVW as reinforcement material and two different grades of bolts; 4.8 grade (about 530 MPa tensile strength) and 10.9 grade (about 1040 MPa tensile strength). The load was applied in tension to induce the bending moment in the connection area. Figure 2.34 shows the geometry of the test set up and the failure mode of the connection. Specimens exhibited brittle failure due to splitting of column member along the row of bolts. Specimens with DVW and 10.9 grade bolts

showed the highest moment capacity and rotational stiffness, which were approximately 95% and 90% higher than the unreinforced specimens with the same grade of bolts. Specimens with plywood and plybamboo also showed superior mechanical performances compared to unreinforced specimens but they were lower than specimens with DVW. This is because the embedment strength of DVW is approximately 3.5 times and 1.5 times higher than the plywood and plybamboo. These findings confirmed the results of Leijten et al. which highlighted the suitability of DVW in structural applications [177].

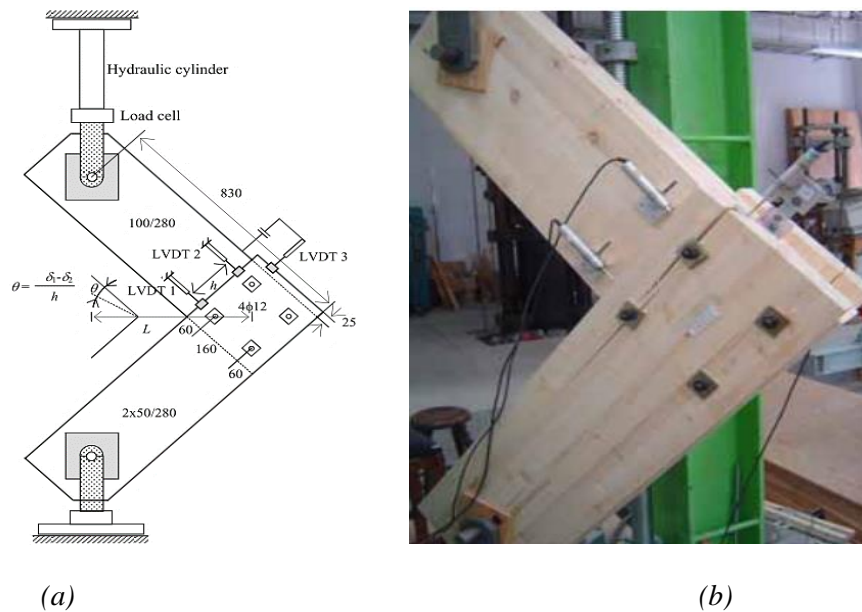


Figure 2.34- Beam-column connections, (a) simplified test geometry, (b) splitting failure [176]

Similar to beam-beam connections with metallic fasteners, beam-column connections with slotted-in steel plates and steel dowels are often seen in heavy timber structures. The capacity of the connections can be improved by using higher capacity steel components and localised reinforcements (such as screws and high density DVW, plybamboo, plywood) within the connection area to prevent premature tensile and shear splitting of the timber members. Furthermore, the current study did not find literature on connections that are suitable for DLT timber construction.

2.4.4 Timber connections using thermo-mechanically compressed wood

Recent studies found that CW can strengthen existing joint systems when used in combination with other conventional fasteners [118,178]. CW of Japanese cedar was used as a substitute for high-density hardwood for making shear dowels [25]. The CW with its annual ring radial perpendicular to the loading direction (0°) had a unique double shear performance characteristic and showed good properties as a dowel material in terms of its enhanced strength and ductility. Kitamori et al. [79] developed a friction joint system using CW wedges

and metallic bolt-nut connections for timber buildings. The proposed joint system was shown to have superior mechanical performances in terms of high stiffness, strength and ductile behaviour. Jung et al. [95] examined the use of CW dowels to improve the strength of glued-in-rod (GIR) joints system. Their test results demonstrated that GIR joints with CW dowels showed around 1.6 times higher strength than those with maple dowel in pull-out tests.

To make use of the high strength properties of CW connectors, Jung et al. [78,80,179] also utilised CW plates and dowels within column-sill and beam-column connections as an alternative to steel fasteners. Figure 2.35 shows the arrangement of CW plates using CW dowels in connections. Jung et al. [78,80] evaluated the pull-out strength and moment resistance of the timber-CW connections. Test results showed that good structural performance of the connection can be achieved by using CW dowels to resist high shear forces and using the CW plates to resist bending moment. However, these findings are based on the limited number of test configurations and smaller sample size, hence, further tests are required.

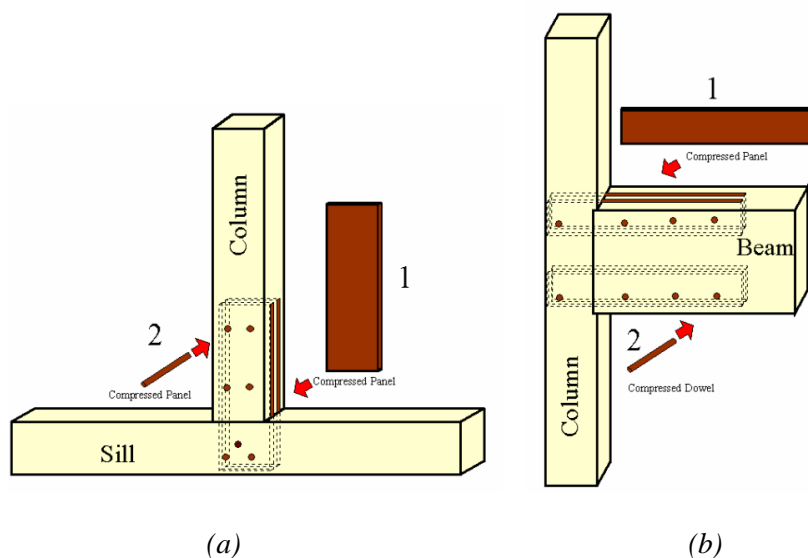


Figure 2.35- Slotted-in CW plates using CW dowels, (a) column-sill connection, (b) beam-column connection [80]

2.5 Conclusion

This chapter has given a brief introduction to wood as a structural material and has detailed up to date findings on wood modification techniques and timber connections suitable for heavy timber construction. The important highlights of the chapter are as follows:

- Literature indicates that carpentry connections with hardwood dowels have high volumetric shrinkage which leads to loosening of the connections over a period of time [62,63]. However, the current study did not find any quantitative information to validate this. Therefore, moisture dependent swelling and shrinkage of the timber-hardwood dowel connections could be an area of investigation.

- Also, a large number of studies have highlighted that thermo-mechanically CW is dimensionally unstable due to springback behaviour when exposed to moisture and heat which may be a primary limitation to its use in structural applications. There are only a few studies that showed the positive side of springback. In timber structures, where the tightness of the connections is required for lateral stability, springback could be utilised as a beneficial characteristic. Previous studies were mainly focused on short-term testing of springback. Thus, there is scope for a thorough investigation of the mechanical properties of CW as a connector material and the long-term testing of springback behaviour. Further, literature shows limited studies on the mechanical properties of thermo-mechanically CW as a connector material. This highlights the need for extensive research on embedment, yield moment capacity and shear performance of these connectors.
- Heavy timber structures can involve carpentry and metallic connections. Carpentry connections are usually adhesive-free and non-metallic. They can be interlocking type within oriental carpentry, whereas scarf and mortise and tenon joints are commonly used in other parts of the world. On a positive side, these connections can be easily disassembled and reconfigured for replacement or repair. However, these connections require a high level of craftsmanship, skill and effort. Another important issue that is associated with these connection types is the use of large cross-sections of solid timber which is not feasible in modern timber construction due to cost and limited availability of larger diameter trees. Therefore, the usage of carpentry connection has declined rapidly in favour of quicker, efficient and profitable connection designs using mechanical connectors in the last century. However, in recent years, the use of robotic technologies and the development of mass timber products made it possible to produce desirable shapes and geometries of carpentry connection types for heavy timber structures. However, the lack of codified design guideline for such connections is still a barrier. When it comes to metallic connectors, the dowel-type connectors are widely used in heavy timber connections in conjugation with steel plates. Particularly, dowelled connections using slotted in steel-plates are one of the most widely used and researched connection types. These connection types are often simpler to assemble and have high structural and fire performance. In the last decade, a few studies have also shown the suitability of CW plate and CW dowels in timber as a potential alternative to metallic fasteners. However, these studies were carried out with a limited number of specimens and need further validation with a larger sample size.
- Literature highlighted that moment-resisting connections exhibit brittle failure due to tension perpendicular to the grain. Brittle failure is an undesirable failure mode which

can result in the sudden collapse of the structure. Therefore, to avoid this failure, the effect of various reinforcement materials (DWW, plybamboo, plywood and screws) have been studied in the vicinity of fasteners to increase per unit area load-carrying capacity of the wood. In the context to the current study, reinforcement by means of wood screws or threaded dowels could be a potential solution to minimise the tension perpendicular to the grain failure.

Chapter 3 Material characterisation of CW and uncompressed wood

3.1 Introduction

The research objective of this PhD thesis, outlined in Chapter 1, is to develop and characterise the structural behaviour of non-metallic and adhesive-free semi-rigid type timber-timber moment connections using compressed wood (CW) dowels and plates. The structural behaviour of such connections is dependent on the mechanical properties of the connected components, namely timber, CW plates and CW dowels. Thus, an experimental test programme was designed to characterise the mechanical properties of each of these individual components.

Additionally, the obtained material test results were compared with other non-metallic construction materials such as hardwoods and composites. The relevant mechanical properties of the aforementioned construction materials were obtained from the literature. While collecting data, the density of the material was considered as a critical parameter irrespective of the material type, manufacturing technique (in case of CW connectors) and test procedure. Finally, some of the material properties (embedment strength and yield moment capacity) were also determined using the empirical formulas/ design guidelines of EC 5 [55]. A comparison was carried out between experimentally obtained results and material properties predicted from EC 5 equations to check their suitability for high-density CW materials.

3.2 Selection of material characterisation tests

The existing material characterisation test protocols only cover uncompressed softwoods and hardwoods. Thus, it is desirable to first check the suitability of existing standards for the characterisation of the material behaviour of CW connectors. For this reason, in this study, EC 5 design guidelines for dowel-type timber connections were used as a reference for the selection of material characterisation tests.

As per EC 5, apart from the connection geometry parameters, prior knowledge of two other parameters are necessary to calculate the load-carrying capacity of connections using strength equations, namely, the embedment strength of the connected timber members (f_h) and the yield moment capacity of the fastener (M_y). For this reason, relevant material characterisation tests were included in the experimental program to calculate the embedment strength of the selected uncompressed timber and CW plates along with the yield moment capacity of the CW dowels. For timber-timber connections based on wood-based connectors additional failure modes must be considered. Schmidt et al. [136] and Sandberg et al. [180] proposed two additional failure

modes and relevant strength equations for embedment failure and cross-grain shear failure of the dowels. Therefore, in addition to embedment and yield moment tests, a cross-grain shear test was carried out to investigate the transverse shear (cross-grain shear) strength of the CW dowels. For comparison purposes, cross-grain shear tests were also carried out on uncompressed beech wood dowels.

Finally, three-point bending tests were conducted on three different CW plate materials to select one material type suitable for the mass production of CW plates to be utilised in the experimental testing discussed in Chapter 5 and Chapter 6.

The CW connectors used in the material characterisation tests were produced using different types of softwood species and a varying level of compression ratio (CR). Table 3.1 summarises the various tests presented in this chapter.

Table 3.1- List of material characterisation tests included in this chapter

Test type	Loading direction	Softwood (SW)	Hardwood (HW)	Compressed Wood (CW) with a varying compression ratio (CR)		
				54%	60%	68%
Embedment	Parallel to grain	✓ (20)				✓ (5)
	Perpendicular to grain	✓ (20)				✓ (5)
Yield moment	Parallel to the growth rings		✓ (5)	✓ (5)		
	Perpendicular to the growth rings		✓ (5)	✓ (5)		
	45° angle to growth rings		✓ (5)	✓ (5)		
Cross-grain shear	Parallel to the growth rings		✓ (5)	✓ (5)		
	Perpendicular to the growth rings		✓ (5)	✓ (5)		
Three-point bending	Perpendicular to grain (edgewise)				✓ (5)	✓ (10)

Note: Number of replications is within parentheses.

3.3 Materials

This section describes the materials used in the study. There were several different materials tested which include CW, hardwood and softwood. The hardwood material in the form of

beech wood dowels was used only as a reference material to compare the yield moment capacity and cross-grain shear strength of CW dowels. They were not used for structural testing presented in Chapter 5 and Chapter 6. The selection of wood species for the current study was based on the commercial availability of the species in Ireland and United Kingdom as agreed among AFTB project partners.

3.3.1 Compressed wood

CW connectors in the form of CW dowels and plates were procured from the University of Liverpool, Liverpool, United Kingdom. The following section describes the manufacturing process of CW dowel and plate material. Both CW dowels and plates were produced using a 200-tonne capacity, 400 °C hydraulic press as shown in Figure 3.1.

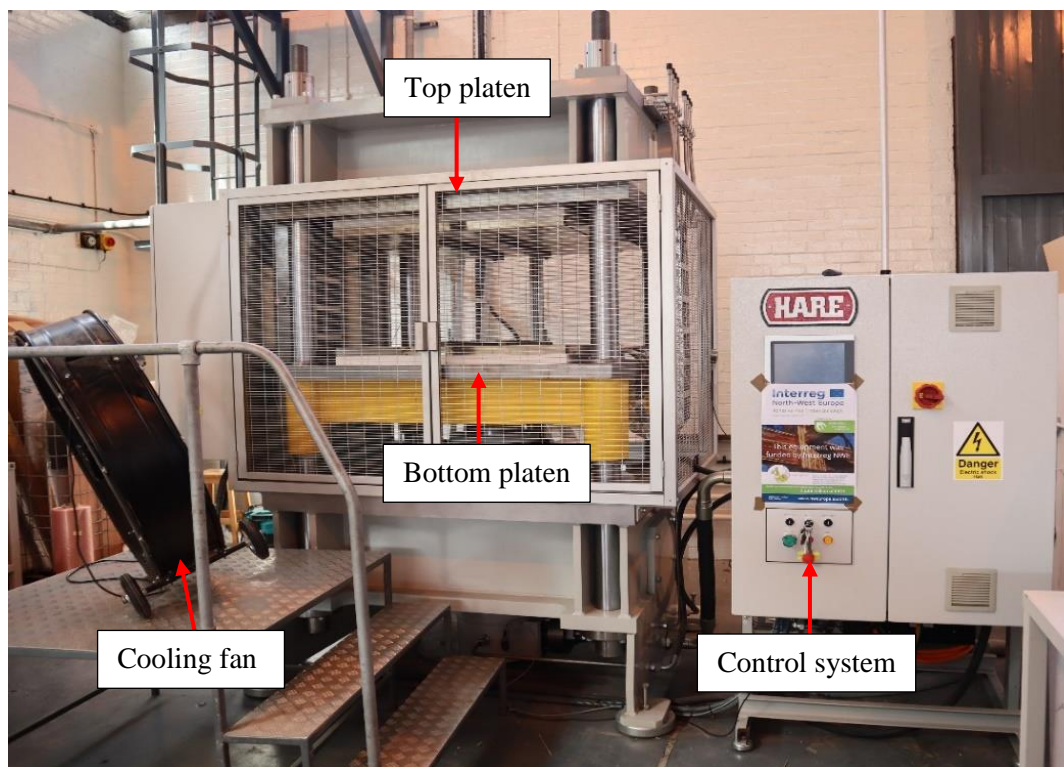


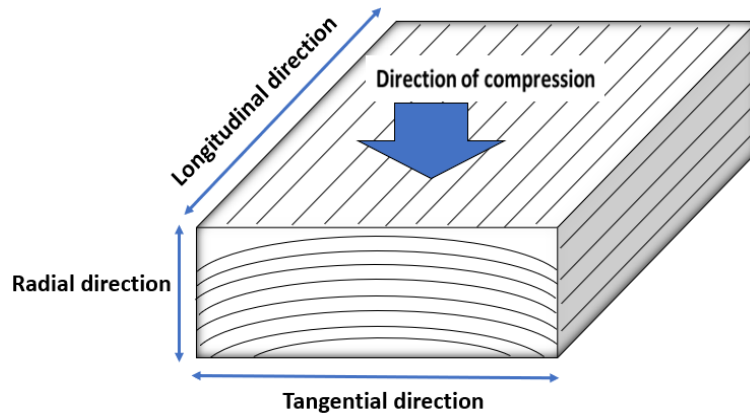
Figure 3.1- Hydraulic press used for production of CW dowels and plates, University of Liverpool, Liverpool, United Kingdom

3.3.1.1 Manufacture of compressed wood (CW) plates

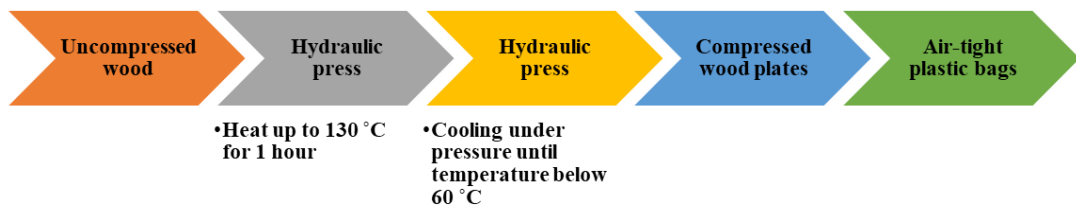
Clear specimens of uncompressed Western hemlock (*Tsuga heterophylla*) and Douglas fir (*Pseudotsuga menziesii*) were used for the production of CW plates. The mean mass densities of the uncompressed Western hemlock and Douglas fir were 500 kg/m³ and 589 kg/m³, respectively. The width and depth of the clear specimens were limited by the commercial availability of defect-free uncompressed wood. Based on the preliminary laboratory trials, clear uncompressed specimens of 67 mm (radial direction) x 63 mm (tangential direction) x 510 mm (longitudinal direction) dimensions were chosen to produce 68% radially compressed Western hemlock (CWH68) plates. The 68% CR was chosen because it was the maximum CR

that was achievable without causing any visible damage to western hemlock specimens. For the 68% radially compressed Douglas fir (CDF68), the initial thickness (radial direction) was 70 mm whereas the tangential and longitudinal dimensions were similar to the CWH68 plates. Figure 3.2a shows the direction of compression. Prior to compression, a steel plate of 1 mm thickness was attached to both top and bottom platens of the hydraulic press to prevent resin from the wood contacting the platens. Dimensioned uncompressed specimens were thermo-mechanically compressed in the radial direction up to 21 mm in thickness at 130°C using the hydraulic press at a rate of 2 mm/sec. The densification process was carried out in multiple steps. Firstly, an initial compression load of 100 kN was applied on the wood specimens and maintained for one hour at 130°C. The heat transfer allows plasticisation (softening) of non-crystalline components of wood: lignin, hemicellulose, and amorphous cellulose. Once softened, wood can be deformed easily without damage. Subsequent compression loads were applied in 10 mm increments, and each increment was maintained for five minutes before the load corresponding to the final stage was applied and maintained for one hour. Afterwards, the compressed plates were cooled under the maximum compressive load (2000 kN) until the temperature was below 60° C. The cooling stage was aided with the use of a large fan. The whole process plus the cooling step takes approximately five hours. Finally, the compressed wood plates were removed from the hydraulic press and stored in air-tight plastic bags to minimise moisture-dependent swelling.

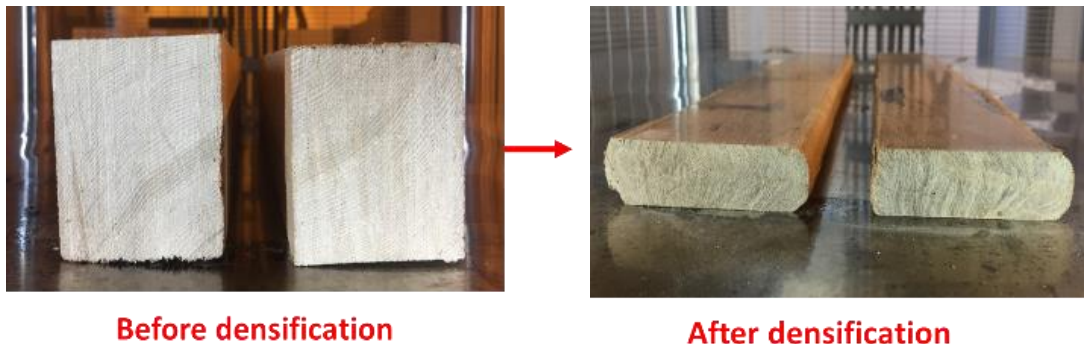
The final finished quality of both the CWH68 and CDF68 specimens was compared visually. The CDF68 specimens showed significant damage at the edges compared to the CWH68 specimens, which may be attributed to the relatively higher initial density of uncompressed Douglas fir compared to the Western hemlock. For this reason, another batch of Douglas fir CW plates was produced using a lower CR of 60%. The main intent of changing the CR from 68% to 60% to produce compressed wood plates with better finishing and lower damage when compared to CDF68 specimens. The 60% radially compressed Douglas Fir (CDF60) was produced using similar initial dimensions as CDF68 with the only difference being the final thickness which was 27 mm. Figure 3.2c shows the specimens of Western hemlock before and after compression. The oven-dry density of the compressed plates used in this study varies from 1300 kg/m³ to 1503 kg/m³.



(a)



(b)



(c)

Figure 3.2- Compressed wood plates, (a) direction of compression, (b) flowchart of manufacturing process, (c) radially compressed specimens before and after compression (University of Liverpool)

3.3.1.2 Manufacture of compressed wood (CW) dowels

CW dowels were produced using visually graded kiln dried uncompressed Scots pine (*Pinus sylvestris*) boards. The initial moisture content of the boards varied from 10%-15% and mass density was between 500 – 600 kg/m³. Small clear specimens of 200 mm (length, longitudinal direction) x 9 mm (width, tangential direction) x 22 mm (thickness, radial direction) were thermo-mechanically compressed in the radial direction using a specialised aluminium mould. Dimensions of the uncompressed specimens were determined through an initial trial to achieve a dowel diameter of 10 mm. To achieve a density of over 1100 kg/m³, for 10 mm dowels the CR was 54%. Figure 3.3 shows a flowchart of the CW dowel manufacturing process.

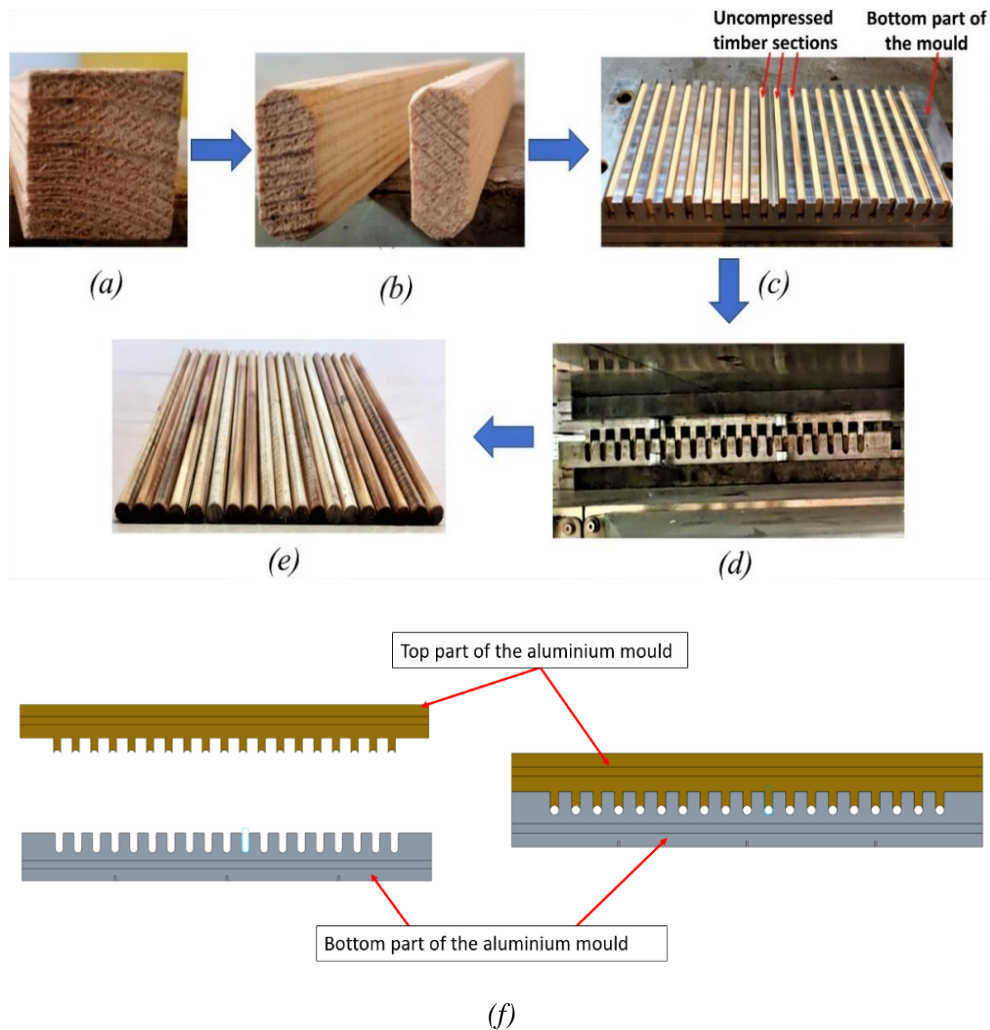


Figure 3.3- Flow chart of production of 54% radially compressed Scots pine dowels (University of Liverpool), (a) cross-section of the radially uncompressed specimen, (b) dimensioning and filleting of specimens, (c) arrangement of specimens on aluminium mould, (d) radial compression of specimens, (e) finished product – 54% radially compressed dowels, (f) drawing of mould

Before placing the clear uncompressed wood specimens in the mould, they were filleted using a finishing machine as shown in Figure 3.3b. The filleted specimens were then arranged on the bottom platen of the mould as shown in Figure 3.3c. The mould was then fixed between top and bottom platens of the press as shown Figure 3.3d. Afterwards, the aluminium moulds were placed in the hydraulic press and heated at 130°C for one hour. The heat transfer was achieved by ensuring the top part of the aluminium mould was in contact with the timber sections that were placed on the bottom part of the mould (see Figure 3.3f). The timber sections were then compressed radially, at a rate of 2 mm/sec. Initial increments of loads of 50, 100 and 150 tonnes were maintained for five minutes before a maximum load of 200 tonnes was applied and maintained for one hour. Once compressed, the specimens were left in the press to cool down under the 200-tonne load. The cooling stage was aided with the use of a large fan. Finally, the densified specimens in the form of cylindrical dowels were de-

moulded once the temperature reached below 60°C. The oven-dry density of the CW dowels used in the material characterisation tests varied from 1165 kg/m³ to 1188 kg/m³.

3.3.1.3 Summary of CW materials used in this study

Table 3.2 shows the specification of the materials used in this study. To measure the density, the specimens were oven-dried at 103 ± 2 °C until no significant change in weight was observed in accordance with EN 408 [181].

Table 3.2- Specification of the CW material

Type of the material	Test type	Mean density at the time of testing (kg/m ³)	Compression Ratio (CR) in %	Species
CW dowels	Yield moment (dowel bending)	1178.3 (68.0)	54	Scots pine (<i>Pinus sylvestris</i>)
	Cross-grain shear	1273.6 (104.3)		
CW plates	Embedment	1301.2 (95.2)	68	Western hemlock (<i>Tsuga heterophylla</i>)
	Three-point bending	1423.2 (33.8)		
		1400.0 (86.4)	60	Douglas fir (<i>Pseudotsuga menziesii</i>)
		1503.6 (86.4)	68	

Note: Standard deviations are within parentheses.

3.3.2 Hardwood

Commercially available uncompressed beech wood (*Fagus sylvatica*) dowels were chosen for comparison with CW dowels. The mean density of the beech wood dowels used for yield moment and cross-grain shear tests was 710.5 (standard deviation = 28.7) kg/m³ and 707.7 kg/m³ (standard deviation = 33.5), respectively. For the density measurement, specimens were oven-dried at 103 ± 2 °C until no significant change in weight was observed. The moisture content of specimens was determined according to EN 13183-1 [56].

3.3.3 Softwood

Irish grown Douglas fir was chosen for manufacturing of the structural elements for testing of the beam-beam and beam-column connections presented in Chapter 5 and Chapter 6. The mean density of the specimens was 572.1 kg/m³ (standard deviation = 57.0 kg/m³). For the density measurement, specimens were oven-dried at 103 ± 2 °C until no significant change in weight was observed. The moisture content of specimens was determined according to EN 13183-1 [56].

3.4 Test procedures

This section outlines the test procedures of embedment, yield moment, cross-grain shear and three-point bending tests. All the test specimens were conditioned for 30 days at a temperature of $20 \pm 2^\circ\text{C}$ and RH of $65 \pm 5\%$ before testing.

3.4.1 Embedment test

As discussed in Section 3.2, embedment strength (f_h) of the timber is important parameters to calculate the load-carrying capacity of the dowel-type timber connections. For this reason, the embedment strength of uncompressed Douglas fir and 68% radially compressed Western hemlock (CWH68) was examined parallel and perpendicular to the grain direction in accordance with EN 383 [182]. All tests were conducted using the same testing rig as shown in Figure 3.4. A gap of 1 mm was kept on each side between the side steel plates and faces of the specimens to avoid friction.

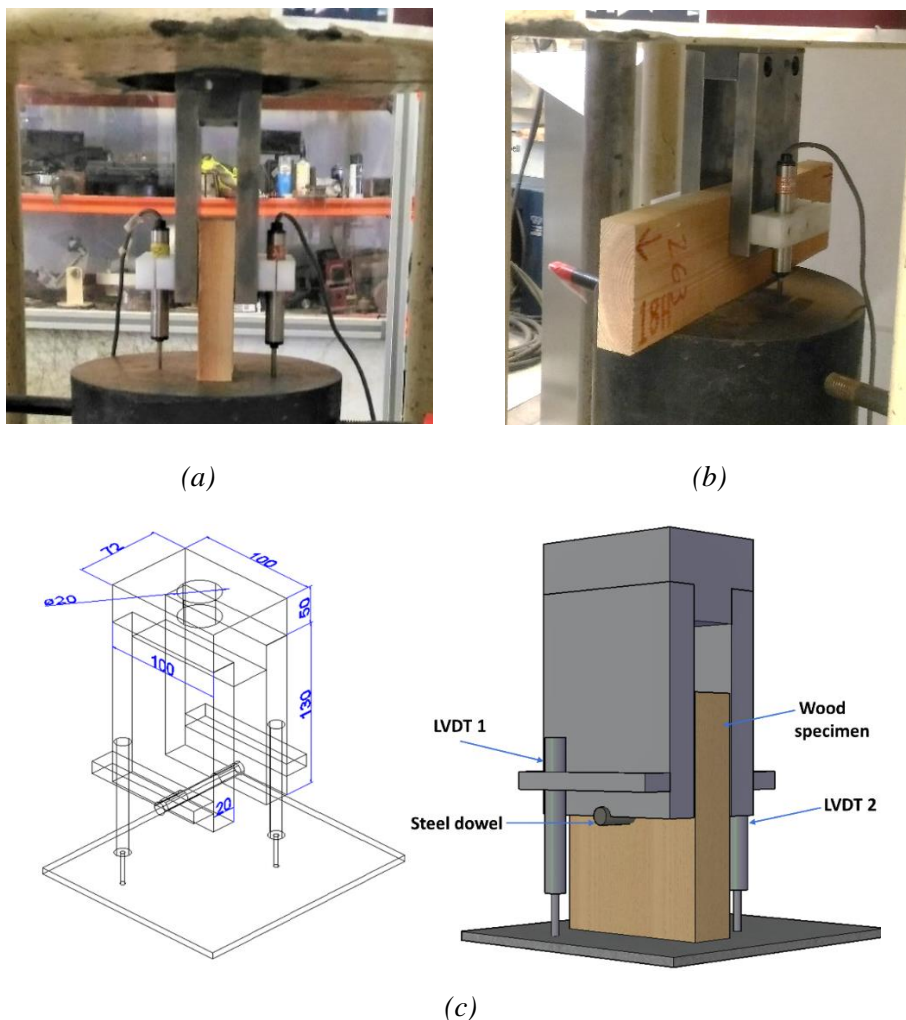


Figure 3.4- Embedment test set up, (a) parallel to the grain, (b) perpendicular to the grain and, (c) dimensions of the test rig (mm)

Table 3.3 shows the specification of the test specimens. The dimensions of uncompressed Douglas fir was based on EN 383 [182]. However, the dimensions of CW specimens had to be adapted due to the limited thickness and width of the CW material available.

Table 3.3- Dimensions of embedment test specimens

Material	Loading type and direction to the grain	Dimensions of the test specimen (l x w x t) in mm	Length of Dowel (mm)
Uncompressed Douglas fir	Compression parallel to grain ()	140 x 100 x 30	72 mm
	Compression perpendicular to grain (⊥)	400 x 100 x 30	
Compressed Western hemlock (CWH68)	Compression parallel to grain ()	140 x 50 x 20	62 mm
	Compression perpendicular to grain (⊥)	350 x 50 x 20	

A total of 50 tests were carried out. Tests were performed using a Denison model T42B, hydraulic testing machine rated to 500 kN, under load control mode. There were 2 linear variable displacement transformers (LVDTs) fixed on each side of the specimen to measure the relative displacement between the steel dowel and the base plate. The diameter of the dowel remained constant (10 mm) for both uncompressed Douglas fir and CWH68. A steel dowel of grade S275 was used for uncompressed Douglas fir. However, when S275 grade steel dowels were used for embedment test of CWH68, this resulted in bending failure of the dowel (see Figure 3.5) without attaining the maximum failure load or code specified displacement. As per EN 383 [182], the dowel must behave as a stiff linear fastener without bending during the test. Therefore, commercially available EN24T grade high tensile strength (850-1000 MPa) steel dowels were used for CWH68 to avoid bending of the dowel due to higher density of the CW material. Prior to testing, a calibration test was performed using a steel block and a steel dowel to measure the slack in the testing apparatus.



Figure 3.5- Deformation of S275 grade steel dowel

A block loading regime was programmed as per the standard EN 383 [182]. At first, specimens were loaded to 40% of the maximum estimated load and cross-head position was held for 30s. After this phase, specimens were unloaded to 10% of the maximum estimated load and the cross-head position was again maintained for 30 s. Finally, specimens were reloaded to failure or until the displacement reached 6.3 mm (5 mm displacement + 1.3 mm slack of the apparatus, as measured in the calibration test). The embedment strength is calculated by the following expression:

$$f_h = \frac{F_{max}}{dt} \quad Eq. 3.1$$

where,

f_h is the embedment strength (MPa),

F_{max} is the maximum load (N),

d is the diameter of the steel dowel (mm),

and t is the thickness of the test specimen (mm).

Also, stiffness characteristics of uncompressed Douglas fir and CWH68 were evaluated based on the slip modulus (K_{ser}) at serviceability limit state (SLS) using the following expression from EN 26891[183].

$$K_{ser} = \frac{3}{4} \frac{0.4F_{max}}{(v_{04} - v_{01})} \quad Eq. 3.2$$

where

F_{max} is the ultimate failure load/load corresponding to 6.3 mm displacement,

v_{04} and v_{01} represent the slip increment corresponding to load increment $0.1F_{max} - 0.4F_{max}$.

In EC 5 [55], the embedment strength of dowelled connections in parallel to the grain direction is determined according to the following expression:

$$f_{h,0,k} = 0.082 (1 - 0.01d)\rho_k \quad Eq. 3.3$$

where

$f_{h,0,k}$ is the characteristic embedment strength parallel to the grain (MPa),

d is the diameter of the dowel (mm),

ρ_k is the characteristic density of the timber (kg/m^3).

If $f_{h,0,k}$ is known, then embedment strength of a dowelled connection at an angle, α , to the grain direction can be calculated using the following expression [55]:

$$f_{h,\alpha,k} = \frac{f_{h,0,k}}{k_{90}\sin^2\alpha + \cos^2\alpha} \quad Eq. 3.4$$

where

k_{90} is the embedment factor which can be calculated using $k_{90} = 1.35 + 0.015d$ for softwoods and $k_{90} = 0.90 + 0.015d$ for hardwoods.

3.4.2 Yield moment of dowels test

As discussed in Section 3.2, the yield moment capacity ($M_{y,Rk}$) of steel dowels is a necessary parameter to determine the load-carrying capacity of a timber-timber connection using the European Yield Model (EYM) equations. The yield moment capacity of steel dowels can be determined by four-point bending tests in accordance with EN 409 [184]. However, there is no standard to calculate the yield moment ($M_{y,Rk}$) of CW dowels. Metallic dowels have higher shear strength and stiffness compared to CW dowels; thus, bending is the dominant failure mode. The tests results (discussed in detail in Chapter 5) on the evaluation of the structural behaviour of CW dowels in semi-rigid type beam-beam moment connections showed that CW dowels exhibit interlaminar shear failure along the length of the dowel between the interphase of latewood and earlywood which is not the case for steel dowels [2]. This kind of behaviour is also reported for glass fibre reinforced polymer (GFRP) and bamboo composite dowels [21,185]. Therefore, EN 409 may not be suitable for the calculation of $M_{y,Rk}$ of CW dowels.

In order to replicate the interlaminar shear failure in the material characterisation tests, the short beam approach described in ASTM D4475 [186] was adopted for the testing. In this test, $M_{y,Rk}$ of CW dowels was calculated using the Eq. 3.5 [185]. For comparison, tests were carried out on commercially available beech wood dowels. All the dowels (CW and beech wood) were tested under a shear load at varying angles ($0^\circ, 45^\circ$ and 90°) to the growth rings. Figure 3.6 shows the specification of the test set up. The dowel length (90 mm) and diameter (10 mm) were kept constant. Tests were performed using an Instron 30 kN machine, under displacement control mode. A constant displacement at the rate of 0.4 mm/min was applied so that failure was reached within $300 \text{ s} \pm 120 \text{ s}$, as per EN 383 [182]. The ram displacement and load were recorded continuously.

$$M_{y,eff} = \frac{3}{8} \cdot F_y \cdot d \quad \text{Eq. 3.5}$$

where F_y is the yield load (N) and d is the dowel diameter (mm).

Ductility was determined using the following expression as per EN12512 [187]. Here, the ultimate displacement was taken at a load level of $0.8F_{max}$.

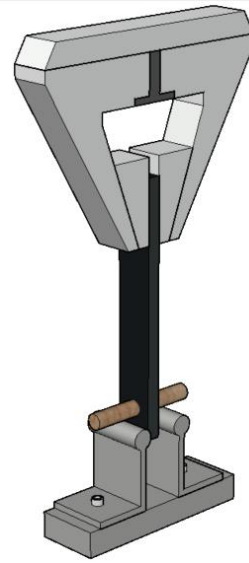
$$D = \frac{V_u}{V_y} \quad \text{Eq. 3.6}$$

where,

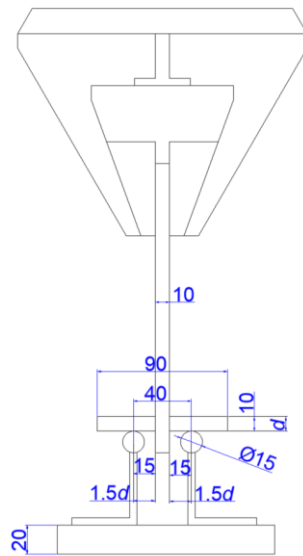
D is the ductility,

V_u is the Ultimate displacement was taken at a load level of $0.8 F_{max}$,

and V_y is the displacement at yield load.



(a)



(b)



0°



90°



45°

(c)

Figure 3.6- Yield moment tests, (a) test set up, (b) geometry of the test set up, and (c) load direction

3.4.3 Cross-grain shear test

As discussed in Section 3.2, wooden dowels can exhibit cross-grain shear failure when used as a shear connector in the dowel-type connections with multiple shear planes. In case of such failure, the load-carrying capacity of the connection is limited by the cross-grain shear strength of the dowel. For this reason, a shear test was conducted to determine the cross-grain shear strength of the CW dowels. The EC 5 does not have any symbol for cross-grain strength of the dowels. In this thesis, cross grain shear strength of the dowels is indicated as f_{sp} . The tests were conducted using a purpose-made device, which comprised two steel support plates fixed 85 mm apart as shown in Figure 3.7a. These plates have round holes of (10.1 mm diameter)

for insertion of the dowels. The dowels were loaded via an 84.5 mm long semi-cylindrical loading head with a central semi-circular groove of 10.1 mm diameter to accommodate the dowel. The groove acts as a support throughout the length of the dowel and prevents it from failing in bending during the test. The apparatus was loaded in compression to apply a shear force on two bearing cross-sections. All the dowels (CW and beech wood) were subjected to a shear load parallel and perpendicular to the growth rings and the obtained test results were compared. Figure 3.7b and Figure 3.7c show the dimensions of the testing apparatus and the dowel fibre orientation compared to the loading direction, respectively. Tests were performed using an Instron 30 kN machine, under displacement control mode. A constant displacement at the rate of 0.7 mm/min was applied so that failure was reached within $300 \text{ s} \pm 120 \text{ s}$ as per EN 383 [182]. The cross-grain shear strength (in double Shear) was calculated using the following formula.

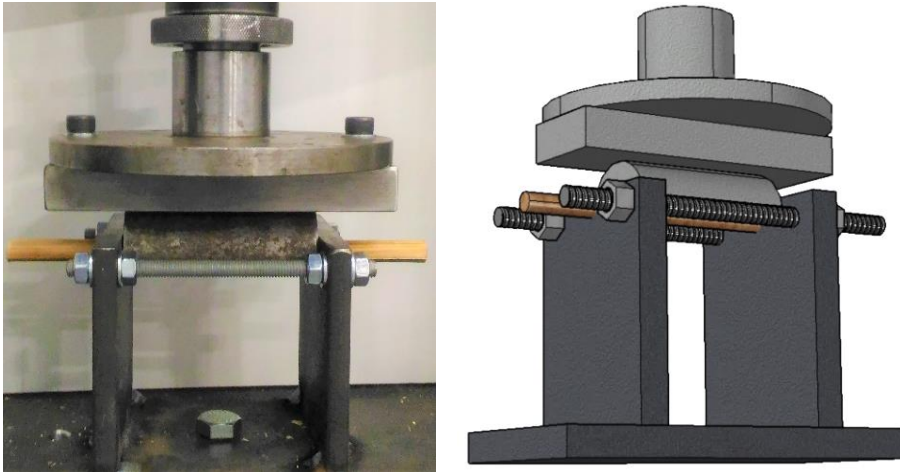
$$f_{sp} = \frac{F_{max}}{2\pi r^2} \quad \text{Eq. 3.7}$$

where

f_{sp} is the cross-grain shear stress per shear plane (MPa),

F_{max} is the maximum load (N),

and r is the dowel radius (mm).



(a)

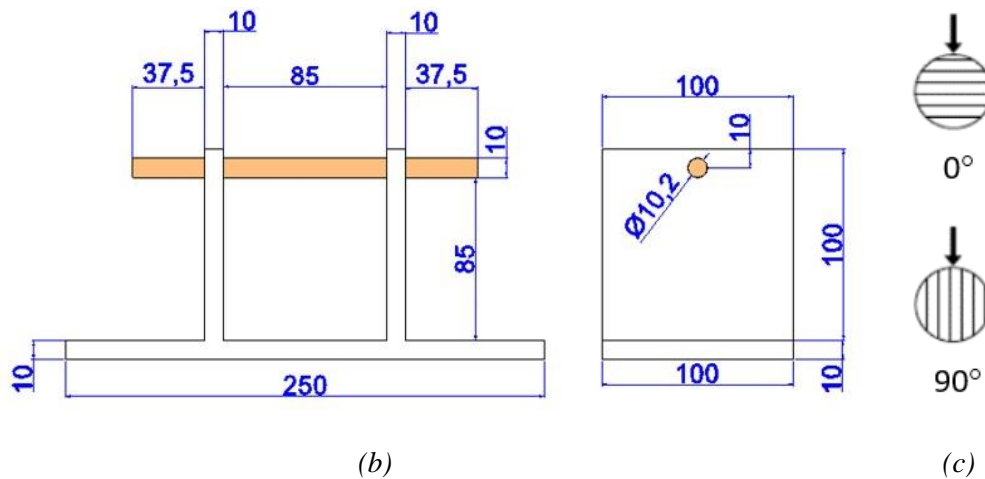


Figure 3.7- Shear test set up, (a) testing rig, (b) rig dimensions, and (c) loading direction (in mm)

3.4.4 Three-point bending test

In this experiment, the strength and stiffness of the CW were evaluated by a three-point bending test in accordance with BS 373 [188]. The main objective of the test was to evaluate the strength and stiffness properties of three different CW materials to select one representative type to be used in the connection plates in the structural testing presented in Chapter 5 and Chapter 6. This experiment involves CW specimens of Western hemlock (CWH68) with 68% CR and Douglas fir with two different CRs of 60% (CDF 60) and 68% (CDF68). A total of 15 specimens (5 replications of each material) were tested in the tangential direction (edgewise). This direction was chosen as this is the direction in which the plates are loaded in the connections. The dimension of each specimen were 300 mm (L) x 20 mm (W) x 20 mm. Tests were performed using a 10 kN Instron machine under displacement control mode at a constant displacement rate of 6.6 mm/min using the test set up as shown in Figure 3.8.

The load and corresponding midspan displacement were continuously recorded during the test. The bending strength and MOE were calculated using the following expressions.

$$f_m = \frac{3FL}{2bh^2} \quad \text{Eq. 3.8}$$

$$E = \frac{(F_{40} - F_{20})L^3}{4(\Delta_{40} - \Delta_{20})bh^3} \quad \text{Eq. 3.9}$$

where

f_m is the bending strength (MPa),

E is the modulus of elasticity (MPa),

F is the maximum load (N),
 F_{20} is the 20 % of maximum load (N),
 F_{40} is the 40% of maximum load (N),
 L is the span of the specimen (mm),
 b is the width of the specimen (mm),
 h is the height of the specimen (mm),
 Δ_{40} is the displacement corresponding to 40% load (mm),
 and Δ_{20} is the displacement corresponding to 20% load (mm).

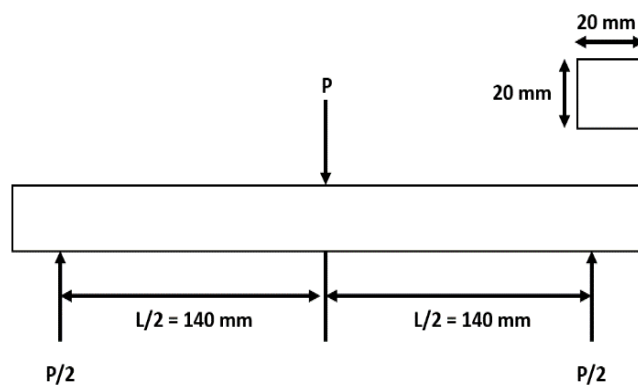
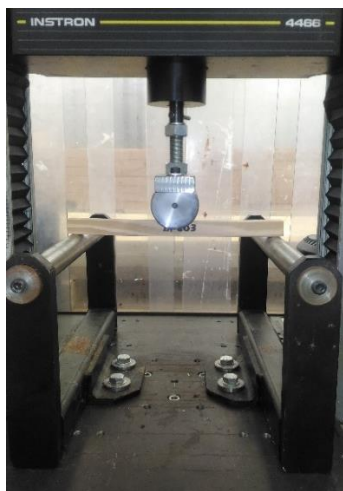


Figure 3.8- Bending test set up and specimen geometry

3.5 Test results and discussion

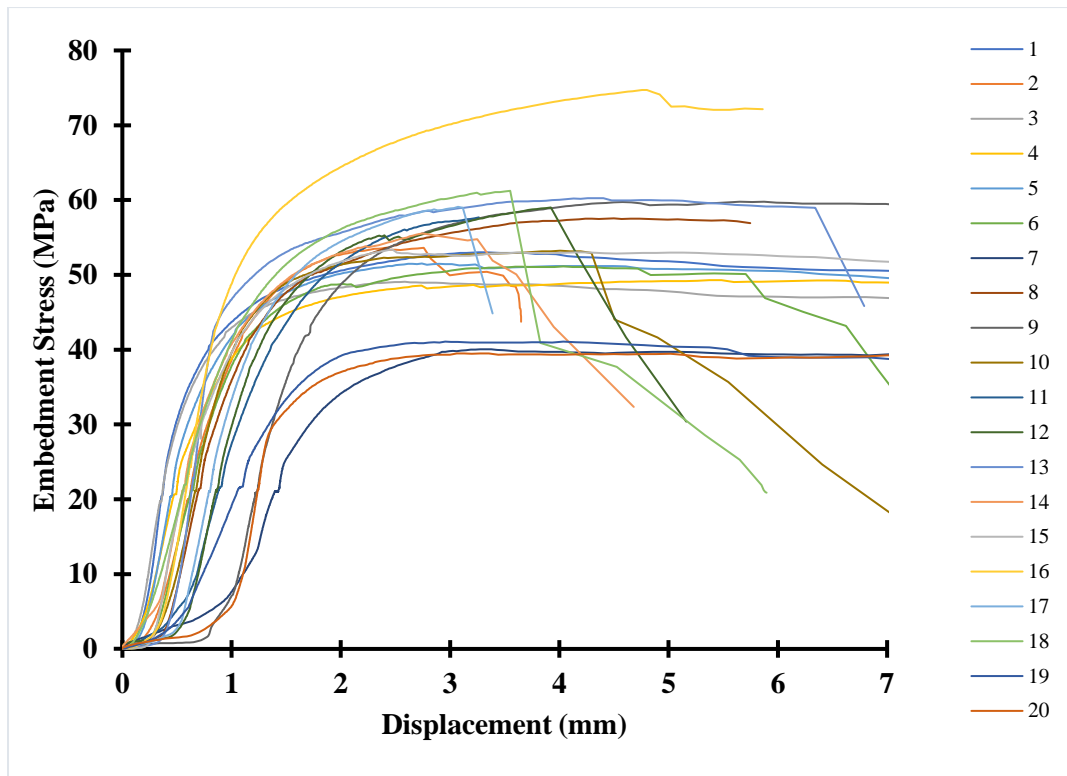
This section describes the test results of all material characterisation tests. Experimental test results were also compared with the results calculated using relevant empirical formulas given in EC 5. In addition to this, obtained test results were compared with available literature.

3.5.1 Embedment test results

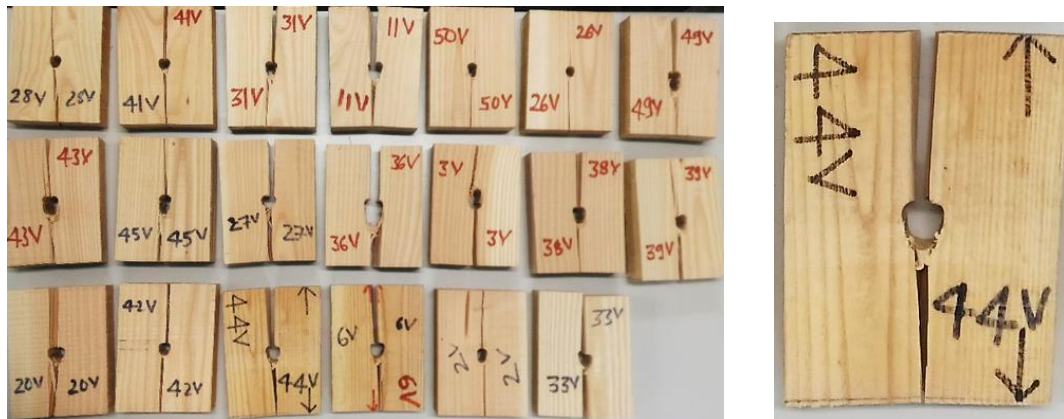
3.5.1.1 Embedment stress – displacement graph and failure modes

3.5.1.1.1 Uncompressed Douglas fir– parallel to the grain

Figure 3.9a shows the embedment stress-displacement graphs for the twenty uncompressed Douglas fir specimens that were tested in the parallel to the grain direction. The parallel to grain embedment tests were characterised by embedment stress-dowel displacement curves with an embedment stress plateau. The stress plateau is followed by an abrupt failure due to the initiation of a crack starting from the dowel hole which subsequently resulted in the collapse of the specimens. Figure 3.9b shows the failure modes of specimens tested parallel to the grain.



(a)



(b)

Figure 3.9- Uncompressed Douglas fir – parallel to the grain, (a) embedment stress-displacement graph, and (b) failure modes of the tested specimens with a close-up view showing typical failure

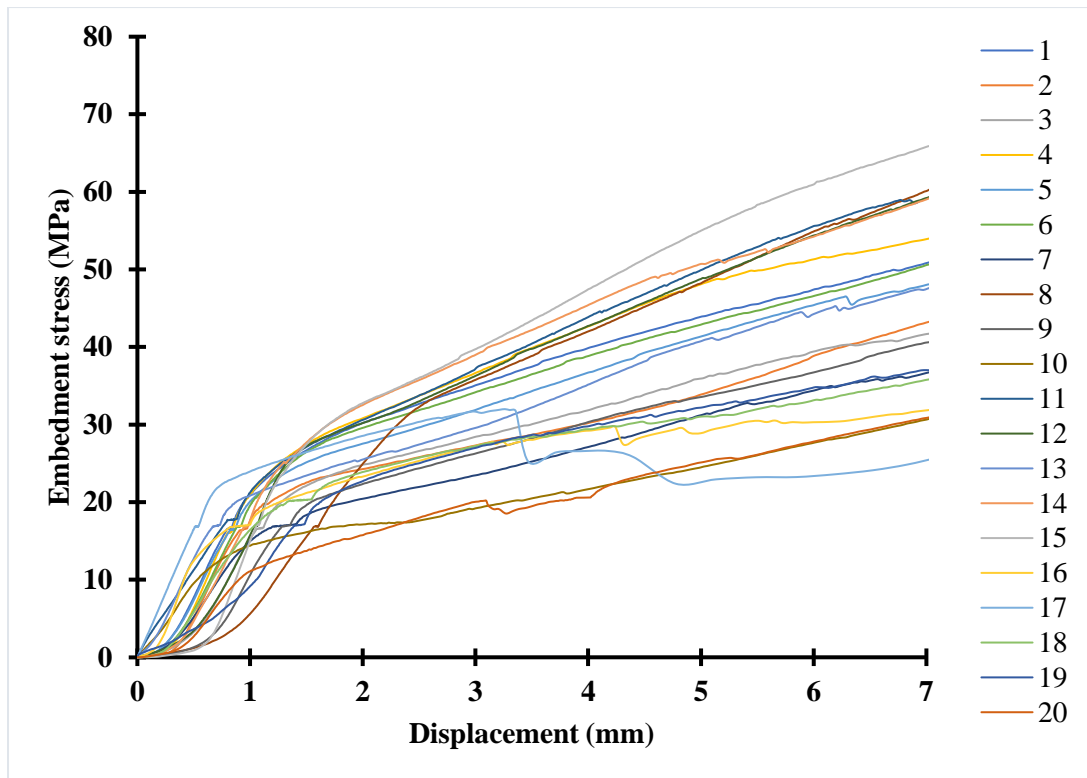
Table 3.4 shows the test results of individual specimens of the uncompressed Douglas fir tested in parallel to the grain direction. The embedment strength and slip modulus were determined using Equation (3.1) and (3.2), respectively. Characteristic values for density and strength are the 5th percentile values and were calculated in accordance with EN 14358 [189]. The characteristic slip modulus is the mean value. The mean and characteristic embedment strength of uncompressed Douglas fir specimens tested in parallel to the grain direction were 54.0 MPa and 37.4 MPa, respectively, and the slip modulus was 18.4 kN/mm.

Table 3.4- Results of individual specimens of the uncompressed Douglas fir tested in parallel to the grain direction

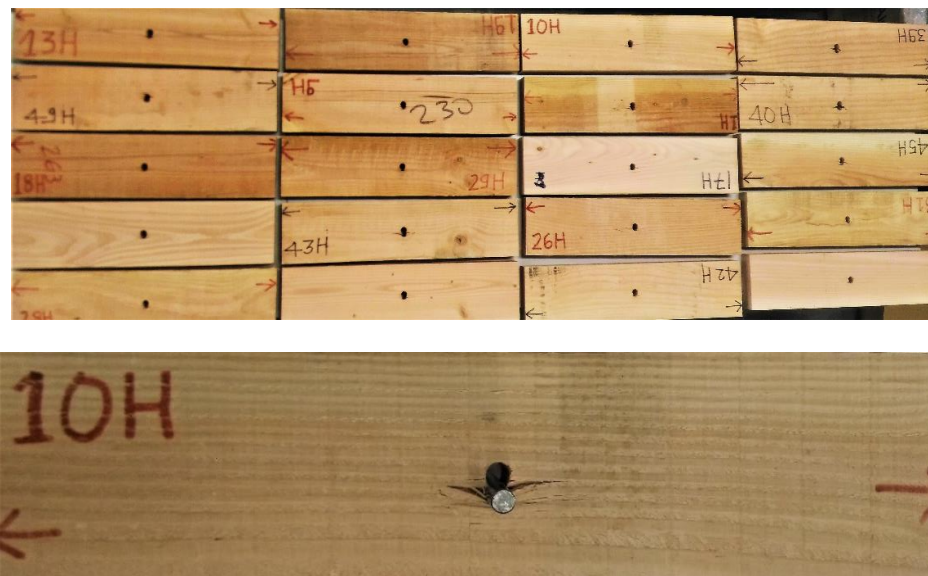
Uncompressed Douglas fir (parallel to the grain)			
Specimen	Oven-dry density (kg/m ³)	Embedment strength (MPa)	Slip modulus (kN/mm)
1	554.8	53.0	28.8
2	557.6	53.6	16.7
3	564.3	49.1	24.0
4	554.5	49.3	16.3
5	549.0	51.5	21.5
6	557.4	51.1	16.5
7	482.6	40.1	6.2
8	611.4	57.5	19.5
9	636.9	59.8	16.5
10	595.2	53.2	17.6
11	598.3	57.7	13.2
12	598.1	59.0	19.8
13	571.4	60.2	28.7
14	595.5	55.5	18.8
15	549.8	53.4	20.4
16	707.6	74.7	26.2
17	638.1	59.1	21.3
18	627.4	61.2	16.0
19	514.8	41.1	9.1
20	511.9	39.6	11.1
Mean	578.8	54.0	18.4
Standard deviation	50.1	8.2	5.9
Characteristic value	482.2	37.4	18.4

3.5.1.1.2 Uncompressed Douglas fir – perpendicular to the grain

Figure 3.10a shows the embedment stress-displacement graphs for the twenty Douglas fir specimens tested in the perpendicular to the grain direction. The perpendicular to grain embedment tests exhibited monotonically increasing load beyond the proportional limit. The crushing of wood fibres beneath the dowel results in localised densification of the wood in the contact area which induces a hardening response. This hardening response was not observed in parallel to the grain direction. The maximum embedment stress was that corresponding to the 6.3 mm dowel displacement. Figure 3.10b shows the failure modes of specimens tested perpendicular to the grain.



(a)



(b)

Figure 3.10- Uncompressed Douglas fir – perpendicular to the grain, (a) Embedment stress-displacement graph, and (b) failure modes of the tested specimens with a close-up view showing typical failure

Table 3.5 shows the test results of individual specimens of the uncompressed Douglas fir tested in perpendicular to the grain direction. The embedment strength and slip modulus were determined using Equation (3.1) and (3.2), respectively. Characteristic values for density and strength are the 5th percentile values and were calculated in accordance with EN 14358 [189].

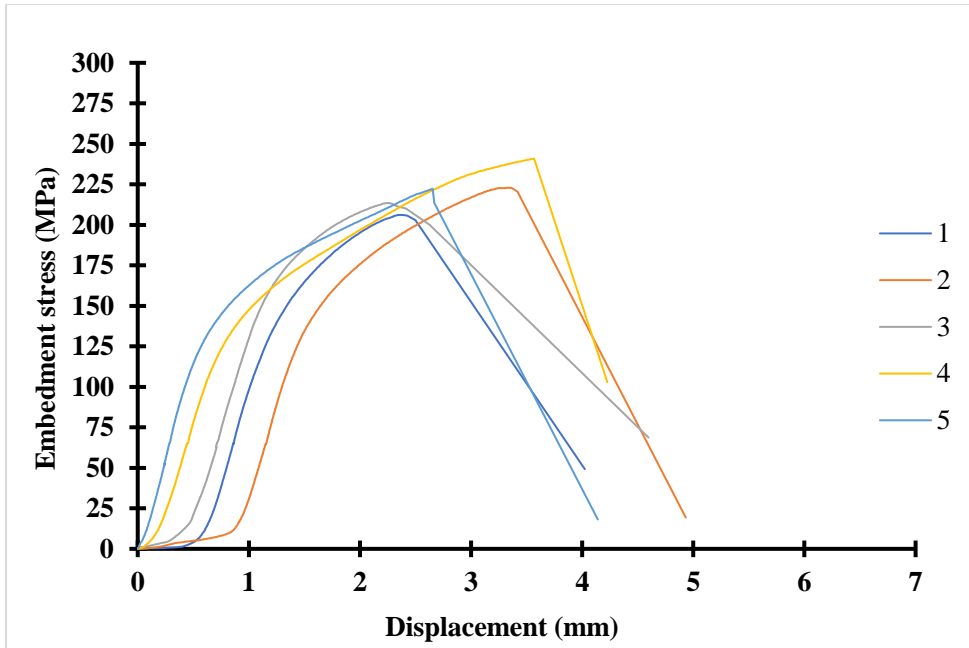
The characteristic slip modulus is the mean value. The mean and characteristic embedment strength of uncompressed Douglas fir specimens tested in perpendicular to the grain direction were 43.0 MPa and 21.9 MPa, respectively, and the slip modulus was 6.2 kN/mm.

Table 3.5- Results of individual specimens of the uncompressed Douglas fir tested in perpendicular to the grain direction

Uncompressed Douglas fir (perpendicular to the grain)			
Specimen	Oven-dry density (kg/m ³)	Embedment strength (MPa)	Slip modulus (kN/mm)
1	595.8	48.4	8.1
2	604.6	40.2	7.2
3	599.3	40.3	6.5
4	599.2	52.0	8.9
5	592.9	45.5	7.4
6	591.7	47.7	8.4
7	536.8	35.3	3.6
8	635.3	56.4	5.9
9	584.9	37.9	6.0
10	523.9	28.5	5.8
11	586.7	57.1	5.4
12	586.7	55.9	9.5
13	578.3	44.9	7.8
14	636.1	55.7	8.1
15	634.2	62.6	8.9
16	438.2	30.6	4.2
17	447.5	24.1	6.9
18	520.4	33.8	3.1
19	581.2	35.3	1.9
20	433.0	28.9	0.8
Mean	565.3	43.0	6.2
Standard deviation	62.7	11.2	2.4
Characteristic value	444.3	21.9	6.2

3.5.1.1.3 Compressed Western hemlock plates (CWH68) – parallel to the grain

Figure 3.11a shows the embedment stress-displacement behaviour for the five 68% radially CWH68 plates tested in the parallel to the grain direction. At the initiation of the elastic phase, a relatively flexible stage was observed due to the non-uniform contact between the dowel and CW plates, which resulted in a rapid localised deformation. Once the contact is uniform across the thickness of the CW plate, an increase was observed in the embedment stress, which was directly proportional to the dowel displacement until the yield point. In contrast to the uncompressed Douglas fir tested in parallel to grain direction, CWH68 specimens showed a brittle failure once the maximum embedment load was attained. Figure 3.11b shows failure modes of specimens tested parallel to the grain.



(a)



(b)

Figure 3.11- Compressed Western hemlock (CWH68) – parallel to the grain, (a) embedment stress-displacement graph, and (b) failure modes of the specimens (specimens 1 to 5 are shown in sequence)

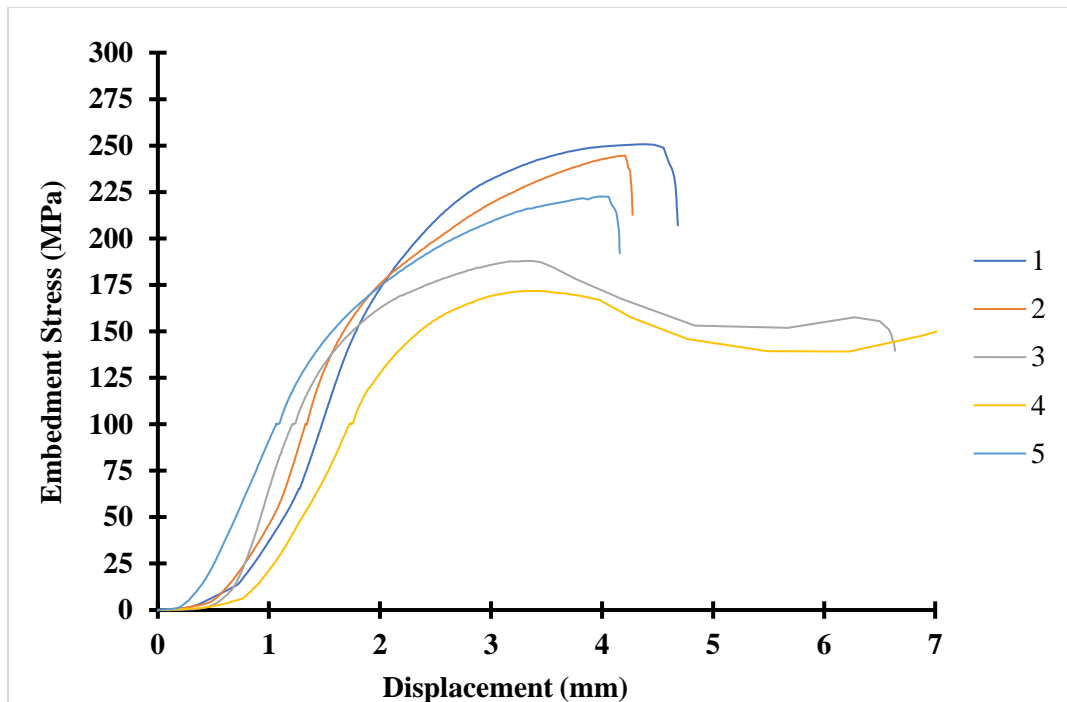
Table 3.6 shows the test results of individual specimens of the CWH68 tested in parallel to the grain direction. The embedment strength and slip modulus were determined using Equation (3.1) and (3.2), respectively. Characteristic values for density and strength are the 5th percentile values and were calculated in accordance with EN 14358 [189]. The characteristic slip modulus is the mean value. The mean and characteristic embedment strength of CWH68 specimens tested in parallel to the grain direction were 221.1 MPa and 189.1 MPa, respectively, and the slip modulus was 41.2 kN/mm.

Table 3.6- Results of individual specimens of the CHW68 tested in parallel to the grain direction

Compressed Western hemlock (parallel to the grain)			
Specimen	Oven -dry density (kg/m ³)	Embedment strength (MPa)	Slip modulus (kN/mm)
1	1138.9	206.1	47.0
2	1333.3	222.9	18.0
3	1194.4	213.5	43.3
4	1222.2	240.8	44.0
5	1305.6	222.3	53.8
Mean	1238.9	221.1	41.2
Standard deviation	80.0	13.0	13.6
Characteristic value	1042.0	189.1	41.2

3.5.1.1.4 Compressed Western hemlock plates (CWH68) – perpendicular to the grain

Figure 3.12a shows the embedment stress-displacement behaviour of the five 68% radially compressed CWH68 plates tested in the perpendicular to the grain direction. Similar to the CW specimens tested in the parallel to grain direction, the specimens of this category also showed a relatively flexible behaviour initially due to non-uniform contact between the dowel and CW plates. Once the contact is uniform across the thickness of the CW plate, an increase was observed in the embedment stress, which was directly proportional to the dowel displacement until the yield point. After the yield load, there was a rapid increase in the deformation. However, bending of the dowel was observed in the samples almost after 3 mm of dowel displacement. Thus, the test was stopped, and the peak value of the load was taken for measurement of the embedment strength. Figure 3.12b shows failure modes of the tested specimens with localised crushing perpendicular to the grain without longitudinal splitting of the specimens.



(a)



(b)

Figure 3.12- Compressed Western hemlock (CWH68) – perpendicular to the grain, (a) embedment stress-displacement graph, and (b) failure modes of the tested specimens with a close-up view showing typical failure

Table 3.7 shows the test results of individual specimens of the CWH68 tested in perpendicular to the grain direction. The embedment strength and slip modulus were determined using Equation (3.1) and (3.2), respectively. Characteristic values for density and strength are the 5th percentile values and were calculated in accordance with EN 14358 [189]. The

characteristic slip modulus is the mean value. The mean and characteristic embedment strength of CWH68 specimens tested in perpendicular to the grain direction were 218.9 MPa and 142.3 MPa, respectively, and the slip modulus was 26.6 kN/mm.

Table 3.7- Result of individual specimens of the CWH68 tested in perpendicular to the grain direction

Compressed Western hemlock (perpendicular to the grain)			
Specimen	Oven-dry density (kg/m ³)	Embedment strength (MPa)	Slip modulus (kN/mm)
1	1392.9	250.7	24.7
2	1404.8	244.7	26.1
3	1250.0	187.9	36.0
4	1392.9	184.9	19.8
5	1381.0	222.6	26.5
Mean	1364	218.1	26.6
Standard deviation	64.4	30.9	5.9
Characteristic value	1205.8	142.3	26.6

3.5.1.1.5 Characteristic embedment strength properties from test data and EC 5

Design of dowel-type connections in accordance with EC 5 is based on characteristic (5th percentile) embedment strength values. The standard provides empirical expressions for the embedment strength parallel and perpendicular to the grain (Equations (3.3) and (3.4)) based on the characteristic density and dowel diameter. In order to investigate the suitability of these expressions for use in the current study, characteristic values of the experimental embedment strength ($f_{h,k}$) for uncompressed and compressed wood are compared with those determined using the EC 5 equations. Table 3.8 shows a comparison of the embedment strength of uncompressed Douglas fir and compressed Western hemlock, CWH68. Results show that the characteristic embedment strength of CWH68 specimens tested parallel to the grain direction was 405.6% higher than that of uncompressed Douglas fir specimens tested in a similar direction. Similarly, the mean embedment strength of CWH68 specimens tested perpendicular to the grain was 549.7 % higher than that of uncompressed Douglas fir specimens. Compared to uncompressed wood the embedment strength of CW seems to be less affected by load direction which may be attributed to the less variability of density distribution in all principal directions. However, this needs to be validated with larger sample size.

Table 3.8- Comparison between characteristic embedment strength of uncompressed Douglas fir and compressed Western hemlock (CWH68) from experiments and EC 5 values (MPa)

	Douglas fir Uncompressed loaded		Compressed Western hemlock loaded	
	parallel to the grain direction ()	perpendicular to the grain direction (⊥)	parallel to the grain direction ()	perpendicular to the grain direction (⊥)
Experimental results	37.4	21.9	189.1	142.3
EC 5 expressions	35.6	25.4	76.9	54.9

The EC 5 expressions give reasonable approximations for the uncompressed softwood material. However, these significantly underestimate the embedment strength of the CW material. The embedment strength of the CW is underestimated by 59.3% and 45.9% in the parallel and perpendicular to the grain directions, respectively. Thus, new equations will have to be developed to estimate the embedment strength of CW. In this study, only five replications of CW were tested in each direction and additional testing is required to derive a suitable equation to determine the embedment strength of CW. For design of timber-CW connections, the characteristic value of the embedment strength of CW from the experiments can be utilised as a conservative value. Additionally, as the embedment strength of uncompressed wood is significantly lower, this study concluded that the embedment strength of CW is unlikely to be a critical factor for designing timber-CW connections.

3.5.1.1.6 Comparison of embedment strength of CW specimens with literature

A comparison between experimentally-determined embedment strength values for CW and equivalent high density bio-based material reported in the literature [21,22,25,177,190–192] is presented in Figure 3.13. To allow the comparison, embedment strength data for wood and bamboo-based material with a density greater than or equal to 900 kg/m³ was collected irrespective of the wood species, testing standard, dowel diameter, type of loading (tension or compression), end distances, edge spacing and manufacturing process.

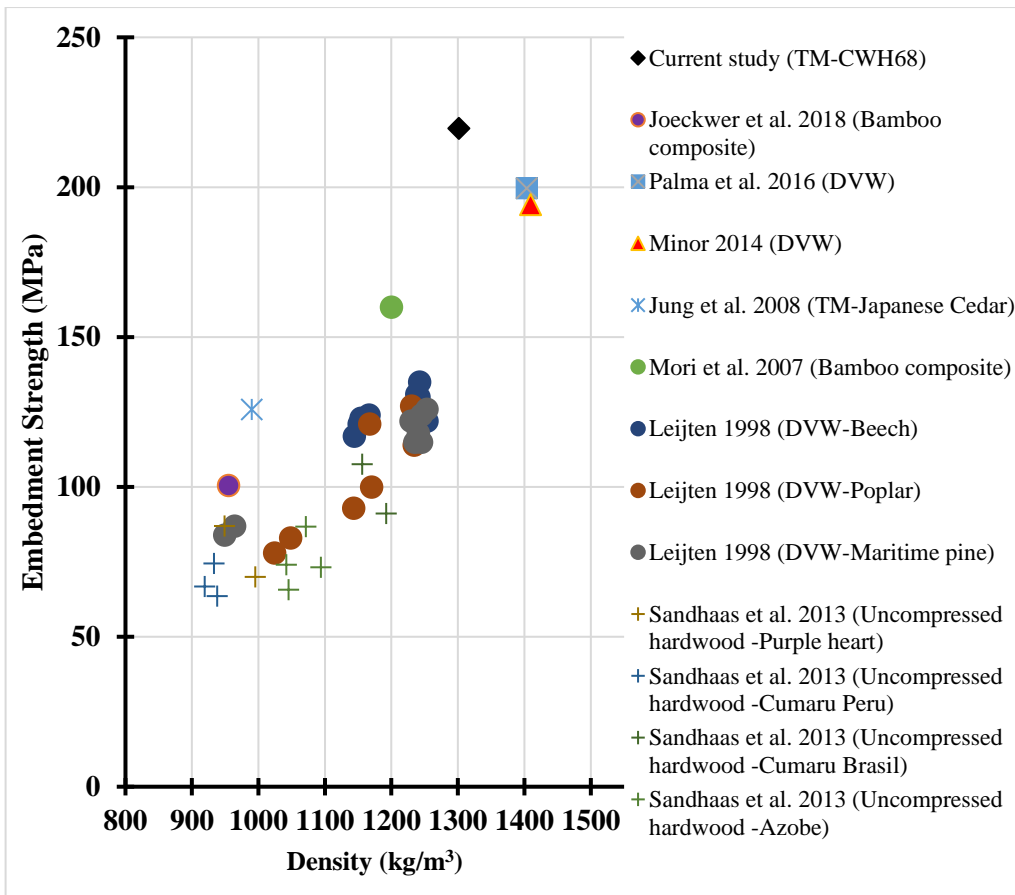


Figure 3.13- Embedment strength comparison of CW between mean values of experimental results and existing literature (TM – Thermo-mechanically densified wood, DVW- Densified Veneer Wood)

The comparison shows that the experimental results are in line with existing research on the embedment strength of high-density wood/bamboo-based material. Based on the results, it can be concluded that the embedment strength of wood is significantly improved by an increase in the density through the densification process and other wood modification techniques. It is also observed that the embedment strength of adhesive-free thermo-mechanically (TM) densified wood is approximately equal to the densified veneer wood (DVW) produced using synthetic adhesives. Thus, TM densified wood may potentially be utilised in similar applications to DVW i.e. reinforcement material in the moment-resisting timber-timber connections.

3.5.2 Yield moment of dowels test results

3.5.2.1 Load – displacement behaviour and failure modes of CW and beech wood dowels

Figure 3.14 shows the load vs. mid-span displacement graph for all the tested specimens with solid lines for the CW dowels and dashed lines for the beech wood dowels. CW dowels loaded at in tangential direction (CW_T) showed a sudden failure once the maximum load was attained. In contrary to this, the CW dowels loaded in the radial direction and at 45° angle (CW_F) to the growth rings showed a greater plastic behaviour beyond the yield load. There

was a gradual decline in the load capacity with a continuous increase in the midspan-displacement due to interlaminar shear failure along with the growth rings (see Figure 3.15) and formation of partial plastic hinges (see Figure 3.16) in the dowels.

All beech wood dowels demonstrated lower stiffness behaviour when compared to the CW dowels. The load-displacement behaviour of all the beech wood dowels followed a similar curve irrespective of the orientation of growth rings to the loading direction. Once the yield load was attained, a gradual increase in the midspan-displacement was observed without any significant increase in the load capacity. Once the maximum load was attained, all dowels showed a sudden decline in the load capacity followed by tension failure in the bottom side of the dowels as shown in Figure 3.17. It should be noted here that indentation of the dowels by the loading head was observed for the beech wood dowels whereas there was no such deformation on compressed wood dowels. Therefore, the results for beech wood dowels should be considered conservative.

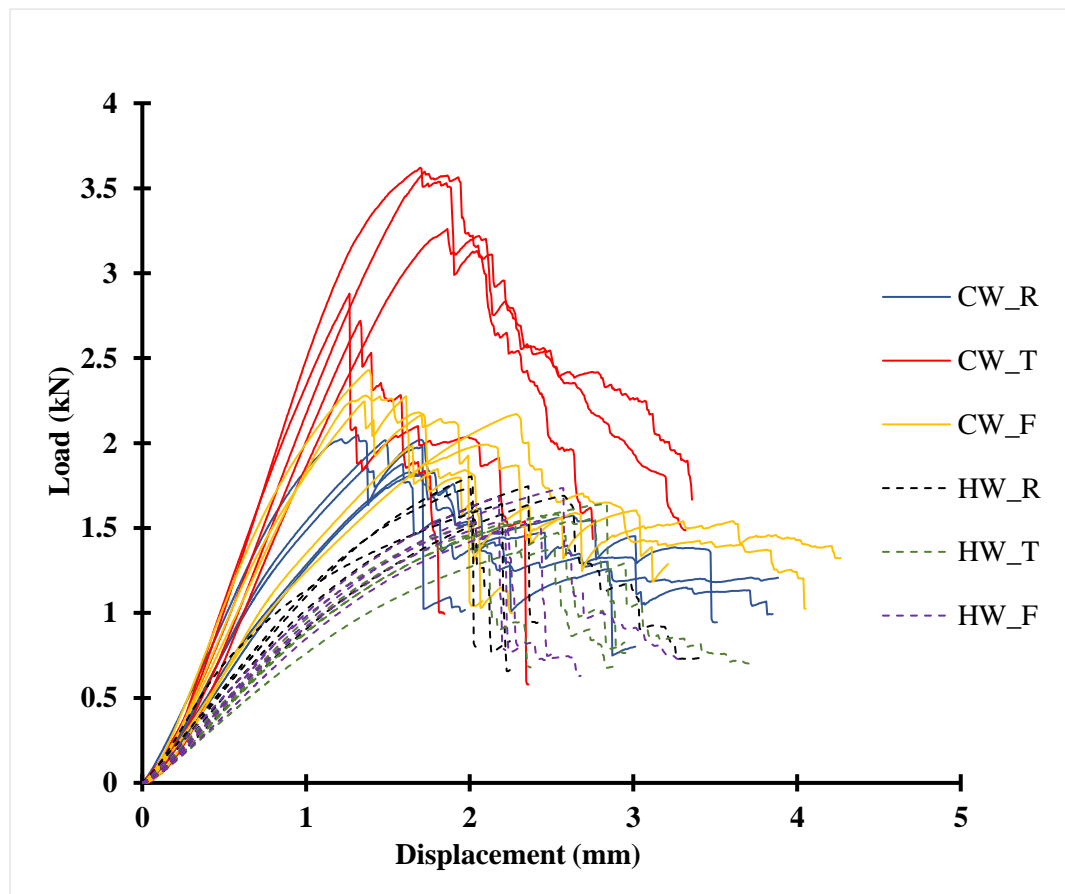


Figure 3.14- Load-displacement behaviour of CW and beech wood dowels (CW_R = CW dowels tested at 0° angle to load; CW_T = CW dowels tested at 90° angle to load; CW_F = CW dowels tested at 45° angle to load; HW_R = beech wood dowel tested at 0° angle to load; HW_T = beech wood dowel tested at 90° angle to load; HW_F = beech wood dowel tested at 45° angle to load)

Failure modes during the testing were one of the following:

1. **Interlaminar shear:** This failure mode describes a shear “delamination” along the specimen length and parallel to a growth rings as shown in Figure 3.15.



Figure 3.15- Interlaminar shear failure of CW dowels

2. **Interlaminar shear and bending:** This failure is a combination of (1) and tensile failure with the formation of plastic hinges at midspan and/or over the supports as shown in Figure 3.16. Interlaminar shear failure was observed on the cross-section of the dowels as shown in Figure 3.15.

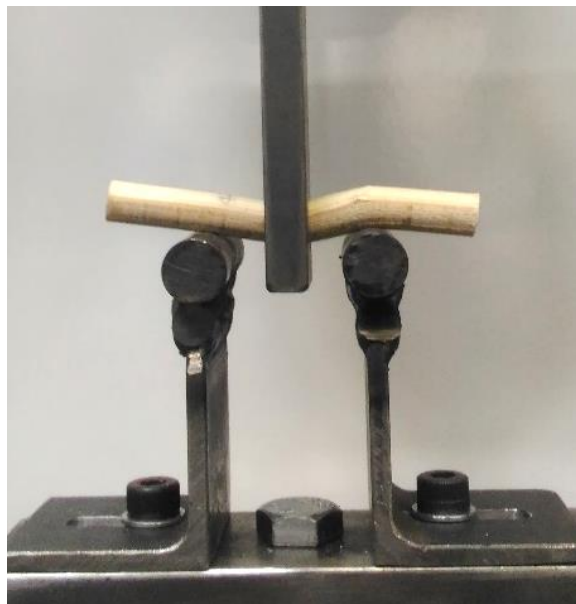


Figure 3.16- Formation of plastic hinges at midspan and over the supports

3. **Bending:** Tensile failure at the midspan on the bottom surface as shown in Figure 3.17.



Figure 3.17- Tensile failure at the midspan

Figure 3.18 shows failure modes of all the tested specimens.

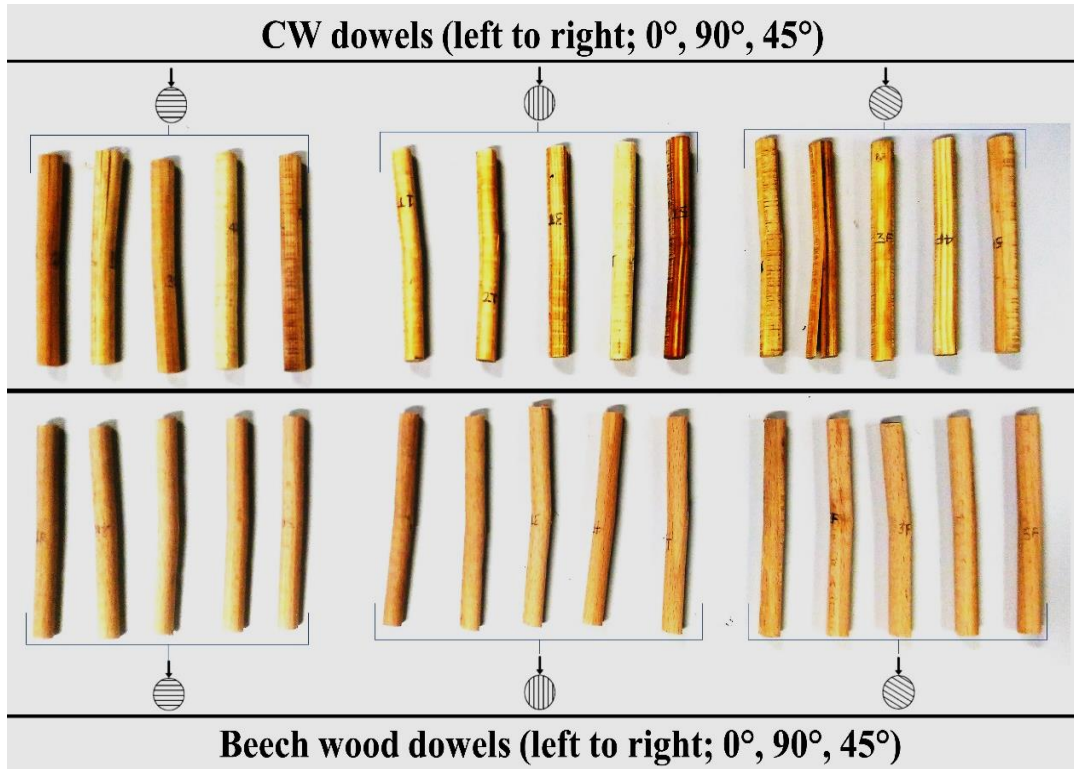


Figure 3.18- Failure modes of the tested specimens

3.5.2.2 Comparison between experimental yield moment capacity of CW and beech wood dowels

Table 3.9 shows the yield moment test results of CW dowels tested at 0° (CW_R), 45° (CW_F) and 90° (CW_T). The mean yield moment capacities of the CW dowels tested at 0°, 45° and 90° were 6686.3 Nmm, 7870.1 Nmm and 11807.1 Nmm, respectively. The characteristic yield moment capacities of the CW dowels tested at 0°, 45° and 90° were 5815.3 Nmm, 6252.4 Nmm and 8351.6 Nmm, respectively. The mean yield moment capacity of CW dowels tested at 90° was approximately 76% and 50% higher than the specimens tested at 0° and 45° directions, respectively. The mean ductility ratio of CW specimens tested at 0°, 45° and 90° were 1.6, 1.7 and 1.2, respectively. The dominant failure mode of CW dowels tested at 0° and 45° was interlaminar shear, whereas this was bending and interlaminar shear for specimens tested at 90°. This may be due to a reduction in interlaminar shear strength of CW caused as a result of densification process. When load is applied at 0° and 45°, the relative slip between

earlywood and latewood is easier due to lower interlaminar shear strength when compared to specimens those are loaded at 90°.

Table 3.9- Yield moment test results for CW dowels

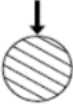
Compressed wood dowels						
Sample ID	Load direction	Oven-dry density (kg/m ³)	Moisture content (%)	Yield Moment (Nmm)	Ductility ratio	Failure mode
1CW_R		1133.2	5.5	6831.0	1.9	Interlaminar shear
2CW_R		1155.8	5.5	6410.6	1.7	Interlaminar shear
3CW_R		1084.6	5.2	6466.4	1.6	Interlaminar shear
4CW_R		1158.4	5.6	6478.0	1.7	Bending
5CW_R		1296.5	4.8	7245.5	1.4	Interlaminar shear
Mean			1165.7	5.3	6686.3	1.7
Standard deviation		78.9	0.3	354.1	0.2	
Characteristic values as per EN 14358 [189]				5815.3		
1CW_F		1134.5	5.4	7379.4	1.7	Bending
2CW_F		1203.1	6.1	8006.0	1.8	Interlaminar shear
3CW_F		1168.9	5.3	7018.9	1.7	Interlaminar shear
4CW_F		1219.5	6.0	8376.4	1.6	Interlaminar shear
5CW_F		1214.0	6.0	8569.8	1.9	Interlaminar shear
Mean			1188.0	5.8	7870.1	1.7
Standard deviation		35.8	0.4	657.6	0.1	
Characteristic values as per EN 14358 [189]				6252.4		
1CW_T		1164.9	5.6	13359.4	1.4	Bending
2CW_T		1186.1	4.9	13046.0	1.5	Bending
3CW_T		1089.6	5.1	10260.0	0.8	Bending and interlaminar shear
4CW_T		1134.2	5.6	11809.9	1.5	Bending and interlaminar shear
5CW_T		1331.2	4.8	10560.2	0.9	Bending and interlaminar shear
Mean			1181.2	5.2	11807.1	1.2
Standard deviation		91.4	0.3	1404.7	0.4	
Characteristic values as per EN 14358 [189]				8315.6		

Table 3.10 shows the yield moment test results of beech wood dowels tested at 0° (HW_R/ radial direction),45° (HW_F) and 90° (HW_T/ tangential direction). The mean yield moment capacities of beech wood specimens tested at 0°,45° and 90° were 5791 Nmm, 5522 Nmm and 5172 Nmm, respectively. The characteristic yield moment capacities of the beech dowels tested at 0°, 45° and 90° were 4445.2 Nmm, 4791.3 Nmm and 4457.4 Nmm, respectively.

Table 3.10- Yield moment test results for beech wood dowels

Beech wood dowels						
Sample ID	Load direction	Oven-dry density (kg/m ³)	Moisture content (%)	Yield Moment (Nmm)	Ductility ratio	Failure mode
1HW_R		702.9	10.6	6063.5	1.5	Bending
2HW_R		722.7	11.9	5875.7	1.7	Bending
3HW_R		730.9	11.9	5747.6	1.6	Bending
4HW_R		667.4	11.6	4904.7	2.5	Bending
5HW_R		733.5	11.8	6364.2	1.4	Bending
Mean			711.5	11.6	5791.2	1.7
Standard deviation		27.4	0.6	547.1	0.4	
Characteristic values as per EN 14358 [189]				4445.2		
1HW_F		716.3	10.9	5790.8	1.5	Bending
2HW_F		740.3	11.9	5302.5	1.7	Bending
3HW_F		700.8	13.4	5898.6	1.6	Bending
4HW_F		657.3	11.6	5313.5	1.5	Bending
5HW_F		698.7	11.9	5304.7	1.6	Bending
Mean			702.7	11.9	5522.0	1.6
Standard deviation		30.3	0.9	297.0	0.1	
Characteristic values as per EN 14358 [189]				4791.3		
1HW_T		717.2	10.7	5336.0	1.5	Bending
2HW_T		744.7	11.9	5333.3	1.9	Bending
3HW_T		745.2	11.9	5275.2	1.9	Bending
4HW_T		665.0	11.7	4655.9	1.7	Bending
5HW_T		714.8	11.9	5262.8	1.7	Bending
Mean			717.4	11.6	5172.6	1.7
Standard deviation		32.7	0.5	290.7	0.2	
Characteristic values as per EN 14358 [189]				4457.4		

In contrast to CW dowels, beech dowels tested at 90° showed the lowest yield moment capacity. The beechwood dowels tested at 0° showed the highest yield moment capacity which was approximately 5% and 11% higher than the specimens tested at 45° and 90° respectively. The mean ductility ratio of beech wood specimens tested at 0°, 45° and 90° were 1.7, 1.6 and 1.8, respectively. In contrast to CW dowels, all beech wood dowels failed in bending irrespective orientation of growth rings to the load direction. This was because densification process lowers interlaminar shear strength of CW dowels which is not the case for beech wood dowels.

Based on the comparison between CW and beech wood dowels, the largest difference was found when CW dowels were tested in the tangential direction (90°). The mean yield moment of the CW dowels was 128% higher than the beech wood dowels. For CW dowels, the yield moment increased as the angle between the load and radial direction increased. Based on the results, it can be concluded that angle between the orientation of growth rings of CW dowels and loading direction is a decisive factor in determining the load-carrying capacity and ductility of the connection. However, while using the CW dowels on-site, ensuring the same direction of dowels is not practical. Therefore, a characteristic value of yield moment capacity can be used based on test results of specimens that are tested in radial, tangential directions and at 45° angle.

3.5.2.3 Comparison between experimental yield moment capacity of CW dowels and literature

Figure 3.19 shows a comparison between the experimental yield moment capacity of CW dowels and the literature [185,190,193]. Literature review on the yield moment capacity of non-metallic dowels showed a scarce availability of data. Thus, the test results were compared with available information on other non-metallic dowel materials. The collected data was from various research papers which focused on the investigation of the feasibility of non-metallic dowels as an alternative to steel dowels in timber connections. The non-metallic dowel materials included in the comparison were glass fibre reinforced polymer (GFRP), carbon fibre reinforced polymer (CFRP) and bamboo composite. Where data was unavailable for 10 mm dowels, a lower dowel diameter was used to allow for comparison.

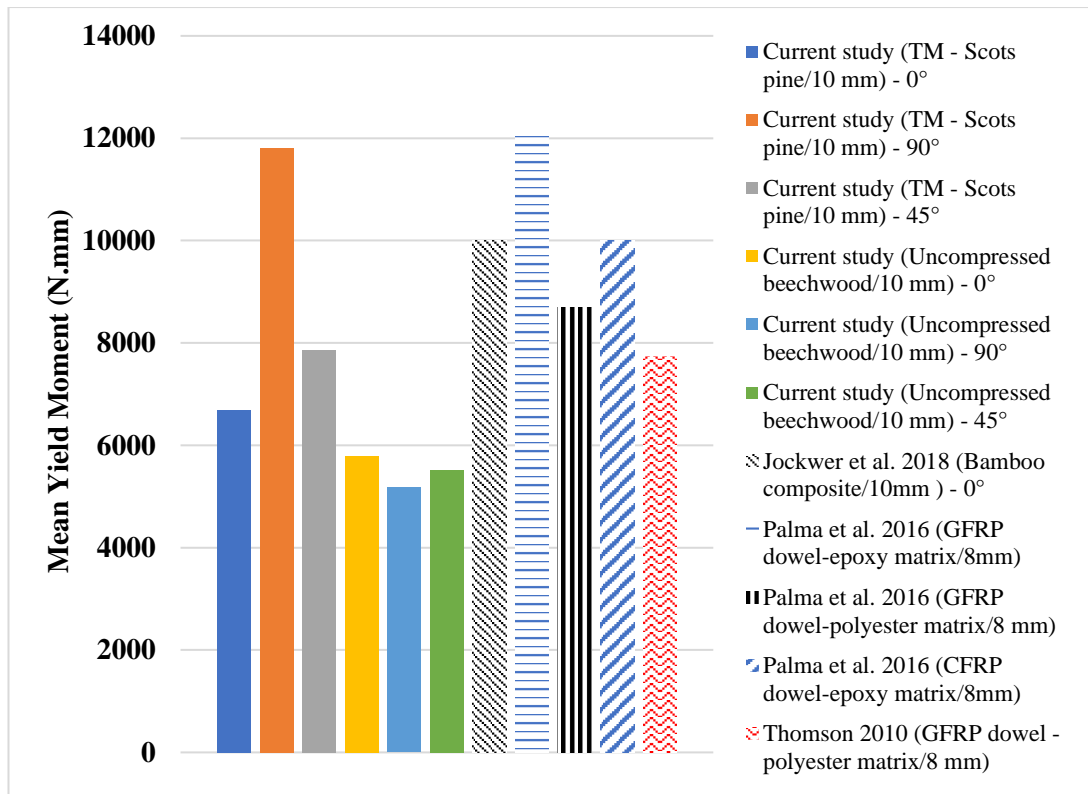


Figure 3.19- Comparison between mean experimental yield moment capacity of CW dowels and literature (0 – radial and 90- tangential direction)

The comparison shows that the yield moment capacity of CW dowels loaded at 90° (CW_T) to the growth rings is approximately equal to the GFRP (produced using an epoxy matrix with a mass fraction of fibres between 50 % -75 %) dowels of 8 mm diameter. The 8 mm CFRP dowels (produced using an epoxy matrix with a fibres mass fraction of between 68%-70%) and 10 mm bamboo-composite dowels showed approximately 15% lower yield moment capacity than the CW dowels tested at 90° (CW_T). As observed from the comparison, 8 mm GFRP dowels (produced using a polyester matrix) showed approximately 1.3-1.7 times lower yield moment capacity compared to the dowels produced using an epoxy matrix. The comparison between CW dowels and FRP dowels showed that CW dowels tested at 90° (CW_T) shows approximately similar (8 mm GFRP dowels with epoxy matrix) or higher (GFRP/CFRP dowels with polyester matrix) yield moment capacity.

As discussed in Section 3.4.2, EC 5 does not provide any guidelines for determining the yield moment capacity of non-metallic dowels. Thus, the results of the current study were also compared with calculated (using Equation 8.30 of EC 5) yield moment capacity of S235 grade (ultimate tensile strength of 360 MPa [194]) steel dowels of 10 mm diameter. The yield moment capacity of S235 grade steel dowel is 42995 Nmm which is approximately 3.6 times higher than the CW dowels tested at 90° (CW_T). Although non-metallic dowels show relatively lower yield moment capacity, it may be possible to use them at a closer spacing than

the steel dowels to achieve similar load carrying capacity per unit area as steel connections. In structural applications where a higher load carrying capacity is required, CW dowels with larger diameter can be used.

3.5.3 Cross grain-shear test results

3.5.3.1 Load – displacement behaviour and failure modes of CW and beech wood dowels

Figure 3.20 shows the load vs. displacement graph for all twenty specimens tested in cross-grain shear. The solid lines indicate the CW dowels results and the dashed lines the beech wood dowels results. The stiffness of the CW dowels was significantly higher than the beech wood dowels. Both the dowel material showed brittle behaviour. However, beech wood dowels showed significantly greater plastic deformation (approximately 5 mm displacement) which may be attributed to the hardening of material beyond the proportionality limit, whereas limited plastic behaviour was observed for the CW dowels. The mean peak loads for the CW dowels tested in the radial and tangential directions was approximately 51% and 82% higher than the beech wood dowels tested in similar directions, respectively.

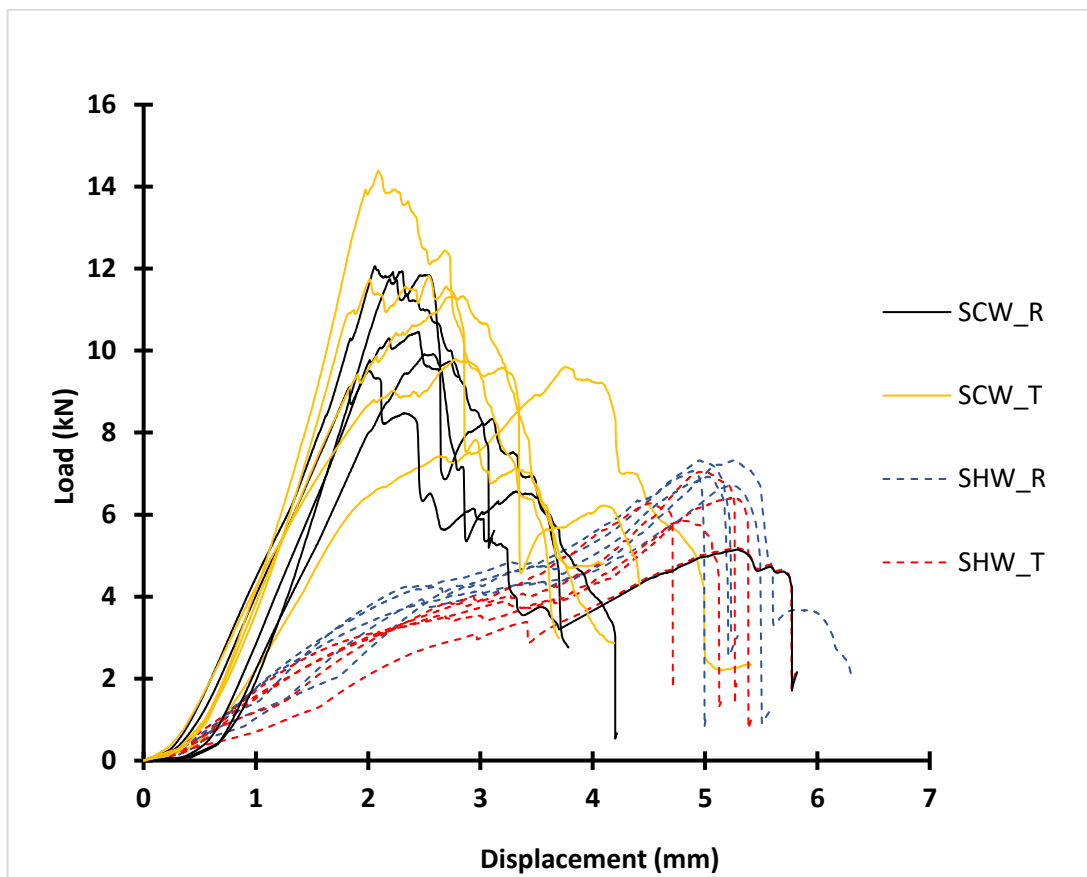


Figure 3.20- Load-displacement behaviour of CW and beech wood dowels tested in shear (SCW_R denotes CW dowels tested at 0° angle to load; SCW_T denotes CW dowels tested at 90° angle to load; SHW_R denotes beech wood dowel tested at 0° angle to load; SHW_T denotes beech wood dowel tested at 90° angle to load)

Figure 3.21 shows the failure modes of all tested specimens. As expected, all specimens showed two cross-grain cuts which are located at the two shear planes between the steel support and the loading head.

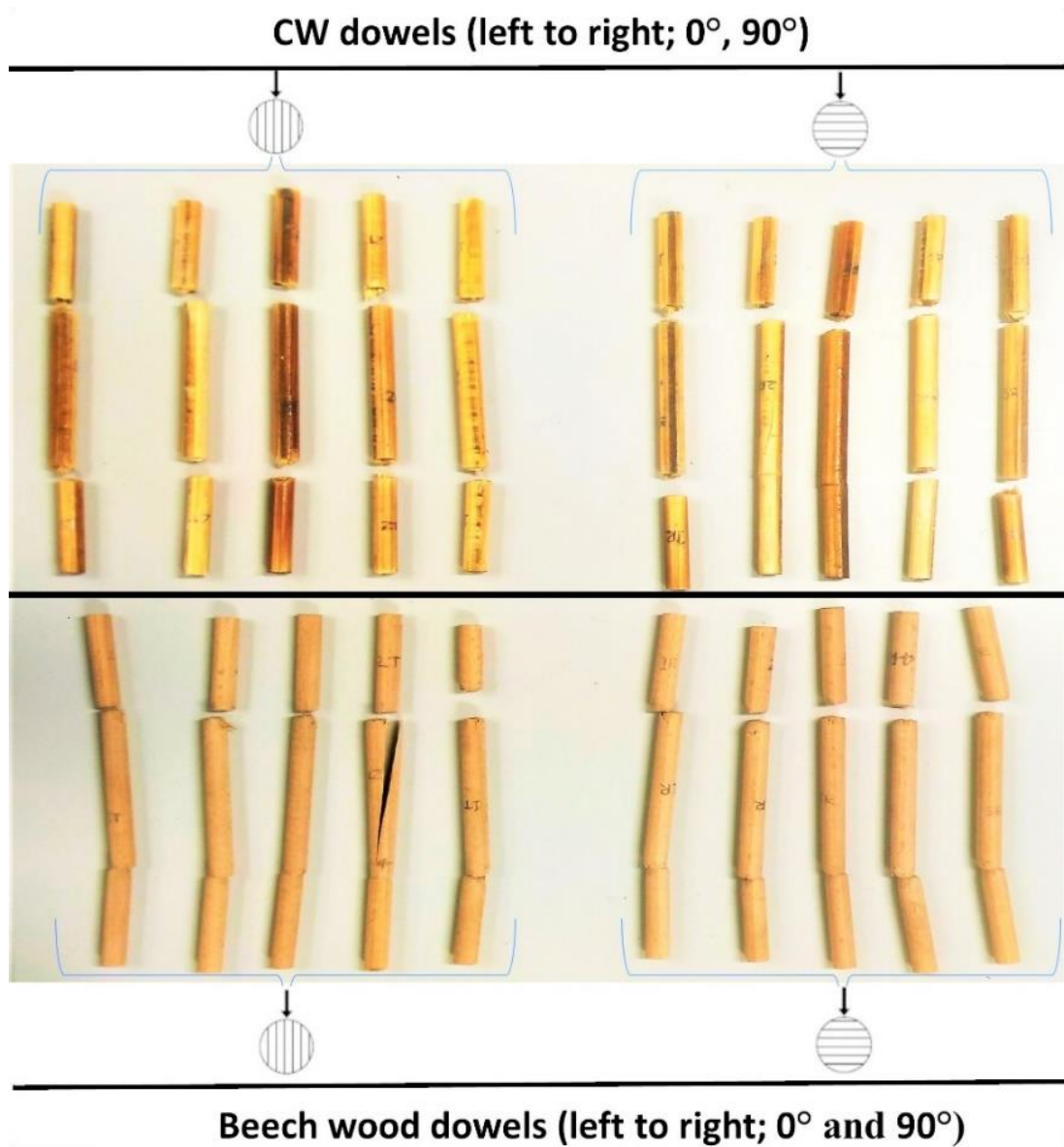


Figure 3.21- Failure modes of the tested specimens in shear

3.5.3.2 Comparison between experimental cross-grain shear strength of CW and beech wood dowels

Table 3.11 shows cross-grain shear test results for CW dowels. The mean cross-grain shear strength per shear plane of CW dowels tested at 0° (SCW_R) and 90° (SCW_T) were 68 MPa and 72 MPa, respectively. The characteristic cross-grain shear strengths of the CW dowels tested at 0° and 90° were 50.8 MPa and 42.3 MPa, respectively. Table 3.12 shows test results for beech wood dowels. The mean cross-grain shear strength per shear plane of beech wood specimens tested at 0° (SHW_R) and 90° (SHW_T) were 44 MPa and 39 MPa, respectively.

The characteristic cross-grain shear strengths of the beech wood dowels tested at 0° and 90° were 40.8 MPa and 28.5 MPa, respectively.

Table 3.11- Cross-grain shear test results of CW dowels

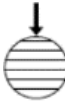
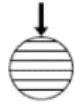
Compressed wood dowels				
Sample ID	Load direction	Oven-dry density (kg/m ³)	Moisture content (%)	Cross-grain shear strength (MPa)
1SCW_R		1323.0	6.5	76.8
2SCW_R		1273.1	6.0	63.2
3SCW_R		1365.2	6.3	74.8
4SCW_R		1245.9	5.9	66.6
5SCW_R		1242.8	5.6	60.5
Mean		1290.0	6.1	68.4
Standard deviation		52.9	0.4	7.1
Characteristic values as per EN 14358 [189]				50.8
1SCW_T		1107.3	7.8	61.1
2SCW_T		1405.4	6.3	91.7
3SCW_T		1404.4	6.2	75.3
4SCW_T		1123.3	6.0	62.5
5SCW_T		1245.3	5.3	72.2
Mean		1257.2	6.3	72.6
Standard deviation		145.1	0.9	12.3
Characteristic values as per EN 14358 [189]				42.3

Table 3.12- Cross-grain shear test results of beech wood dowels

Beech wood dowels				
Sample ID	Load direction	Oven-dry density (kg/m ³)	Moisture content (%)	Cross-grain shear strength (MPa)
1SHW_R		730.3	11.7	45.0
2SHW_R		678.1	11.4	42.7
3SHW_R		752.0	11.5	46.6
4SHW_R		729.9	11.4	46.7
5SHW_R		725.1	11.3	44.1
Mean			723.1	11.5
Standard deviation		27.2	0.1	1.7
Characteristic values as per EN 14358 [189]				40.8
1SHW_T		640.9	11.4	40.8
2SHW_T		675.0	11.1	33.1
3SHW_T		725.6	11.6	40.0
4SHW_T		715.8	11.4	44.9
5SHW_T		704.1	11.4	37.3
Mean			692.3	11.4
Standard deviation		34.4	0.2	4.4
Characteristic values as per EN 14358 [189]				28.5

Based on the comparison between CW and beech wood dowels, it was observed that the mean cross-grain shear strength of CW dowels was higher than that of the beech wood dowels when comparing each tested direction (0° and 90°). The largest difference of 84 % was found when comparing the CW dowels to the beech wood dowels tested in the tangential direction.

3.5.3.3 Comparison of cross-grain shear strength CW dowels with literature

As discussed in Section 3.2, EC 5 [55] does not cover failure modes of non-metallic dowel connectors. Also, the literature review showed limited information on cross-grain shear strength of wood connectors. Figure 3.22 shows the comparison between the mean cross-grain

shear strength of experimentally tested CW dowels with available literature [25,195] based on the density. The results indicate that the cross-grain shear strength was significantly improved by the thermo-mechanical compression process. The cross-grain shear strength of CW dowels was approximately 1.6 -1.7 times higher than the hardwood dowels.

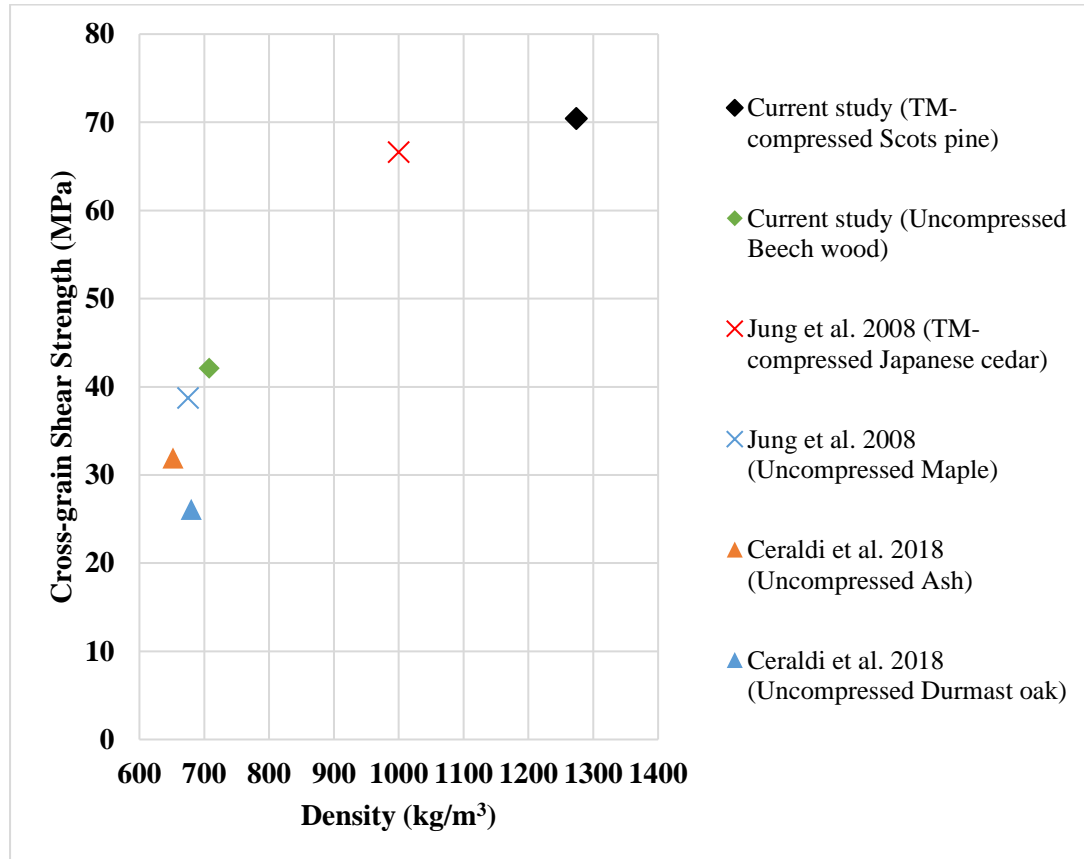


Figure 3.22- Comparison of mean values of experimental cross-grain shear strength with the literature

3.5.4 Bending test results

3.5.4.1 Load – displacement behaviour and failure modes of CW plates

Figure 3.23 shows the load-midspan displacement curve of all fifteen CW plates tested in bending. All specimens behaved in a brittle fashion with a sudden drop in the load capacity beyond the elastic phase. Two of the CWH68 specimens failed at a relatively lower load which may be due to swelling during the conditioning process. Figure 3.24 shows the failure modes of all the specimens. All the specimens showed brittle failure in the tension zone once the peak load was attained. The failure behaviour was similar to uncompressed timber in bending, with failure initiating on the tension face at the loading head location and propagating along the grain.

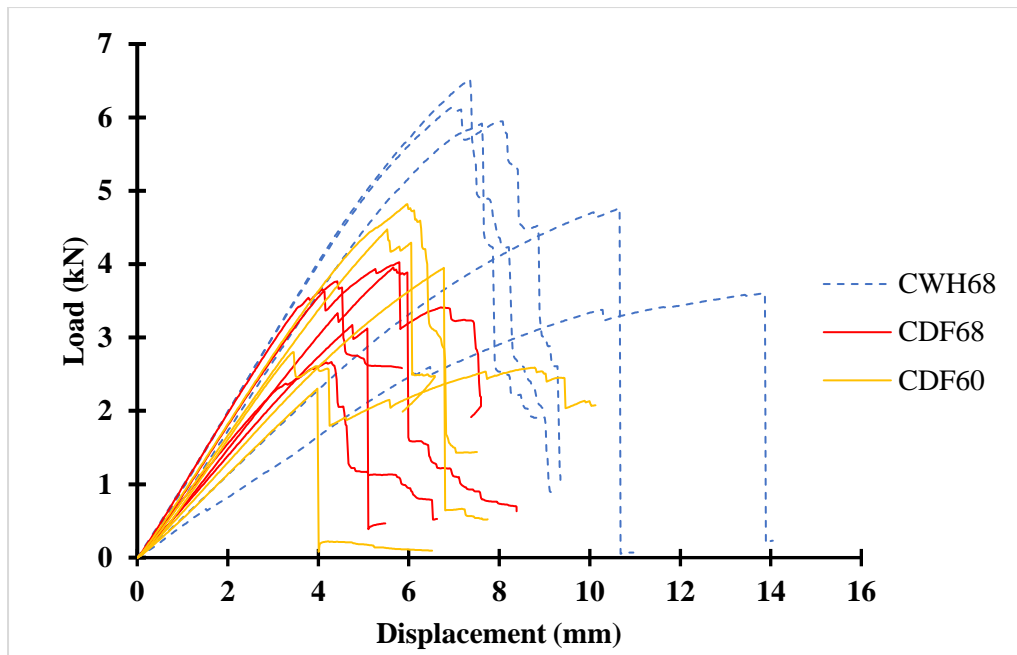


Figure 3.23- Load-displacement behaviour of specimens tested in bending



Figure 3.24- Bending failure of the specimens

3.5.4.2 Comparison of experimental results of bending test

Table 3.13 shows the three-point bending test results. The mean bending strengths of CWH68, CDF68 and CDF60 were 283.1, 184.6 and 192.6 MPa, respectively. The bending strength of CWH68 (mean density of 1423 kg/m³) was 47% higher than the CDF60 (mean density of 1400 kg/m³), whereas it was 53% higher than CDF68 (mean density of 1503 kg/m³). The mean modulus of elasticity of CWH68, CDF68 and CDF60 were 27.5, 29.1 and 27.4 GPa, respectively. MOE of CDF68 specimens was 5.8 % higher than the CWH68 whereas this increase was 6.2 % for CDF60. Based on the results it can be concluded that the bending strength of CW is dependent on the species, whereas MOE is mainly dependent on the density of the material irrespective of the wood species. This finding will need to be confirmed with a larger sample size.

Table 3.13- Results of three-point bending test

Sample ID	Oven-dry density (kg/m ³)	Moisture content (%)	Bending strength (MPa)	Modulus of Elasticity (GPa)
CWH68_1	1383.9	4.82	342.1	35.9
CWH68_2	1437.5	4.35	322.1	35.2
CWH68_3	1437.5	6.21	189.1	13.8
CWH68_4	1464.3	4.88	250.1	20.0
CWH68_5	1392.9	5.77	312.2	32.5
Mean	1423.2	5.2	283.1	27.5
Standard deviation	33.8	0.8	62.8	10.0
CDF68_1	1437.5	4.83	207.6	27.1
CDF68_2	1491.1	5.77	140.0	27.3
CDF68_3	1473.2	4.64	166.5	24.5
CDF68_4	1589.3	5.56	197.7	34.8
CDF68_5	1526.8	4.12	211.4	31.9
Mean	1503.6	5.5	184.6	29.1
Standard deviation	57.7	0.4	30.6	4.1
CDF60_1	1294.6	4.97	120.9	20.4
CDF60_2	1392.9	5.99	252.9	32.7
CDF60_3	1348.2	5.45	207.4	23.2
CDF60_4	1446.4	5.62	147.0	30.3
CDF60_5	1517.9	5.26	234.9	30.4
Mean	1400.0	5	192.6	27.4
Standard deviation	86.4	0.7	56.7	5.3

To understand the difference between the bending strength properties, some of the tested and randomly selected specimens from a fresh lot of all three materials were dissected and

inspected visually. It was then observed that the compressed Douglas fir specimens have significant internal damage along the growth rings in a longitudinal direction as shown in Figure 3.25. No such defects were observed in CWH68 specimens. Based on the test results and quality of finished plates, CWH68 was chosen for mass production of CW plates for the connection test programme.

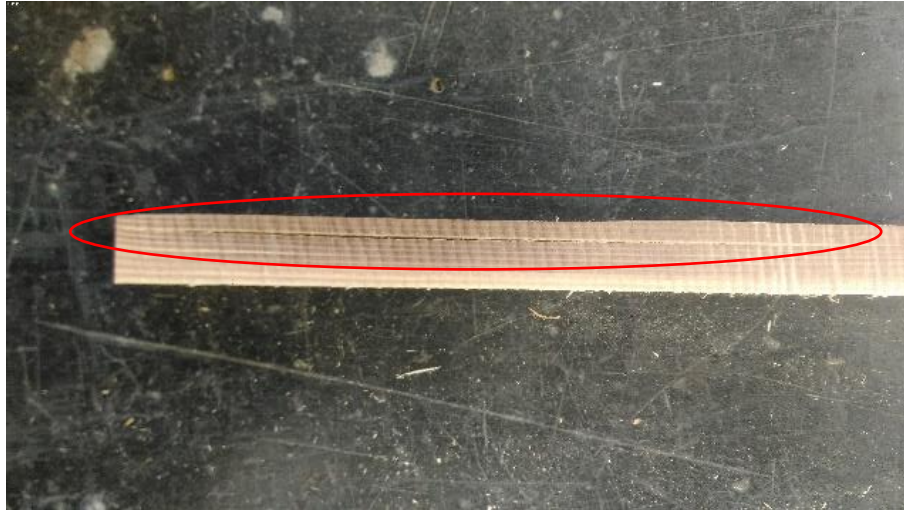


Figure 3.25- Internal damage along with the growth rings in the longitudinal direction of compressed Douglas fir

3.5.4.3 Comparison between experimental bending test results and literature

To allow comparison between experimental results and available literature [18,22,82,102,110,112,113,118,196,197], data was gathered from literature based on the density of the material ($\geq 900 \text{ kg/m}^3$) irrespective of densification process, testing standard, loading direction and wood species. Figure 3.26 shows a bending strength comparison of various densified wood material with the experimental results of this study. The comparison shows that the bending strength of wood can be significantly improved by the densification process. As per EN 338 [50], the characteristic bending strength of uncompressed structural softwoods and hardwoods is within the range of 16 MPa to 80 MPa, which can be further increased by approximately 1.5 to 3.5 times through the densification process. As observed from the experiments, in addition to material density the bending strength may be also affected by the species type. The CDF60 and CWH68 specimens were of approximately of similar density. However, the mean bending strength of CDF60 specimens was 1.5 times lower than CWH68 specimens. This indicates that bending strength is affected by the wood species type which may be attributed to the microscopic structure of individual species. Further study is needed to determine the effect of material density and species type on the bending strength properties.

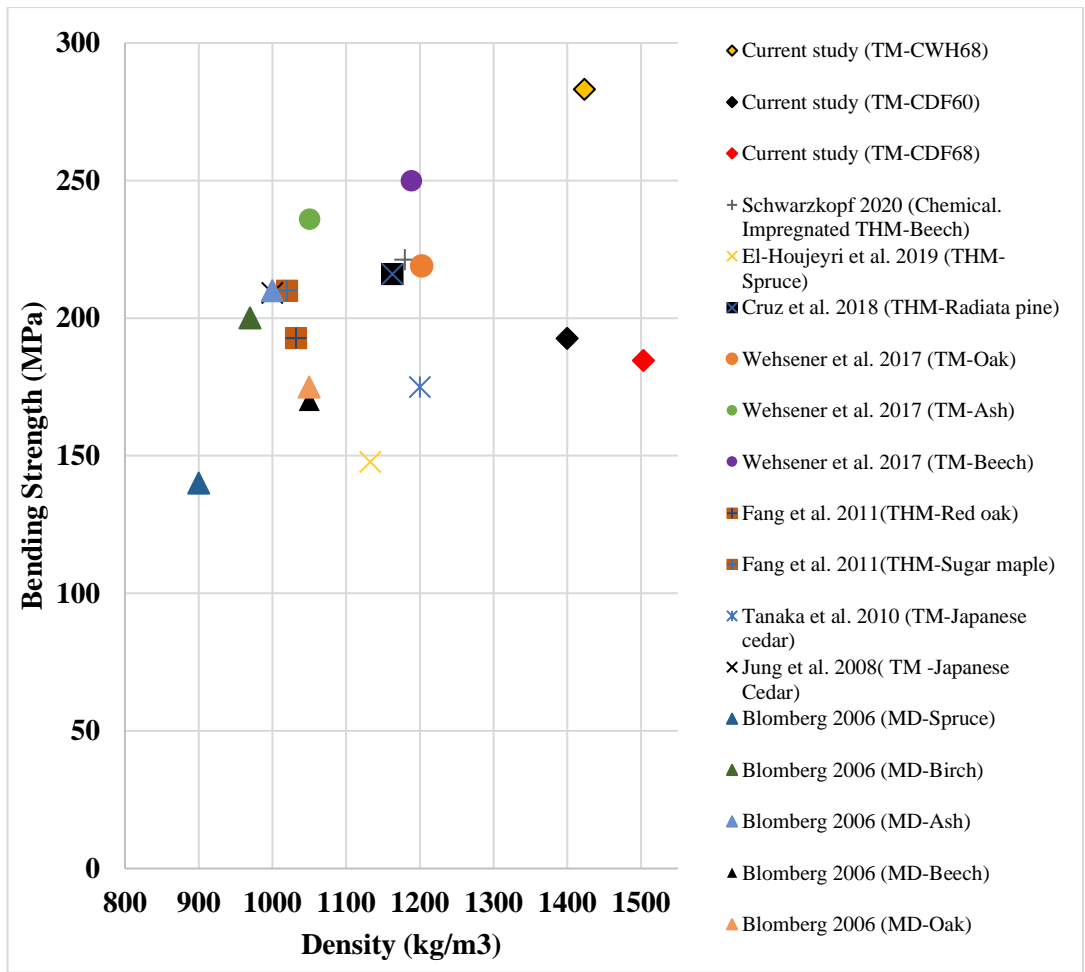


Figure 3.26- Bending strength comparison between mean values of experimental results and literature (TM – Thermo-mechanically densified wood, THM- Thermo-Hydro-Mechanically densified wood, MD – Mechanically Densified wood)

Figure 3.27 shows a comparison of the MOE of the tested specimens with the literature. Similar to the bending strength, MOE of CW is significantly improved by the densification process compared to uncompressed wood. The comparison did not show a clear relationship amongst MOE, density of the material and wood species. An investigation will be needed with a larger sample size to determine the effect of density and wood species on MOE.

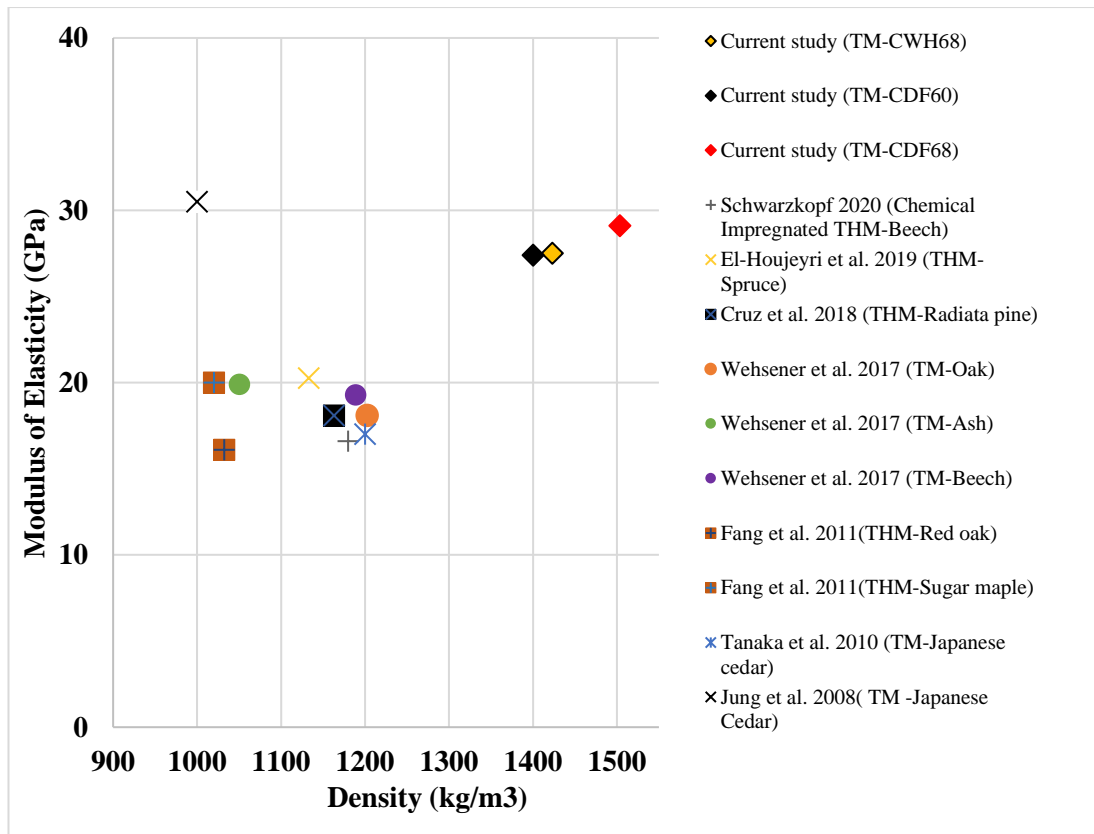


Figure 3.27- Modulus of Elasticity (GPa) comparison between mean values of experimental results and literature (TM – Thermo-mechanically densified wood, THM- Thermo-Hydro-Mechanically densified wood)

Based on the reviewed literature and experimental results presented in Figure 3.26 and Figure 3.27, a comparison of the effect of the manufacturing process on material properties was conducted irrespective of the wood species. Here, it should be noted that the oven-dry density of cell wall constituents remain constant among fibre types and wood species which is approximately 1500 kg/m^3 [45,47,198]. Thus, densifying the wood beyond 1500 kg/m^3 severely damages the cell wall materials and negatively affects the strength properties as observed for specimens of 68% radially compressed Douglas fir (CDF68). The maximum level of densification or compression ratio (CR) that can be achieved for a wood species depends on various parameters such as composition and morphology of fibres, percentage of latewood material, ray volume and loading direction [35,90]. For instance, the CW specimens of CWH68 and CDF68 produced in this study had similar CR of 68%. However, their mean densities and strength properties were significantly different which may be attributed to the aforementioned species-specific parameters. In this study, to allow the comparison, a conservative assumption was made that the researchers [18,25,82,110,112,113,118,196] had used a maximum possible CR or density for a relevant wood species without damaging the cell wall constituents. Based on the comparison, it can be concluded that the thermo-mechanical (TM) compression process (with/ without CDF68) results in the highest density

of the materials studied followed by chemical impregnated thermo-hydro-mechanical (Chemical impregnated THM) densification, thermo-hydro-mechanical (THM) densification and mechanical densification (MD). The TM compression process results in the highest bending strength followed by chemical impregnated THM densification, THM densification and MD. The highest MOE was observed for materials produced using the TM compression process followed by THM densification and chemical impregnated THM densification. However, an investigation with various species type and compression ratio/density is required to determine the effect of manufacturing process on the mechanical properties of the CW material.

3.6 Conclusion

In this chapter, the manufacturing process for CW and CW connectors has been discussed in detail. This is followed by test procedures and test results of various material characterisation tests performed on CW, hardwood and softwood material. Additionally, experimental test results were compared with the literature and results obtained from empirical formulas of EC 5 (in the case of embedment strength). The obtained test results are utilised for the design and analysis of the structural performance of non-metallic and adhesive-free timber-timber moment connections using CW connectors presented in Chapter 5, Chapter 6 and Chapter 7. A summary of the key finding of this chapter is as follows:

1. Embedment response of CW and uncompressed softwood

The embedment test results show that the mean embedment strength of CWH68 in the parallel and perpendicular to the grain directions was approximately 168% and 175% higher, respectively, than that of uncompressed Douglas fir tested in similar directions. The mean slip modulus of uncompressed Douglas fir in parallel and perpendicular to the grain was approximately 55% and 77% lower than that of CWH68 tested in similar directions. The difference between the embedment strength of CW material tested in parallel and perpendicular to the grain direction was insignificant (1.3%) which is probably attributed to the low variation in the density distribution of the CW material. However, the comparison of initial stiffness values represented by the slip modulus in the elastic range shows that the slip modulus of the CW material is not significantly affected by the densification process. The effect of grain direction has a higher influence on the elastic deformation irrespective of the density of the material, whereas the embedment strength was largely affected by the density of the material. From the design perspective of timber-timber connections using CW connectors, it can be concluded that the embedment strength of the CW material is not a critical factor for design purposes. The comparison between

experimental test results and results obtained using the empirical formula of EC 5 shows that the EC 5 underestimates the embedment strength of CW materials by a factor of 2.5 and thus requires further research using statistically valid sample sizes to derive new equations for CW material. The comparison between experimental results and the literature verifies that the embedment strength of the wood is significantly improved by the increase in density through the densification process and other wood modification techniques.

2. Yield moment capacity of CW and beech wood dowels

The results of yield moment tests show that the mean yield moment of the CW dowels was higher than that of the beech wood dowels when comparing each tested direction (0° , 45° and 90°). The largest difference was found when the CW dowels were tested in the tangential direction: CW dowel was 128% higher than the beech wood. For the CW dowels, the yield moment increased as the angle between the load and radial direction increased. The beech wood dowels loaded at 90° showed the highest ductility whereas this was least for CW dowels loaded at 90° . Based on the results, it can be concluded that the angle between the load direction and the radial direction may be a decisive factor in determining the load-carrying capacity and ductility of timber-CW connections. However, it is conservative to use the lowest value of yield moment capacity as the orientation of the dowel cannot always be specified within the connections while working on the site. Finally, it can be concluded that the density of the material positively influences the yield moment capacity. The comparison between experimental results and literature shows that the CW dowels present approximately similar yield moment capacity and failure modes as FRP and bamboo composite material. If CW dowels are used as a substitute of steel dowels, a larger dowel diameter may be required to achieve the same load-carrying capacity.

3. Cross-grain shear performance of CW and beech wood dowels

The results of cross-grain shear tests show that the mean cross-grain shear strength of CW dowels was higher than that of the beech wood dowels when comparing each tested direction (0° and 90°). The largest difference of 84 % was found when comparing CW dowels to beech wood dowels tested in the tangential direction. For the analytical calculations or numerical modelling to predict the moment capacity of the multiple shear plane timber-CW connections, cross-grain shear strength may be utilised if cross-grain failure is the dominant failure mode of CW dowels. The comparison between experimental results and literature shows approximately similar values which confirms that higher density CW dowels produce higher cross-grain shear strength compared to hardwood dowels.

4. Bending response of CW plates

The bending test result was used for the selection of a suitable material type for the mass production of CW plates to be utilised for the development of structural testing presented in Chapter 5 and Chapter 6. The test results show that the bending strength of CW is dependent on the species, whereas MOE is mainly dependent on the density of the material irrespective of the timber species. Based on the bending test results and severity of damage that occurs during the thermo-mechanical compression, Western hemlock was chosen for the mass production of CW plates used in Chapter 5 and Chapter 6.

5. Influence of modification process

Finally, the comparison between experimental results and the literature confirms that thermo-mechanically compressed wood produces approximately similar results to other modified wood materials, and could be utilised in various structural application where higher strength and stiffness properties are required such as reinforcement material to improve the stiffness of beams or as a connector material in timber-timber connections. On the material production side, TM compression is relatively simple compared to other wood modification techniques. For example, THM compression involves three different processes which are relatively time-consuming. On the other hand, production of densified veneer wood (DVW) involves the application of synthetic adhesives prior to the densification process, which compromises the sustainability aspect of using timber.

Chapter 4 Swelling/shrinkage behaviour of CW and timber-CW connections

4.1 Introduction

In this chapter, the swelling/shrinkage behaviour of CW as a plate material and in the form of small-scale timber-CW connections is examined. As discussed in Chapter 2, CW exhibits springback which is responsible for its unstable nature when subjected to moisture/heat or a combination of both [90]. Today, Only a few wood densification techniques have been used at industrial scale with additional physical and chemical additions [113]. However, springback behaviour of the CW could be utilised as a beneficial trait in applications such as dowel-type timber structural connections where the increased tightness of connection caused by springback is desirable.

In recent years, hardwood dowels have also been commercialised as an alternative to adhesives and metallic fasteners in the manufacturing of dowel laminated timber products (DLT) [10,17,63,199,200]. For DLT production, dried hardwood dowels (at a relatively low moisture content) are driven into softwood boards. This induces moisture movement between the hardwood dowels and surrounding softwood boards. Consequently, hardwood dowels swell to establish moisture equilibrium with the surrounding timber and this facilitates form-and-friction locking of the dowel in the timber [17]. However, the long-term behaviour of such products is still unknown. During service life, the moisture content of DLT components (hardwood dowels and softwood) varies with the change of RH of the surrounding environment [63]. This causes swelling/shrinkage within the connection components. As a result, the contact pressure/friction between hardwood dowels and softwood varies and leads to separation of timber lamellae [201]. Philippe et al. [103] reported that a continuous decrease in the RH over a course of time may lead to complete loss of contact pressure between connected components. In another study, Guan et al. [62] reported that hardwood dowels have high-stress relaxation feature which causes loosening of connection over time and necessitates tightening at regular interval.

CW dowels may be utilised as a remedy to solve issues associated with loosening of hardwood dowelled connections. The continuous expansion of CW due to springback may prevent the loosening of connections during the service life. There are a few studies available on structural applications of CW as dowel material for the production of CW dowel laminated timber and jointing of structural members such as beams and columns [18,78,79,102]. However, there is not enough information available on how the springback phenomenon affects the load-carrying capacity of the connections. This requires a valid justification through quantitative

experimental research. For the aforementioned reasons, two minor studies were carried out to address the following questions:

1. If CW dowels are used as a replacement of hardwood dowels in DLT, how long should the CW laminated timber products be conditioned to activate tight friction fit between them and surrounding timbers?
2. Due to springback behaviour, do CW dowels offer any improvement in the load-carrying capacity of the timber-CW connection compared to timber-hardwood connections?

To address the above questions, this chapter is divided into two sub-sections:

1. Unconstrained swelling/shrinkage test of CW
2. Ageing test on CW dowel-timber and hardwood dowel-timber connections

Unconstrained swelling/shrinkage of CW was characterised by means of conditioning of CW plates at 65 ± 5 % RH and 20 ± 2 °C over 510 days. Also, the springback of CW was evaluated through moisture dependent swelling (190 days) and oven drying (26 days) treatments. Section 4.3.1 and Section 4.4.1 detail the test procedure and results of the aforementioned experiments, respectively.

Ageing tests were carried out to develop a better understanding of the long-term behaviour of CW fastened joints. The natural ageing of timber structures and particularly structural connections is normally slow, and a longer time period is required to study their mechanical behaviour on a scientific basis. CW laminated products and connections are relatively new and there is no actual life span data available. Therefore, it has been found necessary to carry out accelerated ageing tests to obtain representative information on connection strength in a significantly reduced time. With the aim of understanding the long-term behaviour of CW fastened connections, accelerated ageing tests were conducted to evaluate the mechanical behaviour of these connections by means of dowel pull-out tests. Prior to pull-out tests, specimens were subjected to cyclic treatment using variable parameters including constant temperature and RH, followed by pressure wetting and rapid drying cycles. Experimentally obtained results of CW fastened connections were compared with similar connections produced using hardwood dowels. Section 4.3.2 and Section 4.4.2 detail the test procedure and results of the accelerated ageing test, respectively.

4.2 Materials

This section describes the materials used in the study. Several different materials were used: CW, hardwood and softwood. The hardwood in the form beech wood dowels was used as reference material to compare the accelerated ageing test results with CW dowels.

4.2.1 Compressed wood

CW in the form of dowels and plates were sourced from the University of Liverpool. The manufacturing process is as described in Section 3.3.1. Moisture content of CW connectors after compression process varied between 5% -6%. To keep the moisture content constant and to prevent the springback, connectors were placed in air-tight plastic bags.

4.2.1.1 Compressed wood plates (CW plates)

The radially compressed Scots pine (*Pinus sylvestris*) plates were used for unconstrained swelling/shrinkage tests. The densities of the uncompressed wood specimens varied from 500 to 700 kg/m³ at 12% moisture content. The initial dimensions of the uncompressed plates were 200 mm (L) x 50 mm (T) x 30 mm (R), which were compressed to 200 mm (L) x 50 mm (T) x 10 mm (R). This is approximately 67% CR. However, there was a mean increase of approximately 1.3 mm in the radial dimension immediately after specimens were removed from the press. At the beginning of the experiment, the mean thickness (R) of CW plates was 11.3 mm. The density of compressed specimens was between 1100-1500 kg/m³ after the thermo-mechanical compression.

4.2.1.2 Compressed wood dowels (CW dowels)

Scots pine (*Pinus sylvestris*) CW dowels were used for the accelerated ageing tests. The diameter of the dowels varied from 9.95 mm to 10.31 mm and the length was 200 mm. The oven-dry density of the dowels varied from 1200 kg/m³ – 1280 kg/m³.

4.2.2 Hardwood dowels

Beechwood (*Fagus sylvatica*) dowels were chosen for the comparison with CW dowels. The diameter of these dowels varied from 9.80 mm to 10.37 mm. The mean oven-dry density of hardwood dowels was approximately 700 kg/m³.

4.2.3 Softwood

Commercially available kiln-dried Irish grown Scots pine (*Pinus sylvestris*) boards were used for the accelerated ageing tests. To minimise the variations among the specimens, two timber boards of the relatively close oven-dry density of 520 kg/m³-540 kg/m³, were selected from a pack of 6 boards. The dimensions of each timber board were 4800 mm (L) x 100 mm(T) x 75 mm (R). Boards with visually smaller and fewer knots were selected and conditioned at 65 ± 5% RH and a temperature of 20 ± 2 °C for 30 days.

4.3 Test procedures

4.3.1 Unconstrained swelling/shrinkage of CW

To achieve the objective of this study, an experimental test program was developed. The study was designed to determine the unconstrained swelling/shrinkage behaviour of CW plates at standard conditions of $65 \pm 5\%$ RH and $20 \pm 2\text{ }^\circ\text{C}$ temperature. As discussed in Section 4.1, CW shows springback behaviour when subjected to moisture/heat or a combination of both. As CW plates used in this study were thermo-mechanically compressed only in the radial direction, the effect of springback is thus expected to be significantly more in the radial direction compared to longitudinal (L) and tangential (T) directions. For this reason, the current study evaluated the swelling/shrinkage behaviour of CW by means of change in radial (R) thickness over a period of 510 days. To understand the relationship between the change in thickness and mass change due to moisture adsorption and desorption, the mass of every specimen was measured during the experiment. Additionally, springback behaviour of CW plates was quantified by means of moisture dependent swelling/shrinkage behaviour. Figure 4.1 shows the scheme of the experiment. The experiment comprised a total of 16 specimens of 200 mm (L) x 50 mm (T) x 10 mm (R). On delivery at the NUI Galway laboratory (April 04, 2018), these specimens had a moisture content between 5% to 7%. All the specimens were removed from the sealed bags and exposed to a controlled environment of $65 \pm 5\%$ RH and $20 \pm 2\text{ }^\circ\text{C}$. The specimens were continuously monitored to determine their swelling behaviour until September 9, 2019. The presented results include change in the thickness and mass of the CW plates during the aforementioned exposure period. To evaluate the springback behaviour of CW plates, two specimens were randomly taken from the batch of 16 specimens after 190 days of the standard conditioning phase. These specimens were oven-dried at $103.5 \pm 2\text{ }^\circ\text{C}$ and the shrinkage behaviour was monitored.

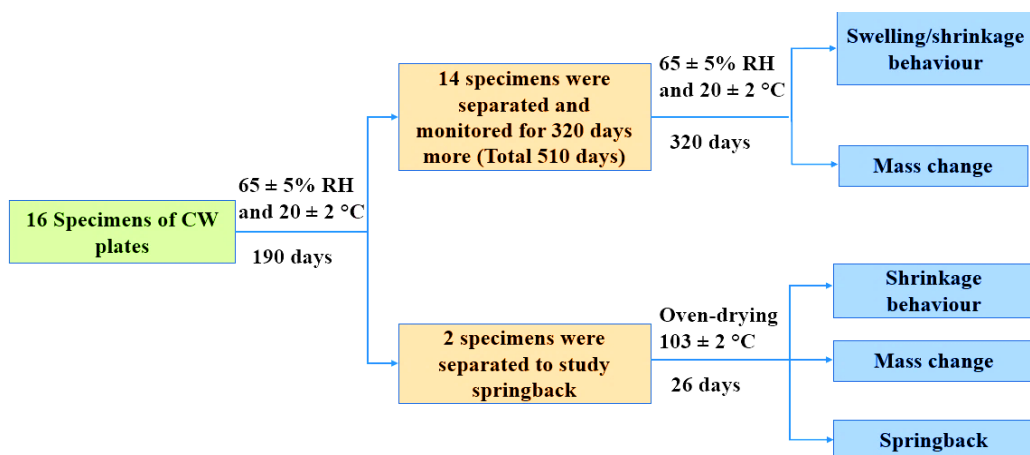


Figure 4.1- Scheme of the experiment

4.3.1.1 Test measurements

As discussed in Section 4.3.1, radially CW tends to expand in the direction of the compression, therefore measurements were taken in the radial direction only. Once taken out from the plastic bags, 6 measurements of the thickness (radial direction) were taken on each specimen using a handheld wireless *MarComprof* vernier calliper with an accuracy of ± 0.03 mm as shown in Figure 4.2a, b and c.

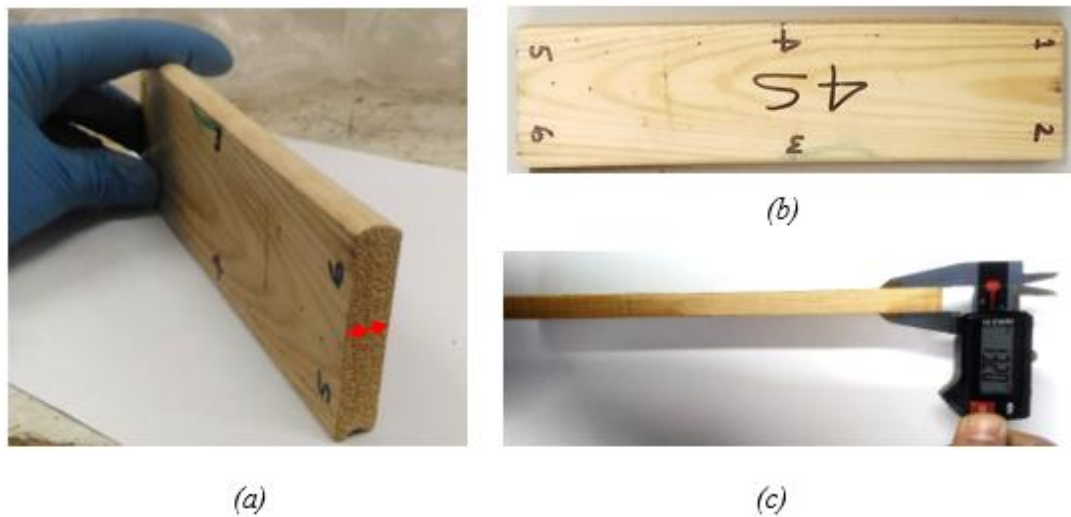


Figure 4.2- Test measurement, (a) direction of the measurement, (b) positions of measurement, (c) thickness measurement using vernier calliper

The relative change in the thickness due to swelling/shrinkage was calculated using the following expression:

$$\Delta t = t_m - t_i \quad \text{Eq. 4.1}$$

where

Δt is the relative change in the thickness (mm),

t_m is the thickness on the day of measurement (mm),

t_i is the initial thickness (mm), which was measured immediately after taking out specimens from the plastic bags.

Percentage change in the thickness was calculated using the following expression:

$$\Delta t_{\%} = \frac{(t_m - t_i)}{t_i} \times 100 \quad \text{Eq. 4.2}$$

where $\Delta t_{\%}$ is the percentage change in thickness (%).

For the specimens, which were used for shrinkage study, the percentage decrease in the thickness was calculated using the following expression:

$$t_d = \frac{(t_b - t_o)}{t_b} \times 100 \quad \text{Eq. 4.3}$$

where

t_d is the percentage decrease in the thickness (%),

t_b is the thickness at the time of start (mm) which was measured after 190 days of conditioning at standard conditions,

t_o is the thickness of the oven-dried specimen (mm).

In order to understand the relationship between change in thickness and mass due to moisture adsorption and desorption, the mass of each specimen was measured during the experiment using an *Ohaus* analytical and precision balance. The relative mass change was calculated using the following expression:

$$\Delta m = m_m - m_i \quad \text{Eq. 4.4}$$

where

Δm is the relative change in the mass (g),

m_m is the mass on the day of measurement (g),

m_i is the initial mass (g) which was measured immediately after taking out specimens from the plastic bags.

Percentage change in the mass was calculated using the following expression:

$$\Delta m_{\%} = \frac{(m_m - m_i)}{m_i} \times 100 \quad \text{Eq. 4.5}$$

where $\Delta m_{\%}$ is the percentage change in the mass (%).

For the specimens which were used for shrinkage study, the percentage decrease in the mass was calculated using the following expression:

$$m_d = \frac{(m_i - m_m)}{m_i} \times 100 \quad \text{Eq. 4.6}$$

where

m_d is the percentage decrease in mass (%).

Springback of CW was calculated using the following expression:

$$t_s = t_{MDS} - t_o \quad \text{Eq. 4.7}$$

where

t_s is the springback of CW (%),

t_{MDS} is the moisture dependent swelling during the conditioning phase (%),

t_o is the thickness of the oven-dried specimen (%).

4.3.2 Accelerated ageing tests on timber-CW and timber-hardwood connections

This study was designed to determine the influence of different environmental conditioning series (including moisture cycling) on the pull-out capacity of dowelled connections in timber. Differential swelling/shrinkage of the dowel and timber substrate is expected to influence the frictional forces between the dowel surface and surrounding hole.

Four different conditioning series were considered as outlined in Figure 4.3. Series A indicates control specimens. Specimens of Series B were subjected to conditioning treatment for 45 days at 65 ± 5 % RH and 20 ± 2 °C temperature. Specimens of Series C and D were subjected to cycles of pressure soaking in water followed by oven drying and finally 24 hrs of conditioning at 65 ± 5 % RH and 20 ± 2 °C temperature. As there is no standard for accelerated ageing test on wooden-dowel type connections, artificial conditions were simulated by means of pressure treatment in accordance with ISO 12580 [202] for Series C and Series D. Three specimens, each containing a single CW and beech wood dowel, were tested in each series. Finally, the specimens all the series were subjected to pull-out tests to evaluate the effect of ageing.

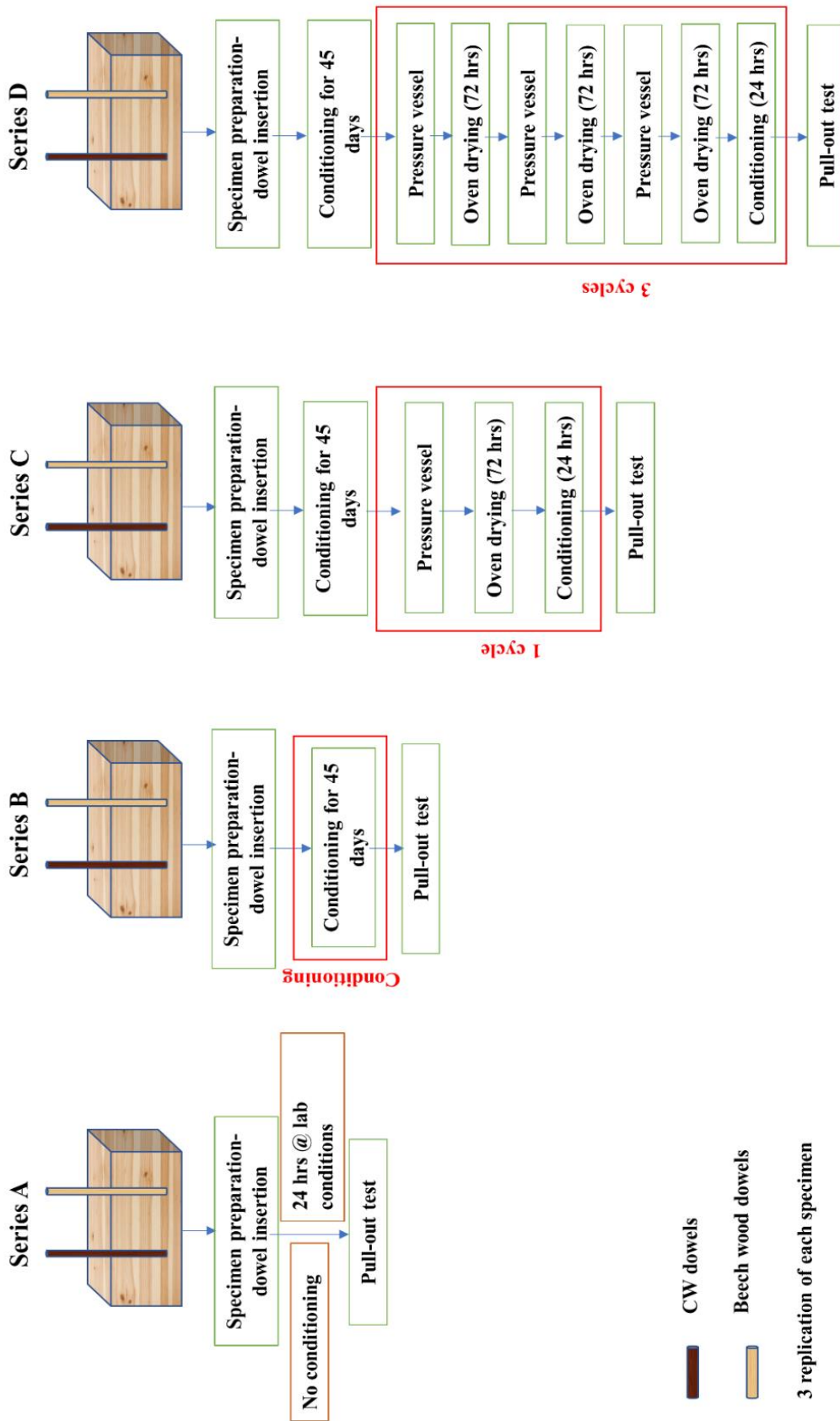
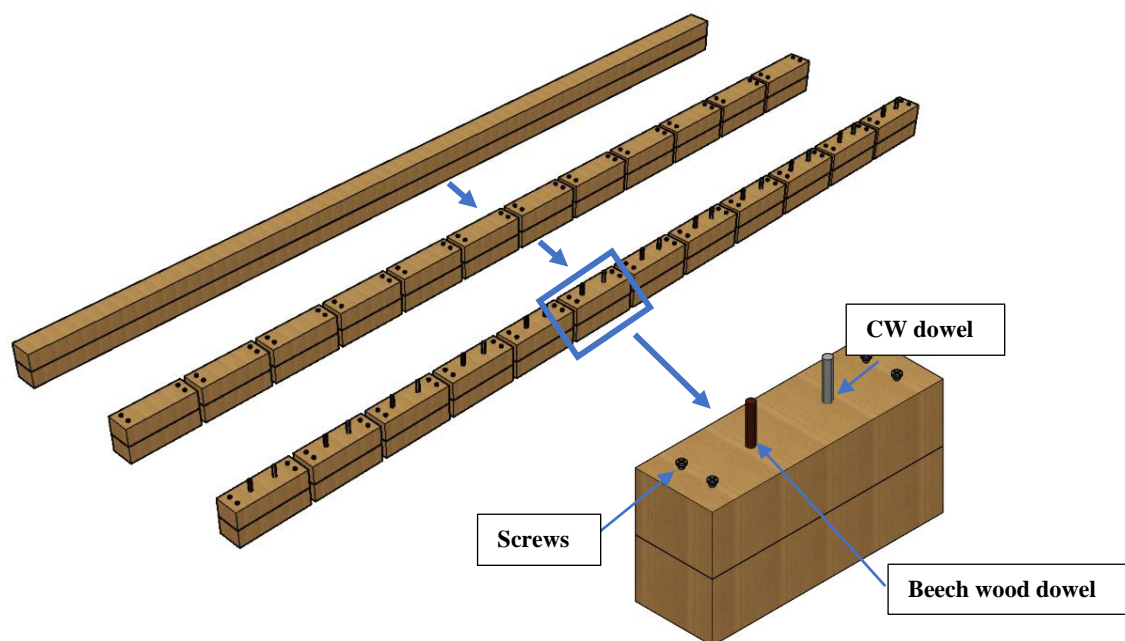


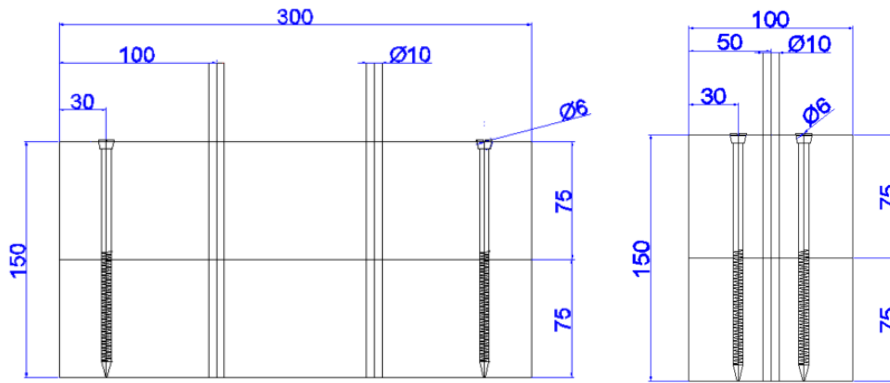
Figure 4.3- Scheme of accelerated ageing test

4.3.2.1 Preparation of test specimens

There were a total of 12 specimens of 300 mm (L) x 100 mm (T) x 150 mm (R) dimensions (three for each series). Dimensions were defined as per EN 13182 [203]. Each specimen comprised of two laminates of 300 mm (L) x 100 mm (T) x 75 mm (R). Conditioned timber boards were cut to the desired length and laminated together using Spax's universal partially threaded flat countersunk-headed screws of 6 mm diameter and 150 mm length as shown in Figure 4.4a. It should be noted that screws were preferred over adhesives for lamination purpose as severe accelerating ageing could potentially cause delamination. Figure 4.4b shows the geometry of the specimens. Once laminated, holes were bored in the specimens using a pillar drilling machine (see Figure 4.4c). Each dowel was 200 mm long, which includes a 150 mm effective length (embedded thoroughly in the timber specimens), a 10 mm gap between the Instron grip and the timber surface and a 40 mm grip length (to clamp using the mechanical grips). In order to ensure a tight fit without damaging the perimeter of the dowels, 10.2 mm drilling bits were used to create holes for all CW dowels. For the hardwood dowels, drilling bits of 10 to 10.2 mm were used due to wide variation in the dowel diameter. For both dowel types, the diameter of the hole was chosen based on the average diameter of the dowel which was measured at three pre-marked points (starting from one randomly chosen end to the other end) as indicated in Figure 4.4d. It should be noted that neither CW nor beech wood dowels were oven-dried before assembly. Table 4.1 shows the mean hole clearance for each series. The initial dowel diameter was measured using a handheld wireless *MarComprof* vernier calliper with an accuracy of ± 0.03 mm. Each specimen was comprised of two dowels (one CW and one beech wood dowel) to minimise the effect of timber substrate variation on the test results.

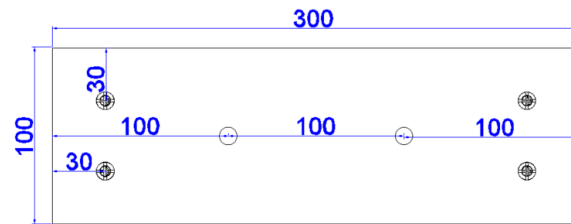


(a)



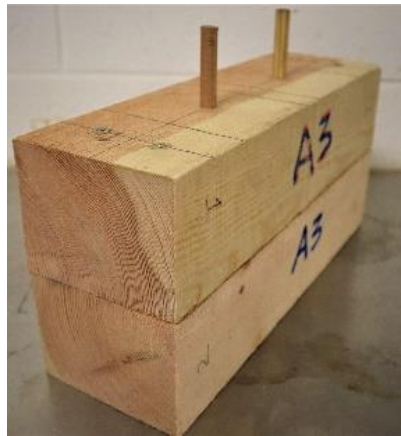
(Elevation view)

(End view)

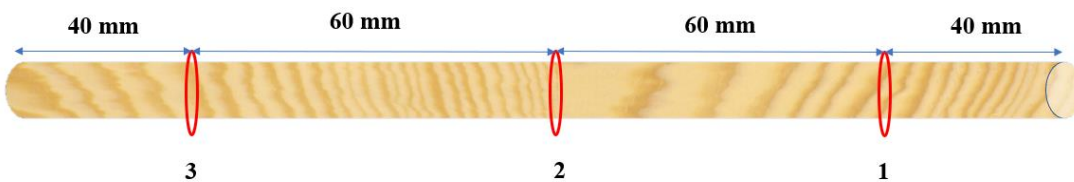


(Top view)

(b)



(c)



(d)

Figure 4.4- Specimen preparation of accelerated ageing test, (a) process , (b) geometry of specimens, (c) assembly process, (d) position of measurement of dowel diameter

Table 4.1- Mean hole clearance for each series

Series type	Mean hole clearance (mm)	
	CW dowels	Beech wood dowels
A	0.13	0.16
B	0.09	0.07
C	0.06	0.09
D	0.10	0.15

4.3.2.2 Accelerated ageing treatments and measurement of swelling/shrinkage of dowels

Specimens of each series were subjected to different sets of treatment as described below:

Series A (control specimens): These specimens were kept at laboratory conditions for 24 hrs after dowel insertion. Dowel diameter and mass of the specimens were measured before and after 24 hours.

Series B: Based on the results of unconstrained swelling/shrinkage tests presented in Section 4.4.1, it was found that the rate of swelling of CW plates significantly reduced after approximately 40-45 days. Therefore, these specimens were subjected to 45 days of conditioning at 20 ± 2 °C and RH of $65 \pm 5\%$. This conditioning treatment may facilitate the locking of dowels in the timber due to springback. Dowel diameter and mass of the specimens were measured at 15-day intervals.

As CW dowels tend to expand mainly in the radial direction, the diameter was only measured in the radial direction at a pre-marked point 1 (10 mm above the timber surface) as shown in Figure 4.5.

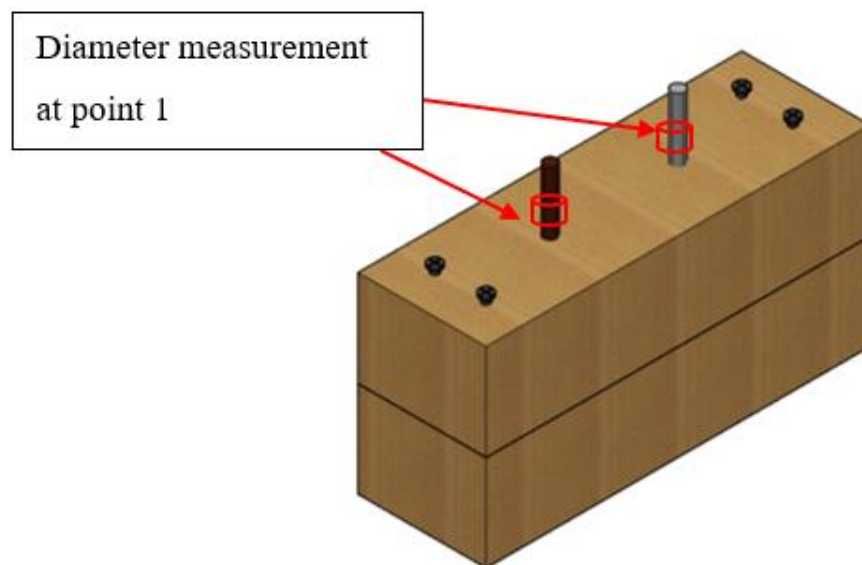


Figure 4.5- Swelling/shrinkage measurement in the radial direction at measurement points indicated by red circles

The change in dowel diameter of both the CW and beech wood dowels were calculated using the following expression:

$$\Delta d = \frac{d_t - d_i}{d_i} \times 100 \quad \text{Eq. 4.8}$$

where,

Δd is the radial change in dowel diameter (%),

d_t is the dowel diameter after the treatment (mm),

d_i is the initial dowel diameter which is measured prior to treatment of the specimens (mm).

Series C: Similar to Series B, all the specimens of this series were subjected to 45 days of conditioning at $65 \pm 5\%$ RH and 20 ± 2 °C temperature. For every specimen, dowel diameter (radial direction) and mass of the specimens were measured at 15-day intervals. On the 46th day, the specimens were subjected to a pressure soaking treatment to accelerate moisture diffusion in the timber and dowels, which in turn induced internal stresses in and around the connection. These specimens were only cycled once as per Method B of ISO 12580 [202]. Initially, specimens were placed in the pressure vessel and submerged in water at room temperature as shown in Figure 4.6a. Specimens were separated using a wire screen in such a manner that all end-grain surfaces were freely exposed to water. Then, the pressure vessel was closed and a vacuum of approximately 70 kPa was drawn and held for 30 minutes using a pressure gauge shown in Figure 4.6b. Subsequently, the vacuum was released and a pressure of approximately 550 kPa was applied for 2 hours. Specimens were then oven-dried at 70 °C temperature until the mass returned to 100 - 115% of the conditioned mass (mass on 45th day after conditioning) as shown in Figure 4.6c. Once the aforementioned mass was attained, specimens were conditioned for 24 hrs at $65 \pm 5\%$ RH and 20 ± 2 °C temperature before the pull-out test.

As this treatment involves four different steps water soaking, pressure treatment, oven drying and conditioning, the changes in dowel diameter are expected in both radial and tangential directions. For this reason, dowel diameter was measured in both the directions after each step at pre-marked point 1. For example, measurements were taken after pressure treatment, then oven drying and finally after conditioning.



(a)

(b)

(c)

Figure 4.6- Accelerated ageing test equipment, (a) pressure vessel, (b) treatment station, (c) drying treatment

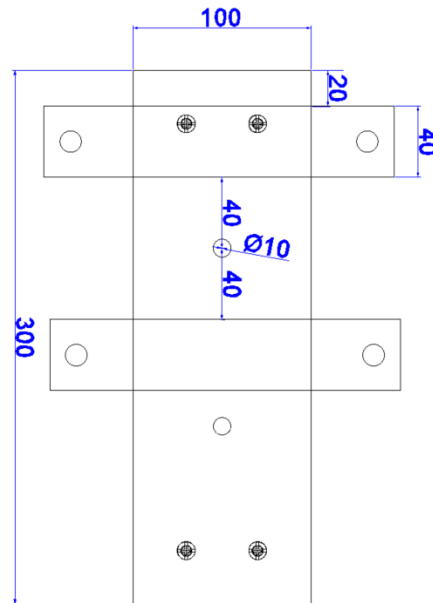
Series D: Specimens of this series were subjected to a treatment similar to Series C. However, 2 extra pressure soaking and drying cycles were added before final conditioning to know their effect on connection strength. Similar to Series C, the diameters of the dowels were measured after completion of each step of the individual cycle in both the directions at pre-marked point 1.

4.3.2.3 Pull-out tests

All treated specimens were subjected to pull-out tests as per EN 13182 [203]. Tests were performed using an Instron machine, model 4466, rated to 10 kN, under displacement control mode at a constant displacement rate of 1.5 mm/min. The testing rig comprised of a 2716 series manual wedge action grip and two steel plates for clamping the specimen on the steel platform using threaded steel bars as shown in Figure 4.7a. The distance between the inner edges (nearest to dowel) of the steel plates and the axis of the dowel was $4d$ (40 mm), as shown in Figure 4.7b. Once the specimen was securely clamped on the testing rig, the grip was tightened enough to pull the dowel axially in the upward direction (tension). And, the maximum pull-out load was recorded.



(a)



(b)

Figure 4.7- Testing rig, (a) test set up, (b) plan view of the test specimen showing edge distances of steel plate from the centre of the dowel

4.4 Test results and discussions

4.4.1 Results of unconstrained swelling/shrinkage of CW plates

4.4.1.1 Radial swelling during the conditioning phase

Figure 4.8 shows the change in the thickness of all CW plates over 510 days of the conditioning phase at the standard conditions of $65 \pm 5\%$ RH and $20 \pm 2^\circ\text{C}$ temperature. The solid lines show the change in the thickness of individual specimens and the dashed line represents the mean thickness change. Two random specimens (number 5 and 8) were separated after 190 days of conditioning to study the shrinkage behaviour of CW. These were represented by dotted lines in the graph. Every specimen showed an increase in the thickness which may be attributed to continuous springback of CW plates due to moisture adsorption. After approximately 180 days of conditioning, a plateau was observed due to a slower rate of swelling.

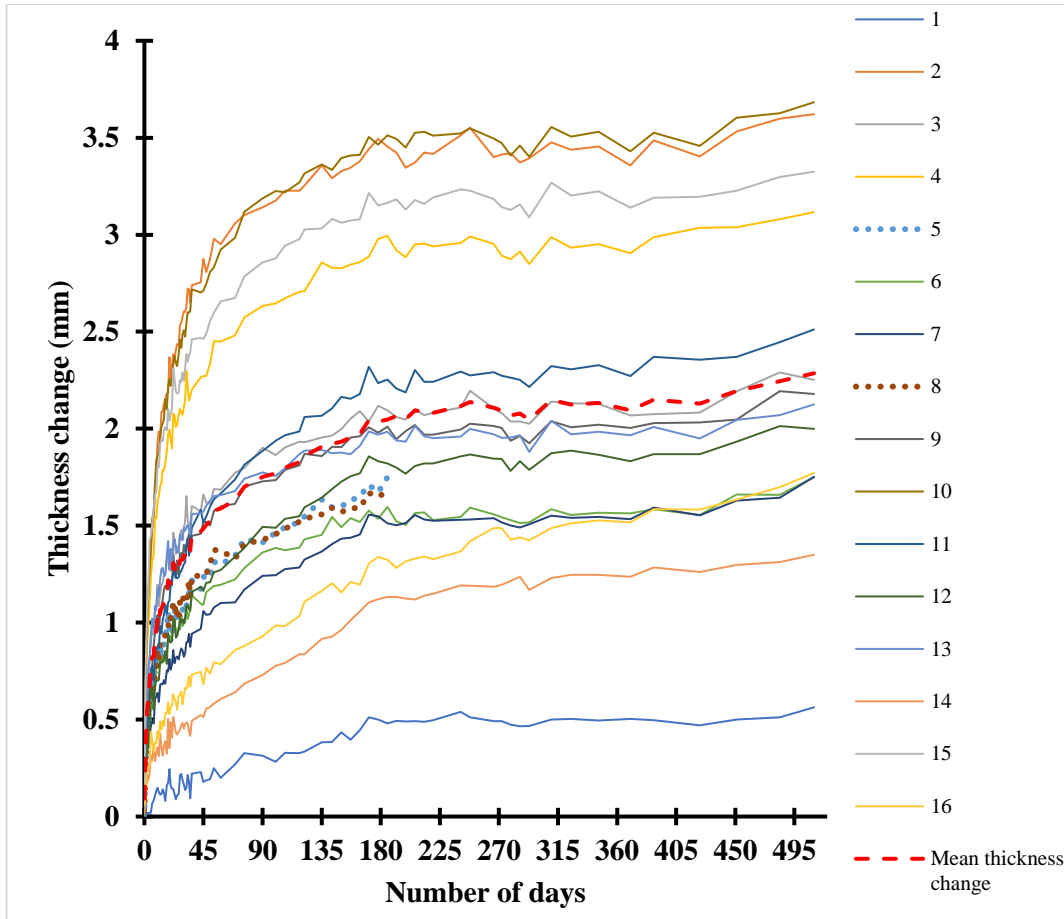


Figure 4.8- Change in the thickness of CW plates over a period of 510 days during conditioning phase (specimen number 5 and 8 were taken out for shrinkage study after 190 days)

Figure 4.9 shows the mean rate of thickness change vs. number of days. There was a rapid increase in the thickness during the first 10 days of exposure with a highest increase of 0.4 mm on first day. The mean rate of thickness increase for the first 10 days of exposure was approximately 0.2 mm/day. The mean rate of thickness increase between 10-20 days was approximately 0.07 mm/day. This was approximately 60% lower compared to the first 10 days of exposure. This rate slowed down with the increase in the number of days. The mean rate of thickness increase between 20-30 and 30-40 days was approximately 90.2% and 92.6% lower compared to the increase of the first 10 days, respectively. Between 40-50 days, this rate further decreased to approximately 96% when compared to the first 10 days of exposure.

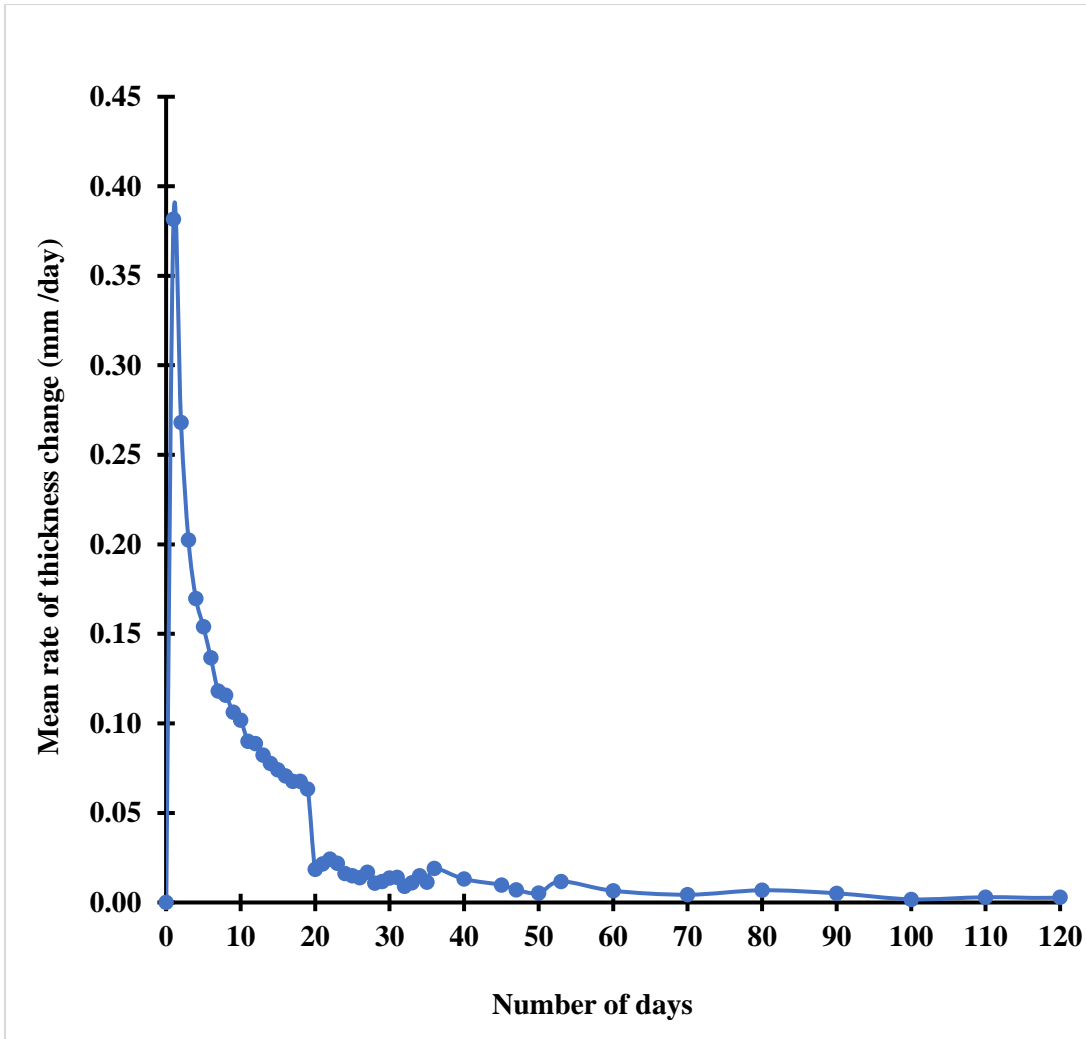


Figure 4.9- Mean rate of thickness change vs. number of days during the conditioning phase

Table 4.2 shows the change in the thickness of the individual specimens. The mean increase in the thickness of plates was 2.3 mm (excluding specimen number 5 and 8). This increase was approximately 20% (excluding specimen number 5 and 8) of the initial thickness. A larger variation was observed in the percentage thickness change, which may be attributed to the intrinsic variability in the properties of wood specimens due to differences in the proportion of latewood and earlywood, amount of resin canals and microscopic structure of the individual specimens.

Table 4.2- Change in the thickness of individual CW plates over a period of 510 days during the conditioning phase.

Specimen	Thickness at the start of experiment (mm)	Thickness on day 190 (mm)	Thickness on day 510 (mm)	Thickness change ΔT (mm)	Percentage thickness change ΔT (%)
1	12.4		12.9	0.6	4.6
2	11.0		14.6	3.6	32.9
3	11.0		13.2	2.3	20.5
4	11.5		14.6	3.1	27.1
5*	11.3	13.0		1.7	14.9
6	11.2		12.9	1.8	15.6
7	10.8		12.5	1.8	16.2
8*	11.8	13.4		1.6	13.7
9	10.7		12.8	2.2	20.5
10	11.0		14.7	3.7	33.6
11	11.1		13.6	2.5	22.6
12	11.8		13.8	2.0	16.9
13	11.8		14.0	2.1	17.9
14	11.3		12.6	1.4	12.0
15	11.6		15.0	3.3	28.5
16	11.3		13.1	1.8	15.6
Mean ^a with standard deviation in parentheses	11.3 (0.5)		13.6 (0.8)	2.3 (0.9)	20.3 (8.1)

Note: * shows the specimens taken for the study of shrinkage behaviour. The thickness change and percentage thickness change for Specimen 5 and 8 were calculated based on the initial thickness and thickness measurement on day 190. And, ^a shows the mean value excluding Specimens 5 and 8.

4.4.1.2 Mass change due to moisture adsorption and desorption during conditioning phase:

Figure 4.8 shows the change in the mass of CW plates due to moisture adsorption and desorption. Solid lines show the change in the mass of individual specimen and the dashed line represents the mean mass change. Specimen numbers 5 and 8 were represented by dotted lines on the graph. As expected, there was a rapid increase in the mass of specimens due to

adsorption of moisture during the initial period of exposure (10 days). During thermo-mechanical compression, wood loses a significant amount of moisture content as the process was carried out at a higher temperature which typically ranges between 120 to 160 °C [52]. This significantly reduces the moisture content (typically 4-5%) of the CW as observed during the manufacturing process. For this reason, when the CW is exposed to higher RH, it starts adsorbing the moisture at a faster rate as observed in the current study. There was a rapid increase in the mass during the first 10 days of exposure which gradually slowed down with the increase in the conditioning time. After approximately 180 days of conditioning, a plateau was observed due to an equilibrium with the surrounding environment.

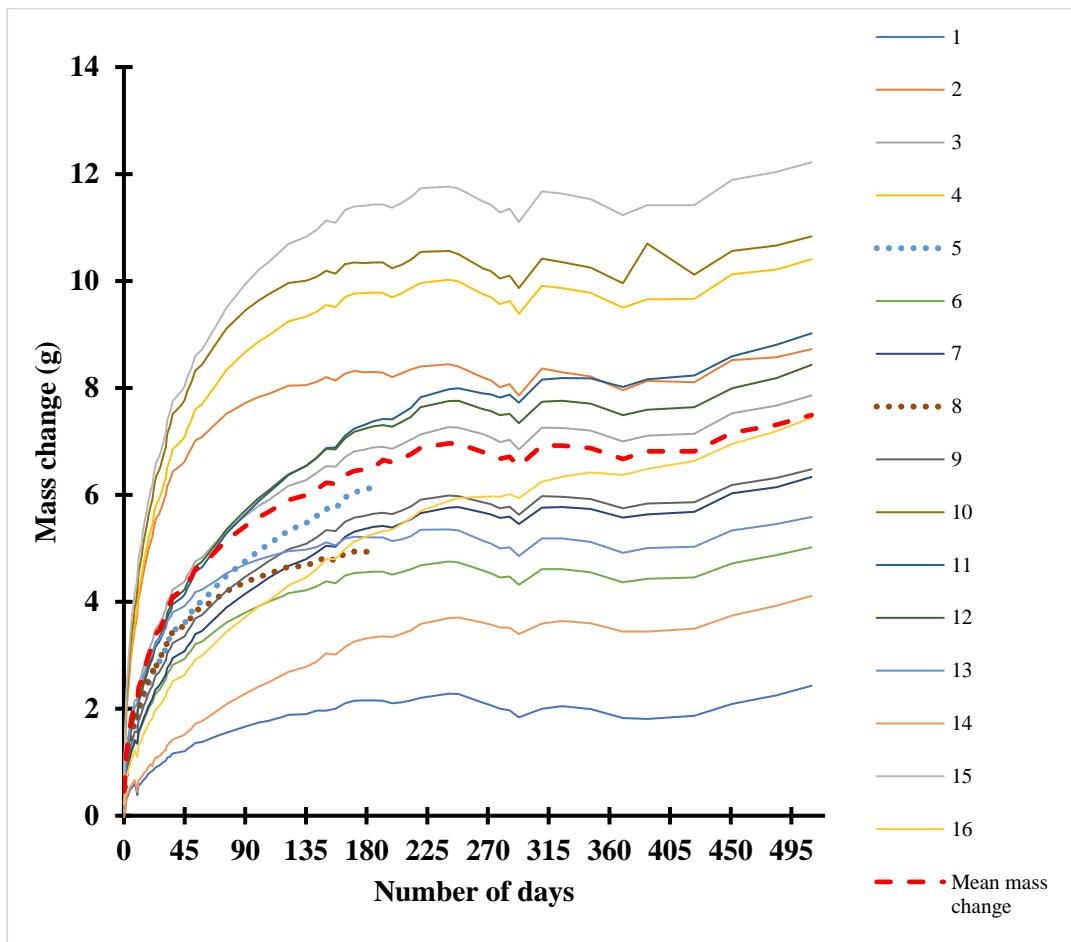


Figure 4.10- Change in the mass of CW plates over a period of 510 days during the conditioning phase (Specimen number 5 and 8 were taken out for shrinkage study after 190 days)

There was a rapid increase in the mass during the first 10 days of exposure with a highest increase of 0.8 grams on first day. The mean rate of mass increase for the first 10 days was approximately 0.3 g/day. The mean rate of mass increase between 10-20 days was approximately 0.2 g/day. This was approximately 49.7% lower compared to the first 10 days of exposure. This rate slowed down with the increase in the number of days. The mean rate of mass increase between 30-40 days was approximately 83.4% lower when compared to the

first 10 days. This rate further decreased to approximately 90.8% between 40-50 days when compared to the first 10 days of exposure.

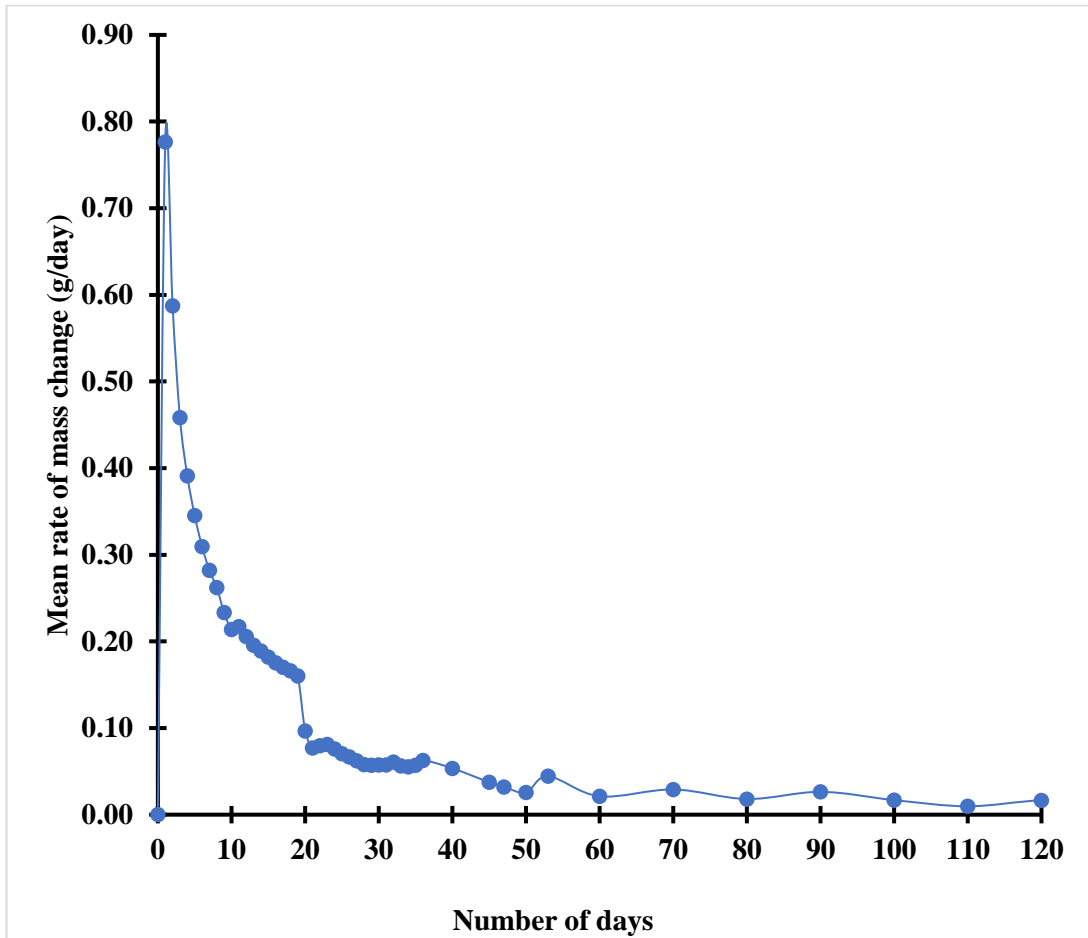


Figure 4.11- Mean rate of mass change vs. number of days during the conditioning phase

Table 4.3 shows the change in the mass of individual specimens. The mean increase in the mass of plates was 7.5 g (excluding Specimen number 5 and 8) of the initial thickness. This increase was approximately 4.7% (excluding Specimen number 5 and 8) of the initial mass.

Table 4.3- Change in the mass of individual CW plates over a period of 510 days during the conditioning phase

Specimen	Mass at the start of the experiment (g)	Mass on day 190 (g)	Mass on day 510 (g)	Mass increase ΔW (g)	Percentage mass increase ΔW (%)
1	178.5		180.9	2.4	1.4
2	124.5		133.2	8.7	7.0
3	170.5		178.4	7.9	4.6
4	152.0		162.4	10.4	6.8
5*	170.1	176.3		6.2	3.6
6	155.1		160.1	5.0	3.2
7	168.3		174.6	6.3	3.8
8*	159.5	164.4		4.9	3.1
9	152.1		158.6	6.5	4.3
10	141.1		152.0	10.8	7.7
11	164.2		173.2	9.0	5.5
12	203.2		211.6	8.4	4.1
13	145.1		150.7	5.6	3.9
14	198.1		202.2	4.1	2.1
15	170.9		183.2	12.2	7.1
16	176.1		183.5	7.4	4.2
Mean ^a with standard deviation in parentheses	164.3 (21.4)	-	171.8 (20.8)	7.5 (2.7)	4.7 (1.9)

Note: * shows the specimens taken for the study of shrinkage behaviour. The mass change and percentage mass change for Specimen 5 and 8 were calculated based on the initial mass and mass measurement on day 190. And, ^a shows the mean value without specimen 5 and 8.

4.4.1.3 Relationship between the change in thickness and mass during the conditioning phase

Figure 4.12 shows a relationship between the change in thickness vs. mass change during conditioning of CW at standard conditions of 65 ± 5 % RH and 20 ± 2 °C temperature. To understand the relationship, regression lines were fitted to experimental results and correlation was presented by the coefficient of determination (R^2). Linear regression line showed a R^2 value of 0.98, whereas polynomial regression line showed R^2 value of 0.99. The polynomial regression line fits well to the initial 2 g increase in the mass which was recorded during the

first 10 days of exposure. After 10 days, a linear relationship was observed between the change in thickness and mass.

The total increase in the thickness comprises of a reversible swelling/shrinkage component and an irreversible swelling component. The reversible swelling/shrinkage was due to the hygroscopic nature of wood and irreversible swelling due to springback. After approximately 180 days of conditioning, the moisture content reached an equilibrium and the mass change was negligible, but the springback continued and resulted in a thickness increase. The mass at equilibrium moisture content was about 6.7 g which is represented by numerous data points in

Figure 4.12. If a line is hand-drawn (black colour) from the origin point, it roughly demarcates irreversible and reversible swelling/shrinkage. The area between black and blue lines show the reversible swelling/shrinkage which eventually reduced to zero due to the constant conditioning phase. The area under the black line shows the irreversible swelling due to springback.

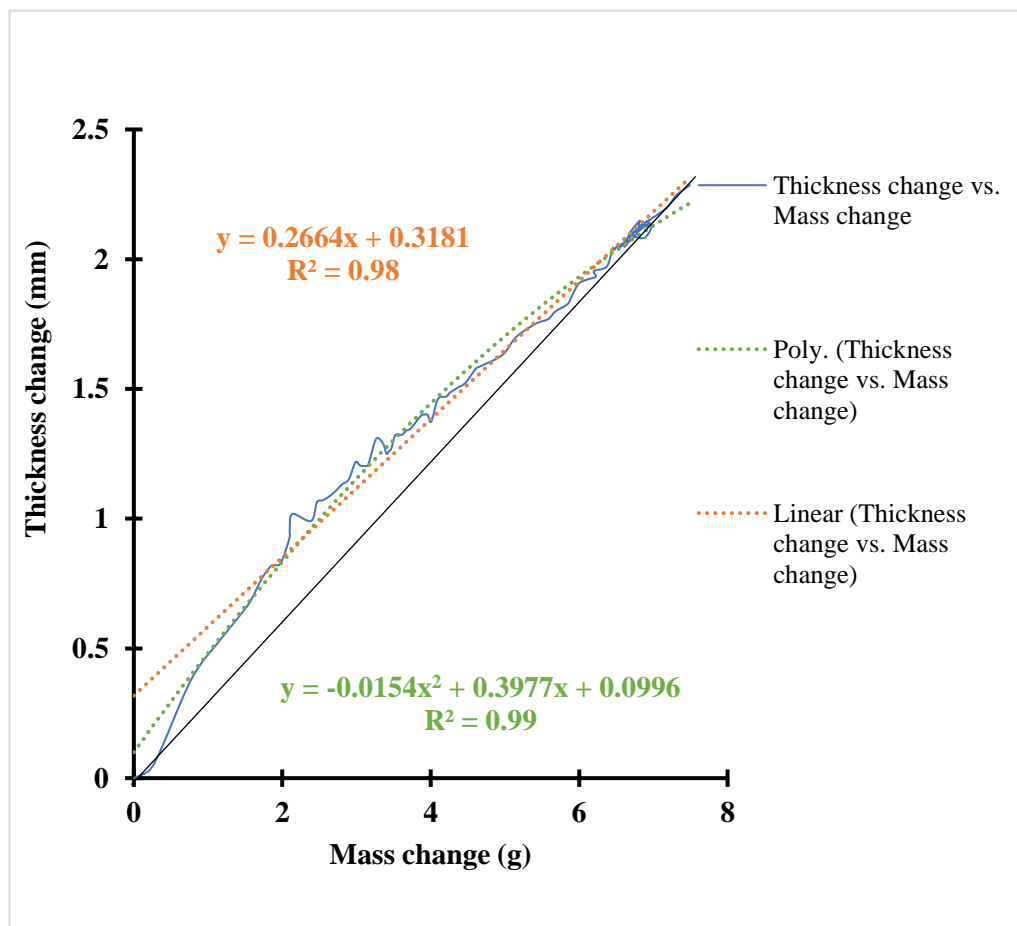
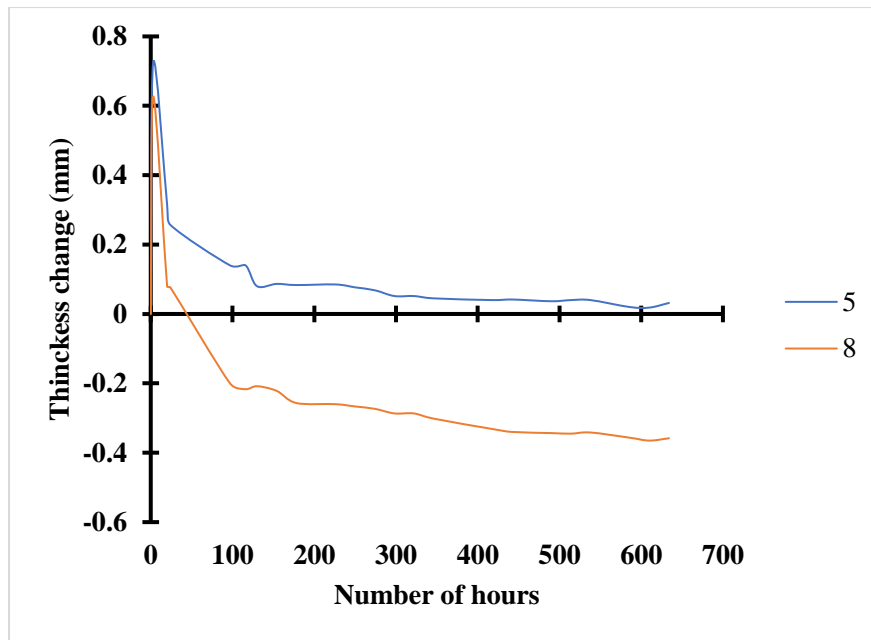


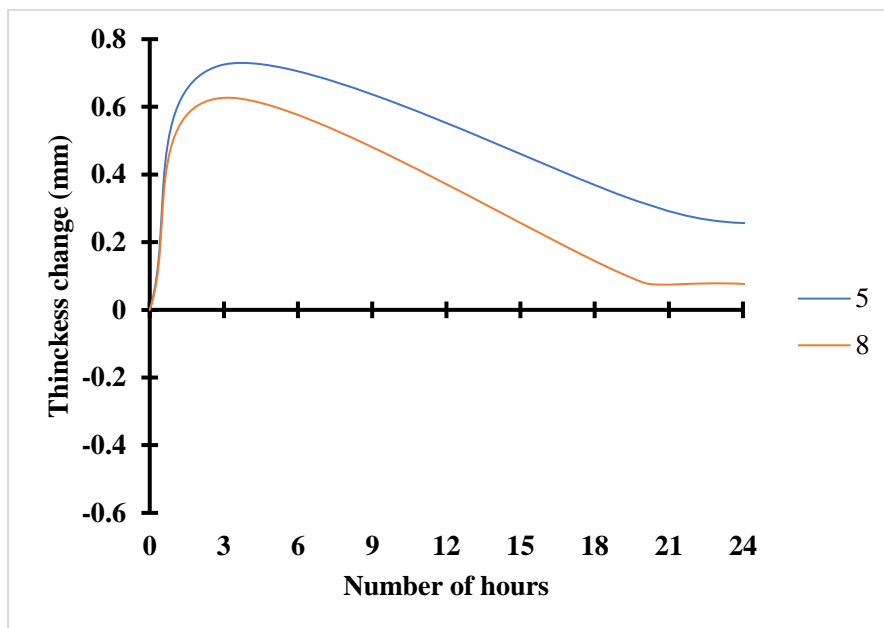
Figure 4.12- Relationship between change in the thickness vs. mass change of CW during the conditioning phase

4.4.1.4 Shrinkage of CW plates during oven drying at 103 ± 2 °C

To understand the springback behaviour of CW, Specimen number 5 and 8 were separated from the standard conditioning phase and placed in an oven at 103.5 ± 2 °C temperature. Figure 4.13a shows change in the thickness of both specimens during oven-drying. It should be noted that these plates were conditioned for 190 days before oven-drying and had gained approximately 3.5% mass due to moisture adsorption. There was a significant increase in the thickness of both specimens during the initial 3 hours of drying treatment as shown in Figure 4.13b. This behaviour is correlated with previous finding [100], which states that if a densified wood specimen is given the same conditions (temperature and moisture) that was used during densification, it tends to regain its original shape. In the current study, specimens were only oven-dried at 103.5 ± 2 °C which is 26.5 ± 2 °C lower than the temperature (130 °C) used during the thermo-mechanical compression process. Also, the moisture content was approximately 12% at the beginning of the compression process which is higher than the net moisture content (moisture content after compression \approx 4-5% + 3.5% moisture gain) of specimens after conditioning period. However, the given conditions are suitable enough to plasticize the cell wall of the specimens because hemicellulose (glass transition temperature \approx 54-56 °C at 15% moisture content) and lignin (glass transition temperature ranges from 72-128 °C at 15% moisture content) are above their glass transition temperatures [91]. It should be noted that lignin act as a restraint to dimensional changes. The plasticization of lignin and hemicellulose due to oven drying led to softening of moisture-laden cell walls of both the plates. This softening rapidly released the stresses that were generated in the plate during the thermo-mechanical compression process and exhibited rapid swelling. Once the moisture had completely evaporated, there was no plasticizing agent remained. And, specimens exhibited a continuous decrease in the thickness with increase in drying duration which is a typical of uncompressed timber.



(a)



(b)

Figure 4.13- Thickness change during oven-drying, (a) overall change in thickness, (b) thickness change during the first 24 hours

Both plates showed a continuous decrease in the mass over the entire period of drying due to moisture desorption as shown in Figure 4.14. The mass was constant after 26 days of oven drying.

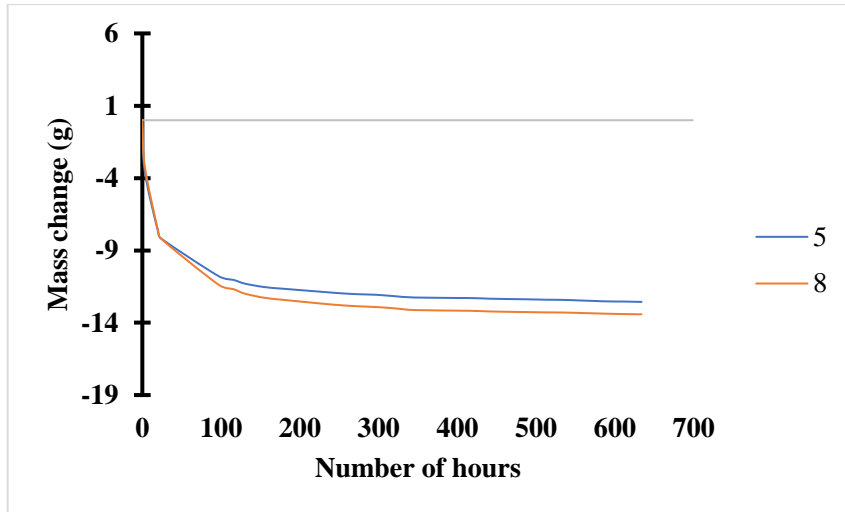


Figure 4.14- Mass change during oven-drying

To calculate the springback, thickness at constant mass was measured. The springback is presented as the difference between the increase in thickness due to conditioning (moisture dependent swelling) and shrinkage during oven-drying. During oven drying, decreases of 0.1% and 3.0 % were observed in the thickness of Specimen number 5 and 8, respectively. A continuous decrease in the mass was observed due to evaporation of moisture. Decreases of 3.7% and 5.3% were observed in the mass of specimen number 5 and 8, respectively. Specimens 5 and 8 showed springback of 14.8% and 10.7%, respectively. The typical behaviour of both plates is graphically presented in Figure 4.15.

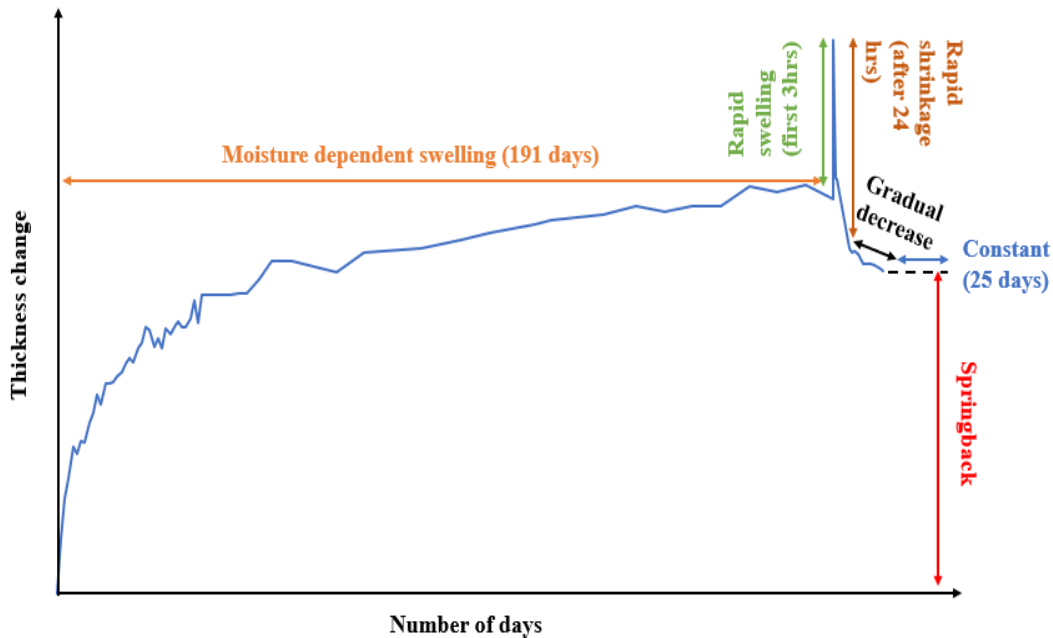


Figure 4.15- Typical behaviour of CW when subjected to moisture and heat

4.4.2 Results of accelerated ageing test

4.4.2.1 Radial swelling/shrinkage of dowels during 45 days of the conditioning treatment

Figure 4.16 shows the mean percentage radial swelling in CW dowels for all the specimens of Series B, C and D. These results confirm the continuous expansion of CW dowels during the conditioning phase, whereas the expansion was negligible in the beech wood dowels. It should be noted CW dowels showed 72% lower swelling compared to CW plates which may be attributed to the surrounding timber acting as a constraint. CW dowels showed approximately 564% increase in the radial swelling compared to beech wood dowels over a period of 45 days. Based on this behaviour, it can be concluded that CW dowels swell at a faster rate compared to beech wood dowels. Therefore, it can be assumed that expansion of CW dowels may facilitate form and friction locking of the dowels with the surrounding timber. This may improve the pull-out strength of specimens with CW dowels compared to the specimens with beech wood dowels.

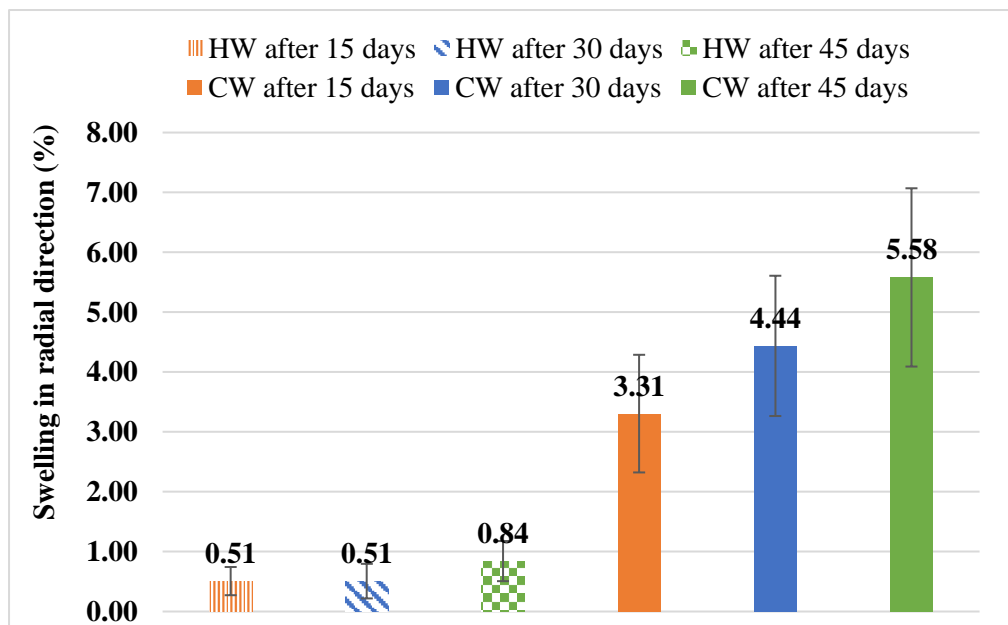


Figure 4.16- Mean percentage radial swelling/shrinkage results of beech wood dowels (denoted as HW) and CW dowels during the conditioning phase at 20 ± 2 °C temperature and 65 ± 5 % RH for 45 days (Series B, C and D)

4.4.2.2 Change in the diameter of the dowel during various treatments (Series B, C and D)

This section describes mean percentage swelling/shrinkage in dowel diameter of Series B, C and D. It should be noted that all specimens of Series B, C and D were conditioned for 45 days. During the conditioning period, change in radial diameter of CW is expected to be significantly higher compared to tangential direction. Thus, the diameter was only measured in the radial direction for aforementioned series. The measurements in the tangential direction were not recorded during the standard conditioning phase. But, for Series C and Series D,

pressure soaking and drying processes are expected to affect both the radial and tangential diameters. Thus, the diameters were recorded in both radial and tangential directions after completion of each cycle. Test results are presented for each series separately. Firstly swelling/shrinkage of dowels was compared with their initial diameters in corresponding directions. Then, swelling/shrinkage results were compared between dowel types (CW and beech wood) for each direction separately. The effect of change in dowel diameter on pull-out strength values is also discussed for each series. Finally, changes in the shape of the dowels are shown pictorially.

Series B: Figure 4.17 shows the change in mean dowel diameter of CW and beech wood dowels during the standard conditioning phase. The solid line indicates CW dowels and the dashed line indicates beech wood dowels. CW dowels exhibited a mean increase of 5.3% in radial diameter when compared to the initial diameter after 45 days of conditioning. The beech wood dowels showed a mean increase of only 1% of their initial radial diameter.

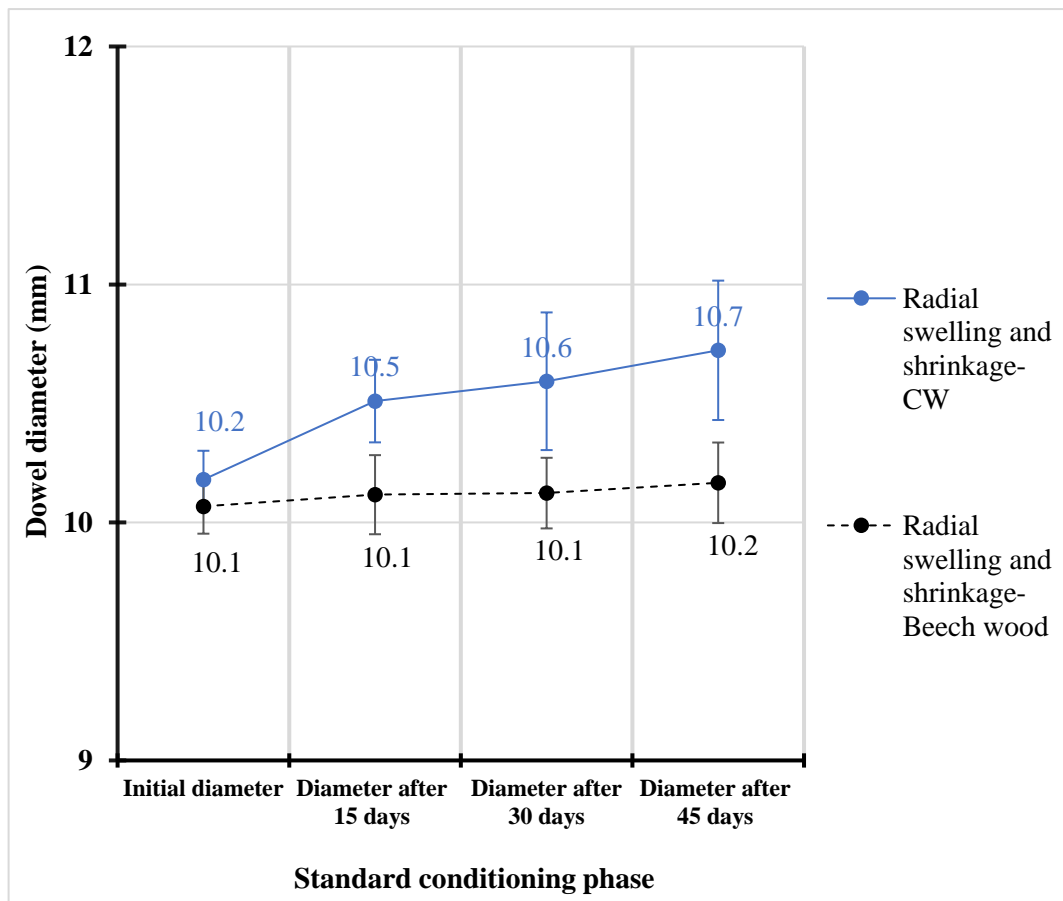


Figure 4.17- Change in dowel diameters of CW and beech wood dowels for series B

CW dowels expanded due to the springback in the radial direction and exhibited an elliptical shape. However, beech wood dowels maintained their circular shape as shown in Figure 4.18.

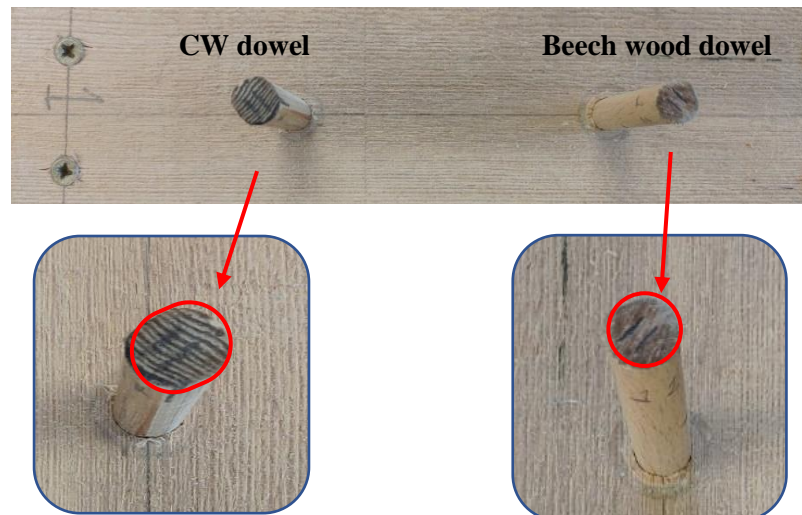


Figure 4.18- Shape of the dowels of Series B after 45 days of the conditioning phase

Series C: Figure 4.19 shows the change in mean dowel diameters of CW and beech wood dowels during various steps of treatment. CW dowels showed a mean increase of 34% in radial diameter when compared to the initial diameter. This increase in radial diameter was only 2.3% for the beech wood dowels. In the tangential direction, CW dowels showed a negligible increase of 0.4% in mean diameter, whereas this increase for beech wood dowels is about 1.2%. When mean dowel diameter of CW dowels are compared with beechwood dowels in corresponding radial and tangential directions, they showed swelling of 31% in the radial direction and 0.9% shrinkage in the tangential direction. Irrespective of swelling/shrinkages in both dowel types, their corresponding diameters were higher than the substrate hole diameters which were 10 mm and 10.2 mm. The mean radial swelling of CW dowels of this series was 28.7% higher than CW dowels of Series B. This was expected because of water soaking and pressure cycle. The mean radial swelling of beech wood dowels of this series was 1.3% (negligible) higher than beech wood dowels of Series B. Thus, an increase can be expected in pull-out test results in comparison to dowels of Series B.

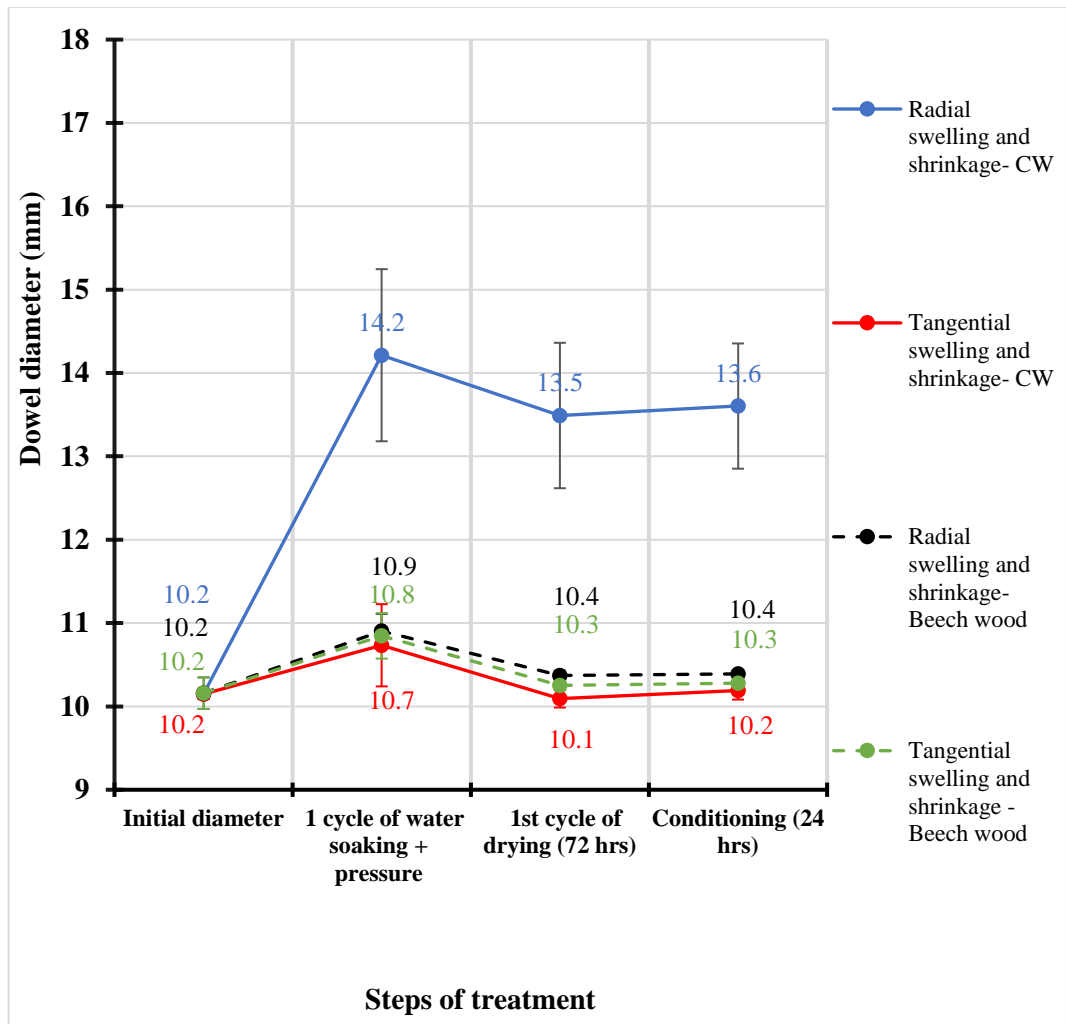
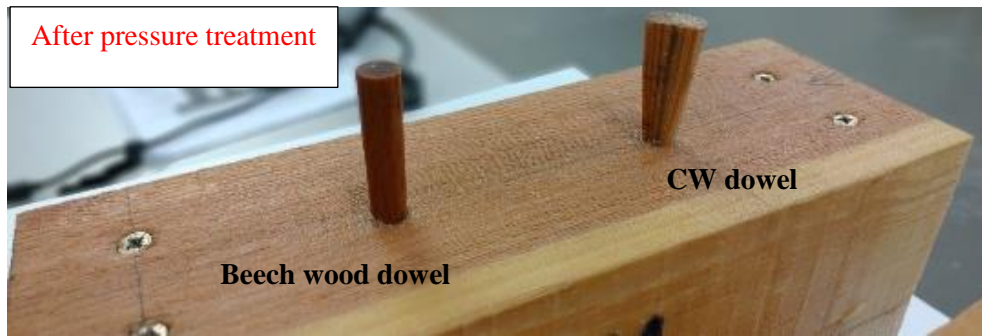


Figure 4.19- Change in dowel diameters of CW and beech wood dowels for series C

CW dowels expanded due to springback in the radial direction and formed a funnel shape geometry after the pressure treatment as shown in Figure 4.20a. This shape remained stable during subsequent drying and conditioning as shown in Figure 4.20b. However, beech wood dowels maintained their cylindrical shape.



(a)



(b)

Figure 4.20- Shape of the dowels of series C, (a) after water soaking and pressure treatment (b) after oven drying

Series D: Figure 4.21 shows the change in mean dowel diameters of CW and beech wood dowels during various steps of treatment. CW dowels showed a mean increase of 42% of the initial diameter in radial direction. Whereas, this increase was only 2.5% for the beech wood dowels. In the tangential direction, CW dowels showed a negligible decrease of 0.5% in mean diameter, whereas beech wood dowels showed an increase of 2.5% (similar to radial diameter). When mean dowel diameter of CW dowels are compared with beechwood dowels in corresponding radial and tangential directions, they showed 42.5% increase in radial direction and 1.1% shrinkage in the tangential direction. The mean radial swelling of CW dowels of this series was 8% higher than CW dowels of Series C. This was expected because of two additional pressure soaking cycles. The CW dowels of this series showed about 0.9% higher tangential shrinkage compared to Series C. The mean radial swelling of beech wood dowels of this series was 0.2% (negligible) higher than beech wood dowels of Series C. The beech wood dowels of this series showed about 1.4% higher tangential swelling compared to Series C. Because of tangential shrinkage of CW dowels of this series, they may show lower pull-out load values. Whereas, beech wood dowels of this series may show higher pull-load due to increase in diameter in both radial and tangential directions.

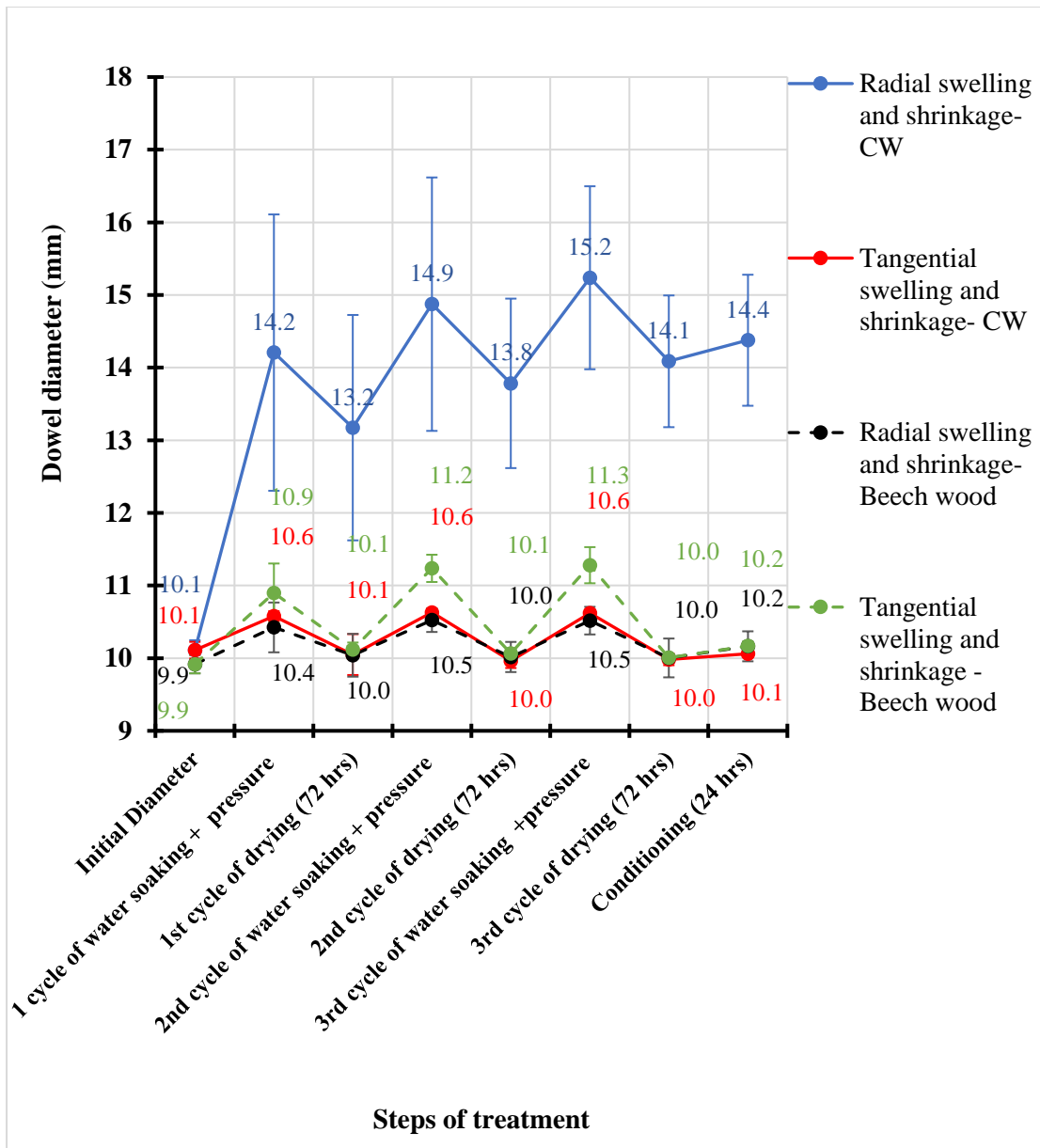
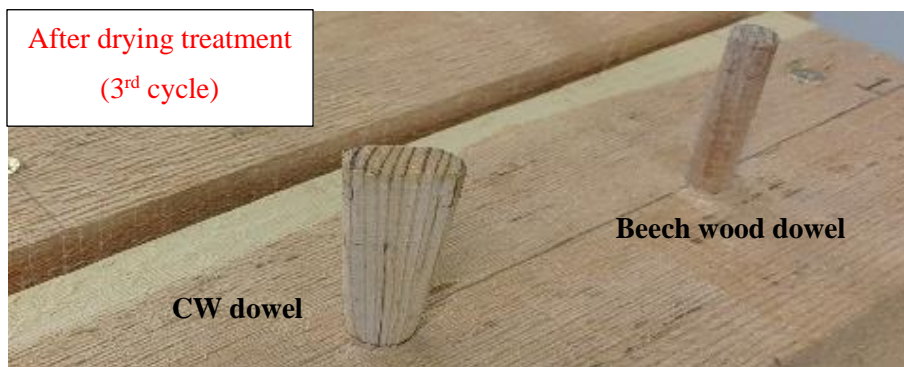


Figure 4.21- Change in dowel diameters of CW and beech wood dowels for series D

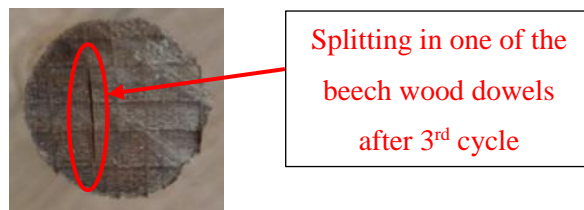
CW dowels expanded due to sprinback in the radial direction and formed a funnel shape geometry after 1st cycle of pressure treatment as shown in Figure 4.22a. This shape further enlarged (about 10% higher) during subsequent pressure cycles. However, beech wood dowels maintained their cylindrical shape as shown in Figure 4.22b. Splitting was observed in one of the beech wood dowels in the radial direction as shown in Figure 4.22c.



(a)



(b)



(c)

Figure 4.22- Shape of the dowels of series D after 3rd cycle, (a) after water soaking and pressure treatment (b) after final drying treatment, (c) splitting in one of the beech wood dowels

Also, timber substrates developed serious cracks after completion of 3rd cycle as shown in Figure 4.23. These cracks resemble as to natural weathering in timber because when timber is exposed to moisture variations, stresses develop in the cell wall and between cells and, these lead to damage and the formation of cracks [204]. However, a long-term natural weathering study is needed to evaluate the effect of these cracks on the mechanical performance of connection with time. In the current study, it is expected that cracking may release the stresses that had developed during ageing cycles and may impact the failure mechanism and pull-strength of the connection.

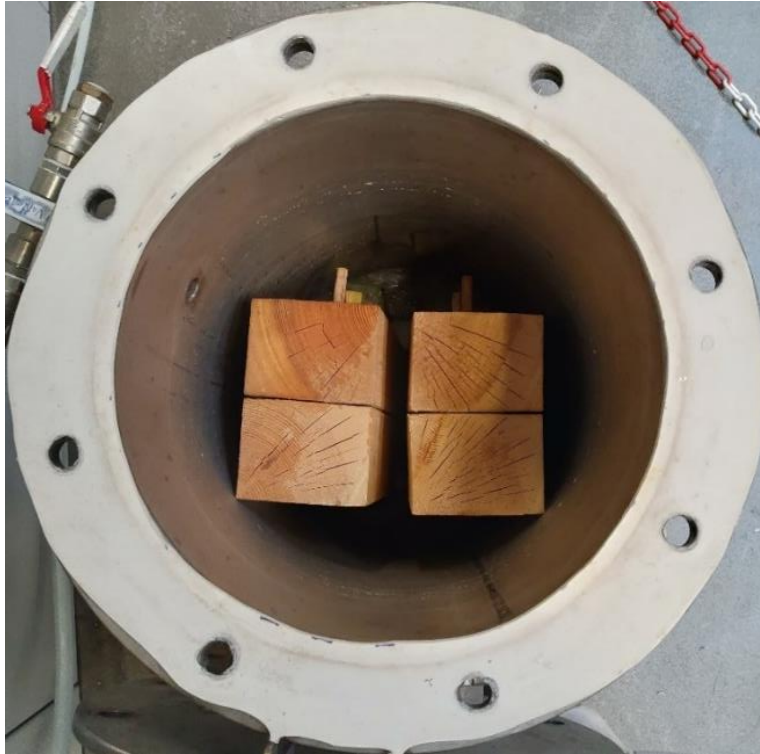


Figure 4.23- Cracks on the surface of specimens after 3rd pressure cycle

4.4.2.3 Pull-out test results and failure modes

This section details the pull-out test results of all specimens of Series A, B, C and D. The load vs. ram displacement behaviour of each series are discussed separately with corresponding failure modes shown pictorially. For all the load vs. ram displacement graphs, solid lines indicate connections with CW dowels and dashed lines indicate connections with beechwood dowels. Also, the test results of each series were compared between CW dowels and beech wood dowels, which were given the same treatment.

Series A: Figure 4.24 shows the pull-out load vs. ram displacement behaviour of this series. Specimens of this series were kept at laboratory conditions (19 °C temperature and 82% RH) for only 24 hrs after dowel insertion. Thus, a negligible amount of dowel expansion is expected. As expected, there was no significant difference between the pull-out strength of CW dowels and beech dowels. The mean pull-out strength of beech wood dowels was only 10% lower than the CW dowels which may be due to the effect of hole clearance.

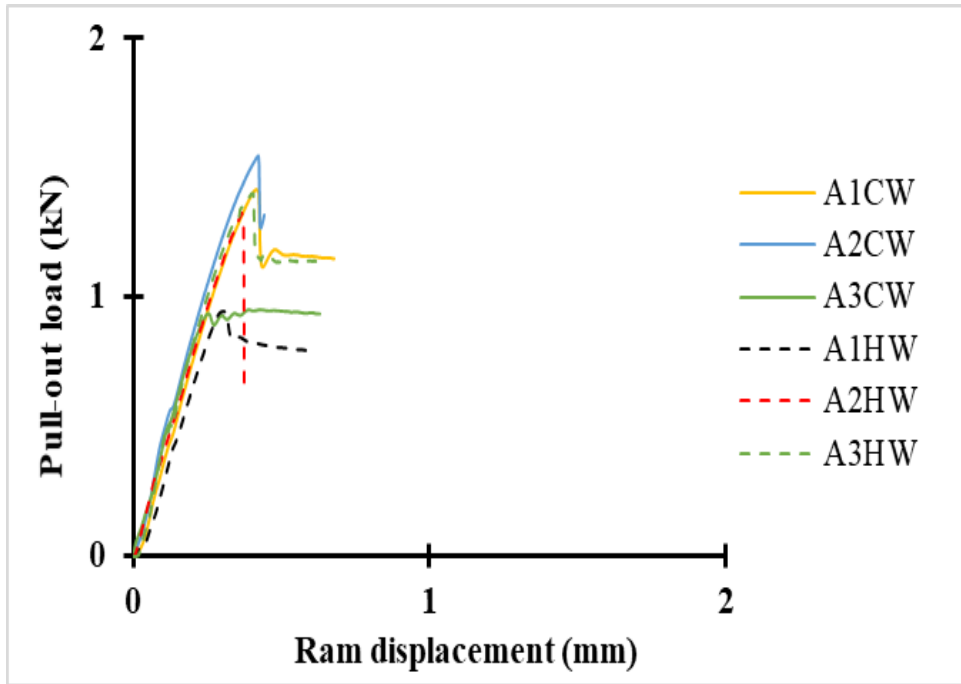


Figure 4.24- Pull-out load vs. ram displacement graph for Series A

Tested specimens are shown in Figure 4.25. Both CW and beech wood dowels were pulled out easily once the maximum load attained.

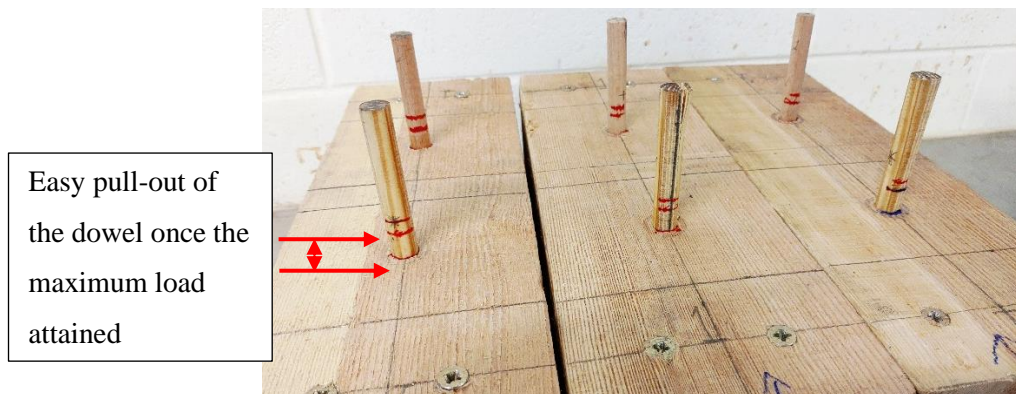


Figure 4.25- Failure of CW dowels and beech wood dowels of series A

Series B: Figure 4.26 shows the pull-out load vs. ram displacement graph of this series. The specimens with CW dowels did not show consistent load-displacement behaviour. This behaviour may be due to non-uniform expansion of CW dowels throughout the embedded length within the timber substrate. CW shows large variations (4% - 33%) in radial expansion as observed from the unconstrained swelling/shrinkage tests results (see Table 4.2). These variations may be attributed to intrinsic characteristics of wood such as percentage of earlywood/latewood material and ray volumes in the cross-section of CW dowels [35,93]. CW dowels with a higher amount of earlywood are expected to expand at a faster rate when compared to dowels with a higher amount of latewood [104]. In a practical situation, to have an equal proportion of latewood/earlywood in every specimen of CW dowel may not be

possible. Thus, uniform expansion of CW dowel throughout the embedded length may not be possible and such variations are inevitable. In this study, the expansion of CW dowels was not measured within the embedded length. Thus, it is difficult to point out the exact cause of variations in the test results. Nevertheless, the maximum pull-out strength values of all the specimens with CW dowels were relatively closer (3.6 kN to 4 kN). The pull-out strength of the connections with CW dowels was 387% higher than connections with beech wood dowels. Conditioning of connections allows continuous expansion of CW dowels in the radial direction and facilitates form and friction locking. Beech wood dowels for this series showed loosening of connections relative to Series A even though the hole clearance for this series was approximately 56% lower. Also, the diameter of the dowels was 1% higher in the radial direction when compared to the diameter at the beginning of the experiment. However, it is well reported for normal timber that it swells and shrinks more in tangential direction compared to longitudinal and radial directions [30,54]. Shrinkage in tangential direction may loosen the connection which may be correlated to higher volumetric shrinkage in hardwoods than softwoods. The loosening of beech wood connections may be due to natural variability or tangential or volumetric shrinkage of beech wood dowels. A larger sample with both radial and tangential diameter measurements would be needed to investigate this. Similar to Series A, no failure was observed in the timber and dowels (CW and beech wood). A continuous increase in the displacement was observed once the maximum load was attained.

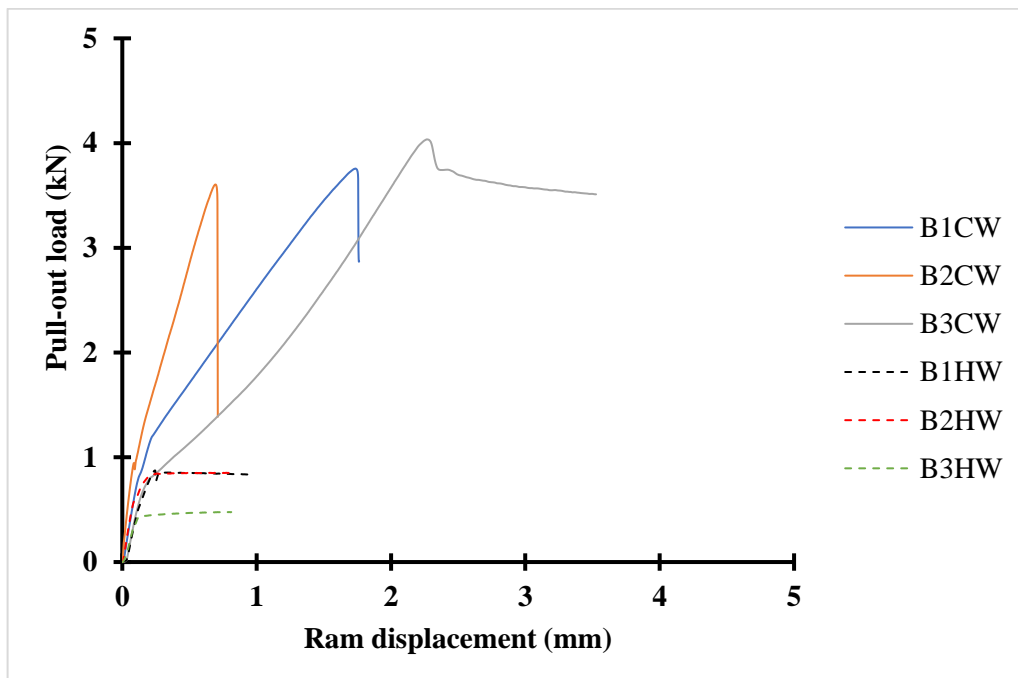


Figure 4.26- Pull-out load vs. ram displacement graph for Series B

Series C: Figure 4.27 shows the pull-out load vs. ram displacement behaviour of this series. The pull-out strength of the connections with CW dowels was 75% higher than the

connections with beech wood dowels. When compared with CW connections of Series A and B, there were increases of 353% and 55% in the pull-out strength values, respectively. Similarly, when the beech wood connections of this series were compared with Series A and B, results showed increases of 184% and 331%, respectively.

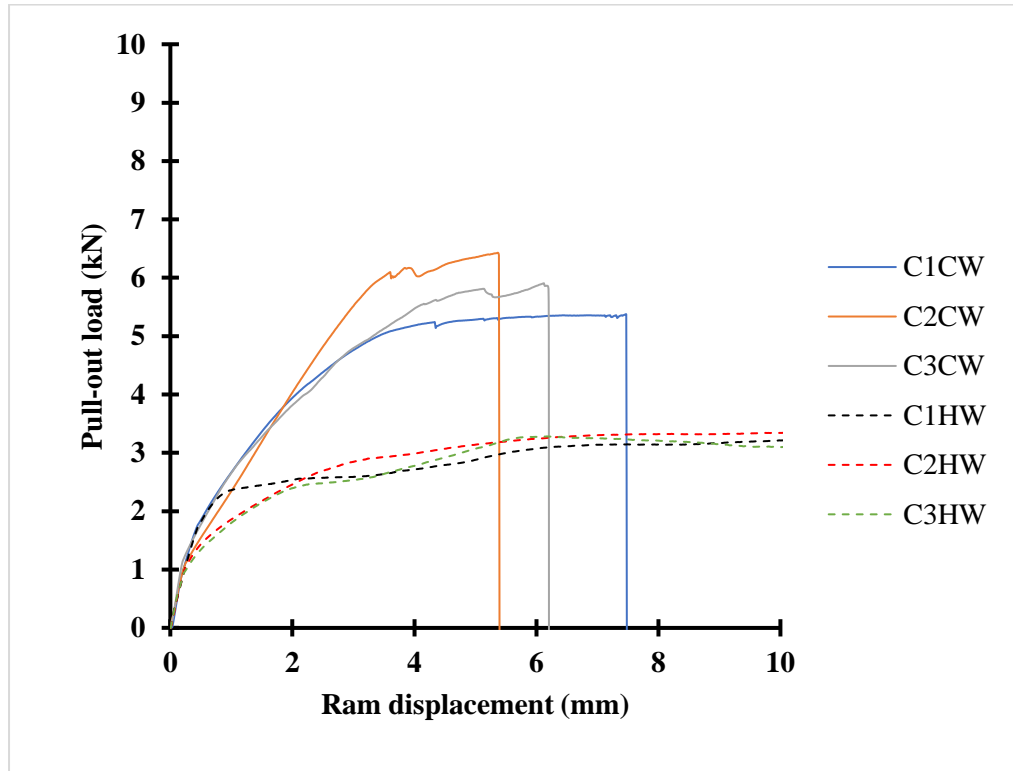


Figure 4.27- Pull-out load vs. ram displacement graph of Series C

As expected, diffusion of water due to pressure treatment induced swelling of both CW and beech wood dowels and facilitated form and friction locking. After the 1st cycle, both CW and beech wood dowels did not recover their initial diameter, and this resulted in the tightening of the connections. The CW dowel connections showed brittle failure (see Figure 4.28) of the dowels once they attained maximum load at an average withdrawal displacement of 6.3 mm. This means the pull-out strength of the connection is higher than the tensile strength of the CW dowel. In contrast to this, beech wood dowels pulled out easily once they achieved the maximum load with a continuous increase in the displacement.

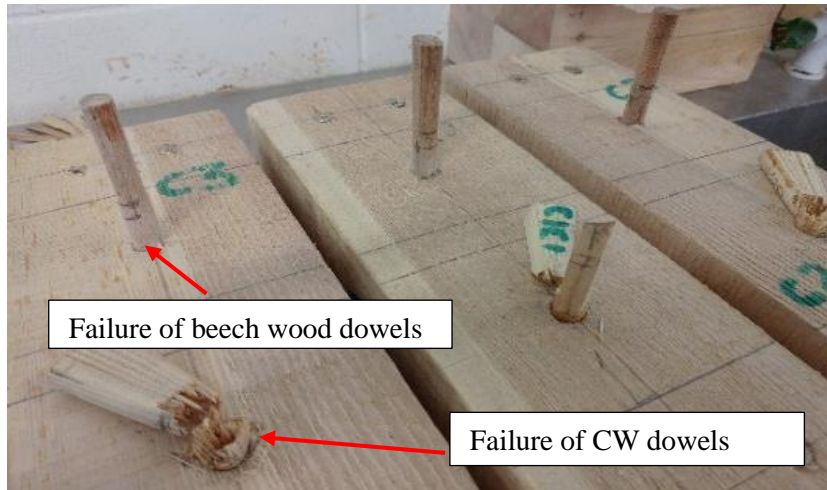


Figure 4.28- Failure of CW and beech wood dowels of Series C

Series D: Figure 4.29 shows the pull-out load vs. ram displacement behaviour of this series. It was expected that ageing cycles (or treatment) may result in lower pull-out strength values. However, increasing the number of ageing cycles positively affected the pull-out strength of the CW connections. They showed a 145% higher pull-out strength than connections with beech wood dowels. When compared with the pull-out strength of the CW connections of Series A, B and C, there were increases of 429%, 81% and 17%, respectively. This was possibly due to a relatively tighter fit of CW dowels of this series with the timber substrates. It should be noted that the specimen of Series C showed brittle failure at relatively lower mean pull-out load. Thus, a brittle failure (tensile failure) similar to Series C could be expected from this series as well. However, the CW dowels of this series pulled out easily without any brittle failure (see Figure 4.30) once the maximum load was attained.

When the pull-out strength values of beech wood dowels of this series were compared with beech wood connections of Series A and B, there were increases of 137 % and 259%, respectively. In comparison to beech wood connections of Series C, specimens of this series showed a 17% lower pull-out strength. It should be noted that the radial expansion of this series (2.5%) was relatively higher than the Series C (2.3%). Also, tangential expansion was 1.4% higher than that of Series C. This means a higher pull-strength can be expected as the expansion was higher. However, the obtained pull-out strength values showed an opposite trend. When comparing the failure mechanism of beech wood dowels of this series with Series A, B and C, a similar failure was observed with the continuous increase in the displacement once the maximum load was attained as shown in Figure 4.30.

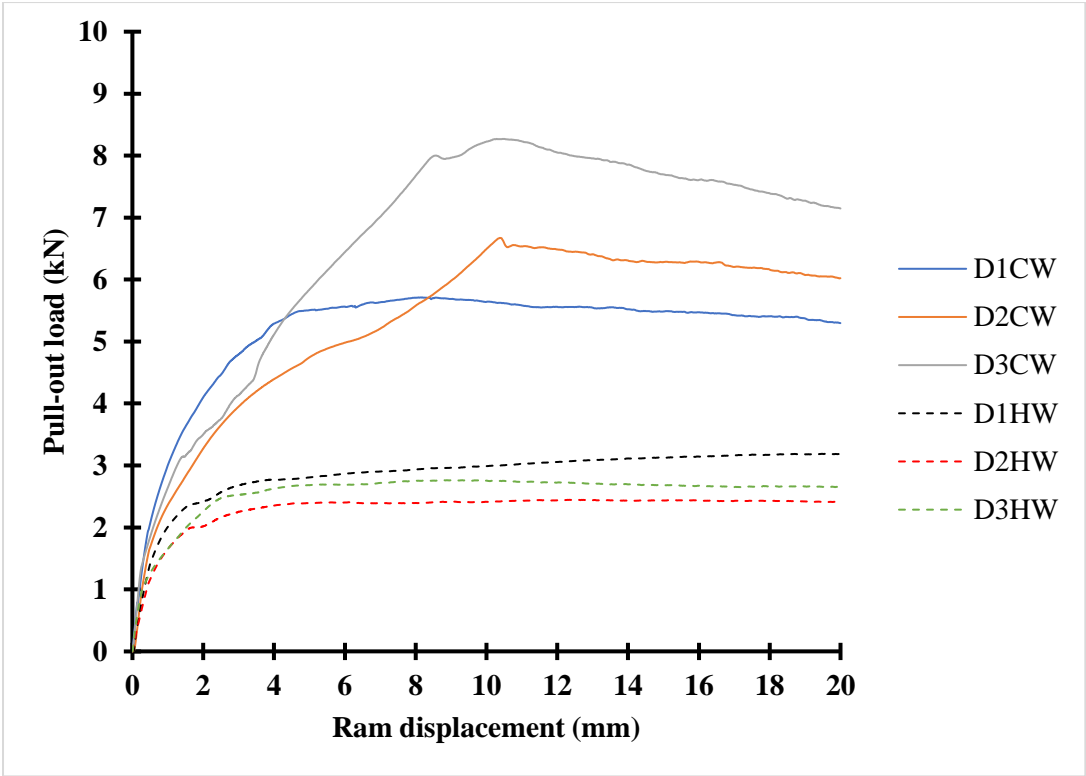


Figure 4.29- Pull-out load vs. ram displacement graph of Series D

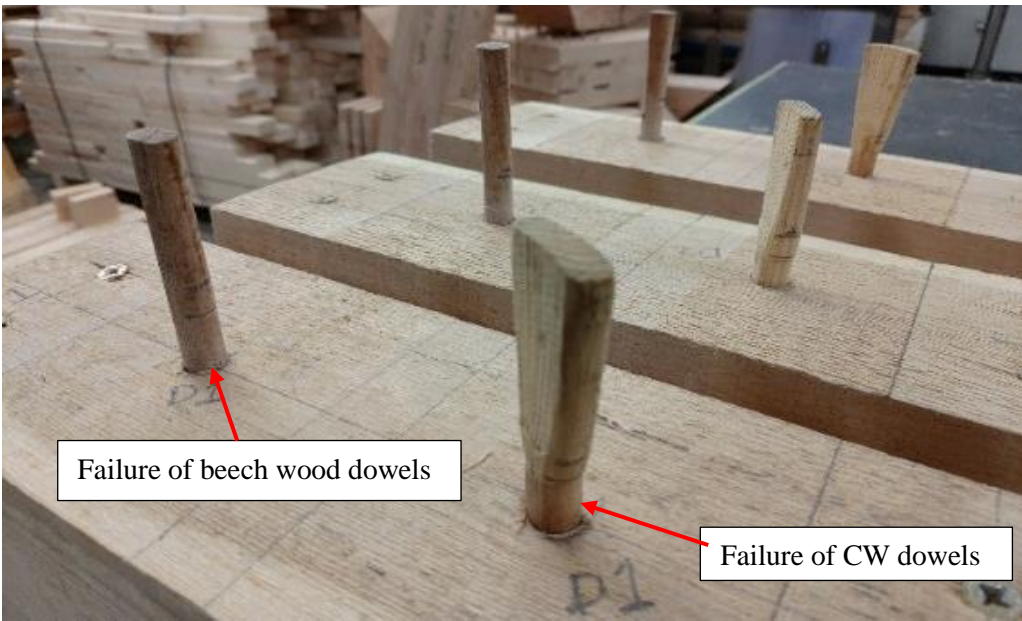


Figure 4.30- Failure of CW and beech wood dowels of series D

4.4.2.4 Results summary of pull-out test results

Table 4.4 shows test results of all individual specimens of Series A, B, C and D for pull-out tests.

Table 4.4- Results of pull-out tests

Series type	Dowel type	Specimen ID	Pull-out load (kN)	Mean Pull-out load (kN) with standard deviation in parentheses
A	Beech wood	A1HW	0.9	1.2 (0.2)
		A2HW	1.3	
		A3HW	1.4	
	CW	A1CW	1.4	1.3 (0.3)
		A2CW	1.5	
		A3CW	1.0	
B	Beech wood	B1HW	0.9	0.8 (0.2)
		B2HW	0.9	
		B3HW	0.6	
	CW	B1CW	3.8	3.8 (0.2)
		B2CW	3.6	
		B3CW	4.0	
C	Beech wood	C1HW	3.4	3.4 (0.1)
		C2HW	3.4	
		C3HW	3.3	
	CW	C1CW	5.4	5.9 (0.5)
		C2CW	6.4	
		C3CW	5.9	
D	Beech wood	D1HW	3.2	2.8 (0.4)
		D2HW	2.4	
		D3HW	2.8	
	CW	D1CW	5.7	6.9 (1.3)
		D2CW	6.7	
		D3CW	8.3	

4.4.2.5 Explanation on variations in failure mechanism and pull strength values of Series C and D

Variations were observed in the pull-out strength values and failure mechanism (only for CW dowels) of Series C and D. Therefore, the following questions can be discussed to explain the variations:

1. Lower pull-out strength values were expected for Series D due to the increasing number of ageing cycles, why CW connections of this series showed higher pull-out strength values when compared to Series C?
2. As the CW dowels of Series C showed brittle failure at relatively lower pull-out load (mean) when compared to Series D, why the failure mechanism of CW dowels was not similar to Series C?
3. Although the radial and tangential expansion of beechwood dowels of Series D were higher than that of Series C, why beech wood dowels of Series D showed lower pull-out strength values?

To answer the above questions, the effect of the following parameters was investigated:

1. Effect of hole clearance on the pull-out strength and failure mechanism of Series C and D

The mean hole clearance of CW dowels of Series D was 0.04 mm higher than Series C. This means CW dowels of Series C had a tighter fit compared to the dowels of Series D. Hence, specimens of Series C should exhibit a higher pull-out strength compared to Series D. However, the results were opposite. It should be noted that the specimens of Series C were given only one cycle of treatment, whereas specimens of Series D were cycled three times. It was understood that the water soaking and pressure treatment will diffuse water molecules within the CW dowels and timber substrate, and particularly increase the radial diameter of CW dowels due to springback effect. To evaluate the effect of hole clearance on pull-out strength of Series C and Series D, the mean diameters of CW dowels of both the series were compared in radial and tangential directions after the first cycle of water soaking and pressure treatment. The mean radial diameter of CW dowels of both the series was same (14.2 mm). And, the mean tangential diameters of Series C and D were 10.7 mm and 10.6 mm, respectively. The radial and tangential diameters of both the series were relatively higher than the substrate hole (dowel hole) diameter which was 10.2 mm (constant).

Similar to CW dowels, beech wood dowels also expanded after the first cycle of treatment. The mean radial diameters of beech wood dowels for Series C and Series D were 10.9 mm and 10.4 mm, respectively. Also, the mean tangential diameters for Series C and Series D were 10.8 mm and 10.9 mm, respectively. The radial and tangential diameters of both the series were relatively higher than the substrate hole diameters which were 10.0 mm and 10.2 mm.

Based on the above discussion, it can be concluded that the radial and tangential diameters of both the series were significantly higher than the substrate hole diameter irrespective of dowels type. This means that the effect of hole clearance could be nullified as both CW and beech

wood dowels are exerting swelling forces on the walls of the substrate hole based on their material behaviour. From the above discussion, it was clearly understood that ageing cycles facilitated the tight fit of both the dowel types with the respective timber substrates. This means that the effect of hole clearance should not influence the pull-out strength of both the Series C and D irrespective of dowel types.

2. Effect of radial and tangential swelling/shrinkage of CW dowels and timber on pull-out strength and failure mechanism on Series C and D

As observed, CW dowels expanded in both radial and tangential direction after completion of corresponding ageing cycles. Due to two additional pressure soaking cycles, a higher swelling is expected within the dowels of Series D when compared to Series C. To validate this, radial and tangential diameters of both CW and beech wood dowels were measured immediately after the completion of corresponding ageing treatment. For the clarity purposes, results were compared separately for each dowel type.

i. Comparison between radial and tangential swelling of CW dowels for Series C and Series D

As expected, the swelling of CW dowels in the radial direction was significantly higher than the tangential direction due to radial springback. For Series C, the mean radial diameter was 13.6 mm after completion of the corresponding ageing cycle, whereas this was 14.4 mm for Series D. In percentage, the mean radial dowel diameter of Series D was 8.2% higher when compared to Series C. These findings confirmed that the increase in the number of ageing cycles results in a significant swelling of dowels in a radial direction. Each cycle is releasing the stresses which were developed during thermo-mechanical compression and consequently improving the tightness of the connection. In contrast to this, the tangential diameter of CW dowels of Series D was lower than Series C. For Series C, the mean tangential diameter was 10.2 mm after completion of corresponding treatment, whereas this was 10.1 mm for Series D. This means dowels shrunk tangentially with a greater number of cycles. The ratio of radial to tangential dowel diameter for CW dowels of Series C was 1.3, whereas this was 1.4 for Series D. Table 4.5 shows the individual measurement of each specimen of the corresponding series. As the difference between tangential dowel diameter of Series C and D were negligible, it can be said that the only radial swelling affects the pull-out strength. And radial swelling was higher for Series D compared to Series C. This may be a possible reason for higher pull-out strength values of Series D compared to Series C.

Table 4.5- Radial and tangential swelling of CW dowels for Series C and Series D after corresponding ageing treatment

Specimen ID	Number of treatment cycles	Diameter after completion of corresponding treatment cycles (mm)		Ratio of radial to tangential dowel diameter	Mean values of Ratio of radial to tangential dowel diameter
		Radial direction	Tangential direction		
C1CW	1	12.9	10.1	1.3	1.3
C2CW		14.4	10.2	1.4	
C3CW		13.6	10.3	1.3	
D1CW	3	14.7	10.0	1.5	1.4
D2CW		15.1	10.1	1.5	
D3CW		13.4	10.1	1.3	

ii. Comparison between radial and tangential swelling of beech wood dowels for Series C and Series D

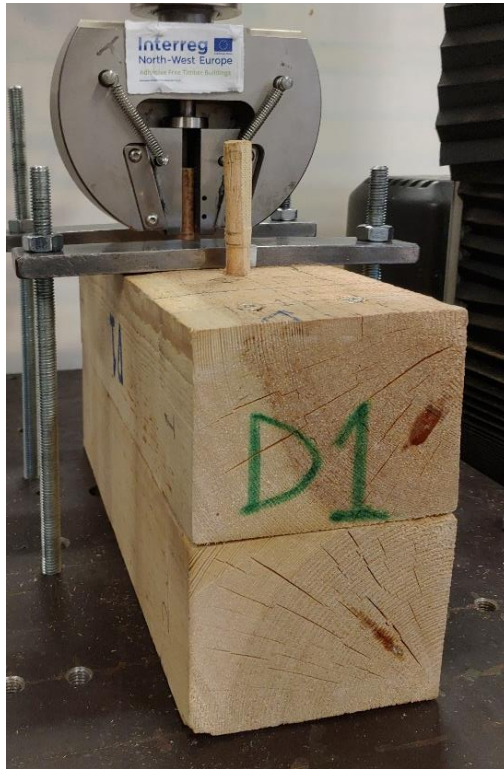
For Series C, the mean radial diameter was 10.4 mm after completion of corresponding treatment, whereas this was 10.2 mm for Series D. In percentage, the mean radial dowel diameter of Series D was approximately 2% lower when compared to Series C. Also, the tangential diameter of beech wood dowels of Series D was 1% lower than Series C. For Series C, the mean tangential diameter was 10.3 mm after completion of corresponding treatment, whereas this was 10.2 mm for Series D. The ratio of radial to tangential dowel diameter for CW dowels of Series C and Series D was same (1.0) as shown in Table 4.6. However, the radial and tangential swelling of Series C was higher than the Series D. This may be a possible reason for higher pull-out strength values of Series C compared to Series D.

Table 4.6- Radial and tangential swelling of beech wood dowels for Series C and Series D after corresponding ageing treatment

Specimen ID	Number of treatment cycles	Diameter after completion of corresponding treatment cycles (mm)		Ratio of radial to tangential dowel diameter	Mean values of Ratio of radial to tangential dowel diameter
		Radial direction	Tangential direction		
C1HW	1	10.4	10.1	1.0	1.0
C2HW		10.4	10.3	1.0	
C3HW		10.4	10.4	1.0	
D1HW	3	10.0	10.1	1.0	1.0
D2HW		10.1	10.2	1.0	
D3HW		10.4	10.2	1.0	

To understand the difference between failure mechanism of CW dowels of Series C and Series D, their diameters in radial and tangential directions were compared with their substrate hole diameter (10.2 mm) after completion of corresponding treatment. As discussed earlier, the radial swelling is relatively higher than the substrate hole diameter for both the series as shown in Table 4.5. Thus, a tighter fit is expected as the CW dowel is exerting higher swelling force on the inner walls of the substrate hole which are in contact with the radial surfaces of the dowel. When CW dowel swells in the radial direction, it facilitates elongation of the substrate hole in the direction of swelling. At the same time, the substrate hole tries to shrink in tangential direction due to the Poisson effect. The substrate hole shrinks at a certain level that it is in contact with the tangential surface of CW dowels on each side. Due to the interference fit, CW dowel and timber try to maintain a form and friction locking.

The form and friction locking is positively affected by the springback in a radial direction. But this may be negatively affected by (1) cracking/checking/splitting of CW dowels or timber or combination of these, and (2) change in tangential dowel diameter resulted from severe accelerated ageing treatment. Generally, the formation of cracks/checks in timber releases the drying stress which develops due to alternative water soaking and drying treatments [59]. In the current study, cracks were observed on the cross-sectional ends of the timber substrate of both series after the completion of corresponding ageing cycles. The cracks on timber substrates of Series D were longer and more in numbers (visually evaluated) compared to Series C Figure 4.31.



(a)



(b)

Figure 4.31- Development of cracks due to ageing treatments, (a) timber substrate of Series D, (b) timber substrate of Series C

Due to severe cracks on timber specimens of Series D, it was expected that the timber may not shrink and swell with CW dowel to maintain the form and friction locking and may result in the loosening of the connection. This loosening may be further severed by shrinkage in dowel diameter in the tangential direction. After the first ageing cycle, the mean tangential dowel diameter of Series C was approximately 10.2 mm which was as same as the substrate hole diameter. In contrary to this, the mean tangential dowel diameter for Series D was approximately 10.1 mm, which was 0.1 mm lower than the substrate hole diameter. For Series D, the combination of reduced swelling/shrinkage of timber substrate (due to cracks) and tangential shrinkage of dowel created a gap between the inner walls of the substrate hole and tangential surface of the dowel. This led to an easy pull-out of the dowels of Series D without any failure when compared to dowels of Series C which had higher restrain to pull-out due to tangential swelling. Figure 4.32 shows a typical swelling/shrinkage mechanism of CW dowels during ageing cycles.

In practical situations, connections are exposed to moisture fluctuations and temperature changes. These variations in the surrounding environment negatively affect the dimensional stability of the structural timber members during their service life. As a result, they exhibit cracks/splitting/checks which negatively impacts the tightness and load-carrying capacity of the connections [37]. As timber shrinks and swells more in the tangential direction, chances

of loosening of connection is higher when RH is low. Low RH may lead to the creation of a gap between the dowel hole and hardwood dowel. However, the effect of loosening can be minimised/ eliminated by using CW dowels as they maintain the tightness of connection due to their significantly higher radial springback.

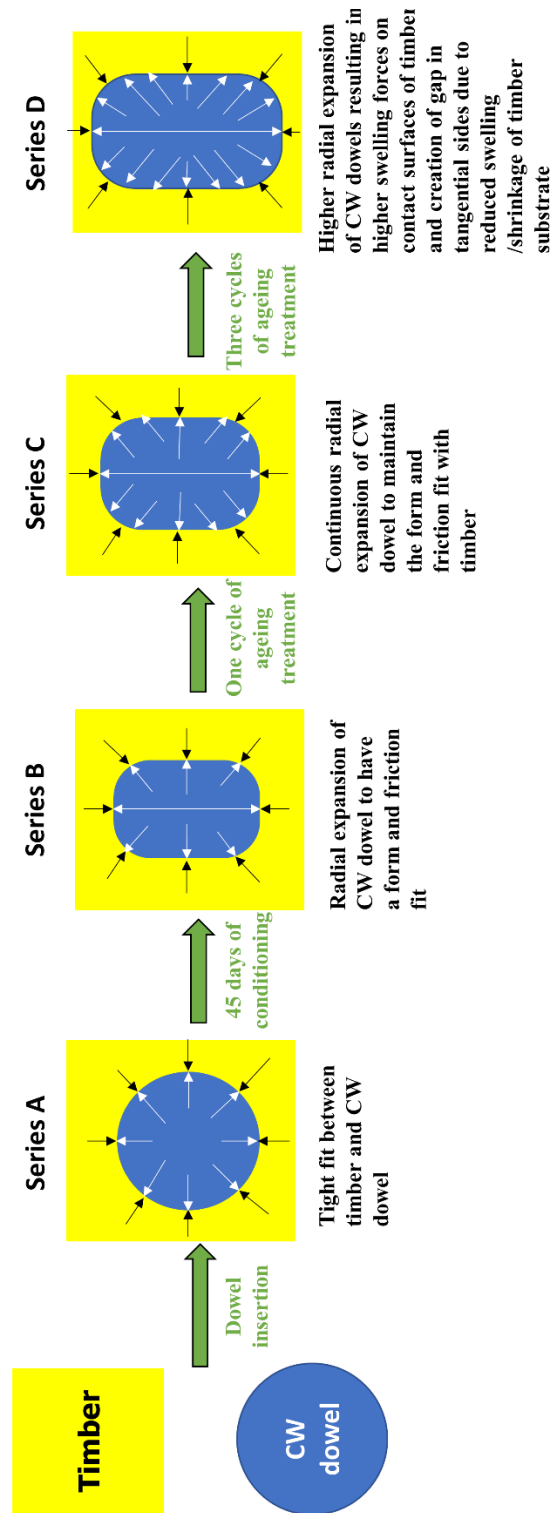


Figure 4.32- Typical swelling/shrinkage mechanism of CW dowel during ageing cycles

4.5 Conclusion

In this chapter, the swelling/shrinkage behaviour of CW as a plate material and in small-scale dowel type timber-CW connections are discussed. The chapter was designed to answer two important questions which had to be addressed for the development of non-metallic and adhesive-free EWPs and timber-CW connections using CW connectors. To address question number one, which was how long CW laminated EWPs should be conditioned to activate the form and friction locking of the CW dowels with surrounding timber, an unconstrained swelling/shrinkage test was carried out using CW plates. The CW plates were conditioned at standard conditions of 65 ± 5 % RH and 20 ± 2 °C temperature for 510 days. Also, the springback behaviour of CW was characterised through moisture dependent swelling (190 days) and oven drying (26) for 216 days. To address question number two, which was how springback affects the load-carrying capacity of dowel type timber-CW connections, an accelerated ageing test was carried on timber-CW and timber-beech wood dowel connections. The obtained test results were compared to check the feasibility of CW dowels as an alternative to hardwood dowels in DLT and timber-CW connections.

1. Unconstrained swelling/shrinkage results

The results of unconstrained swelling/shrinkage tests showed that CW material continuously expands during the conditioning phase (510 days). During thermo-mechanical compression, wood significantly loses moisture and develops residual stress due to densification. These stresses are eventually depleted during the conditioning phase as the moisture of the surrounding environment plasticizes (softens) the wood constituents. The conditioning of CW showed a net increase in the thickness, which was approximately 20% (mean) of the initial thickness. Similar to thickness change, all CW specimens showed a net increase in the mass which was approximately 5 % (mass) of the initial mass. A polynomial relationship was found between change in thickness and mass during the first 10 days of exposure. After the first 10 days, a linear relationship was observed between change in thickness and mass. The rate of expansion is faster during the initial period (10 days) of exposure, which may be attributed to rapid moisture adsorption. This rate was decreased to approximately 95% between 40-50 days of exposure when compared to the first 10 days. Based on the results, it can be concluded that CW dowel laminated timber products and timber-CW connections could be conditioned at least for 45 days at the standard condition of 65 ± 5 % RH and 20 ± 2 °C temperature to activate the form and friction locking between timber and CW dowels.

The results of springback study showed that when moisture-laden CW is oven-dried at high temperature, it rapidly swells. This may be attributed to the increased molecular motion in the cell wall constituents which consequently assists in stress relaxation [35]. The results of springback study showed that the CW shows approximately 13% (mean) springback after 190 days of conditioning treatment. As the results of springback were only based on two specimens, a larger sample will be needed to obtain statistically valid results.

2. Accelerated ageing test on CW and beech wood dowel connections

Results showed that the connections with CW dowels have higher pull-out strength for all sets of accelerated ageing treatments compared to connections with beech wood dowels. During the service life, connections with CW dowels may retain/improve the load-carrying capacity of connections for longer duration due to springback behaviour of CW. The results of Series A did not show any significant difference in the pull-out strength values irrespective of the dowel type as they were only conditioned for 24 hrs at room temperature. It was expected because 24 hrs are relatively a shorter duration than the time required to activate the form and friction fit. Results of the Series B, C and D showed that springback effect of CW dowels continuously increases the tightness of connections and improves the pull-out strength. In contrast to this, connections with beech wood dowels showed a lower pull-out strength when conditioned at a standard temperature of 20 ± 2 °C and RH of $65 \pm 5\%$, which may be due to natural variability or tangential or volumetric shrinkage of beech wood dowels. A larger sample with both radial and tangential diameter measurements would be needed to investigate this further. In contrast to this, specimens with beech wood dowels of Series C and D showed a significant improvement in the pull-out strength when artificial conditioning (pressure treatment and drying) was given. However, the pull-out strength of connections with beech wood dowels was still lower than the CW connections irrespective of the number of cycles. In a practical situation, the load-carrying capacity of CW dowelled connections may not be similar to test results obtained in this study. This is because the service conditions are not as severe as accelerated ageing treatments used in this study. Results showed that CW dowels continuously expand with an increase in the number of ageing cycles. This means a continuous increase in the radial diameter of CW dowels can be expected during service life which positively

affects the load-carrying capacity of connections. The comparison of the failure mechanism of CW dowels between Series C and Series D showed that CW dowels exhibit tangential shrinkage. In service conditions, the combinations of tangential shrinkage of dowels and timber cracks may develop due to ageing and consequently result in the loosening of the connection in perpendicular directions to the springback. This loosening may lead to pull-out of dowel with a minimum or without any damage during service conditions. However, the effect of tangential loosening may be counteracted by the significantly higher radial swelling of dowels. In contrast to CW dowels, beech wood dowels may shrink due to their higher volumetric shrinkage and cause loosening of connection during service life. The obtained test results of this study were based on a limited number of specimens, thus, a confirmation will be required with respect to large sample size. The study shows that springback of CW dowels could be utilised as a beneficial trait in timber connections.

Chapter 5 Development of semi-rigid timber connections using CW connectors

5.1 Introduction

This chapter details the development and structural testing of small-scale semi-rigid type timber-timber moment connections using CW connectors. Based on the literature review of carpentry and timber-steel connections, the available sizes and material properties of CW connectors presented in Chapter 3, a range of beam-beam and beam-columns connection designs were developed. These connections were experimentally tested and assessed based on their structural performance in terms of load-carrying capacity, moment capacity, rotational stiffness, and ductility.

The work divided into four phases. Beam-beam connections were investigated in Phase-I and Phase-II while beam-column connections were the focus of Phase-III and Phase-IV. Each phase comprised the development of connection design and associated experimental testing. The development process involves selection of connection design, configuration of connection components (CW connectors and structural members), manufacturing process and assembly. Experimental testing involves destructive tests in accordance with EN 26891[183].

Figure 5.1 shows the outline of these four phases. In Phase-I, beam-beam connections were developed using glued structural members and CW connectors. The main objective of this phase was to evaluate the structural feasibility of CW connectors as an alternative to steel connectors in semi-rigid type timber moment connections. For this reason, connections were also developed using steel connectors of approximately equivalent capacity. Both connection types (with CW and steel connectors) were tested using a destructive method. Based on the test results of Phase-I and available geometries of CW connectors, connection designs were optimised in Phase-II. In Phase-III, seven different designs of beam-column connections were developed using glued structural members and CW connectors. The main objective of this phase was to select a suitable connection design that can be used for the development of beam-column connections using CW dowel laminated (CWDLT) structural members and CW connectors. Finally, in Phase-IV, an initial design of beam-column connections was produced using CWDLT members and CW connectors based on the results of Phase-III. Based on the initial results, the design was optimised to improve the structural behaviour of these connections.

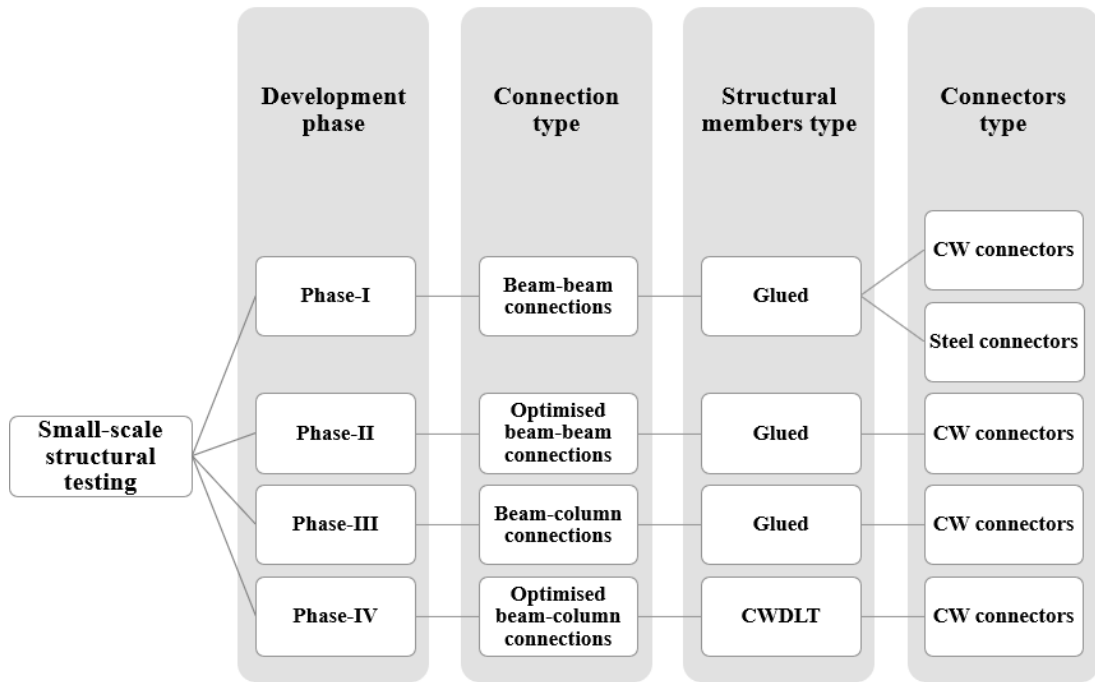


Figure 5.1- Scheme of small scale-structural testing

5.2 Selection of connection designs

The objective of the current study was to develop semi-rigid type timber moment connections using CW connectors. Therefore, the design of the connection had to be developed based on the type and geometry of the available CW connectors and size of the structural members. In the current study, the types and geometry of the CW connectors are critical parameters compared to the size of the structural members. As the CW connectors used in this study were developed at laboratory scale and were available only in the form of dowels and plates, a dowel type connection with connector plate is the preferred option over any other connection types such as interlocking (contact type) and glued connections.

Prior to finalising an appropriate connection design, the positive aspects of CW dowels and plates were evaluated. The literature review (see Section 2.3.5) showed that CW dowels exhibit higher shearing performance compared to dense hardwood dowels. This was also confirmed from the material characterisation tests presented in Chapter 3. Therefore, to make use of higher cross-grain shear strength and yield moment capacity of the CW dowels, the connection design should consist of multiple shear planes.

Another component that can improve the structural performance of timber-CW connections is the CW plate. Generally, timber beams fail in tension. Inclusion of stiffer reinforcement material in the tensile face of beams can improve their overall bending performance. In recent years, many materials were tested for this purpose such as steel and fibre reinforced polymer (FRP) plates [49,205,206]. These materials offer higher tensile strength, stiffness and embedment behaviour compared to timber. Similar to the aforementioned materials, the CW

plate also has higher strength (embedment and bending) and stiffness properties compared to uncompressed wood as presented in Chapter 3. Thus, these plates can be either glued or mechanically attached to locally reinforce the connection area to prevent premature splitting of the timber around the connectors. However, the aim is to produce a non-metallic and adhesive-free connection design, thus a possible solution could be connecting CW plates to timber using CW dowels.

Multiple shear plane slotted-in steel plate dowel-type timber connections are widely used in Europe for jointing of larger cross-sections of glued laminated timber [148,153,207]. These connections are mainly designed in trusses, arches, bridges etc., to transmit heavier loads. The provision of slotted-in steel plates increases the load-carrying capacity of the connection. In similar fashion, multiple shear plane connection designs with slotted-in CW plates and CW dowels are well suited for the current study.

In this study, based on the above discussion and reviewed literature, multiple shear plane slotted-in CW plate and mortise-tenon connections with CW dowels were selected in this study to develop non-metallic and adhesive-free timber moment connections. Both beam-beam and beam-column connections were designed using multiple shear plane arrangements. The detailed geometries and connection designs for each connection type are discussed in detail in the corresponding sections.

5.3 Material

This section describes the materials used for beam-beam and beam-column connections. The four material types used were CW, compressed laminated wood, steel and softwood.

5.3.1 Compressed wood

The CW in the form of CW plates and CW dowel were used as connectors. They were sourced from the University of Liverpool, United Kingdom. The detailed manufacturing processes of both CW plates and CW dowels are presented in Section 3.3.

5.3.1.1 Full-depth CW plates

The term full-depth CW plate refers to CW plates which are fixed within routed grooves and which have a depth similar to the entire cross-section depth of the beam as shown in Figure 5.2. In this study, these plates were only used for beam-beam connections developed in Phase-I. These plates were manufactured using Scots Pine (*Pinus sylvestris*) wood compressed in the radial direction. The initial density (at 10%-15% moisture content) of timber boards was between 500 – 600 kg/m³. The initial dimensions of the uncompressed plates were 500 mm (L) x 180 mm (T) x 30 mm (R), which were compressed to 500 mm (L) x 180 mm (T) x 10 mm (R). This is approximately 67% CR. However, there was a mean increase of approximately 1.2 mm in the radial direction immediately after the specimens were removed

from the press. Plates were delivered in air-tight plastic bags to avoid moisture dependent swelling. Prior to insertion of these plates in the beam-beam connections (Phase-I), the mean thickness (R) was 11.3 mm. The oven-dry density of the plates varied from 1100-1500 kg/m³.



Figure 5.2- Full-depth CW plates

5.3.1.2 Narrow-depth CW plates

The term narrow-depth CW plate refers to a CW plate which is smaller in depth and only limited to a certain depth of the cross-section of the beam as shown in Figure 5.3. The narrow depth plates were used for all remaining product development phases (Phase-II, Phase-III and Phase-IV). The reason for using narrow-depth CW plates instead of full-depth CW plates was due to lack of commercial availability of defect-free wider and deeper cross-section of uncompressed timber for mass production of CW plates. Initial manufacturing trials showed that knots are responsible for variations in the thickness of the CW plates. The narrow-depth plates were manufactured from clear and uncompressed timber boards of Western Hemlock (*Tsuga heterophylla*) wood. The mean mass density of the uncompressed Western hemlock was 500 kg/m³. The initial dimensions of the uncompressed plates were 510 mm (L) x 63 mm (T) x 67 mm (R). They were compressed in a radial direction to up to 21 mm (R). Similar to full-depth CW plates, these plates were also delivered in air-tight plastic bags to avoid moisture dependent swelling. The dimensions of plates were adjusted according connection configuration. The oven-dry density of the CW plates varied from 1300 kg/m³ – 1470 kg/m³.

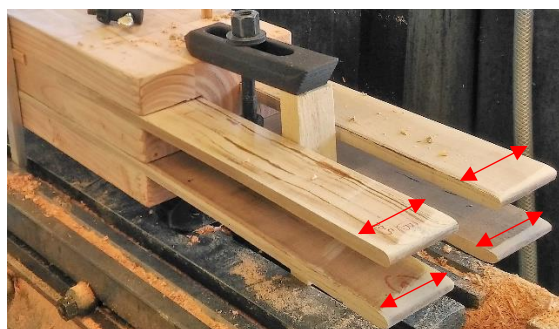


Figure 5.3- Narrow-depth CW plates

5.3.1.3 Compressed wood dowels (CW dowels)

CW dowels were produced using visually graded kiln dried uncompressed Scots pine (*Pinus sylvestris*) boards. The manufacturing procedure of dowels is as described in Section 3.3.1.2.

The initial densities (at 10%-15% moisture content) of timber boards were between 500 – 600 kg/m³. Small clear specimens of 200 mm (length, longitudinal direction) x 9 mm (width, tangential direction) x 22 mm (thickness, radial direction) were thermo-mechanically compressed. They were compressed in a radial direction to up to 10 mm (R). This is approximately 54% CR. All dowels were delivered in air-plastic bags. After removing from the plastic bags dowel diameter was measured and it varied from 10 mm - 10.3 mm. The average oven-dry density of the CW dowels was 1285 kg/m³.

5.3.2 Compressed laminated wood

Commercially available compressed laminated wood in the form of threaded beechwood dowels (species – *Fagus sylvatica*) of 10 mm (nominal diameter) was procured from Permal Deho Ltd, United Kingdom (see Figure 5.4). These dowels were used only in the connection area of CWDLT beam/column (see Section 5.7). The purpose of using these dowels instead of smooth CW dowels was to avoid separation of timber lamellae forming the members.

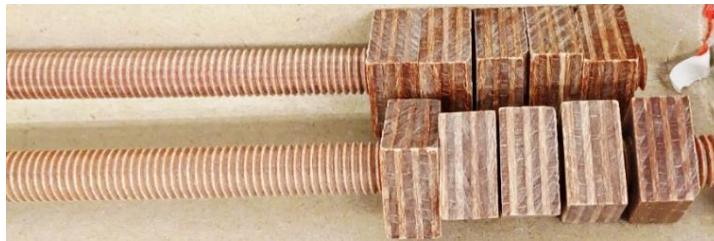


Figure 5.4- Threaded beechwood dowels

5.3.3 Steel connectors

The steel connectors were used only in Phase-I for comparison with timber-CW connections. The commercially available S275 steel grade was used for dowels and steel plates. The steel plates were 480 mm long, 10 mm thick and 152 mm wide. To allow the comparison with timber-CW connections, steel dowels of 8 mm diameter were used.

5.3.4 Structural members (softwood)

For all small-scale structural testing, structural members were manufactured using kiln-dried timber boards of Irish-grown Douglas fir (*Pseudotsuga menziesii*). The boards were conditioned at a temperature of 65 ± 5 % RH and 20 ± 2°C temperature for 3 months. The oven-dry density measured on small clear specimens ($n= 40$) varied from 433 - 703 kg/m³. There were two types of structural members produced from Douglas fir (1) glulam and (2) CWDLT.

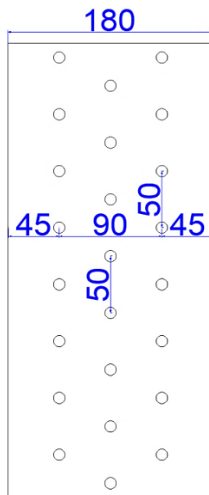
5.3.4.1 Glulam

Glulam members were used for Phase-I, Phase-II and Phase-III. The manufacturing process was the same for all glulam members. The laminates were glued together using a one-component PU adhesive and were clamped in a rig to a minimum pressure of 0.6 MPa in

accordance with EN 14080 [208]. During the development phases, cross-sectional areas of the members were varied. The cross-sectional areas of the beams for Phase-I and Phase-II were 115 mm (b) x 157.5 mm (h) and 130 mm (b) x 160 mm (h), respectively. Beams with 115 mm (b) x 157.5 mm (h) dimensions were manufactured with three laminates, whereas four laminates were used for beams of 130 mm (b) x 160 mm (h) cross-sectional area. Each beam and column used for Phase III had a cross-sectional area of 180 mm (b) x 180 mm (h). Each beam consisted of five laminates of 36 mm thickness. The lengths of the glulam members were specific to connection types and are given below in the assembly and fabrication section for the respective connection type.

5.3.4.2 CW dowel laminated timber (CWDLT)

CWDLT were manufactured using CW dowels to connect the timber laminates. These members were used as the beams and columns for development and testing of beam-column connections presented in Section 5.7. For comparison with test results of Phase-III, all geometric parameters (180 mm x 180 mm) of beams remained the same as glued members with the only difference being, the way timber boards were connected to produce the laminated members. The CW dowels had a nominal diameter of 10 mm and were made from 54% radially compressed Scots Pine. Each CW laminated member consisted of five laminates of 36 mm thickness. The laminates were held together using manual clamps and 10.2 mm diameter holes were drilled using a K2I CNC Hundegger [209]. The holes were drilled in a staggered pattern as shown in Figure 5.5a. Practically, the staggered dowel arrangement has a relatively lower reduction in the net cross-sectional area compared to the row arrangement. This prevents possible splitting along the row of dowels. For this reason, all the CWDLT members were manufactured using the staggered arrangement. Once the holes were drilled, laminates were fastened together by inserting the CW dowels using a hammer as shown in Figure 5.5b. To facilitate easy insertion of the CW dowels, the insertion ends were chamfered to a conical shape.



(a)



(b)

Figure 5.5- Manufacturing of CW dowel laminated timber beams, (a) staggered arrangement of dowels with dowel spacing (mm), (b) insertion of dowels

5.4 Beam-beam connections using full-depth CW/steel plates and glued structural members (Phase-I)

This section details the experimental programme for Phase-I. The primary objective of this phase was to check the structural feasibility of CW connectors as an alternative to steel connectors in beam-beam connections. To realise this objective, two types of semi-rigid beam-beam connections were developed. Type-1 included connections with full-depth CW plates and CW dowels. Type-2 included connections with full-depth steel plates and steel dowels. To allow the comparison, timber-steel connections were designed with approximate capacity to the timber-CW connections. All connections were tested using a four-point bending test set up. Obtained test results are presented in terms of load-midspan displacement, moment capacity, rotational stiffness, ductility ratio and failure modes. Finally, results are also compared to examine the difference in structural performance of both connection types.

5.4.1 Connection configuration, fabrication and assembly

A total of four semi-rigid type beam-beam connections were developed and tested in this phase. Two connections were developed using full-depth CW plates and CW dowels and two using full-depth steel plates and steel dowels. The connection configuration was the same for both connection types. Each spliced connection configuration comprised of two vertically oriented full-depth CW or steel plates, which extended to the entire depth of the beam as shown in Figure 5.6a. Each glulam beam was routed with two 11 mm wide slots to accommodate two CW or steel plates of 10 mm thickness. The fabrication of the connection is as shown in Figure 5.6b. For assembly, the beams were fixed in position using clamps and the CW or steel plates were inserted prior to dowel insertion. In all cases, 10 dowels were used

to connect the plates on each side. For timber-steel connections, plates and beams were pre-drilled prior to insertion in the slots. An 8 mm hole diameter was used for the steel dowels of 8 mm to ensure a tight-fit as per EC 5 [55] guidelines for steel dowels. Once drilled, steel plates were positioned in the slots and steel dowels were inserted manually. For timber-CW connections, holes were drilled after positioning the CW plates in the slots using a pillar drill. After this, CW dowels were inserted using a hammer. In initial tests it was observed that a 10 mm hole diameter was too small to fit CW dowels of 10 ± 0.3 mm as it damaged the perimeter of the dowels. It must be noted that EC 5 [55] recommends a similar size of the hole to the diameter of the steel dowel. However, this criterion cannot be applied for the CW dowels until manufacturing tolerances of CW products are codified in design standards. For the selection of appropriate drilling bits, 10 mm and 10.2 mm were tried on a few timber pieces. It was found that a 10.2 mm hole diameter is appropriate for dowels of 10 mm - 10.3 mm diameter. Also, to facilitate easy insertion of the CW dowels, the insertion ends of the dowels were roughly chamfered (about 0.5 mm) to a conical shape.

The assembled beams with the connection at mid-span had an overall length of 3160 mm. This ensured that the assembly could be tested in flexure over a span of 2835 mm, which is 18 times the depth of the beam as specified in EN 408 [181]. A gap of 10 mm was used between the connected beams to avoid contact/ friction during testing based on previous studies [120,158,159]. Figure 5.6c shows edge spacing and end distances in the connection area as per Table 8.5 of EC 5 [55]. It should be noted that EC 5 does not provide a guideline on edge spacing and end distances of moment connections. Thus, it was decided to choose existing guidelines which are formulated for designing connections subjected to tension or compression. After fabrication, the assembled connections were conditioned for one month at $65 \pm 5\%$ RH and $20\text{ }^{\circ}\text{C}$ temperature prior to testing. Table 5.1 summarises the number of replications, plate thickness, number of dowels and labelling system for each connection type.

Table 5.1- Test programme of Phase-I

Connection type	Number of replications	Nominal dowel diameter (mm)	Total number of dowels/connection	Label
Timber-CW	2	10	20	BB-CW-FP-1
		10	20	BB-CW-FP-2
Timber-steel	2	8	20	BB-ST-FP-1
		8	20	BB-ST-FP-2

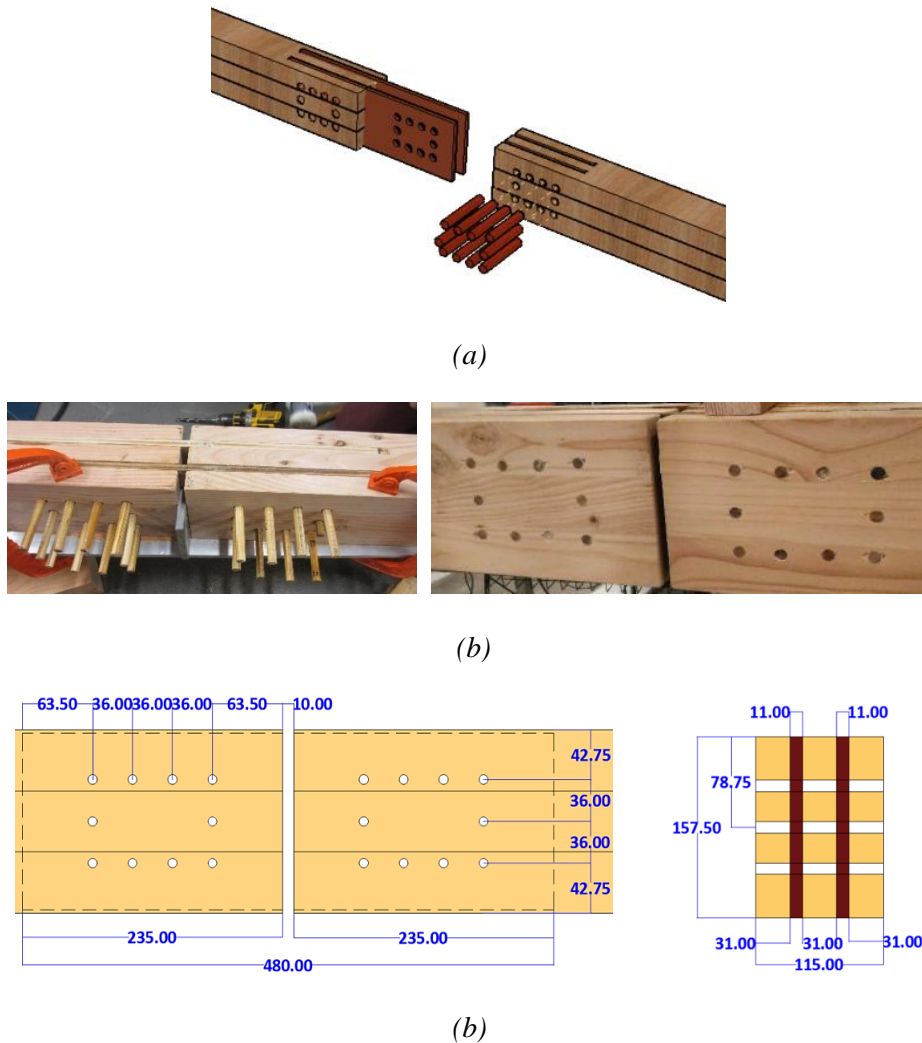


Figure 5.6- Beam-beam connection using full-depth CW/steel plates (all dimension are in mm) (a) connection configuration, (b) edge spacing, end distances and cross section

5.4.2 Test set-up and procedure

All connected beams were tested in flexure over a simply supported span in four-point bending in accordance with EN 408[181]. The connection was located at mid-span in the shear-free zone, so it was subjected to pure bending. The loading apparatus included a hydraulic jack and a steel girder. The load was applied vertically in downward direction using the hydraulic jack. The load was then divided into two-point loads by the girder. Two small steel plates were inserted between the beam and either load points to minimise local indentation. Simple lateral supports were placed at the end of the beams to avoid lateral movement during the test. Figure 5.7a and Figure 5.7b shows the test set up and geometry of the specimen, respectively.

$$M_{exp} = \frac{F_{max}}{2} \times l \quad Eq. 5.2$$

where $F_{max}/2$ is the load at one point, and l is the lever arm distance which was 945 mm, here. Each beam-beam connection system is comprised of two separate and similar connections connected in series. So, the experimental rotational stiffness of the connection (k_{exp}) was calculated using the following equations [54]:

$$k_{exp} = \frac{1}{\left(\frac{1}{k_{exp,1}} + \frac{1}{k_{exp,2}}\right)} \quad Eq. 5.3$$

where $k_{exp,1}$ and $k_{exp,2}$ are the rotational stiffnesses of each side of the connection. The experimental rotational stiffness of each side of the connection was assumed to be equal due to symmetrical connection geometry and loading condition. It was calculated using the following expression:

$$k_{exp,1} = k_{exp,2} = \frac{M_{exp,40} - M_{exp,10}}{\theta_{exp,40} - \theta_{exp,10}} \quad Eq. 5.4$$

where $M_{exp,10}$ is the 10% value of the M_{exp} , $M_{exp,40}$ is the 40% value of the M_{exp} , $\theta_{exp,10}$ is the rotational angle corresponding to the $M_{exp,10}$, and $\theta_{exp,40}$ is the rotational angle corresponding to the $M_{exp,40}$.

The ductility ratio (D) was calculated as per EN 12512 [187] using the below expression:

$$D = \frac{V_u}{V_y} \quad Eq. 5.5$$

where V_u is the ultimate midspan displacement taken at a load level of $0.8F_{max}$, and V_y is the yield midspan displacement was calculated based on the 1/6 method (detailed in Section 6.3).

5.4.3 Test results and discussion

This section details the load-midspan displacement, moment-rotation behaviour, ductility ratio and failure modes of both connection types.

5.4.3.1 Load-midspan displacement and moment-rotation behaviour of connections of Phase-I

Figure 5.8 shows the load-midspan displacement behaviour of the connections. Solid lines indicate connections with CW connectors and dashed line indicate connections with steel connectors. The behaviour can be seen to be linear elastic until failure when the splitting on the timber beam occurs.

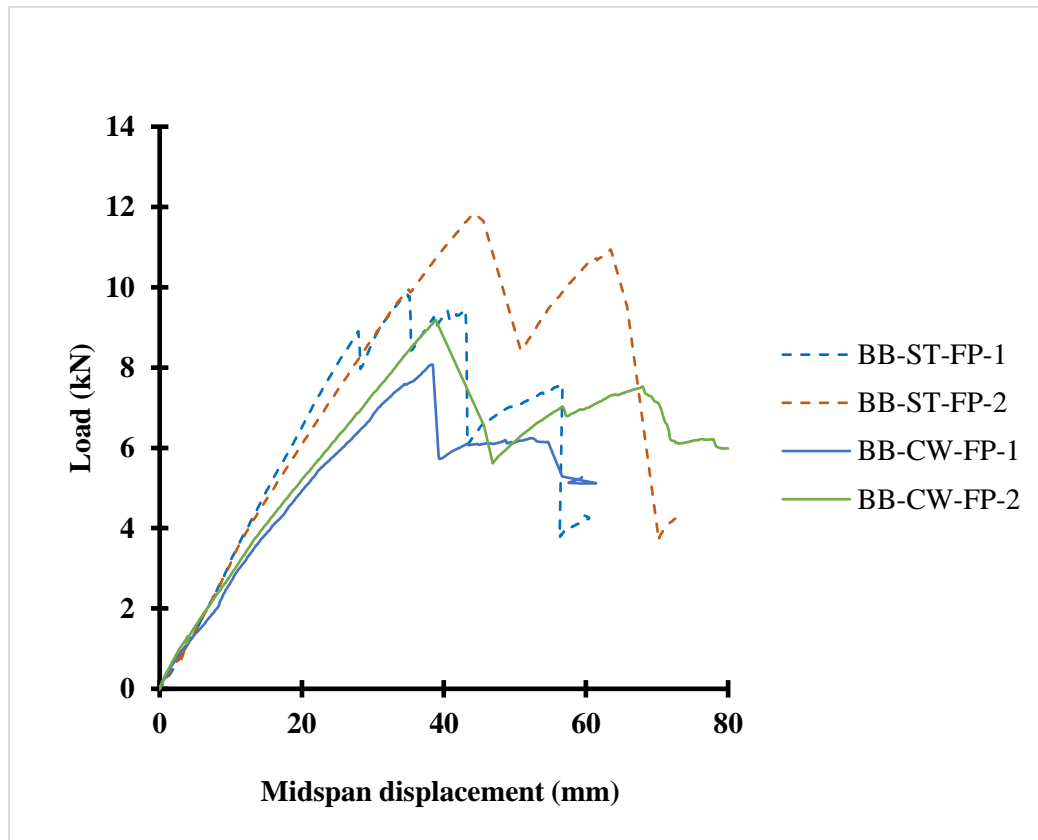


Figure 5.8- Load-midspan displacement of beam-beam connections using full-depth CW and steel plates

Figure 5.9 shows the moment-rotation behaviour of the connections. The graph only shows the linear elastic region of the curve as both connection types experienced brittle failure once the maximum moment capacity attained. The connections with CW connectors showed consistent moment-rotation behaviour in the elastic region. The steel connections showed relatively lower rotational stiffness which may be attributed to localised imperfections in the assembly of components.

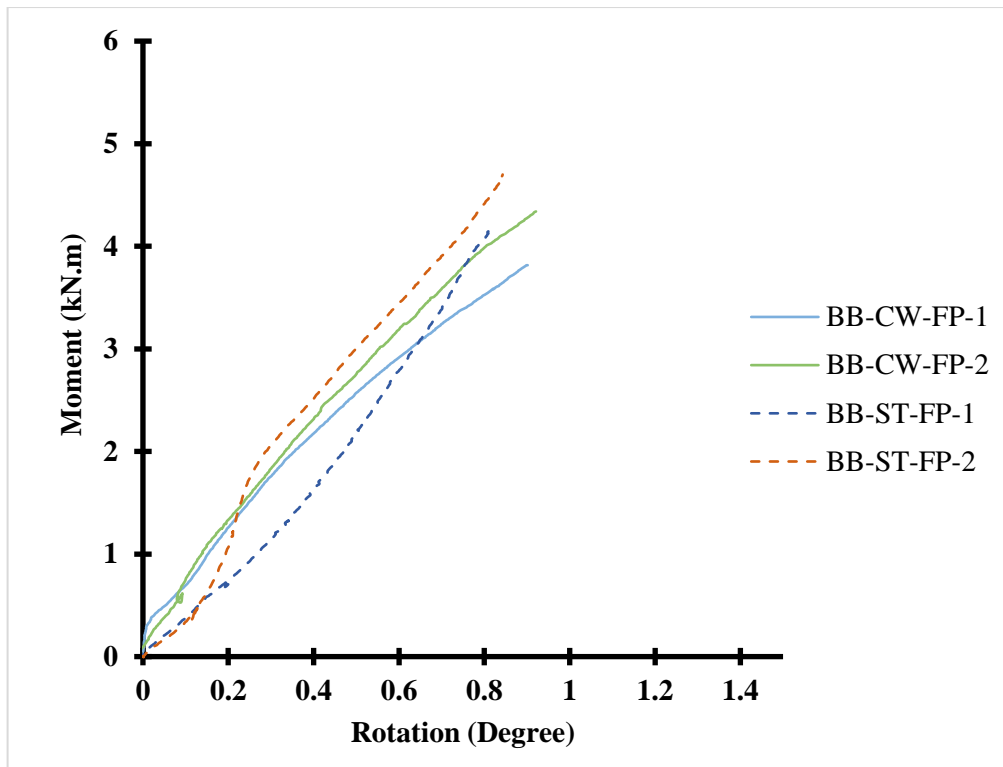


Figure 5.9- Moment-rotation behaviour of connections with CW connectors and steel connectors

5.4.3.2 Failure modes

(a) 10-dowel connection using 10 mm full-depth CW plates

Initially, when the vertical load was applied, the connection at mid-span began to rotate and the beams moved closer to each other at the top of the connected beams and moved further apart at the bottom of the connection. The 10 mm gap at the spliced connection ensured no additional friction or compression parallel to grain in the compression zone. Loading continued until splitting took place in the timber along the bottom row of one of the connected ends in the tension zone. The splitting initiated at dowel number 1 as shown in Figure 5.10. With increasing load, splitting propagated along the bottom row of the dowels. This brittle failure may be attributed to low end/edge-distances and inter-dowel spacing.



Figure 5.10- Failure mode of connection with full-depth CW plates

The dissected sections of the tested specimens showed cross-grain shear failure of the CW dowels. Figure 5.11 shows typical dowel failure modes in these connections. As expected, dowels which were located at maximum distance (lever arm) from the geometric centre of the connection showed larger deformation due to higher moment. This can be clearly seen in the dowel number 1 and 10.

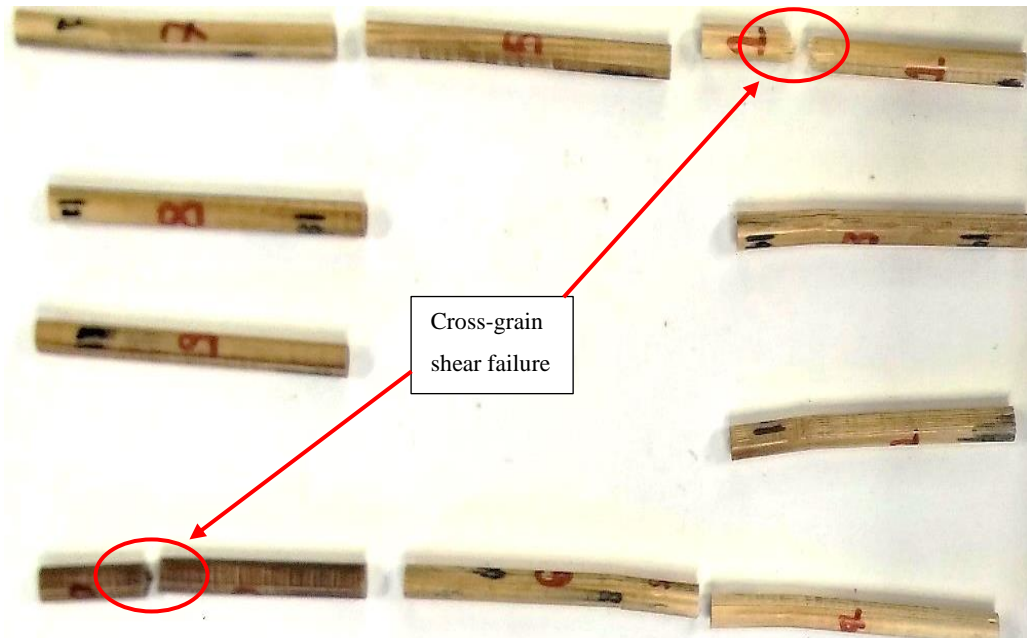


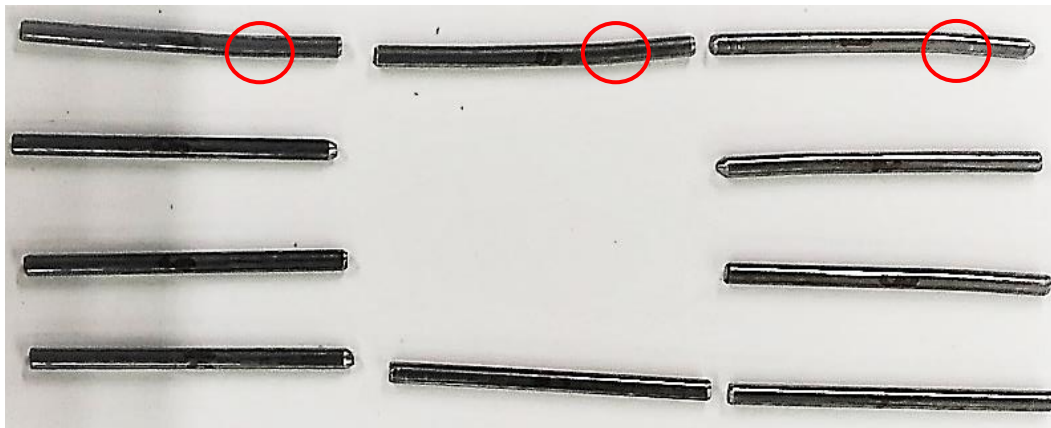
Figure 5.11- Cross-grain shear failure of dowels

(b) 10-dowel connection using 10 mm full-depth steel plate

Similar to connections with full-depth CW plates, these connections also showed a continuous increase in the load until the splitting took place in the timber along the bottom row of one of the connected ends in the tension zone. The splitting initiated at dowel number 1 as shown in Figure 5.12a. With increasing load, splitting was also observed along the upper row of dowels (dowel number 7 to 10). Dowels which were located closer to loaded end showed formation of partial plastic hinges (see Figure 5.12b). They did not show typical plastic behaviour which is generally observed in the timber-steel connections. This may be because these connections were designed with a dowel spacing criterion which is essentially used for connections working in tension or compression. This indicates larger spacing should be used to avoid brittle failure of timber and to facilitate plastic deformation within the dowels.



(a)



(b)

Figure 5.12-Failure mode of connection with full-depth steel plates(a) splitting along the row of dowels in tension zone, (b) red circles shows partial plastic hinges in dowels

5.4.4 Results summary and discussion

Table 5.2 summarises test results of Phase-I. The mean failure load of 10.8 kN was achieved for the timber-steel connections and mean load of 8.6 kN was achieved for timber-CW connections. The mean moment capacity of connections with steel connectors was of 5.1 kN.m and this was 4.1 kN.m for timber-CW connections. There is an overall percentage decrease of approximately 20% for the connections with CW connectors. However, the mean rotational stiffness of the connections with CW connectors was approximately 13% higher than the timber-steel connections. The mean ductility ratio of timber-steel connection was 21% higher than the timber-CW. The design calculations for both timber-steel and timber-CW connections are discussed in Chapter 7.

Table 5.2- Test results of Phase-I

Connection type	Specimen number	Load-carrying capacity (kN)	Moment capacity (kN.m)	Rotational stiffness (kN.m/rad)	Ductility ratio
Using CW connectors	BB-CW-FP-1	8.1	3.8	141.3	1.3
	BB-CW-FP-2	9.2	4.3	169.1	1.5
	Mean	8.6	4.1	155.2	1.4
	Standard deviation	0.7	0.4	19.6	0.1
Using steel connectors	BB-ST-FP-1	9.8	4.6	124.2	1.5
	BB-ST-FP-2	11.8	5.6	145.5	1.8
	Mean	10.8	5.1	134.8	1.7
	Standard deviation	1.4	0.7	15.1	0.2

5.5 Beam-beam connections using narrow-depth CW plates and glued structural members (Phase-II)

In this phase, beam-beam connections were developed using narrow-depth CW plates and glued structural members. The connection with full-depth CW plates was discontinued due to quality issues (i.e. thickness variations and knots) and non-availability of clear timber specimens of wider cross section. Figure 5.13 shows the test program of this phase. A total of four different connection types were developed. They were classified based on thickness of CW plates, number and arrangement of CW dowels. The connection configuration for each connection type is detailed in Section 5.5.1. All connections were tested using a four-point bending test set up. Obtained test results are presented in terms of load-midspan displacement, moment capacity, rotational stiffness ductility ratio and failure modes for each connection type. Finally, results are also compared to examine the difference in structural performance.

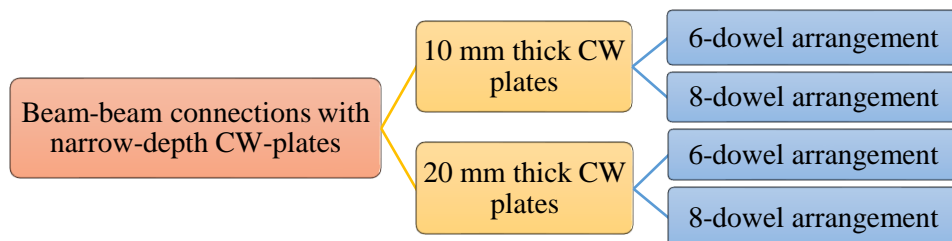


Figure 5.13- Test program of Phase-II

5.5.1 Connection configuration, fabrication and assembly

Figure 5.14 shows the configuration of beam-beam connections with narrow-depth CW plates and CW dowels. To insert the CW plates, vertically oriented grooves were routed at the end of each beam starting from top/bottom surface up to 60 mm depth. Assembly process was similar to connections with full-depth CW plates. Each connection design comprised four slotted-in compressed wood plates, two in the compression zone and two in the tension zone of the beams. For the 6-dowels arrangement as shown in Figure 5.14a, six dowels were used to connect the CW plates to each beam (3 top and 3 bottom; 12 dowels in total). There was a total of five connections of the 6-dowel arrangement that involved two specimens using 10 mm thick CW plates and three specimens using 20 mm thick CW plates. For the 8-dowel arrangement as shown in Figure 5.14b, eight dowels with reduced spacing were used to connect the CW plates to each beam (4 top and 4 bottom; 16 dowels in total). There was a total of five connections of the 8-dowel arrangement that involved two specimens using 10 mm thick CW plates and three specimens using 20 mm thick CW plates. The test span of the specimen was 2880 mm in accordance with EN 408[181]. The edge spacing and end distances of each specimen given in Figure 5.15.

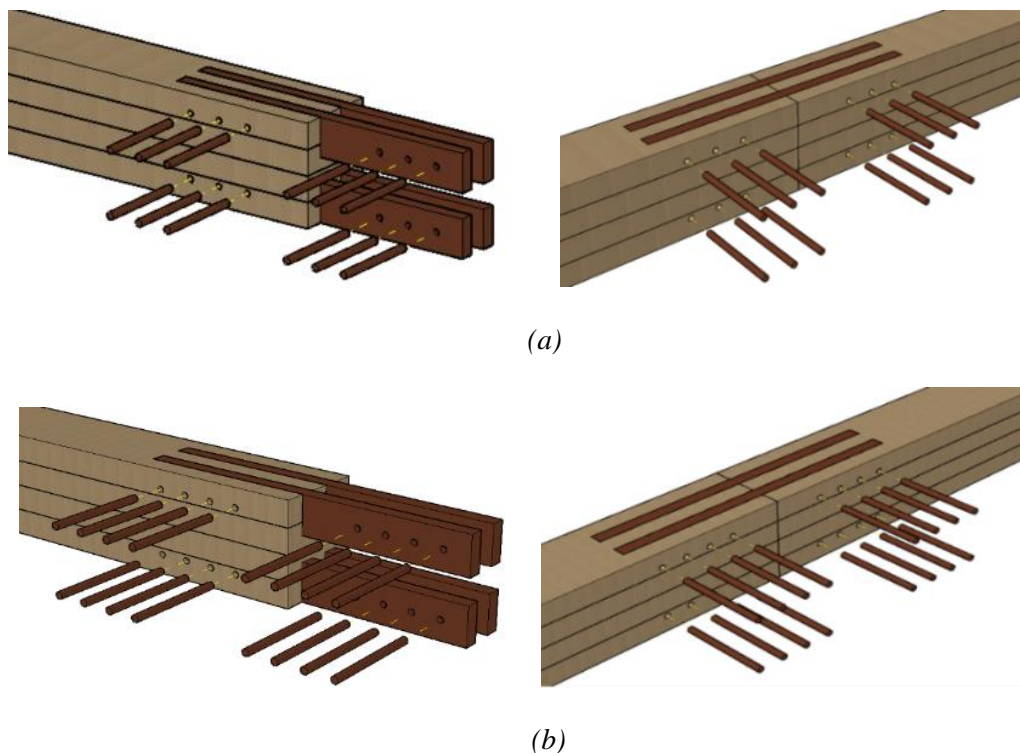


Figure 5.14- 3D design configuration, (a) 6-dowel arrangement, (b) 8-dowel arrangement

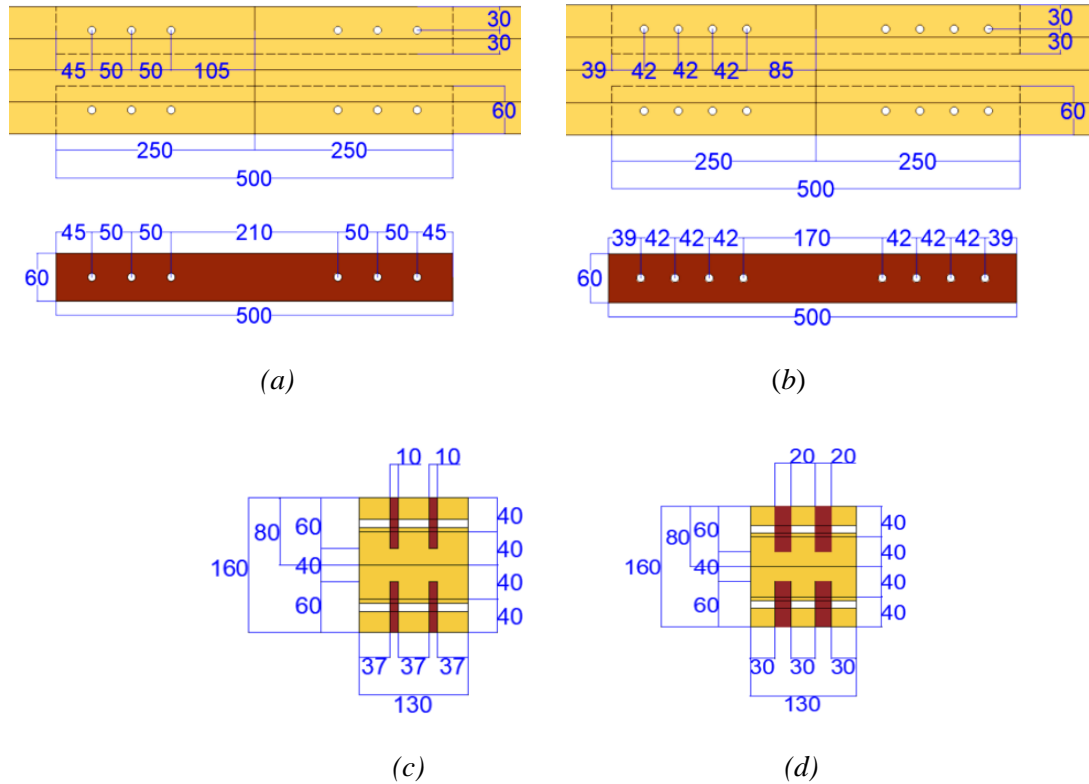


Figure 5.15- Edge spacing and end distance (all dimensions are in mm) (a) 6-dowel arrangement, (b) 8-dowel arrangement, (c) cross-section of the connection using 10 mm thick CW plates, (d) cross-section of the connection using 20 mm thick CW plates

Table 5.3 summarises number of replications, plate thickness, number of dowels and labelling system for each connection type.

Table 5.3- Test scheme of Phase-II

Connection type	Number of replications	Thickness of CW plates (mm)	Total number of dowels / connections	Label
6-dowel arrangement	2	10	12	BB-6-10-1
			12	BB-6-10-2
	3	20	12	BB-6-20-1
			12	BB-6-20-2
			12	BB-6-20-3
8-dowel arrangement	2	10	16	BB-8-10-1
			16	BB-8-10-2
	3	20	16	BB-8-20-1
			16	BB-8-20-2
			16	BB-8-20-3

$$\theta_{avg} = \frac{\theta_L + \theta_R}{2} \quad Eq. 5.6$$

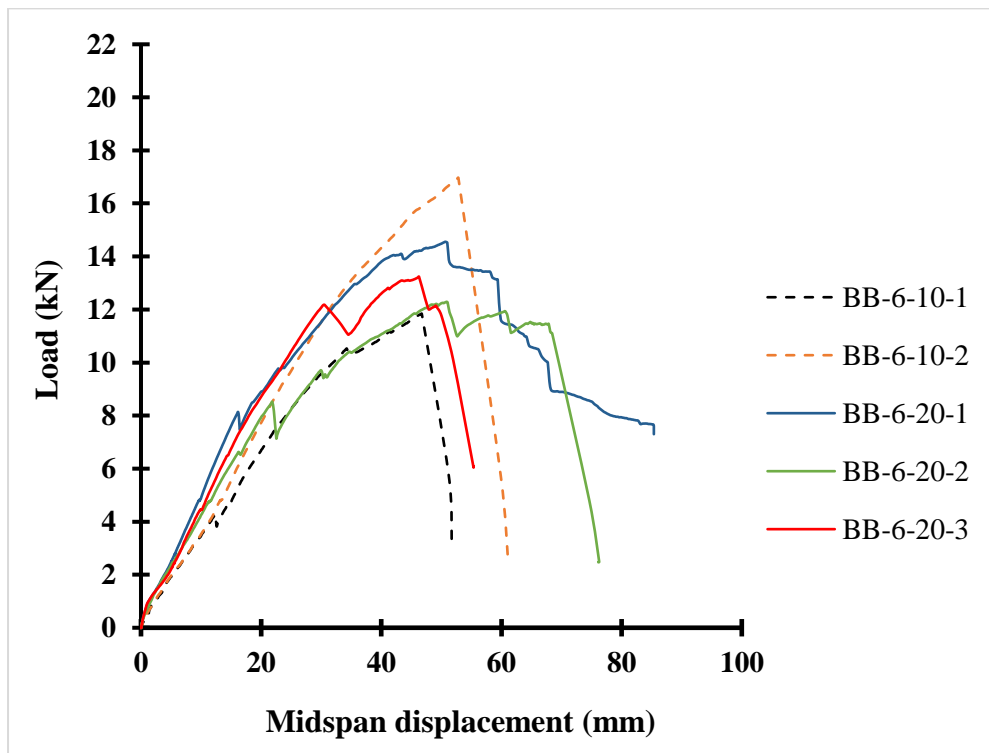
The experimental moment capacity (M_{exp}), rotational stiffness and ductility ratio of each connection type was calculated using Eq. 5.2, Eq. 5.3 and Eq. 5.5, respectively.

5.5.3 Test results and discussion

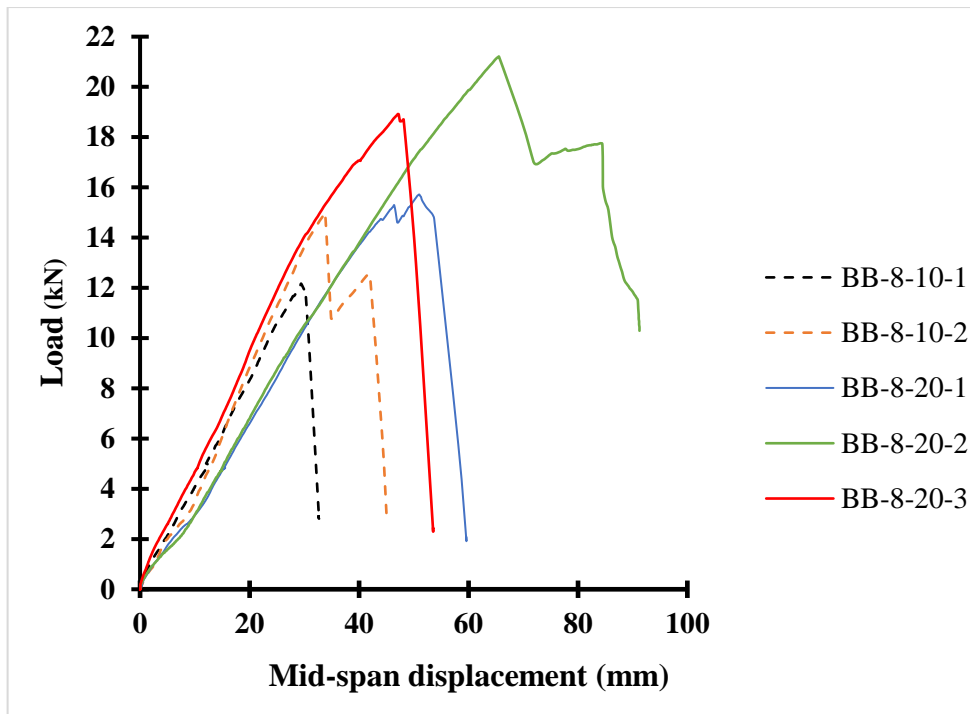
This section details the load-midspan displacement, moment-rotation behaviour, ductility ratio and failure modes of all connection types.

5.5.3.1 Load-midspan displacement and moment-rotation behaviour of connections of Phase-II

Figure 5.17a shows the load-midspan displacement of connections with the 6-dowel arrangement using 10 mm and 20 mm thick narrow-depth CW plates. Figure 5.17b shows the load-midspan displacement of connections with the 8-dowel arrangement using 10 mm and 20 mm thick narrow-depth CW plates. In both Figure 5.17a and Figure 5.17b, dashed lines indicate connections with 10 mm thick CW plates and solid lines indicate connections with 20 mm thick plates. Connections with the 6-dowel arrangement and 20 mm thick CW plates showed non-linear behaviour post-elastic phase, whereas the remaining connections showed brittle behaviour once the maximum capacity was attained.



(a)

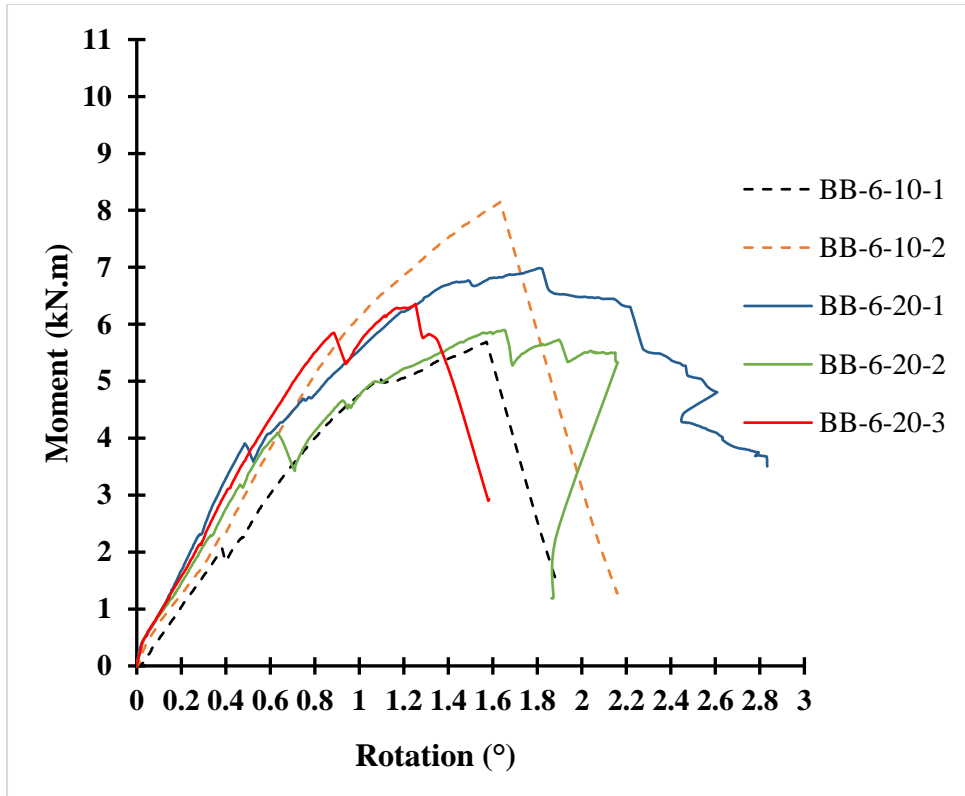


(b)

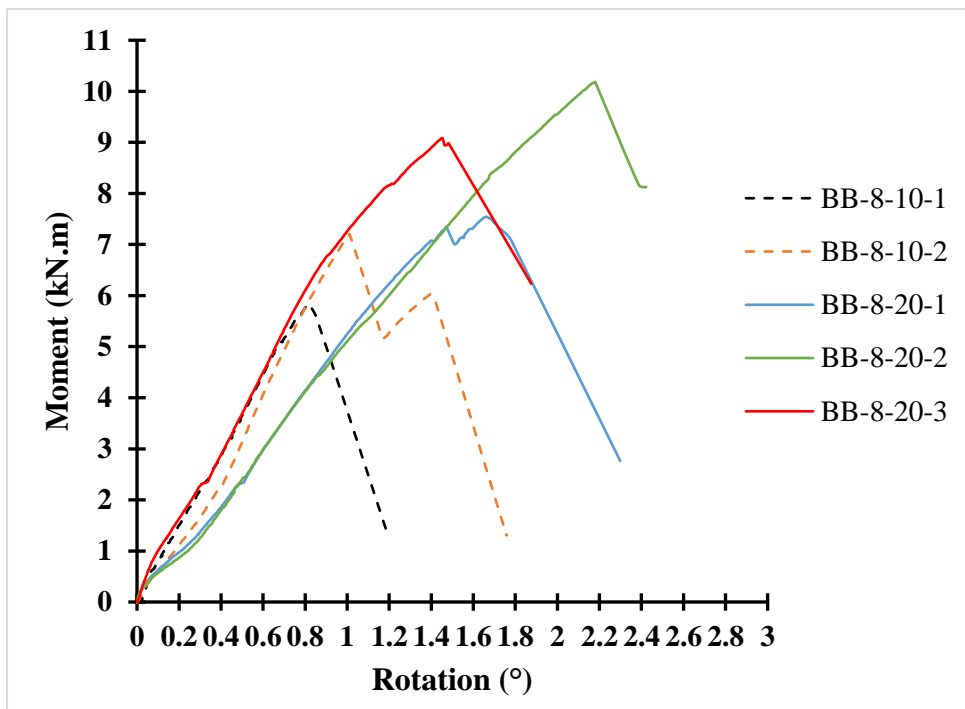
Figure 5.17- Load-midspan displacement behaviour of timber-CW connections of Phase-II, (a) 6-dowel arrangement using 10/20 mm thickness narrow-depth CW plates, and (b) 8-dowel arrangement using 10/20 mm thick narrow-depth CW plates

Figure 5.18a shows the moment-rotation behaviour of connections with the 6-dowel arrangement using 10 and 20 mm thick narrow-depth CW plates. Figure 5.18b shows the moment-rotation behaviour of connections with the 8-dowel arrangement using 10 and 20 mm thick narrow-depth CW plates. Both the 6-dowel and 8-dowel arrangements using 10 mm CW thick plates showed a brittle failure due to splitting in the CW plates along the row of the dowels. The connection design using the 6-dowel arrangement and 20 mm thick CW plates showed significant energy dissipation and ductility once the maximum moment capacity was attained compared to the other three connection designs of Phase-II. Ductility in this connection design was due to deformation (interlaminar shear and cross-grain) of the CW dowels and embedment of the surrounding timber. In contrast to this, the 8-dowel arrangement using 20 mm thick CW plates showed a brittle failure of timber which may be due to lower inter-dowel spacing and end distances.

Based on the results, it can be concluded that higher moment capacity can be achieved by increasing the number of CW dowels and thickness of the CW plates in the connection. The ductility was mainly affected by the spacing of dowels and the thickness of CW plates. Results did not show any clear relationship between the rotational stiffness and other connection parameters such as the number of CW dowels and the thickness of CW plates.



(a)



(b)

Figure 5.18- Moment-rotation behaviour of timber-CW connections of Phase-II, (a) 6-dowel arrangement using 10 and 20 mm thickness narrow-depth CW plates, and (b) 8-dowel arrangement using 10/20 mm thick narrow-depth CW plates

5.5.3.2 Failure modes

(a) 6-dowel connection using 10 mm narrow-depth CW plates

As there was no initial gap between the beams, this resulted in compression parallel to the grain on the top while a gap opened at the bottom of the connection, as shown in Figure 5.19a. All the specimens of this series showed splitting of CW plates along the row of dowels in the tension zone as shown in Figure 5.19a and Figure 5.19b. Due to the brittle failure of the CW plates in tension zone, a sudden decline in moment capacity was observed.

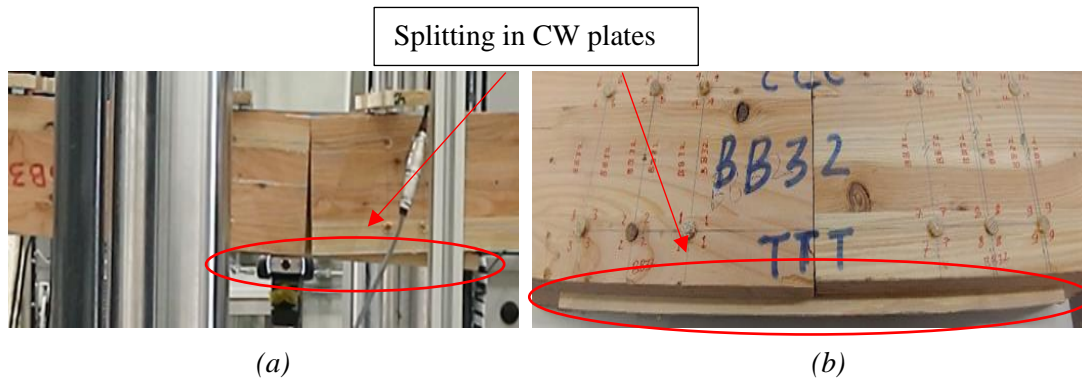
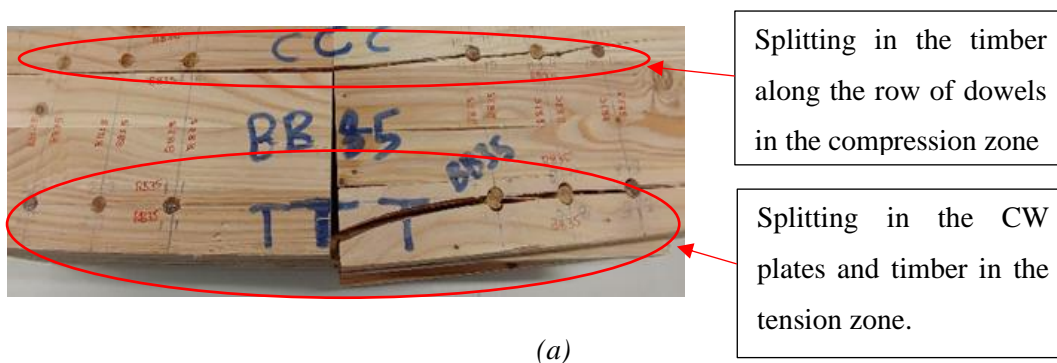


Figure 5.19- 6-dowels connection using 10 mm CW plates, (a) gap opening at the bottom of the connection and (b) splitting of CW plates along the row of dowels in the tension zone

(b) 6-dowel connection using 20 mm narrow-depth CW plates

Increasing to 20 mm thick CW plates resulted in a change in the failure mode of these connections. In all the specimens of this series, initial failure was observed in one of the CW plates in the tension zone due to splitting along the row of the dowels as shown in Figure 5.20a. This resulted in a drop between 8-20% in moment resistance. However, this drop was recovered until an interlaminar and cross-grain shear failure occurred within the CW dowels as shown in Figure 5.20b and Figure 5.20c, respectively. Once the maximum moment capacity was attained, splitting of the beams was observed along the row of CW dowels in the tension zone Figure 5.20a. Also, splitting was observed along the row of CW dowels in the compression zone due to pressing of beams against each other (see Figure 5.20a).



(a)



(b)

(c)

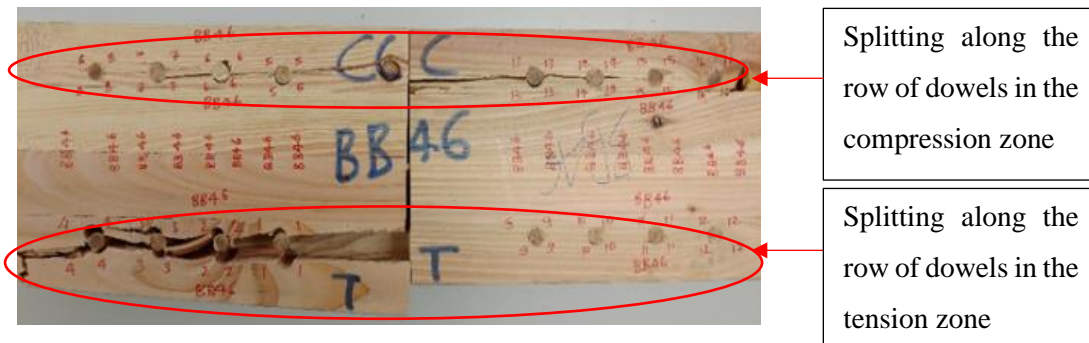
Figure 5.20- 6 dowels connection using 20 mm CW plates, (a) tension failure perpendicular to the grain in timber and splitting in the CW plates, (b) interlaminar shear failure of CW dowels, (c) cross-grain shear failure of the CW dowels

(c) 8-dowel connection using 10 mm narrow-depth CW plates

Similar to 6-dowel connections using 10 mm CW plates, all the specimens of this series exhibited the splitting failure of the CW plates in the tension zone along the row of dowels. When one of the CW plates failed, a rapid decline in the moment capacity was observed without any further increase. As expected, these connections showed a higher rotational stiffness than the 6-dowel arrangement using 10 mm CW plates, which may be attributed to the inclusion of two extra dowels on each side of the beams.

(d) 8-dowel connection using 20 mm narrow-depth CW plates

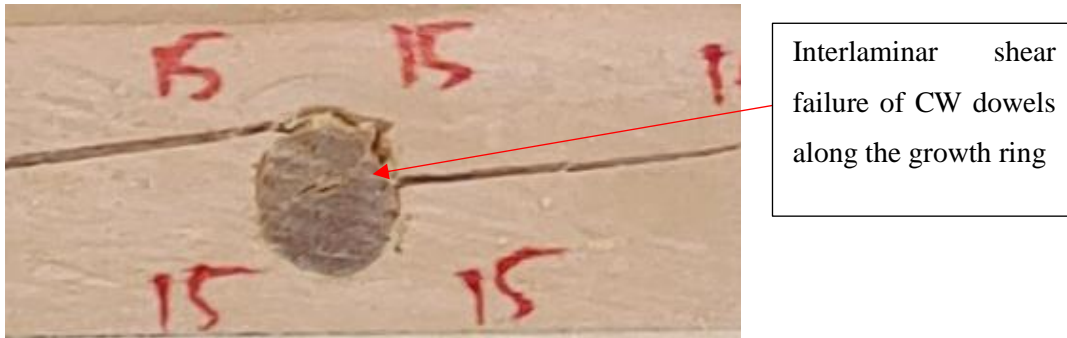
Similar to the 6-dowel arrangement using 20 mm CW plates, the inclusion of 20 mm thick CW plates in the 8-dowel arrangement changed the failure modes of the connection. Unlike the other three connection types, no failure was observed in the CW plates. Once the connection attained the maximum moment capacity, splitting was observed in the timber along the row of CW dowels in the tension zone as shown in Figure 5.21a. Additionally, the CW dowels showed interlaminar shear failure along the growth rings (see Figure 5.21b). Further increase in the load resulted in splitting in the compression zone along the row of dowels due to pressing of beams against each other without any increase in the moment resistance.



Splitting along the row of dowels in the compression zone

Splitting along the row of dowels in the tension zone

(a)



(b)

Figure 5.21- 8 dowel connection using 20 mm CW plates, (a) splitting in the timber in tension zone and compression zone, (b) interlaminar shear failure of CW dowels

5.5.4 Results summary and discussion

Table 5.4 summarises experimental test results of Phase-II. The connection design using 8-dowel arrangement with 20 mm thick CW plates has shown the highest mean moment-resistance which is approximately 39% higher than the lowest value that was observed for 6-dowel arrangement using 20 mm thick CW plates. However, 6-dowel arrangement using 20 mm CW thick plates has shown the highest mean rotational stiffness which is approximately 27% higher than the lowest value that was observed for 6-dowel arrangement using 10 mm thick CW plates. The connection design using 6-dowel arrangement with 20 mm thick CW plates has shown the highest mean ductility ratio which is approximately 140% higher than the lowest value that was observed for 8-dowel arrangement using 10 mm thick CW plates. Results indicate that higher moment capacity can be achieved by increasing the number of CW dowels and thickness of the CW plates. A more ductile response with higher rotational stiffness was shown to be achieved by through larger dowel spacing and thicker CW plates. Designers may choose an appropriate design based on the end use and strength/ductility requirement. These findings are based on the limited number of specimens of each connection type tested in this study. A large number tests are required in future for conformation.

Table 5.4- Test results of beam-beam connections with narrow-depth CW plates (Phase-II)

Connection type	Specimen number	Load-carrying capacity (kN)	Moment capacity (kN.m)	Rotational stiffness (kN.m/rad)	Ductility ratio
6-dowel arrangement using 10 mm CW plates	BB-6-10-1	11.8	5.7	115.0	1.3
	BB-6-10-2	17.0	8.1	170.7	1.4
	Mean	14.4	6.9	142.9	1.4
	Standard deviation	3.6	1.7	39.3	0.0
6-dowel arrangement using 20 mm CW plates	BB-6-20-1	14.6	7.0	224.3	2.4
	BB-6-20-2	12.3	5.9	168.2	2.5
	BB-6-20-3	13.2	6.4	197.0	2.2
	Mean	13.4	6.4	196.5	2.4
	Standard deviation	1.1	0.5	28.1	0.2
8-dowel arrangement using 10 mm CW plates	BB-8-10-1	12.2	5.8	195.1	0.9
	BB-8-10-2	15.0	7.2	177.6	1.1
	Mean	13.6	6.5	186.4	1.0
	Standard deviation	1.3	1.0	12.4	0.1
8-dowel arrangement using 20 mm CW plates	BB-8-20-1	15.7	7.5	148.9	1.1
	BB-8-20-2	21.2	10.2	160.3	1.4
	BB-8-20-3	18.9	9.1	192.9	1.2
	Mean	18.6	8.9	167.4	1.2
	Standard deviation	2.8	1.3	22.9	0.2

5.6 Beam-column connections using glued structural members (Phase-III)

In Phase-III, seven different designs of semi-rigid type beam-column timber moment connections were developed using glued structural members and CW connectors (plates and dowels). The primary objective of this testing was to select a connection design for the development of beam-column connections using CWDLT members and CW connectors. For each design, only one specimen was manufactured and tested to failure. The developed connection designs were classified into two main categories as shown in Figure 5.22. The classification was done based on the presence or absence of CW plates and their similarity

with the modern and carpentry type beam-column connection designs. Modern connections are often produced using slotted-in plates, whereas carpentry connections were comprised of mortise and tenon configuration without any plates.

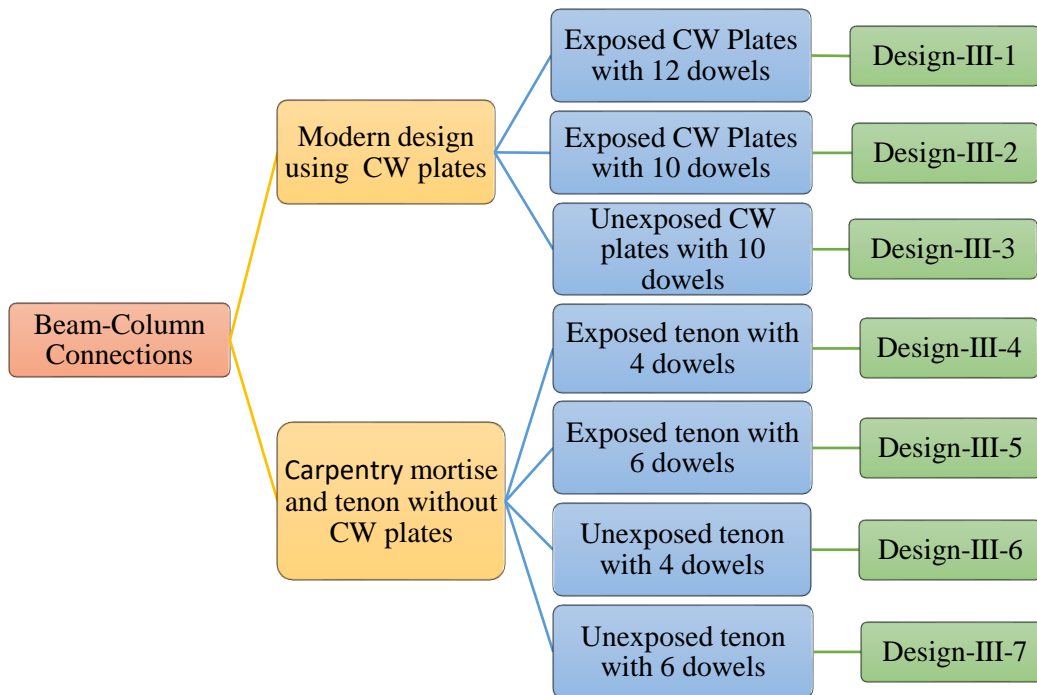


Figure 5.22- Classification of connections designs for beam-column connections

In the modern connection types, four CW plates (2 in the compression zone and 2 in the tension zone) were accommodated in slots routed in the connected members as shown in Figure 5.23. The CW plates of compression zone were hidden in the column area and they were visible in both tension and compression zone of the beam in all modern connection designs. In Design-III-1 and Design-III-2, CW plates of tension zone were not hidden in the column, whereas in Design-III-3 plates were hidden by the shouldered column which extended beyond the connection. Similarly for carpentry mortise and tenon connections, the tenons were not hidden in Design-III-4 and Design-III-5, whereas Design-III-6 and Design-III-7 had hidden tenon members (see Figure 5.23). It was expected that hidden CW plates/ tenons may improve the rotational stiffness of the corresponding design by restricting the rotation of the CW plates/tenons. For explanation purposes, the term “Unexposed” is used for connection designs with hidden CW plates/tenons and “Exposed” for the opposite case.

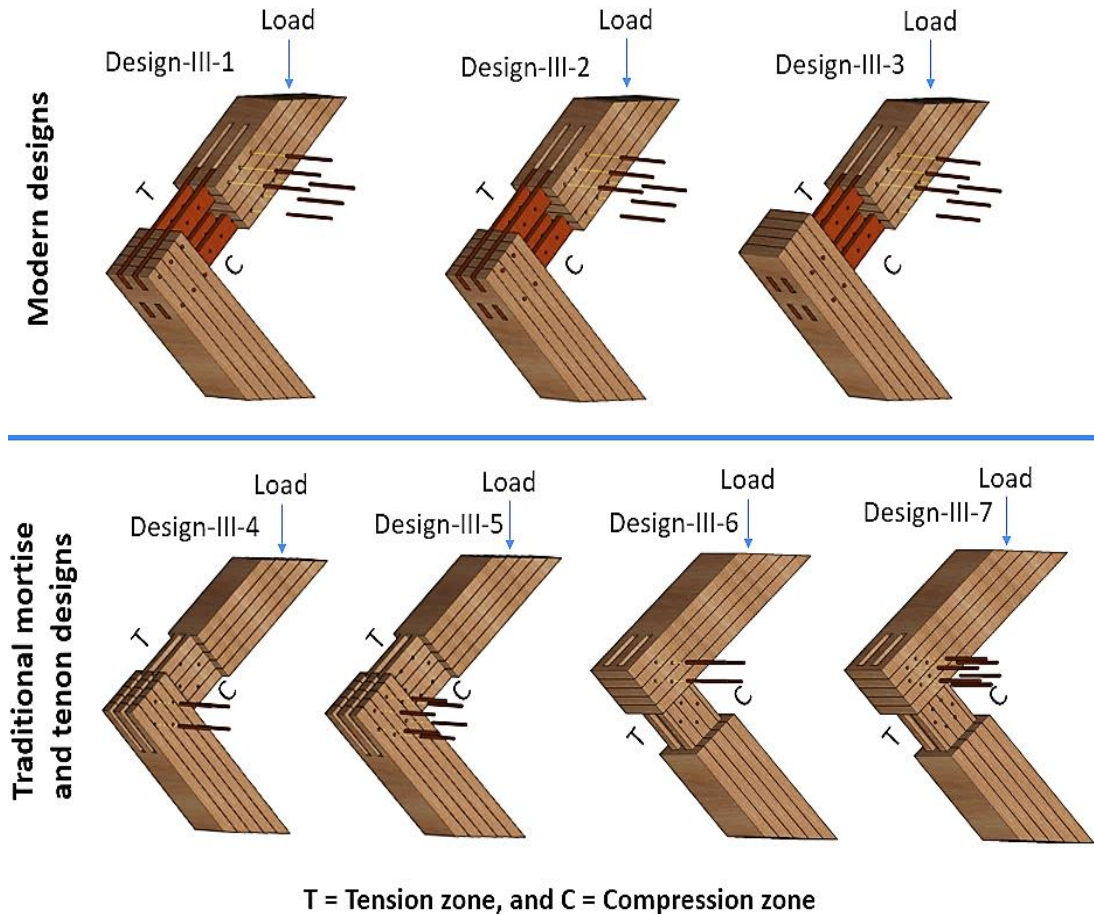


Figure 5.23- 3D models of beam-column connection designs

5.6.1 Connection configuration, fabrication and assembly

Based on the results of the beam-beam connections (Phase-II), 20 mm thick CW plates were chosen to obtain superior structural performance in terms of moment capacity, rotational stiffness and ductility. For modern connections using CW plates, both columns and beams were routed at one end to accommodate the CW plates of 20 mm thickness. The routed slot was 20.5 mm wide and 60 mm deep. While for carpentry mortise and tenon connections, mortises of 30 mm width were routed at one end to accommodate the 28.5 mm thick tenons. The detailed connections geometries are shown in Appendix-A.

Slots dimensions and plate arrangements of Design-III-1 and Design-III-2 were the same with a varying number of CW dowels. Design-III-1 was fastened using 12 CW dowels; 6 CW dowels in each column and beam areas, whereas Design-III-2 was fastened using 10 CW dowels; 4 CW dowels were in the column and 6 CW dowels in the beam. These changes in the number of dowels were used to examine the effect of the number of dowels on the load-carrying capacity and rotational stiffness of the connections. Design-III-3 consisted of 10 dowels similar to Design-III-2. However, it was designed in such a manner that the two CW plates in the tension zone of the column remain unexposed as shown in Figure 5.23. As

mentioned in the previous section, this geometrical change was expected to improve the rotational stiffness of the connection due to restricted rotation of CW plates.

Carpentry mortise and tenon connections were manufactured without CW plates and with a varying pattern and number of dowels. The mortises and tenons were precisely cut using a CNC machine and assembled. Design-III-4 consisted of 4 CW dowels arranged in a cross-shape pattern, whereas Design-III-5 involved 6 dowels arranged in a hexagonal pattern. Inter-dowel spacing, dowel end distances and edge spacing are as shown in Appendix-A.

Another configuration of the mortise and tenon type connections was designed where slots (Pocket slots) of 30 mm were routed in the beam at 20 mm distance from the unloaded end. Tenons of 140 mm x 28.5 mm were routed in the column to ensure easy insertion into the mortise. Design-III-6 was fabricated using 4 CW dowels arranged in the cross pattern whereas Design-III-7 involved 6 dowels arranged in a hexagonal pattern. However, it should be noted that the inter-dowel spacing was lower due to a reduced cross-section of tenon compared to Design-III-4 and Design-III-5. Inter-dowel spacing, dowel end distances and edge spacing are shown in Appendix-A.

Figure 5.24 shows the fabrication and assembly process of the connections. For modern designs, beam and column were fixed in a position and the CW plates were positioned prior to dowel insertion as shown in Figure 5.24a. For carpentry designs, tenon and mortise were held together using a timber board fixed using screws (see Figure 5.24) and then holes were drilled using a pillar drill (see Figure 5.24c). Similar to beam-beam connections, 10.2 mm hole diameter was used for CW dowels (10 mm to 10.3 mm). Also, to facilitate easy insertion of CW dowels, the insertion end of dowel was chamfered to conical shape (Figure 5.24d) using a disc sander. The loaded end of both beam and column were cut with an angle of 45° in such a way that when the specimen was vertically loaded, it induces a bending moment in the connection. Assembled connections were conditioned at $20 \pm 2^\circ\text{C}$ temperature and $65 \pm 5\%$ RH for 30 days before testing.



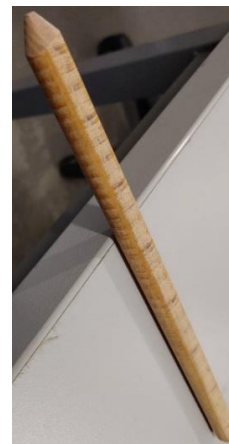
(a)



(b)



(c)



(d)

Figure 5.24- Assembly of the connection, (a) modern connection design, (b) carpentry mortise and tenon, (c) drilling of holes, (d) chamfered end of CW dowels

5.6.2 Test procedure

Tests were performed using a Denison hydraulic testing machine, model T42B [211], rated to 500 kN, under displacement control mode. All tests were carried out in accordance with EN 26891 [183] at a constant displacement rate of 3.2 mm/min. The ram displacement and load were recorded continuously. Each specimen was placed on the flat platform in such a way that loading head above them would compress the levelled surface of beam as shown in Figure 5.25a. LVDTs with an accuracy of 0.1 %, were placed on each side of the column to measure the relative beam-column displacement of the connection at two points spaced 120 mm apart as shown in Figure 5.25a and Figure 5.25b. When the bending moment was induced in the connection, the beam starts rotating at the bearing point. Plungers of the LVDTs were carefully aligned with the centre of the stoppers attached on the beam. The corresponding rotation angle was calculated using Eq. 5.1. The average rotation angle of the connection was calculated using Eq. 5.6. The moment on the connection is the product of load on the beam and perpendicular distance to the bearing point that is approximately 244 mm. The experimental

rotational stiffness of the connection was calculated based on 10% and 40% of the maximum moments and the corresponding rotational angles using Eq. 5.4. The ductility ratio was calculated using Eq. 5.5.

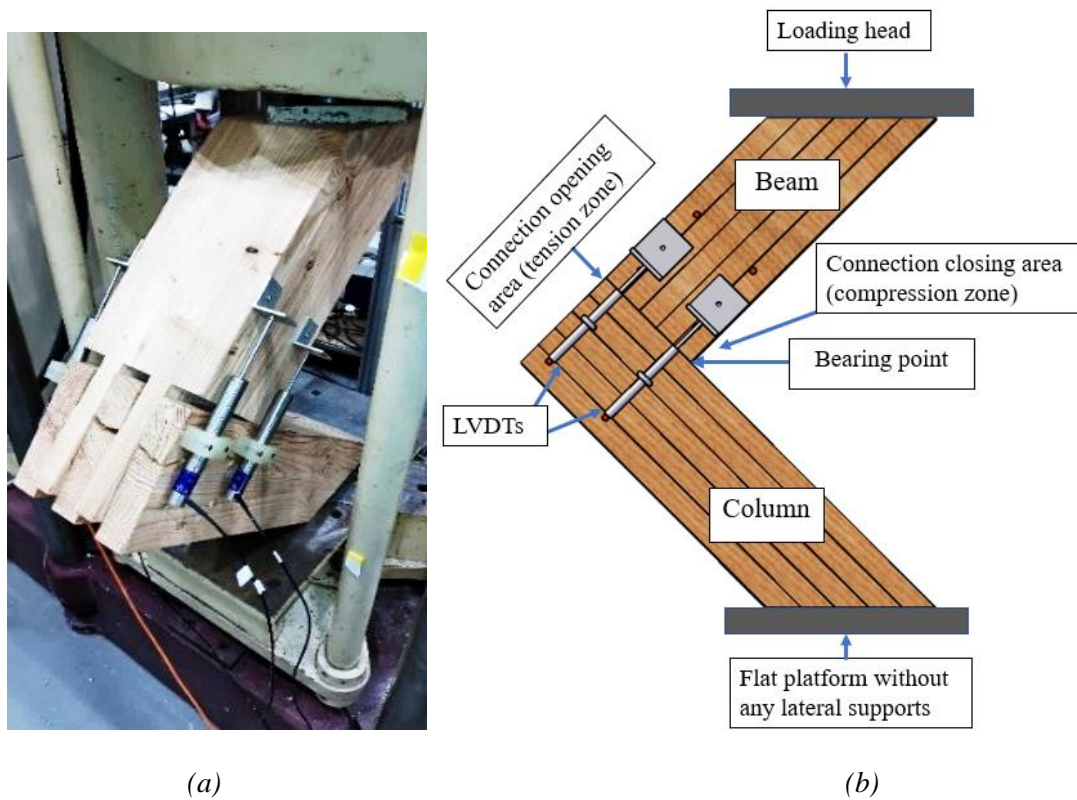


Figure 5.25- Test set up, (a) orientation of the test specimen under load, (b) position of the LVDTs

5.6.3 Test results and discussion

This section details the load-ram displacement behaviour, moment-rotation behaviour and failure mode of each connection design.

5.6.3.1 Load-ram displacement and moment-rotation behaviour

Figure 5.26 shows the load-ram displacement behaviour for all the connection designs. Design-III-1 showed the highest load-carrying capacity, which is approximately 89% higher than the lowest value observed (Design-III-4). All modern connection designs showed a relatively higher yield load compared to the carpentry designs. The mean yield load for modern connection designs was approximately 33.8 kN, whereas this was 26.6 kN for carpentry designs. This is an increase of 33% in the yield load of modern connection designs, which is probably due to the relatively higher number of CW dowels and significantly higher embedment strength of CW plates.

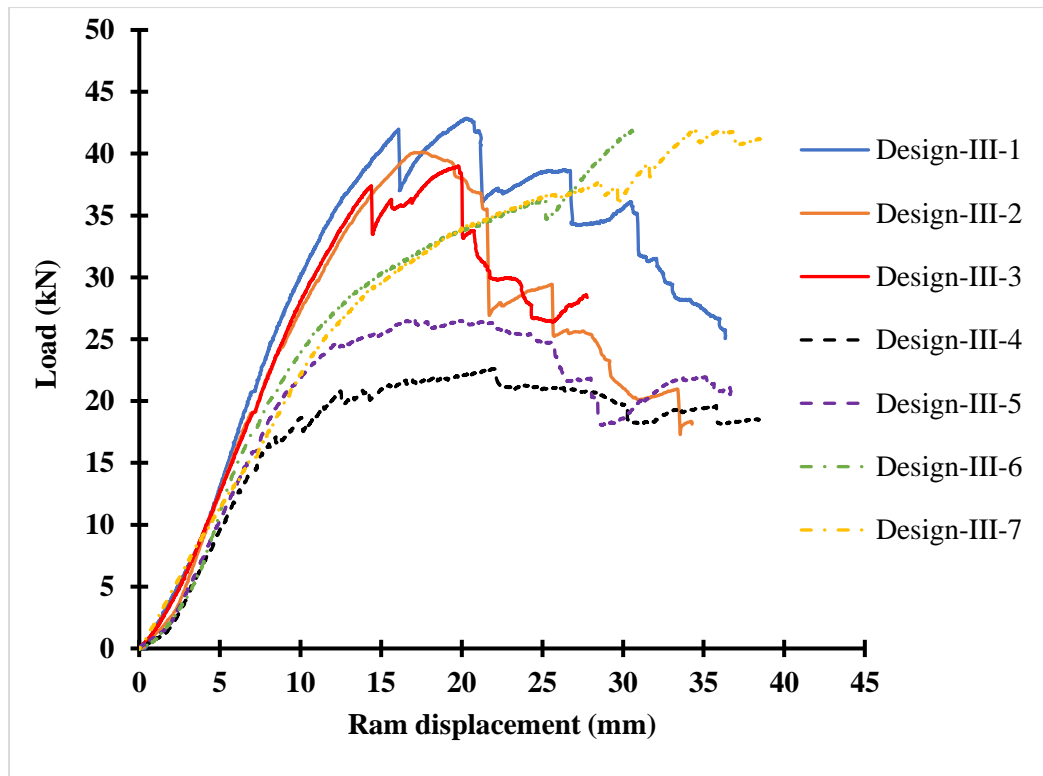


Figure 5.26- Load-ram displacement behaviour of beam-column connections using glued structural members and CW connectors

Figure 5.27 shows moment-rotation behaviour of all the connection designs. Design-III-1 showed highest moment capacity, but the rotational stiffness was the least among all other connection designs. The reason for lower rotational stiffness is due to significantly higher initial rotation compared to other connection designs. The higher rotation is probably due to localised imperfections during the assembly process. The coefficient of variation (COV) of rotational stiffness of modern connection designs was 22.5%, whereas this was only 8.6% for the carpentry connection designs. Among modern connection designs, Design-III-3 showed the highest rotational stiffness which was expected due to restricted movement of CW plates. Among all connection designs, Design-III-6 showed the highest rotational stiffness, which is approximately 74% higher than the least value observed for Design-III-1. Design-III-4 showed the highest ductility ratio, which is approximately 123% higher than the least value observed for Design-III-3. The mean ductility ratio of carpentry connections designs was two times higher than the modern connection designs.

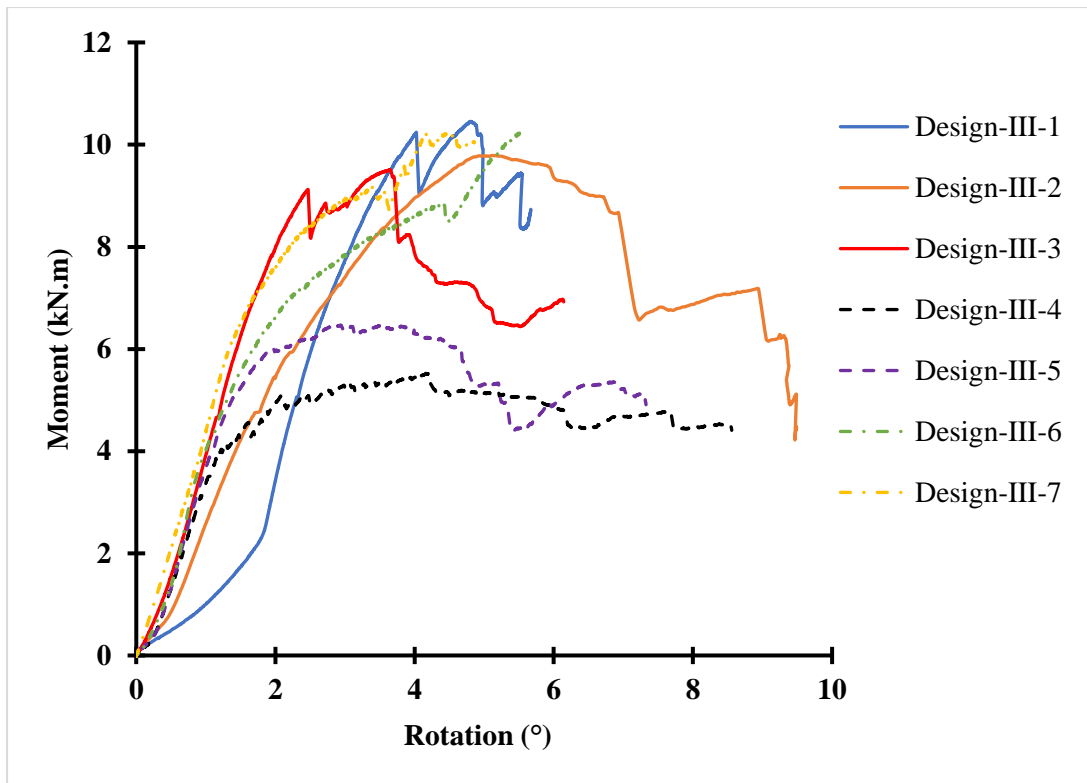


Figure 5.27- Moment-rotation behaviour of beam-column connections using glued structural members and CW connectors

5.6.3.2 Failure modes

(a) Design-III-1

The dowels in the column at the farthest distance from the bearing point, shown in Figure 5.28a, were subjected to higher moment and thus, showed higher deformation compared to dowels in the compression zone (bottom row of dowels in the column and beam). There was no significant damage in the bottom row of dowels, which was possibly due to the smaller distance of the bottom row of dowels from the bearing point. Initially, splitting in one of the exposed CW plates was observed along the row of CW dowels as shown in Figure 5.28b. It was due to higher tensile stresses in the tension zone at approximately 10 kN.m and 4° rotational angle. This resulted in a sudden drop of approximately 1 kN.m. The moment capacity increased again during this loading period due to deformation of dowel number 1 and 2 (which were at the farthest distance from the bearing point) until the tension failure perpendicular to grain observed in the column around dowel 3 at approximately 10.2 kN.m (see Figure 5.28a). The dowels 1 (see Figure 5.28c) and 2 (see Figure 5.28d) showed failure at the interface of CW plates and column. Ductility in the connection resulted from energy dissipation due to deformation of CW dowels and crushing of the surrounding timber.

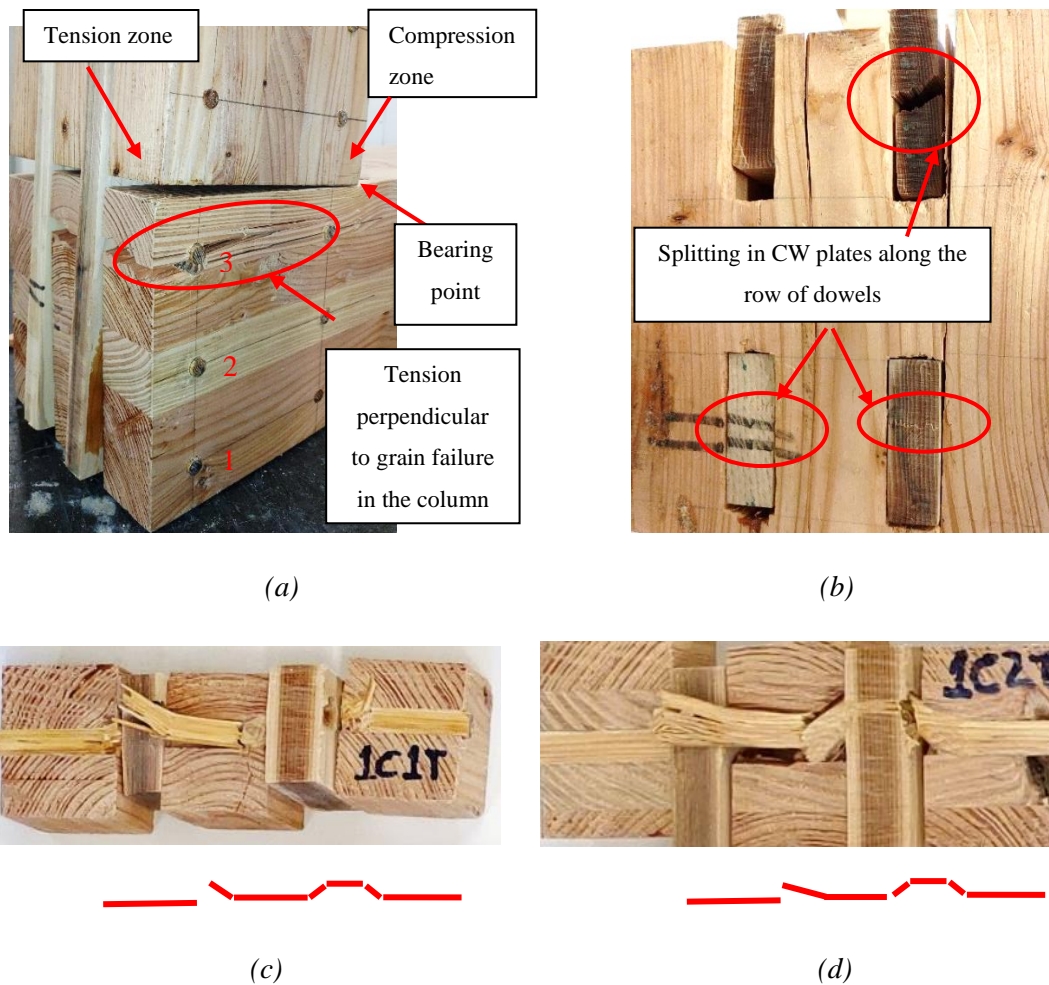


Figure 5.28- Failure mechanism, (a) Splitting in CW plates in the tension and compression zone, (b) tension perpendicular to grain failure in the column, (c) formation of partial plastic hinges in the dowel of tension zone, (d) formation of partial plastic hinges in the dowel 2 of the tension zone

(b) Design-III-2

Similar to Design-III-1, the dowels in the column, which were at the farthest distance from bearing point, showed higher deformation. The dowels of the compression zone remained undamaged compared to dowels in the tension zone (bottom row of dowels in column and beam). Initially, premature splitting was observed in the column area due to tension perpendicular to the grain failure at approximately 6 kN.m and 2° rotational angle (Figure 5.29a). This failure increased the connection rotation without any decrease in the moment capacity of the connection. With the increasing rotation of CW plates, deformation in dowel number 1 was observed which was located at the farthest distance from the bearing point. Another failure was observed due to tension failure perpendicular to the grain in the column at approximately 7 kN.m with the rotation of 3° around dowel number 2. The dissected section around dowel number 1 and 2 are shown in Figure 5.29b and Figure 5.29c, respectively. These consecutive failures in timber, further increased rotation of the connection without a decrease in the moment capacity. The connection attained a maximum moment of approximately 9.7

kN.m before splitting in one of the CW plates of compression zone as shown in Figure 5.29d. The premature splitting around the dowel holes in the column resulted in this connection type being the least ductile among all three modern connection designs.

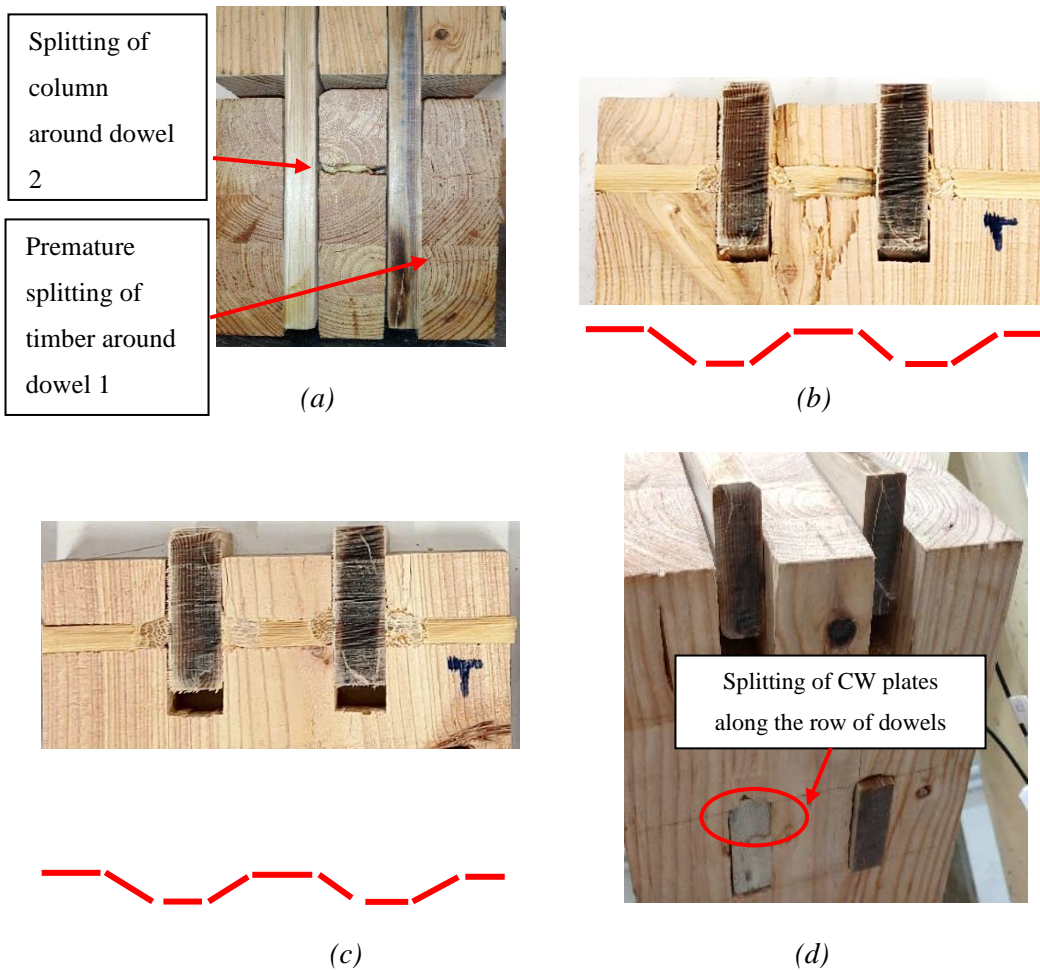


Figure 5.29- Failure mechanism, (a) tension perpendicular to grain failure in the column, (b) formation of partial plastic hinges in dowel 1 of tension zone, (c) formation of partial plastic hinges in dowel 2 of tension zone, (d) splitting in CW plate of the compression zone

(c) Design-III-3

As expected, Design-III-3 showed a different failure mechanism compared to Design-III-1 and Design-III-2. This may be due to restricted rotation of CW plates. Dowels in the column area did not show any significant damage. Splitting was observed in the tension zone of the beam at approximately 7 kN.m moment and 1.6° rotational angle (see Figure 5.30a). This failure further propagated along the row of dowels from dowel number 1 to 3. In contrast to Design-III-1 and Design-III-2, tension perpendicular to grain failure of the column was eliminated through the extended length of the column. CW plates in the compression zone failed one by one as shown in Figure 5.30b. The first CW plate failed at 9.1 kN.m at a rotational angle of 2.5° , which is the first peak in the moment-rotation curve. This resulted in 1 kN.m drop in the moment capacity. After this point, a continuous increase was observed up

to moment of 9.5 kN.m. This may be due to shearing of CW dowels. The dissected section confirmed deformation within dowels of tension zone in the beam. Figure 5.30c and Figure 5.30d shows deformation of dowels. The second CW plate in the compression zone failed once the connection attained its maximum moment capacity of 9.5 kN.m at 3.6° rotation. Ductility in the connection was due to shearing of the dowels and embedment in timber.

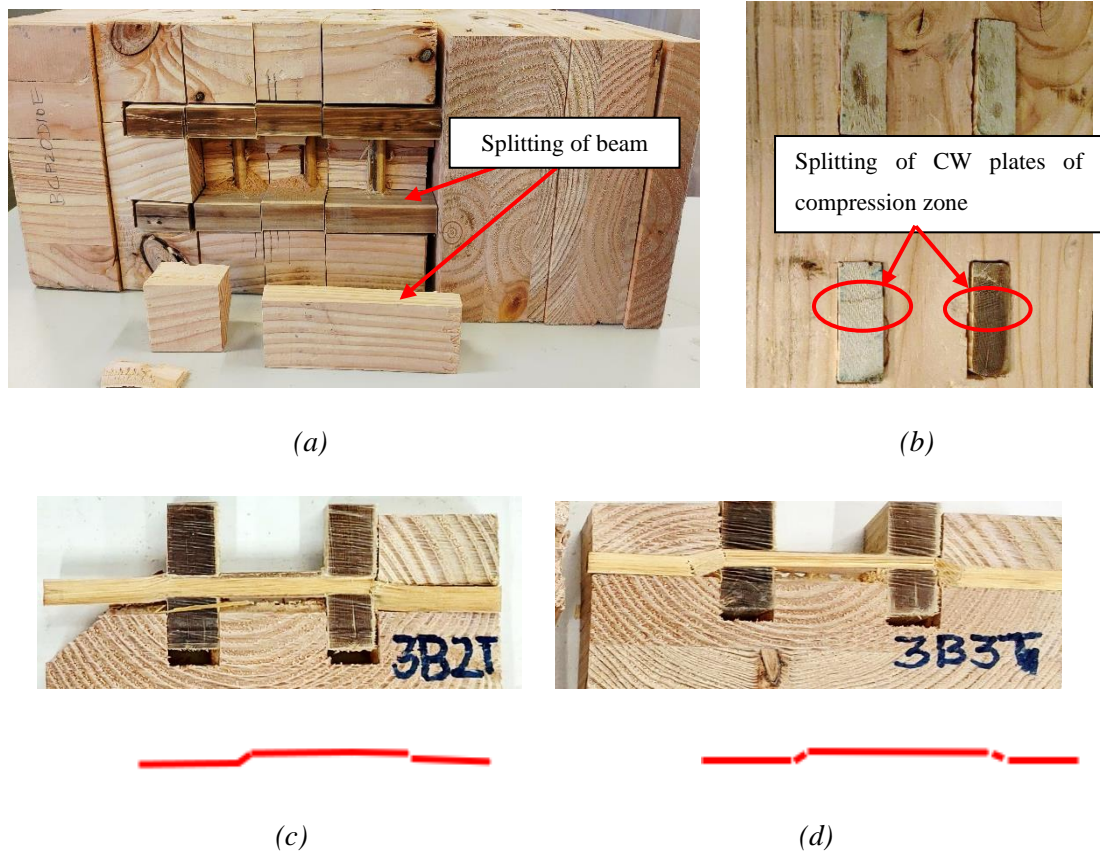


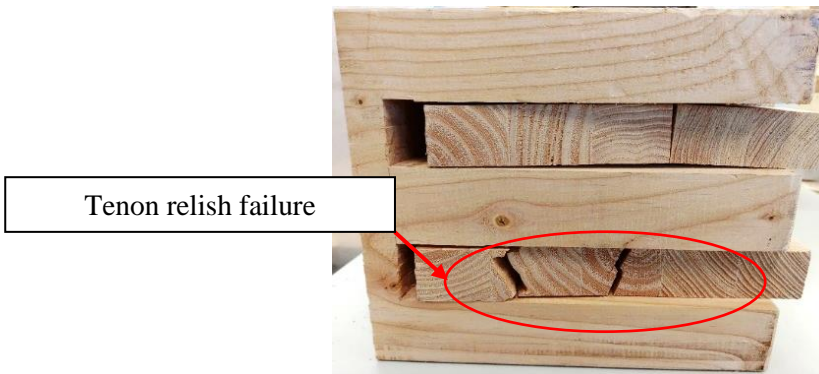
Figure 5.30- Failure mechanism, (a) splitting of CW plates in the compression zone, (b) splitting in the beam, (c) deformations of dowel 2 of the beam, (d) deformation of dowel 3 of the beam

(d) Design-III-4

An elastic phase was observed up a moment of 4 kN.m. After the elastic phase, non-linear behaviour was observed. However, there was no visible failure in the tenon or mortise. The non-linearity may be attributed to the shearing and bending of CW dowels. This was later confirmed when dissected sections were analysed. The CW dowels showed a formation of partial plastic hinges (see Figure 5.31a). During this process, a large amount of energy was absorbed, which favoured the ductile behaviour of this design. Finally, splitting failure was observed in the tenon at 5.5 kN.m moment (see Figure 5.31b). This type of failure in tenon is commonly called a tenon relish failure and it is characterised by a single split or a block shear failure behind the dowel hole [212].



(a)

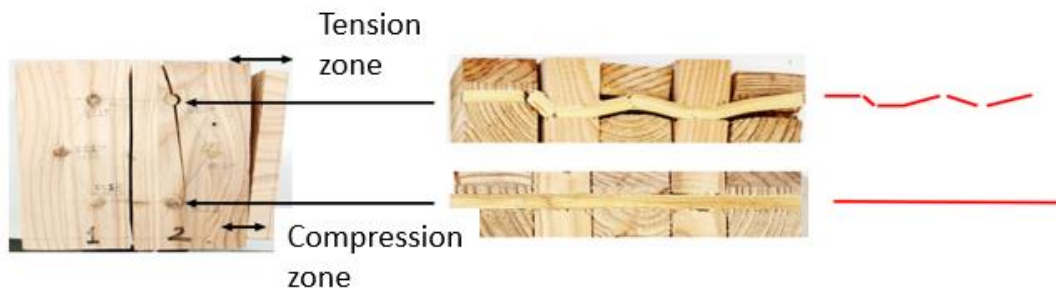


(b)

Figure 5.31- Failure mechanism, (a) typical failure mechanism of the CW dowels with the formation of partial plastic hinges, (b) tenon relish failure

(e) Design-III-5

Similar to Design-III-4, non-linear behaviour was observed in the moment-rotation curve after the elastic phase. There was no visible failure in the tenon and mortise. The dissected components showed the formation of partial-plastic hinges in the CW dowels (see Figure 5.32a). This could be a possible reason for the non-linear behaviour. Tenon relish failure (Figure 5.32b) was observed at 5.8 kN.m. It was observed that the tenon split did not affect the moment capacity significantly. A continuous increment in the rotation was observed without any significant decrease in the moment capacity until the tension failure perpendicular to grain was observed in the column) at 6.4 kN.m (see Figure 5.32b). It should be noted that the rotational stiffness was 23% higher than Design-III-4, whereas the moment capacity had increased by 17%. This improvement was expected due to the inclusion of two extra dowels.



(a)

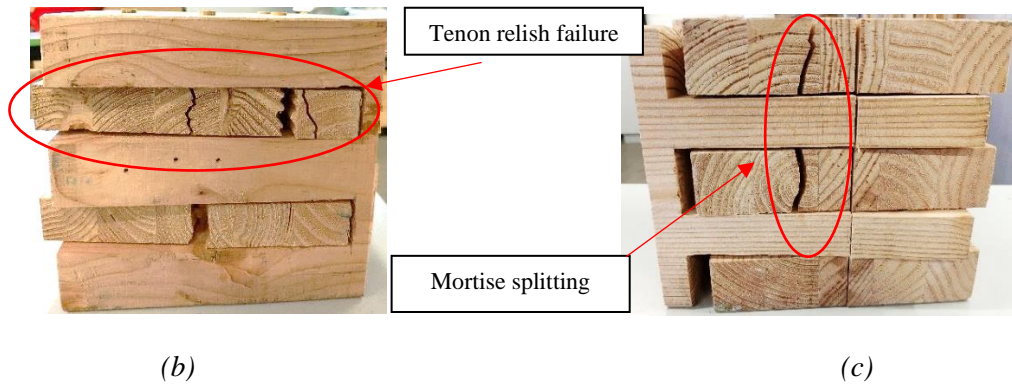
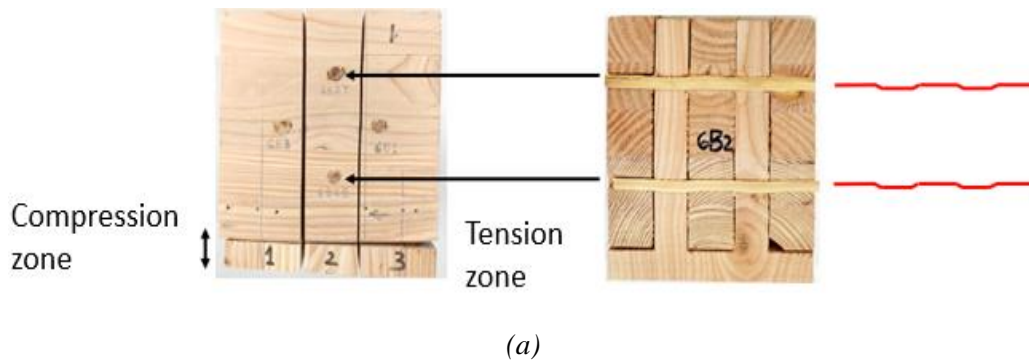
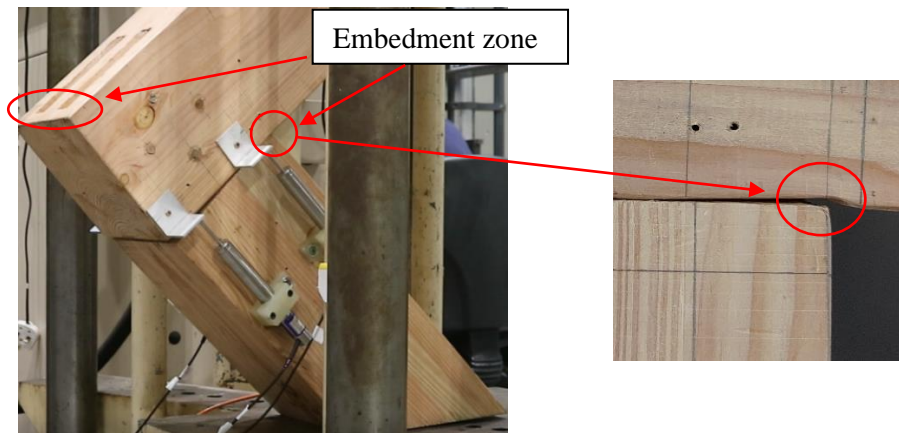


Figure 5.32- Failure mechanism, (a) typical failure mode of CW dowels, (b) tenon relish failure, and (c) mortise failure

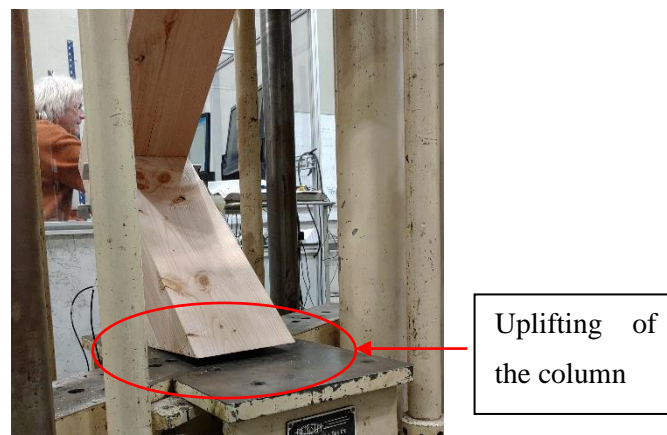
(f) Design-III-6

In this connection, no visible failure was observed in the connected members. CW dowels, which were at the furthest distance from the bearing point, showed shearing and bending failure. Figure 5.33a shows the typical failure of CW dowels. In contrast to Design-III-4 and Design-III-5, rotation of the beam was restricted due to interlocking of tenon and mortise. This led to embedment between mortise and tenon as shown in Figure 5.33b. At moment of 8.2 kN.m, strain hardening can be seen in the moment-rotation graph due to compression perpendicular to the grain in the beam around the bearing point. The test was stopped at 10.2 kN.m due to the uplifting of the column from the bottom end (see Figure 5.33c). Therefore, the result (ultimate load) presented for this connection should be considered conservative.





(b)



(c)

Figure 5.33- Failure mechanism, (a) deformation of CW dowels, (b) embedment of beam-column, (c) uplifting of column

(g) Design-III-7

Similar to Design-III-6, the formation of partial plastic hinges was observed in the CW dowels located in the tension zone (see Figure 5.34a). Also, cross-grain shear failure was observed in the CW dowels. No failure was seen in the dowels near the connection closing area due to their proximity to the bearing point. This design showed similar moment-rotation behaviour as Design-III-6. The rotation of the beam was restricted due to embedment between the mortise and tenon. Tenon relish failure (see Figure 5.34b) was observed at the 8.8 kN.m. Immediately after the tenon split, strain hardening was observed in the moment-rotation curve due to compression perpendicular to the grain in the beam at the bearing point. Similar to Design-III-6, the test was stopped at 10.2 kN.m due to uplifting of the column from the lower platen of the test machine. Therefore, the result (ultimate load/moment) presented for this connection should be considered conservative.

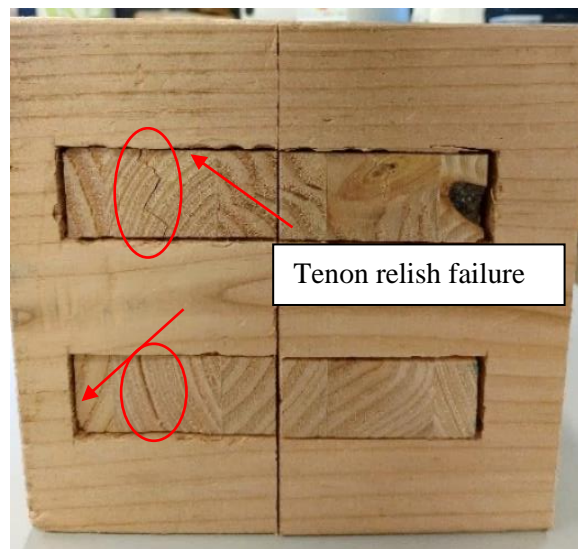
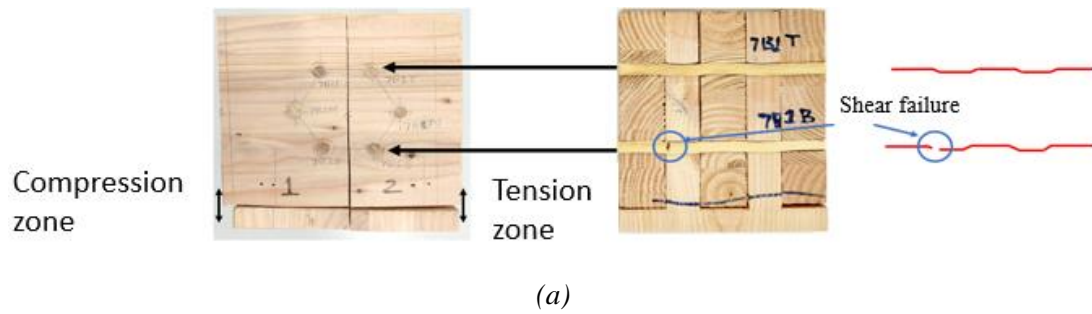


Figure 5.34- Failure mechanism, (a) deformation of CW dowels, (b) tenon relish failure

5.6.4 Results summary and selection of optimum design

Table 5.5 summarises the test results for all connection designs. From a capacity perspective, Design-III-4 and Design-III-5 which were with exposed tenon have lower moment capacities than remaining five connection designs. Design-III-1 and Design-III-3 have significantly lower rotational stiffness compared to other designs. The remaining 3 designs have similar moment capacity and rotational stiffness.

Table 5.5- Results summary of beam-column connections using glued structural members and CW dowels

Design type	Load-carrying capacity (kN)	Moment capacity (kN.m)	Rotational stiffness (kN.m/rad)	Ductility ratio
Design-III-1	42.9	10.5	165.0	2.2
Design-III-2	40.1	9.8	198.4	1.9
Design-III-3	39.0	9.5	255.9	1.7
Design-III-4	22.7	5.5	233.2	3.8
Design-III-5	26.5	6.5	268.8	2.9
Design-III-6	42.0	10.3	286.7	2.7
Design-III-7	42.0	10.2	254.5	1.8

It should be noted that for each connection design only one specimen was tested. The objective was to choose one connection design to produce beam-column connections using CWDLT members and CW connectors. Based on the moment capacity and rotational stiffness values, it can be said that Design-III-6 and Design-III-7 could be an appropriate choice. However, the selection of these designs raises issues from the manufacturing side of CWDLT members. These designs cannot be adopted with their existing geometries due to thinner tenon width which is just 28.5 mm wide (see Figure 5.35). The dowel lamination in thinner tenons may weaken the structural members due to the reduction in net cross-section area while drilling the holes. At the same time, insertion of dowels for connecting member laminates will further need drilling of holes in the tenons and mortises which requires additional care and tight tolerances during manufacturing. Also, increasing the width of structural members was limited in this study by the available length (200 mm) of the CW dowels. Due to aforementioned issues, Design-III-6 and III-7 were not considered suitable for use with CWDLT members. However, they may be used with solid timber and glued members. Based on structural performance and ease of manufacturing, modern connection Design-III-3 was chosen as the basis for the designing of beam-column connections using CWDLT members and CW connectors.

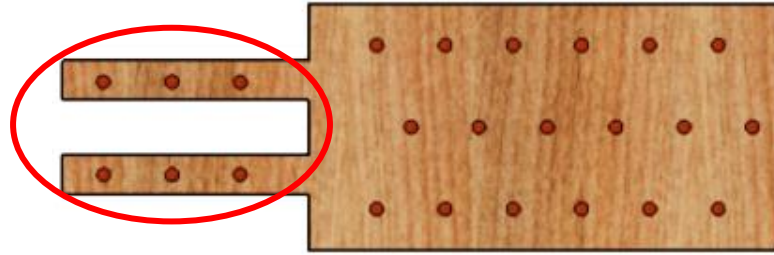


Figure 5.35- Showing constraints in manufacturing of carpentry connection types using CWDLT structural members

5.7 Beam-column connections using CW dowel laminated structural members (Phase-IV)

In Phase-IV, semi-rigid type beam-column timber moment connections were developed using CWDLT structural members and CW connectors (plates and dowels). These connections were developed based on the results of Phase III beam-column connection tests, which were produced using glued structural members (see Section 5.6). The structural members were jointed in a similar fashion to Design-III-3 using four narrow-depth CW plates and ten CW dowels. In this phase, two connection configurations were investigated, which were categorised based on (1) thickness of the CW plates and (2) inter dowel and edge spacing of compressed threaded beechwood dowels. These threaded dowels were located in the connection area of structural members as described in Section 5.7.1. For these two designs, all other connection properties such as the number of CW dowels/CW plates, spacing and end distances of CW dowels of the connections remained constant. Figure 5.36 shows the test program of this phase. The structural performance of developed connections was characterised by means of destructive testing. Finally, obtained test results were examined and compared with Design-III-3 (reference).

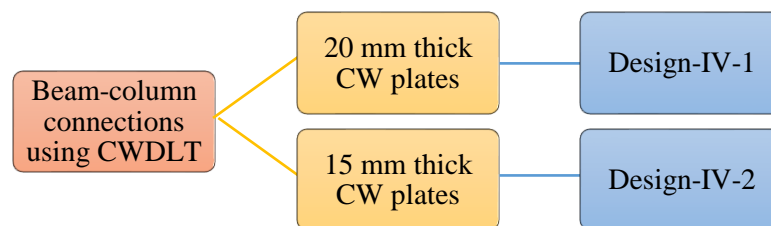


Figure 5.36- Test program of Phase-IV

5.7.1 Connection configuration, fabrication and assembly

A total of 4 beam-column connections were manufactured and tested in this phase. Figure 5.37 shows a 3D configuration of the connection. The column contained 33 smooth CW dowels and 8 compressed threaded beechwood dowels, whereas there were 14 smooth CW dowels and 8 compressed threaded beechwood dowels in the beam.

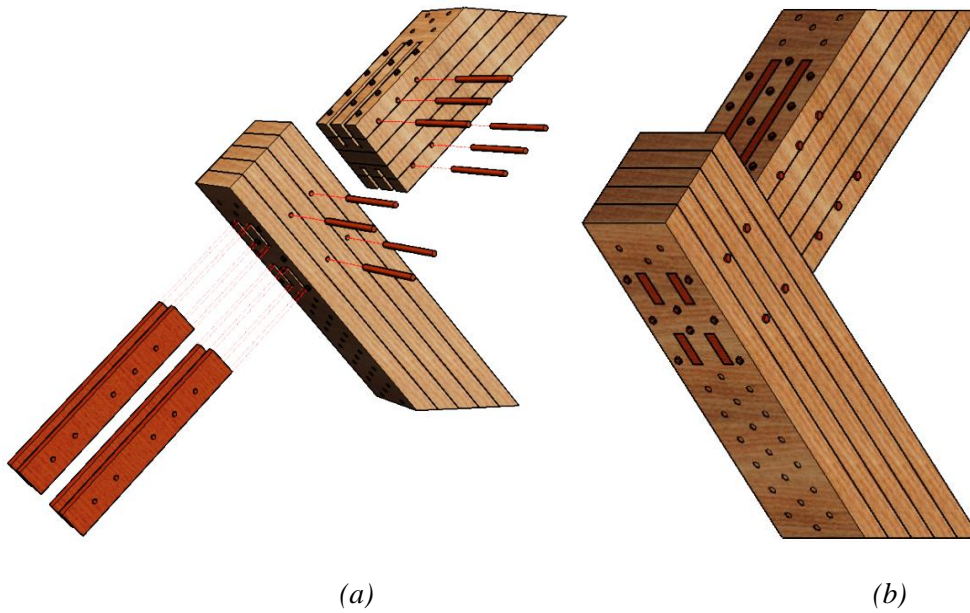


Figure 5.37- 3D design of beam-column connection for CWDLT members, (a) exploded view, (b) assembled connection

The Design-IV-1 comprised of 20 mm thick CW plates. Only a single specimen of this design was developed and tested. This is because of brittle failure of the column in the connection zone for this design (see Section 5.7.3). To avoid this type of failure and to induce more ductile behaviour within the connection, the thickness of CW plates was reduced to 15 mm and the position of compressed threaded beechwood dowels were changed in the subsequent design. This new design referred as Design-IV-2. It was assumed that the 15 mm thick CW plates may reduce rotational stiffness of the connection and facilitate deformation within the CW connectors (used for jointing beam and column) instead of the structural members. Also, the compressed threaded beechwood dowels were moved from the area between the inner edges of slots of compression and tension zone to delay or avoid brittle failure of the column. Figure 5.38a and Figure 5.38b shows a plan view of columns of Design-IV-1 and Design-IV-2, respectively.

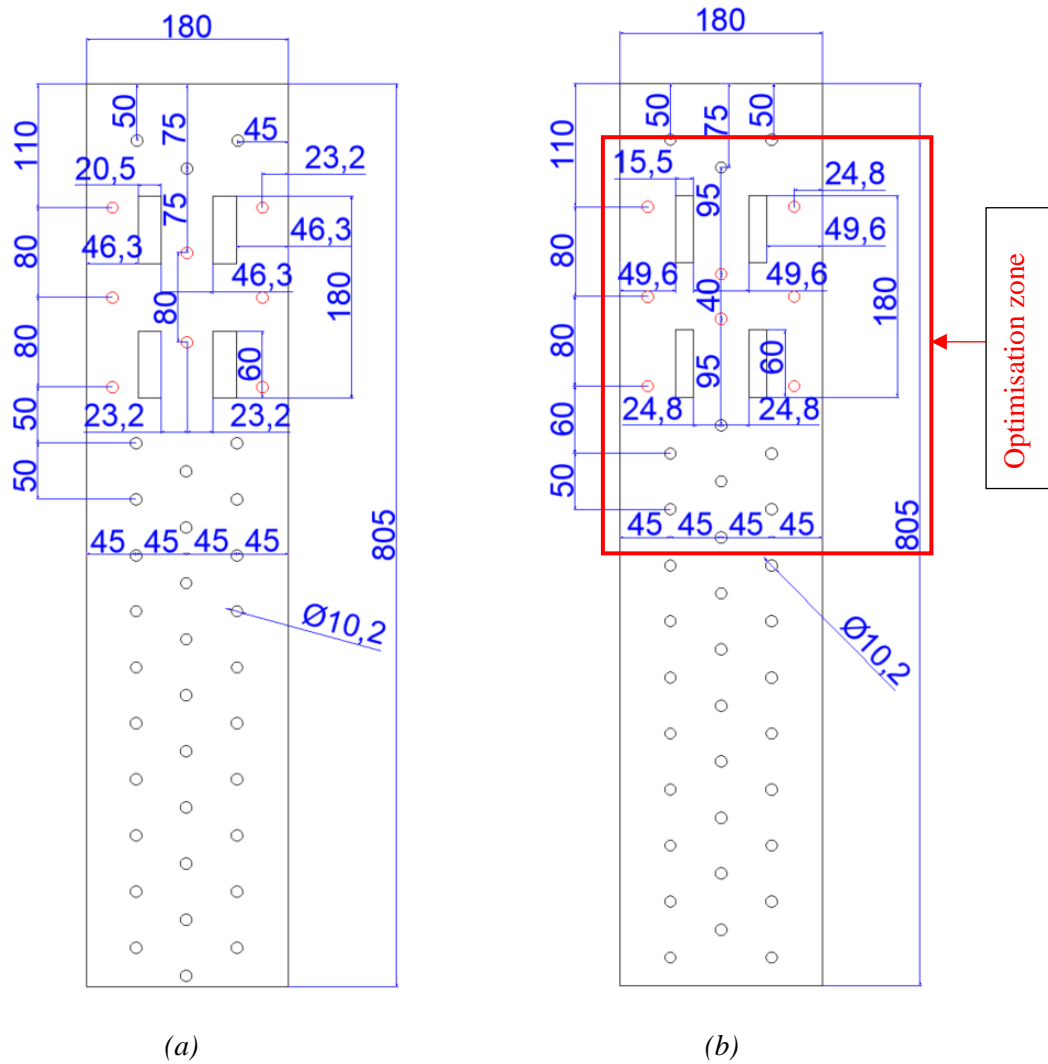


Figure 5.38- Plan view of column, (a) Design-IV-1 (initial design), (b) Design-IV-2 with optimised configuration (all dimensions in mm). Red colour circles indicate compressed threaded beechwood dowels

To assemble the connections, both columns and beams were routed at one end to accommodate CW plates of 20/15 mm thickness as shown in Figure 5.39. The routed slots were 20.5/15.5 mm wide and 60 mm deep. Once routed, members were clamped together and connected using CW dowels. The compressed threaded beechwood dowels were used in the connection area to avoid separation of the laminations at a higher load (see Figure 5.39). In both designs, it was ensured that the compressed threaded beechwood dowels would not intersect with smooth CW dowels (used to connect beam-column). A distance of 15 mm was provided between the axis of the smooth CW dowels and the compressed threaded beech wood dowels. Appendix-B shows the AutoCAD drawings of both designs.

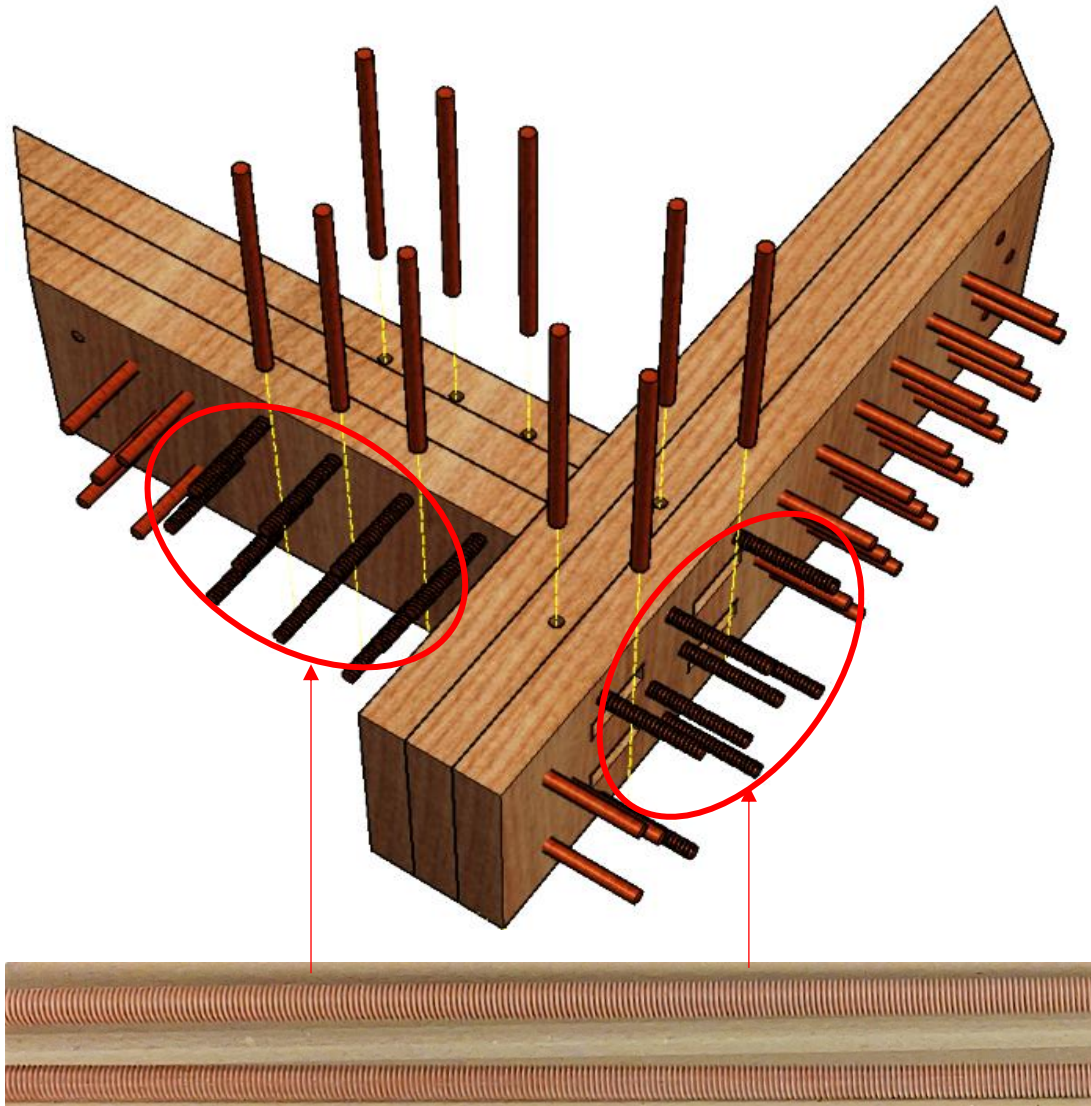


Figure 5.39- Compressed threaded beech wood dowels in the connection area (outer two laminates were removed to show the position of threaded dowels)

Figure 5.40 shows an assembled connection. The assembled connections were conditioned at $20 \pm 2^\circ\text{C}$ temperature and $65 \pm 5\%$ RH prior to testing for 30 days.

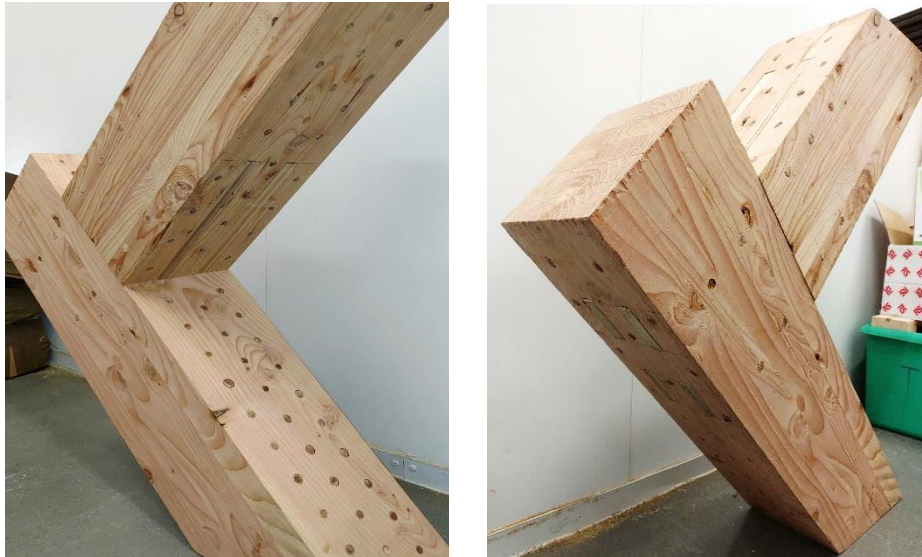


Figure 5.40- Assembled beam-column connections using CWDLT beam-column connections

5.7.2 Test procedure

The test procedure was the same as that used for beam-column connections using glued members (Phase-III) except that the number of LVDTs was increased from four to eight. This improvement was carried out to estimate the rotation of beam and column with respect to CW plates separately. The relative rotation of the CW plates with respect to the column was measured using 4 LVDTs (2 on each side) placed on the column as shown in Figure 5.41. Similarly, 4 LVDTs (2 on each side) were placed on the beam to measure the relative rotation of the beam with respect to the CW plates. The plungers of the LVDTs were carefully aligned with a steel reference plate, which was attached to the CW plates using two 3 mm diameter screws (one on each CW plate on compression zone). The corresponding rotation angle was calculated using Eq. 5.1. The rotation angle of the connection was calculated using Eq. 5.6. The moment on the connection is the product of the load on the beam and perpendicular distance to the bearing point that is approximately 244 mm. The experimental rotational stiffness of the connection was calculated based on 10% and 40% of the maximum moments and the corresponding rotational angles using Eq. 5.4. The ductility ratio was calculated using Eq. 5.5.

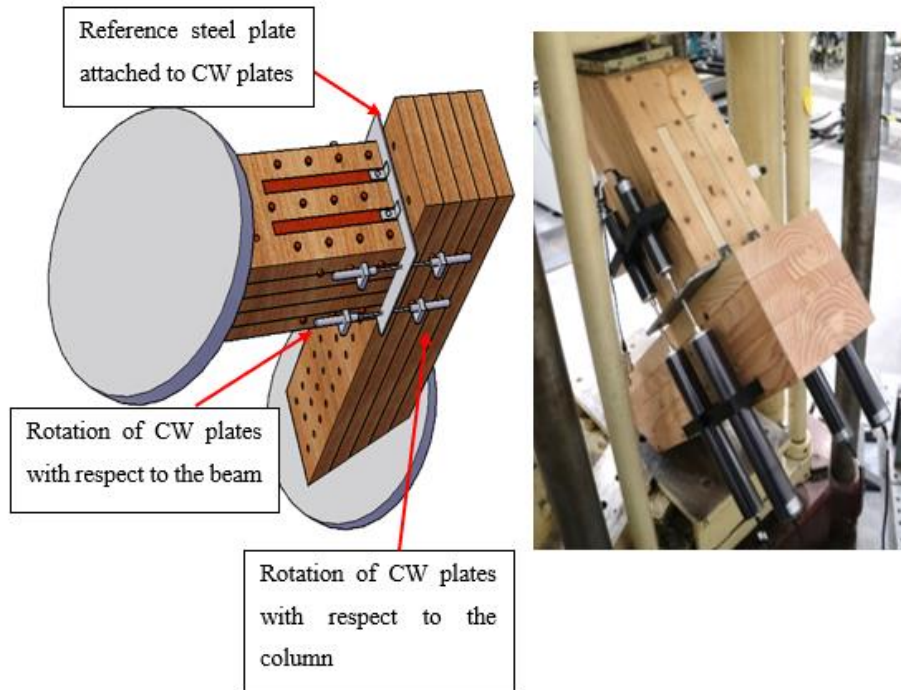


Figure 5.41- Test set up for beam-column connections using CWDLT members

5.7.3 Test results and discussion

This section describes the load-ram displacement, moment-rotation and failure modes of the beam-column connections produced using CWDLT members and CW connectors.

5.7.3.1 Load- ram displacement and moment-rotation behaviour

Figure 5.42 shows a comparison between load-ram displacement behaviour of the Phase IV beam-column connections and a similar connection configuration using glued member (reference). All connections with CWDLT members showed higher ram displacement at failure compared to connections using glued members. This is because CWDLT members offer lower bending stiffness compared to glued members [18,213,214]. The bending stiffness of CWDLT members are approximately 2-3 times lower than the glued members [18,213]. The mean load-carrying capacity of Design-IV-2 was approximately similar to the reference connection Design-III-3, whereas it was only 10% higher than Design-IV-1. The ductility of the Design-IV-1 specimen was found to be lower than the Design-IV-2 specimens. This was primarily due to the early failure of the column without any significant deformation in the connection area.

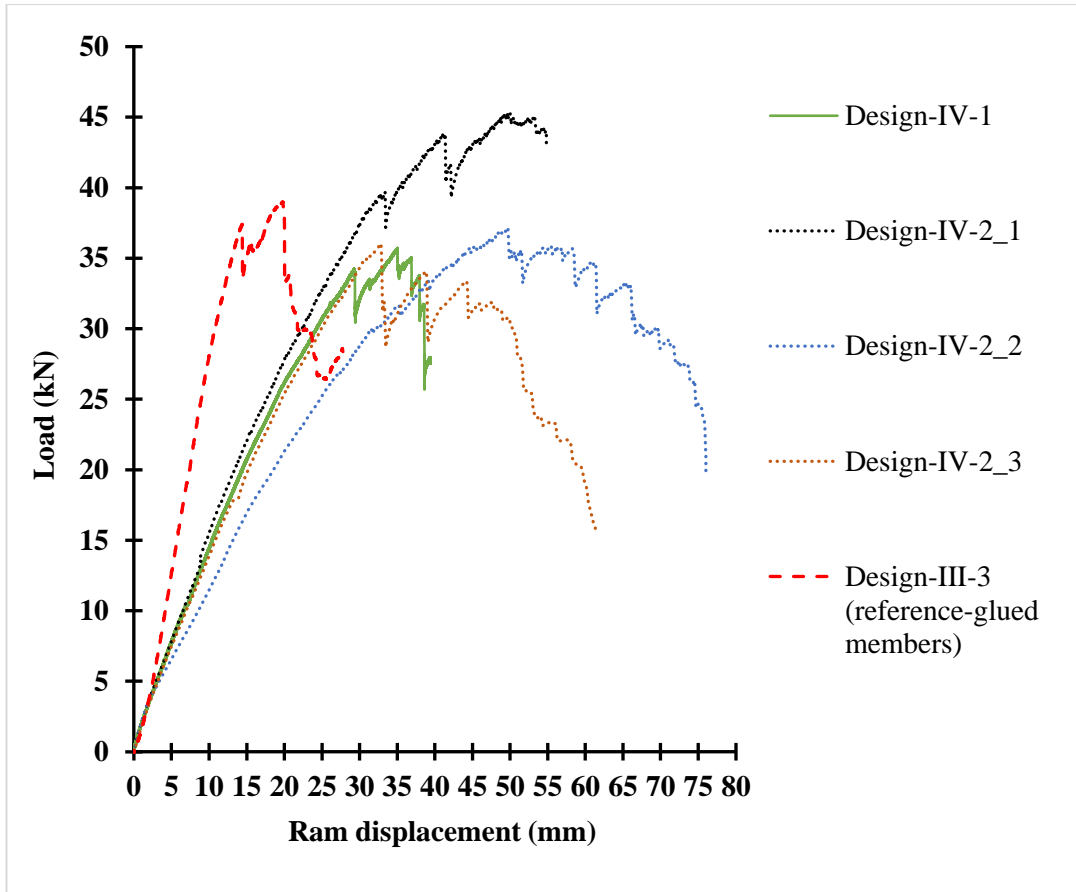


Figure 5.42- Load-ram displacement graph showing a comparison between beam-column connections using CWDLT members and glued members

Figure 5.43 shows a comparison between the moment-rotation behaviour of beam-column connections produced using CWDLT members and similar connection configurations using glued members. The moment-rotation graph confirmed negligible rotation of Design-IV-1 which is just 1.5° at the peak moment. In contrary to this, replications of Design-IV-2 showed a mean rotation of 3.2° which is approximately two times higher than the Design-IV-1 specimen. This was also clearly evident from the failure mechanism of both connection designs (see Section 5.7.3.1).

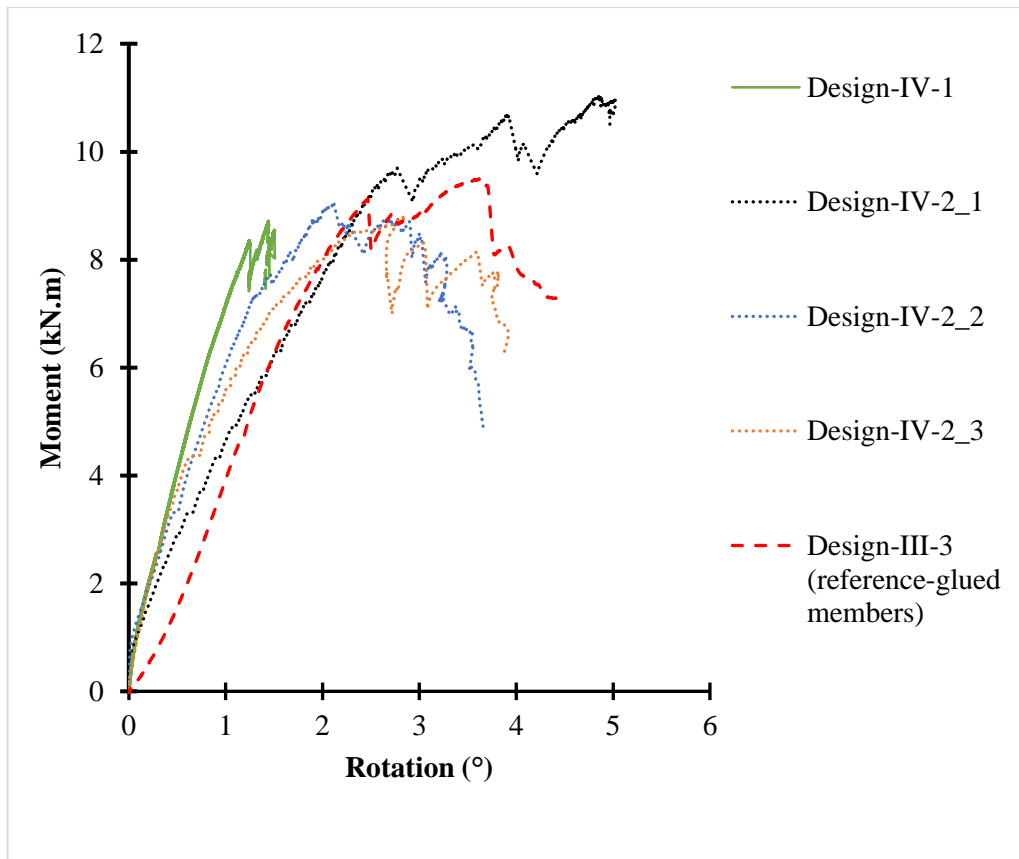


Figure 5.43- Moment-rotation graph showing a comparison between beam-column connections using CWDLT members and glued members

5.7.3.2 Failure modes

When a connection configuration similar to Design-III-3 (with glued members) was manufactured with CWDLT members (Design-IV-1), splitting (brittle failure) was observed in the outermost layer of the column as shown in Figure 5.44. This splitting was observed in the column between two slots of CW plates in the compression zone at a moment of approximately 8.3 kN.m and 1.3° rotation angle. This was initiated from the compressed threaded beech wood dowel, which was located at just 23 mm distance from the inner edges of either side of the slots. In addition to this, inter-laminar slip was observed in the column.

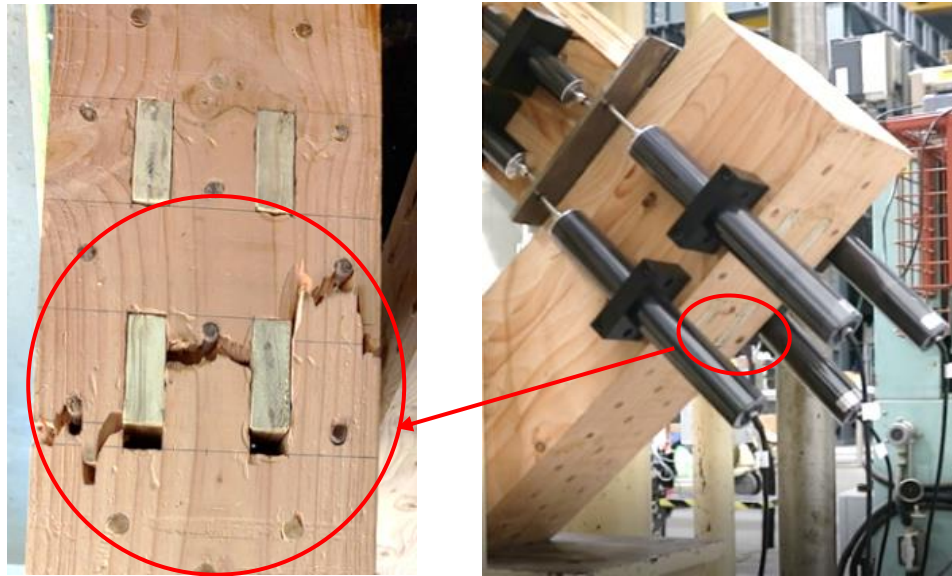


Figure 5.44- Failure mechanism of beam-column connection with 20 mm thick CW plates and CWDLT structural members

To avoid the brittle failure mechanism of the structural members, design changes could be made to optimise the performance of the connection:

- (a) As observed, the rotational stiffness of the connection is higher than the bending stiffness of the structural members. Therefore, it was assumed that the rotational stiffness of the connection can be reduced by decreasing the thickness of CW plates. A lower rotational stiffness may activate deformation in the connection area before any failure in structural members.
- (b) Failure was observed between slots of the compression zone, which is probably due to closer spacing between the slots and compressed threaded beech wood dowels. This can be optimised by increasing the spacing between CW dowels and the slots of the column.
- (c) Increasing the stiffness of the structural members using larger diameter dowels can change the failure to a connection failure. .
- (d) Increasing the cross-sectional area of the structural member so that dowels can be spaced at larger distances will reduce the risk of splitting failure of the member.

From these four possible design changes, (a) and (b) were chosen based on the available dimension of the CW connectors. The final geometry of the connection was manufactured using 15 mm thick CW plates and spacing between the slots and compressed threaded beech wood dowels (see Appendix-B). As mentioned earlier, the cross-sectional area of the structural members could not be increased more than 200 mm, as the maximum available length of laboratory-produced CW dowels was 200 mm. However, option c and d can be investigated in an industrial set up where the length of the CW dowels is not a constraint. Compared to Design-IV-1, a higher rotation was observed in the replications of Design-IV-2 (see Figure

5.45a). Also, none of the replications of Design-IV-2 showed failure in the column (see Figure 5.45b).

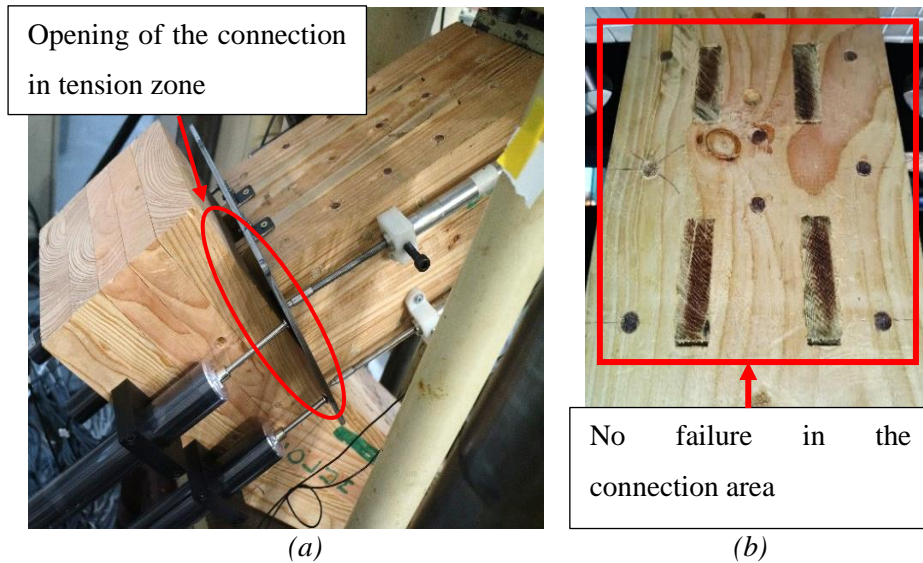


Figure 5.45- Failure mechanism of beam-column connection with 15 mm thick CW plates and larger dowel spacing, (a) opening of the connection in tension zone, (b) no failure in the CWDLT members

5.7.4 Results summary and discussion

Table 5.6 shows a comparison between the beam-column connections using CWDLT members and the reference design using glued structural members (Design-III-3). However, it should be noted that there was only one replication of Design-III-3 and Design-IV-1 each. This may not give a statistical comparison for the whole population. Nevertheless, the mean moment capacity of Design-IV-2 specimens was approximately similar to the reference connection Design-III-3 whereas it was only 10% higher than the Design-IV-1 specimen. The COV between moment capacity values of Design-IV-2 specimens was only 12%. As expected, Design-IV-1 showed the highest rotational stiffness which is approximately 26% higher than the mean rotational stiffness of the Design-IV-2 specimens. The rotational stiffness was least for Design-III-3 which is approximately 38% lower than the Design-IV-1. The COV between the rotational stiffness values of Design-IV-2 specimens was approximately 28%. Such variations in the rotational stiffness values may not be eliminated due to localised deformation around each CW dowels of the connection. Thus, the mean value can be used for design purposes. The mean ductility of the Design-IV-2 specimens was approximately 31% higher than the Design-IV-1, whereas it was approximately 23% higher than the Design-III-3.

Table 5.6- Result summary showing a comparison between beam-column connections using CWDLT members and reference design using glued structural members (Design-III-3)

Design type	Type of structural members	Thickness of CW plates (mm)	Load-carrying capacity (kN)	Moment capacity (kN.m)	Rotational stiffness (kN.m/rad)	Ductility ratio
Design-III-3 (reference)	Glued	20	38.9	9.5	255.9	1.7
Design-IV-1	CWDLT	20	35.7	8.7	413.3	1.6
Design-IV-2_1	CWDLT	15	45.3	11.0	223.4	2.3
Design-IV-2_2		15	37.1	9.1	297.9	2.1
Design-IV-2_3		15	36.1	8.8	395.5	2.0
Mean (Design IV-2)			39.5	9.6	305.6	2.1
Standard deviation (Design-IV-2)			5.0	1.2	86.3	0.2

5.8 Conclusion

Beam-beam and beam-column connections are fundamental connection types in buildings, a range of such connections was developed in this study. The connections were developed in four phases. The first three phases involved the development of semi-rigid type timber moment connections between glued structural members. In the final phase, glued structural members were replaced with CWDLT members. Detailed discussion on the connection configuration, manufacturing process, assembly and structural performance of the developed designs for each phase is presented. The structural performance of the connections was assessed by means of destructive testing. The tests were carried out in accordance with European standards such as EN 408 [181] and EN 26891[183]. The obtained test results are presented in terms of load-carrying capacity, moment capacity, rotational stiffness, and ductility of the connections. A summary of the key findings of the chapter is as follows:

1. Beam-beam connections using full-depth CW/steel plates (Phase-I)

In Phase-I, beam-beam semi-rigid type timber moment connections were developed using glued structural members and CW connectors. Also, timber-steel connections of approximate capacity were developed to allow the comparison with timber-CW connections. Both sets of connections used CW plates extending

over the full-depth of the beam. The geometry of the connected beam-beam specimens and the four-point bending test setup was in accordance with EN 408 [181] with considerations to the principles for determining the strength and deformation characteristics of timber connections specified in EN 26891 [183]. Test results showed that the mean moment capacity of timber-CW was approximately 20% less than that of the timber-steel connections. The mean rotational stiffness of the timber-CW connections was 13% higher than the timber-steel connections. The results of Phase-I demonstrated potential for the use of CW connectors in timber moment connections. However, both connection types showed brittle failure mechanism which is undesirable in the structures and requires further optimisation.

2. Beam-beam connections using narrow-depth CW plates (Phase-II)

In Phase-II, the structural performance of timber-CW beam-beam connections using narrow-depth CW plates and CW dowels. A total of four connection designs were developed. These designs were produced using varying number of CW dowels, thickness of CW plates and arrangement of CW dowels. Similar to Phase-I, the geometry of each specimen and the four-point bending set up was in accordance to EN 408[181] and testing procedure was in accordance with EN 26891[183]. The comparison among designs of Phase-II showed that the higher moment capacity can be achieved by increasing the number of CW dowels and thickness of the CW plates in the connection. The ductility was mainly affected by the spacing of the dowels and the thickness of the CW plates. The test results did not show any clear relationship between the rotational stiffness and connection parameters such as the number of CW dowels and the thickness of CW plates.

3. Beam-column connection using glued members (Phase-III)

In Phase-III, seven different designs of beam-column semi-rigid type timber moment connections were developed using glued structural members and CW connectors. The main objective of this testing phase was to select a connection design for the development of beam-column connections using CWDLT members and CW connectors. The developed designs were classified into two categories based on their resemblance with modern and carpentry timber connection typologies. Modern connection designs were connections with slotted-in CW plates and carpentry connection designs were typical mortise and tenon configuration without the need for CW plates. Based on the findings of Phase-II,

20 mm thick CW plates were preferred over 10 mm thick CW plates. In all of the modern connections, only 20 mm thick CW plates were used to obtain superior mechanical performance and ductile failure modes. All connections were tested using a same test set-up in accordance with EN 26891 [183]. Results have shown that the mean yield load of the modern connection designs was approximately 33% higher than that of the carpentry connection designs, which is probably due to the relatively higher number of CW dowels and significantly higher embedment strength of the CW plates. The mean moment capacity of the modern connection designs was 22% higher than the carpentry connection designs. When comparing the mean rotational stiffness values, the carpentry connection designs showed a 26% increase when compared to the modern connection designs. The mean ductility ratio of carpentry connection designs was 45% higher than the modern connection designs.

Among all specimens irrespective of modern or carpentry connection designs, Design-III-1 showed relatively higher load carrying capacity and moment capacity, but the rotational stiffness was least. For this reason, the remaining designs were considered to select one connection design for beam-column connections using CWDLT members. Design-III-6 and Design-III-7 showed promising results in terms of both strength and stiffness properties. However, these designs were not selected because they were not suitable for CWDLT members. As the strength and stiffness properties of Design-III-3 (modern) was relatively closer to Design-III-6 and Design-III-7, it was selected for development of beam-column connections using CWDLT structural members.

4. Beam-column connections using CWDLT members (Phase-IV)

In this phase, beam-column connections were developed using CWDLT members and CW connectors. Design-III-3 was chosen based on the structural performance and ease of manufacturing. There were two designs developed, which were indicated as Design-IV-1 and Design-IV-2. Design Design-IV-1 was similar to Design-III-3 (Phase-III) with 20 mm thick CW plates. The only difference was that the glued structural members were replaced with CWDLT members. Also, the test protocol was in accordance with EN 26891 [183] with the only difference being the number of LVDTs. A total of four extra LVDTs were used in this phase to precisely measure the rotation of the CW plates with respect to the beam/column on either side (right and left) of the connection. There was the only one specimen of Design-IV-1 tested. This was because of the brittle failure of the column without any significant deformation (rotation) in the connection area. The

literature review showed that the bending stiffness of CWDLT members are 2-3 times lower than similar connections between the glued members. This was evident from the comparison between load-ram displacement graph of the Design-IV-1 and Design-III-3. This needed further optimisation to produce a structurally viable design with equivalent strength and stiffness properties to connections with glued members. Therefore, a new design (Design-IV-2) was produced using 15 mm thick CW plates and larger dowel spacing to prevent/delay the failure of structural members. This design produced favourable results with similar load-carrying capacity, moment capacity and rotational stiffness as the connection design with glued members. Therefore totally 3 replications were tested to check their repeatability. The moment capacity of all three specimens was relatively close with a COV of 12%. However, the variation was relatively higher (COV= 28%) in the case of rotational stiffness values. This needs a larger sample size to perform a precise statistical analysis. However, such variation is mainly dependent on localised deformation of timber and dowels which are inevitable given the anisotropic behaviour of timber and, to some extent, the CW connectors. The mean load-carrying capacity of Design-IV-2 was approximately similar to the reference connection Design-III-3, whereas it was only 10% higher than the Design-IV-1 connection. Similarly, the mean moment capacity of Design-IV-2 specimens was approximately equal to the reference connection (Design-III-3) whereas it was only 10% higher than Design-IV-1. Design-IV-1 showed the highest rotational stiffness which is approximately 26% higher than the mean rotational stiffness of the Design-IV-2 specimens. The rotational stiffness was least for Design-III-3 which is approximately 38% lower than Design-IV-1. Based on the above conclusion, it can be said that the CW connectors could be a possible replacement to metallic connectors and synthetic adhesives both in the manufacturing of layered structural members and timber-timber connections.

Overall, a range of timber-CW semi-rigid type connection designs was proposed for beam-beam and beam-column connections in this study. Designers can choose a particular connection type based on the end uses, strength and stiffness requirement. For example, to obtain higher moment capacities, beam-beam connections systems with narrow-depth CW plates can be preferred over connections with full-depth CW plates. The moment capacity of the connections can be improved by increasing the number of CW dowels and thickness of CW plates whereas high ductility can be achieved by using increased dowel spacing and thicker CW plates. For beam-column connections with glulam and solid timber, carpentry

connections can be used for to obtain higher ductility and rotational stiffness. In some cases, where beam-column has interlocked arrangement, they can be also used in an application where high moment capacity is desired. However, the carpentry connection designs may not be a suitable option when using with CWDLT members. In such cases, connection design with shouldered column and CW plates can be used as they offer similar moment capacity and rotational stiffness compared to carpentry mortise and tenon connections.

Chapter 6 Experimental investigation of laterally loaded laminated timber portal frames with CW connections

6.1 Introduction

Test results of Chapter 5 have shown that CW connectors could be utilised in timber-timber moment connections between glued and CWDLT timber members. However, these findings were based on testing small-scale beam-beam and beam-column connections. Therefore, it is desirable to check the suitability of these CW connectors in large-scale structures such as portal frames. The literature review showed only a few studies on applications of CW connectors in frame structures [62,78]. These studies were carried out using glued structural members and CW connectors with a limited number of replications. Thus, to logically extend the findings of small-scale testing and previous studies, an experimental program was designed in the current study to evaluate the structural performance of CW connectors in portal frames.

This chapter details the manufacturing, assembly and structural performance of the developed portal frames. Two types of frames were investigated. Type-1 frames included glued beam and column elements connected using CW connectors. Type-2 frames were manufactured from CWDLT beam and column elements connected using CW connectors. All frames were tested in a similar fashion using a lateral loading (racking) test set up. The loading protocol was in accordance with EN 26891 [183]. The obtained test results are presented in terms of system (frame) characteristics and localised connection (between beam-column) behaviour. The system characteristics include load-carrying capacity, load-frame rotation, system ductility ratio and failure mechanism. The localised connection behaviour is characterised in terms of moment capacity, rotational stiffness and connection ductility ratio.

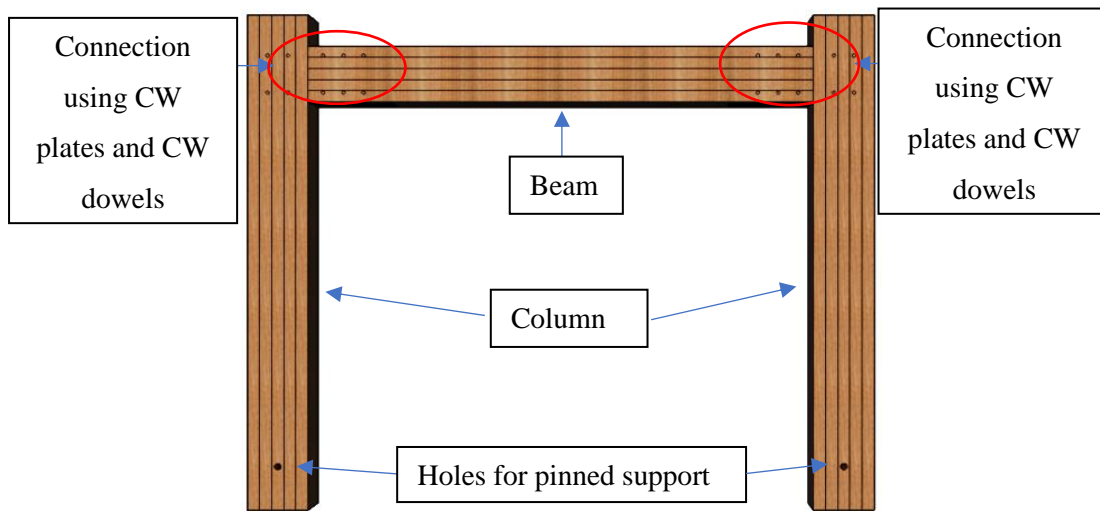
6.2 Material and manufacturing of frames

Three types of materials were used to manufacture both frame types: (1) CW in the form of dowels and plates, (2) compressed laminated wood dowels, and (3) softwood in the form of structural members. The detailed manufacturing processes of both CW plates and CW dowels are given in Section 3.3. The CW dowel diameter varies from 10 mm - 10.3 mm and their mean oven-dry density was 1285 kg/m³. In this study, narrow-depth CW plates of Western hemlock were used with dimensions of 510 mm (L) x 63 mm (T) x 21 mm (R). The oven-dry density of the CW plates varied from 1300 kg/m³ – 1470 kg/m³. The compressed laminated wood dowels were only used within Type-2 frames. The purpose of using these dowels instead of smooth CW dowels was to avoid separation of timber lamellae during the test.

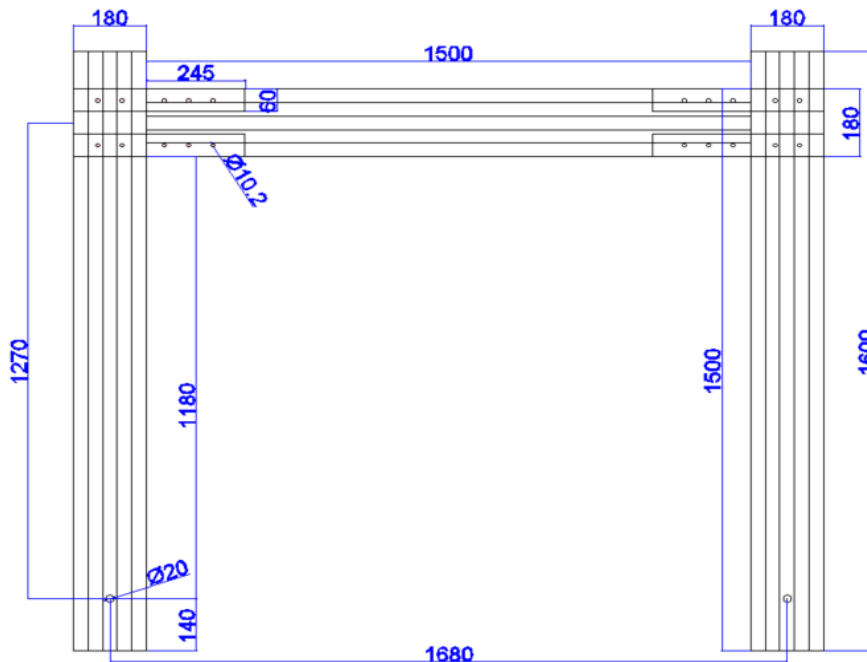
Kiln-dried timber boards of Irish-grown Douglas fir (*Pseudotsuga menziesii*) were used to manufacture the glued and CWDLT members. They were conditioned at a temperature of 65 ± 5 % RH and 20 ± 2 °C temperature for 3 months prior to manufacture. The oven-dry density of the small clear specimens ($n= 40$) of the timber boards varied from 433 -703 kg/m³. Type-1 frames included glulam beams and columns. These beams/columns were produced in accordance with EN 14080 using a one component PU adhesive [208]. Cross-sectional areas of the beams and columns were 180 mm (b) x 180 mm (h). Each beam consisted of five laminates of 36 mm thickness. The length (l) of the column was 1600 mm whereas it was 1500 mm for the beams. The additional 100 mm length of the column was due to shouldered columns. The CWDLT members were used for Type-2 frames. To allow comparison with Type-1 frames, all geometric parameters of the beams remained same as glued members with the only difference being, the way timber boards were connected. Adhesives replaced the CW dowels to join the laminates.

A total of four frames were developed and tested including 2 replications of each frame type. For documentation purposes, the following naming convention was adopted to indicate the frame type. GFR1 and GFR2 indicate Type-1 frames with glued structural members and DFR1 and DFR2 indicate Type-2 frame with CWDLT members. Each frame consisted of three members; two columns and one beam as shown in Figure 6.1a. Each frame was of 1600 mm height and 1860 mm width (measured from the outer edge of the column) as shown in Figure 6.1b. AutoCAD drawings of both frame types are given in Appendix-C.

The column base was designed to act as a pinned support. A 20 mm diameter hole was drilled on each column end (bottom) to accommodate 20 mm diameter steel dowels, which transferred the frame loading to the testing platform. The end distances of these holes were 140 mm ($7d$) from the bottom end of the column. On each CWDLT column, a total of eight threaded beechwood dowels were inserted in a staggered pattern (similar to the smooth CW dowels) at the bottom. These dowels were inserted to reinforce the column ends and were positioned up to 150 mm distance from the bottom end of the column.



(a)



(b)

Figure 6.1- Frame geometry (a) 3D conceptualisation, (b) dimensions (in mm)

In both frame types, the structural members were connected using CW dowels and CW plates. To allow comparison between the structural performance of both frame types, the connection design remained constant. It was based on the test results from small-scale structural testing (Section 5.7). The optimised design-IV-2 using 15 mm thick CW plates and 10 CW dowels, was chosen. Each connection comprised four CW plates (two plates in the compression zone and two in the tension zone). Four slots of 15.5 mm (width) X 60 mm (length) X 180 mm (depth) were routed in the columns to accommodate the CW plates. Figure 6.2a and Figure 6.2b show the connection configuration used in each frame type. AutoCAD drawings of both

connection types are given in Appendix-C. To connect the beam and column, one end of each CW plate was connected to the column and the other end to the beam.

Finally, the assembled frames were conditioned for a month at a temperature of $20 \pm 2^\circ\text{C}$ temperature and $65 \pm 5\%$ RH prior to testing. Conditioning enables expansion of the CW connectors and ensures a tight fit between the laminates and within the connection area.

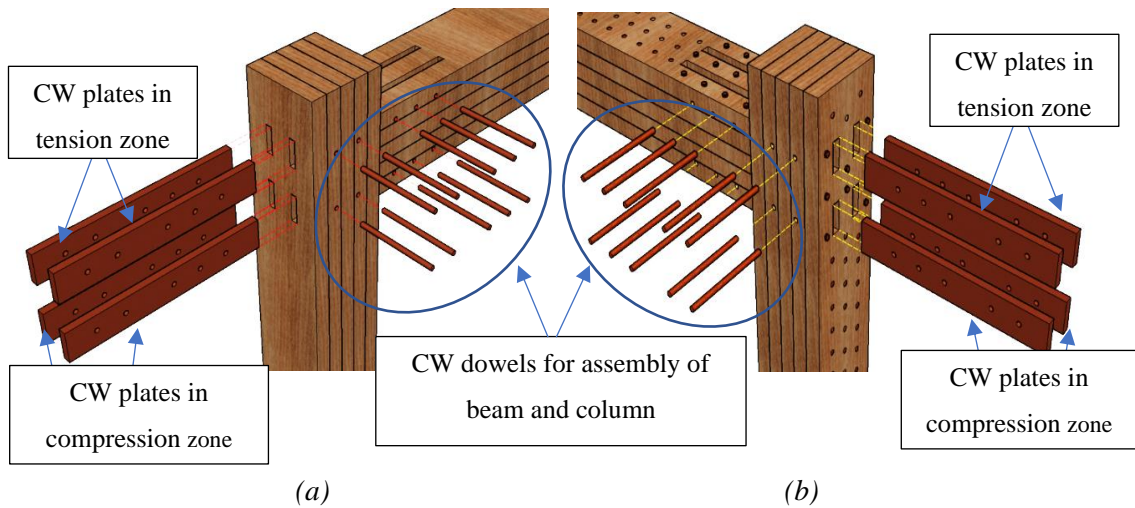
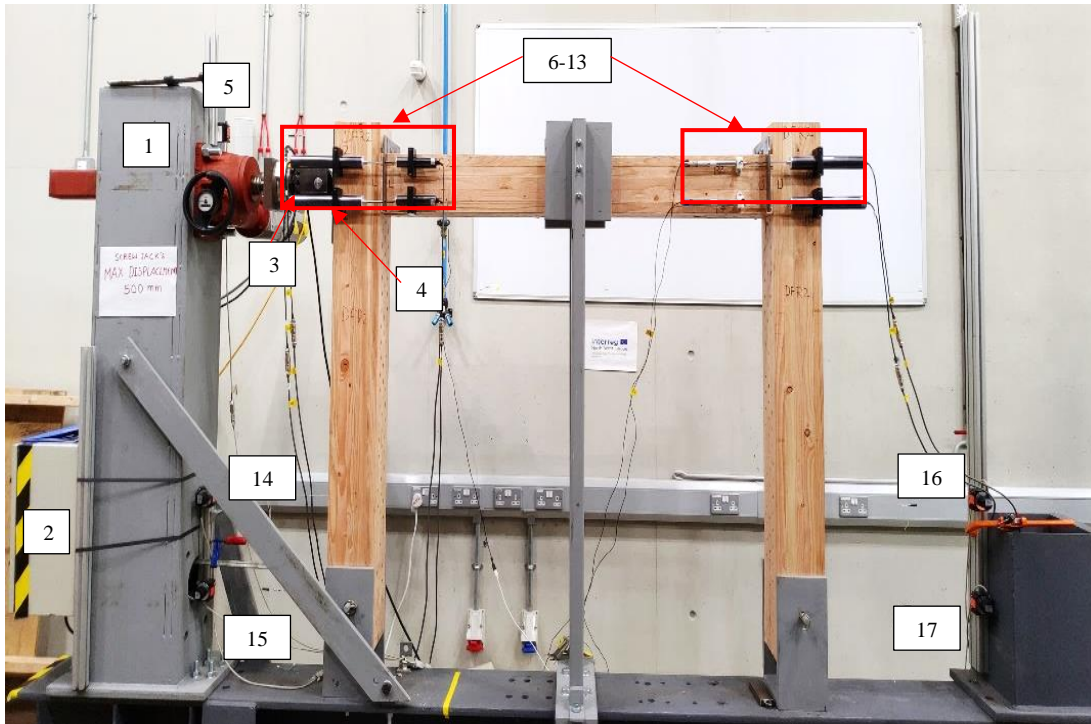


Figure 6.2- Configuration of the connections for frames (a) with glued members (b) CWDLT members

6.3 Test-procedure

Figure 6.3a shows the testing apparatus used in all tests. All relevant components of the loading and data acquisition system are tabulated in Table 6.1. The portal frames were erected on a steel platform using 20 mm diameter pinned supports (steel dowels). Each frame was loaded horizontally using a 500 mm Maschinenfabrik Albert Screwjack [215]. One end of the screwjack was mounted on a box shape steel column and the other end was connected to a load cell. The load cell was further connected to a specifically designed loading head roller to ensure continuous contact as the frame rotates (see Figure 6.3b). A slotted steel plate was fixed to the loaded side of the column in the connection area to avoid any local indentation of the timber (see Figure 6.3c). The slots were positioned so as to avoid contact with the exposed ends of the CW plates. The load was transferred from the screwjack to the frame via the roller and slotted steel plate. The out-of-plane stability of the frames was ensured via steel supports connected to the steel platform.



(a)



(b)



(c)

Figure 6.3- Frame test set up, (a) testing rig, (b) slotted steel plate mounted on loaded side, and (c) rolling load head

Table 6.1- Instruments used in frame testing

Instrument ID	Instrument name	Function
1	Screwjack	For the application of lateral displacement
2	Screw controller	Operation of screwjack
3	Rolling load head	To apply continuous load on the frame
4	Slotted steel plate	To prevent indentation on the surface of the column on the loading side
5	String potentiometer	For measurement of lateral displacement
6-13	LVDTs	For measurement of rotation angle within the connection area between CW plates-column or CW plates-beam
14-17	String potentiometers	For measurement of base rotation of the frame

A string potentiometer was attached to the steel column to continuously record the lateral displacement (translation) of the frame during the test. To measure the rotation of the connections, eight LVDTs (four on each connection) were used. Each connection comprises two separate connections (1) column-CW plates (2) beam-CW plates, which are linked together in the series. The relative rotation of the CW plates with respect to the column was measured using two LVDTs placed on the column as shown in Figure 6.3. Similarly, two LVDTs were placed on the beam to measure the relative rotation of the beam with respect to the CW plates. Each pair of LVDTs was spaced at 120 mm (equivalent to the centre - centre distance of the CW plates in both the tension and compression zones) as shown in Figure 6.4a. The plungers of the LVDTs were carefully aligned with a steel reference plate, which was attached to the CW plates using 5 mm diameter screws. Base rotation of the frame was measured using four string potentiometers. Two potentiometers (one pair) were attached to each column. For each pair, potentiometers were attached in such a way that the first potentiometer was level with steel dowel or pinned support and the second potentiometer was located 300 mm above the first potentiometer (see Figure 6.4b).



Figure 6.4- Instrumentation, (a) arrangement of LVDTs, and (b) arrangement of potentiometers

Static loading tests were carried out in accordance with EN 26891 [183] at a constant displacement rate of 4.5 mm/min. Lateral displacement was applied until failure occurred or to the point when the load dropped to 80% of maximum load. The lateral load-carrying capacity of the frame was the maximum load recorded by the load cell. Figure 6.5 shows a sample load-displacement graph used for the analysis of experimental data. F_{max} indicates maximum load and V_{max} is the corresponding lateral displacement, F_y is the yield load and V_y is the corresponding lateral displacement, and F_u is ultimate load and V_u is the corresponding lateral displacement. V_u was taken at a load level of $0.8F_{max}$ after the F_{max} , while V_y was calculated based on the 1/6 method as per EN 12512 [187]. The system stiffness (frame stiffness) was calculated using the following expression:

$$k_{sys} = \frac{F_{40} - F_{10}}{V_{40} - V_{10}} \quad Eq. 6.1$$

where

k_{sys} is the system stiffness in kN/m,

F_{10} is the 10% value of the F_{max} ,

F_{40} is the 40% value of the F_{max} ,

V_{10} is the displacement corresponding to the F_{10} ,

V_{40} is the displacement corresponding to the F_{40} .

The ductility ratio (D) of the system (frame) was calculated using the following expression:

$$D = \frac{V_u}{V_y} \quad Eq. 6.2$$

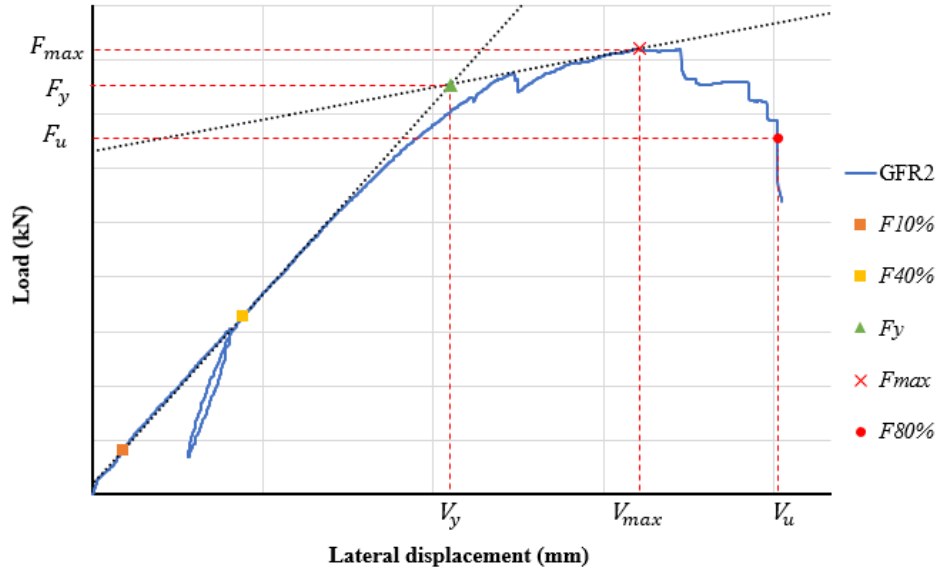


Figure 6.5- Determination of F_{max} , F_y and F_u in accordance with EN 12512 [187]

The base rotation of the frame was calculated using the following expression:

$$\theta = \tan^{-1} \frac{\Delta_1 - \Delta_2}{s} \quad \text{Eq. 6.3}$$

where

Δ_1 (mm) and Δ_2 (mm) are the displacements of the potentiometer pair,

s (mm) is the distance between the potentiometer pair (300 mm).

The rotation within the connection area between the CW plates and beam or column was also calculated Eq. 6.3. In this case, the distance between the LVDT pair was 120 mm.

The experimental rotational stiffness of the localised connection was calculated from 10% and 40% of the maximum moment and the corresponding rotational angle using the following expression:

$$k_{exp,B} = k_{exp,C} = \frac{M_{40} - M_{10}}{\theta_{40} - \theta_{10}} \quad \text{Eq. 6.4}$$

where

M_{10} is the 10% value of the M_{exp} ,

M_{40} is the 40% value of the M_{exp} ,

θ_{10} is the rotational angle corresponding to the M_{10} ,

θ_{40} is the rotational angle corresponding to the M_{40} .

The ductility ratio (D_{con}) of connection was calculated using the following expression:

$$D_{con} = \frac{\theta_u}{\theta_y} \quad \text{Eq. 6.5}$$

where θ_u was taken at $0.8M_{max}$ post maximum moment (M_{max}) attained, while θ_y was calculated based on the 1/6 method as per EN 12512 [187].

6.4 Test results and discussion

This section details the structural characteristics and failure mechanism of both frame types. The structural performance of each frame is evaluated based on the load-lateral displacement and load-frame base rotation behaviour. The moment-rotation behaviour of the localised connections is also discussed. Additionally, the failure mechanism was discussed in terms of localised failure modes in the connection area.

6.4.1 Load-lateral displacement

Figure 6.6 shows a comparison of the load-lateral displacement behaviour of frames with glued and CWDLT members. Solid lines indicate frames with glued members and dashed lines indicate frames with CWDLT. The mean load-carrying capacity of the CWDLT frames was only 4.4% lower than that of the glued frames. The CWDLT frames showed higher lateral displacement compared to glued frames per unit load applied. The mean system stiffness (k_{sys}) of frames with glued members was approximately 53% higher than the frame with CWDLT members. The mean lateral displacement (displacement at maximum load) of CWDLT frames was approximately 19% higher than that of the glued frames. This is attributed to the lower bending stiffness of the CWDLT members [18,20]. The system ductility of frames with glued members was 33% higher than the frames with CWDLT members. Table 6.2 summarises the system characteristics of tested frames.

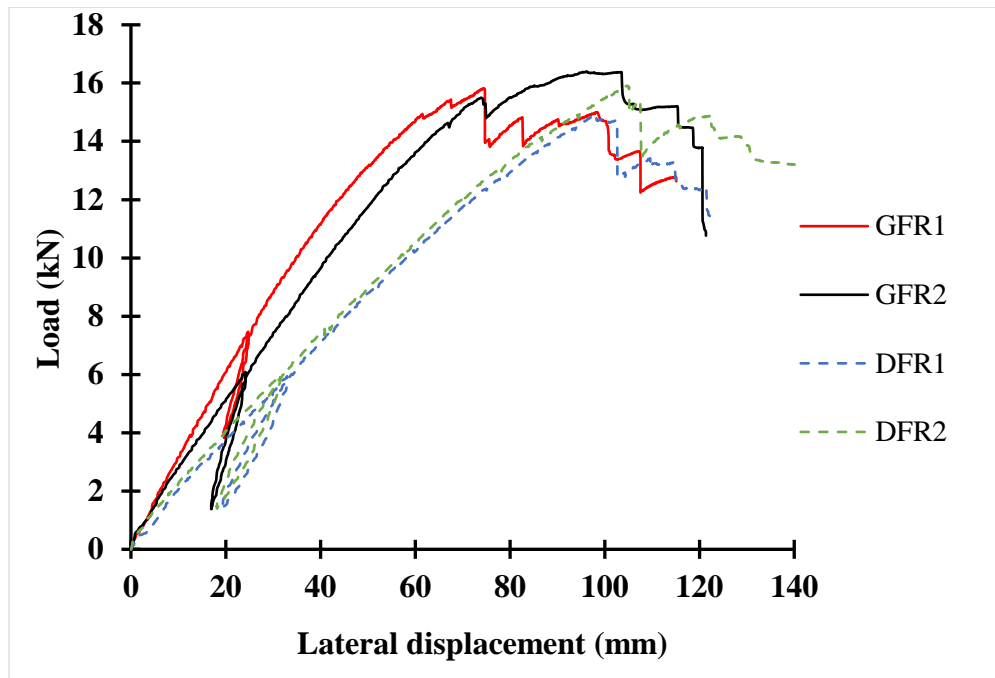


Figure 6.6- Load-lateral displacement graph

Table 6.2- System characteristic of tested frames

Specimen ID	System (frame) characteristics		
	Load-carrying capacity (kN)	System stiffness (kN/m)	System ductility ratio
GFR1	15.8	292.7	2.3
GFR2	16.3	233.4	1.9
Mean	16.1	263.1	2.1
Standard deviation	0.3	41.9	0.3
DFR1	14.9	169.6	1.4
DFR2	15.9	173.4	1.7
Mean	15.4	171.5	1.6
Standard deviation	0.5	2.7	0.2

6.4.2 Load-frame base rotation

Figure 6.7 compares the load-base rotation behaviour of CWDLT frames with glued frames. All CWDLT frames showed higher rotation compared to the glued frame per unit load applied. The mean base rotation (at maximum load) of CWDLT frames was about 22% higher than that of the glued frames. Figure 6.8 shows typical deformation of both frame types.

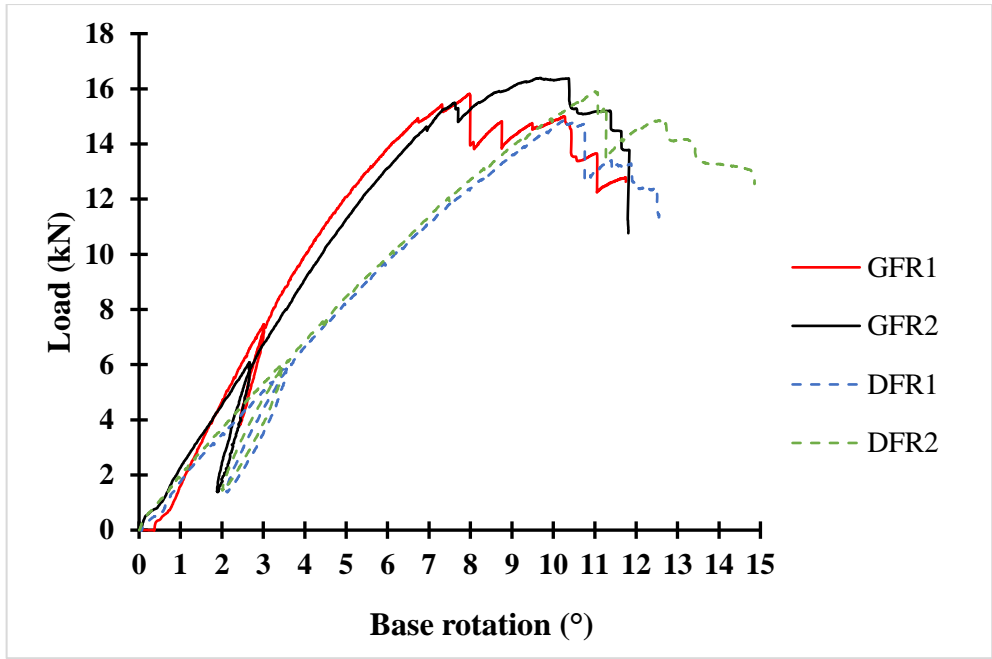


Figure 6.7- Load-base rotation behaviour of glued and CWDLT structural members

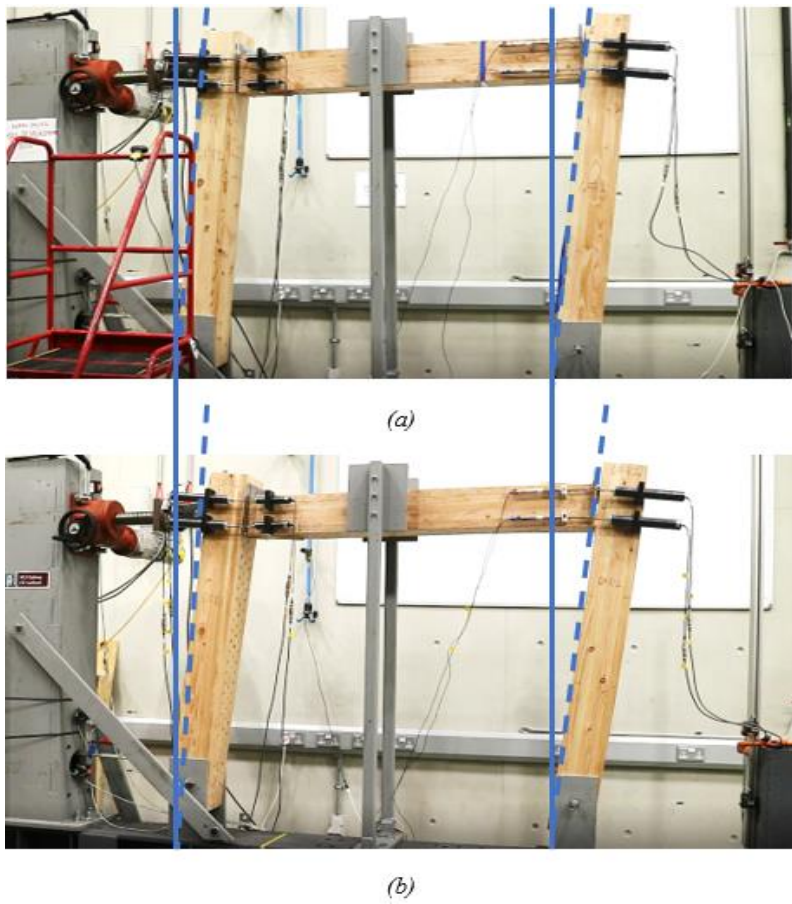


Figure 6.8- Typical deformation of frames, (a) glued frame, and (b) CWDLT frame

6.4.3 Moment- rotation behaviour

Figure 6.9 compares the moment-rotation behaviour of localised connections of the loaded side within both frame types (glued and CWDLT). For clarity purposes, preload cycles were removed from the graph. As both frames were fabricated using common connection design, no difference in the moment capacity was expected. The moment capacity of the connection within the CWDLT frames was only 4% less than that of the glued frames. This is relatively insignificant and could be due to the natural variability in the connection components. The mean rotational stiffness of the connections in frames with CWDLT members was 22% lower than the glued frames. When comparing the variation in rotational stiffness values for each frame type separately, frames with glued members showed a COV of 27%, whereas this was 30.5% for the frames with CWDLT structural members. Although the connection configuration in both frame types was similar, rotational stiffness values were relatively different particularly in the case of frames with CWDLT members. These larger variations could be due to sensitivity of rotational stiffness to a range of connection parameters such as bending stiffness of structural members, friction between connectors and surrounding timber, localised material properties of timber around dowel hole, the surface roughness of connectors [216]. The mean ductility ratio of connections within glued frames was 26% higher than the connections within CWDLT frames. Table 6.3 summarises the connection characteristics of tested frames.

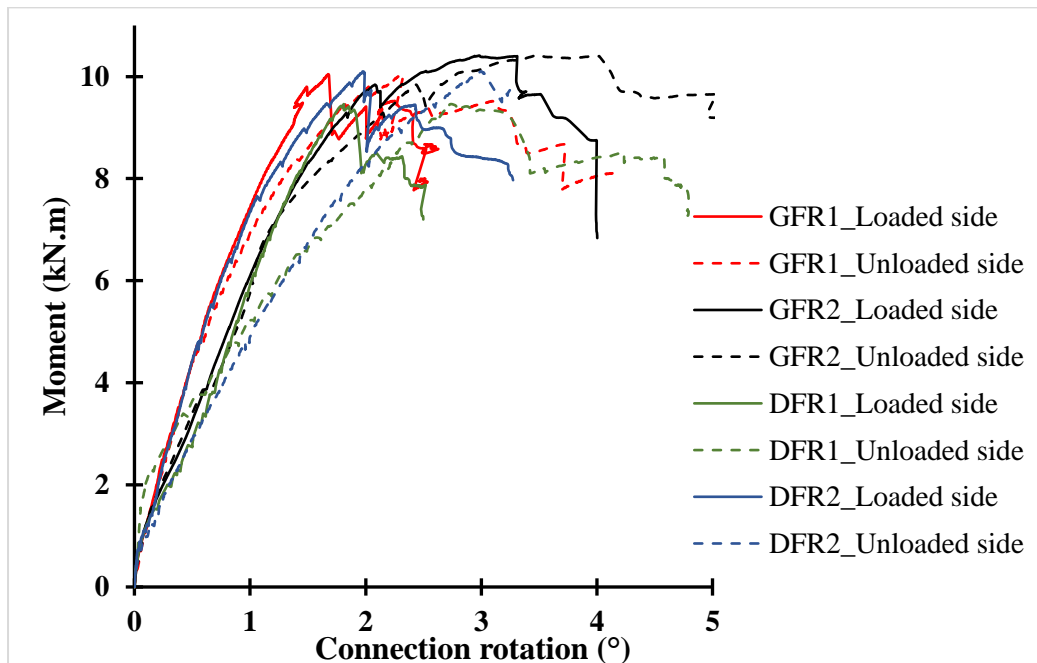


Figure 6.9- Moment rotation behaviour of localised connections of loaded and unloaded sides within both frame types

Table 6.3- Characteristics of localised connections

Connection characteristics			
Connection Label	Moment capacity (kN.m)	Rotational stiffness (kN.m/rad)	Ductility ratio
GFR1_Loaded side	10.0	458.6	2.2
GFR1_Unloaded side	10.0	475.2	3.8
GFR2_Loaded side	10.4	305.1	2.5
GFR2_Unloaded side	10.0	277.3	3.0
Mean	10.2	379.0	2.9
Standard deviation	0.3	102.3	0.7
DFR1_Loaded side	9.5	251.5	1.8
DFR1_Unloaded side	9.5	275.6	2.5
DFR2_Loaded side	10.1	451.4	3.0
DFR2_Unloaded side	10.1	261.9	1.7
Mean	9.8	310.1	2.3
Standard deviation	0.3	94.7	0.6

6.4.4 Failure modes

(a) Frames with glued members (GFR1/2)

Figure 6.10 shows a typical failure mechanism within the connection area of frames with glued structural members. Initially, when the lateral displacement was applied, the frame translated and rotated. The columns rotated around the pinned support as the connection tried to resist the deformation of the frame. The rotation of the CW plates was restricted due to pocket slots in the column. However, the CW plates were exposed and free to rotate in the tension and compression zone of beams. Initial splitting was observed within the CW plates within the

tension zone (connection opening area at the loaded side) (see Figure 6.10a). For GFR1, this was observed at approximately 14.9 kN load at a column base rotation of about 6.8° . This splitting of GFR2 was at approximately 14.6 kN load at 6.9° column base rotation. The splitting was initiated from the CW dowel located within the beam at the farthest distance from the geometric centre of the connection. This did not have a significant effect on the load-carrying capacity. The splitting propagated along the row of CW dowels towards the column edge. As expected, due to the negative bending moment, splitting was observed within the CW plates in the connection opening area on the unloaded side (see Figure 6.10b). This occurred at 15.8 kN load for GFR1, whereas this was 15.4 kN for GFR2. This failure led to approximately 1.8 kN and 0.6 kN drop in the load-carrying capacity of GFR1 and GFR2 frames, respectively.

In case of GFR1, the load recovered slightly (0.8 kN) after this initial failure of CW plates but did not surpass the maximum load (15.8 kN). This recovery was attributed to the deformation of CW dowels. At approximately 7.9° column base rotation, splitting was observed in the remaining CW plates of the loaded and unloaded end. This led to a continuous decrease in the load-carrying capacity of GFR1.

In contrast to GFR1, GFR2 completely recovered the drop in load-carrying capacity and attained a maximum load of 16.3 kN. Splitting in the remaining CW plates was observed at about 10.3° column base rotation. Soon after this, a continuous decrease in the load-carrying capacity was observed. Figure 6.10c and Figure 6.10d show a typical splitting failure of the CW plates in the tension and compression zones at the loaded and unloaded side, respectively. The tests were stopped once the load-carrying capacity dropped to 80% of the maximum load. The frames failed due to deformation in connection components and no failure was observed in the beam and column. The frames demonstrated strong member and weak-connection failure modes.

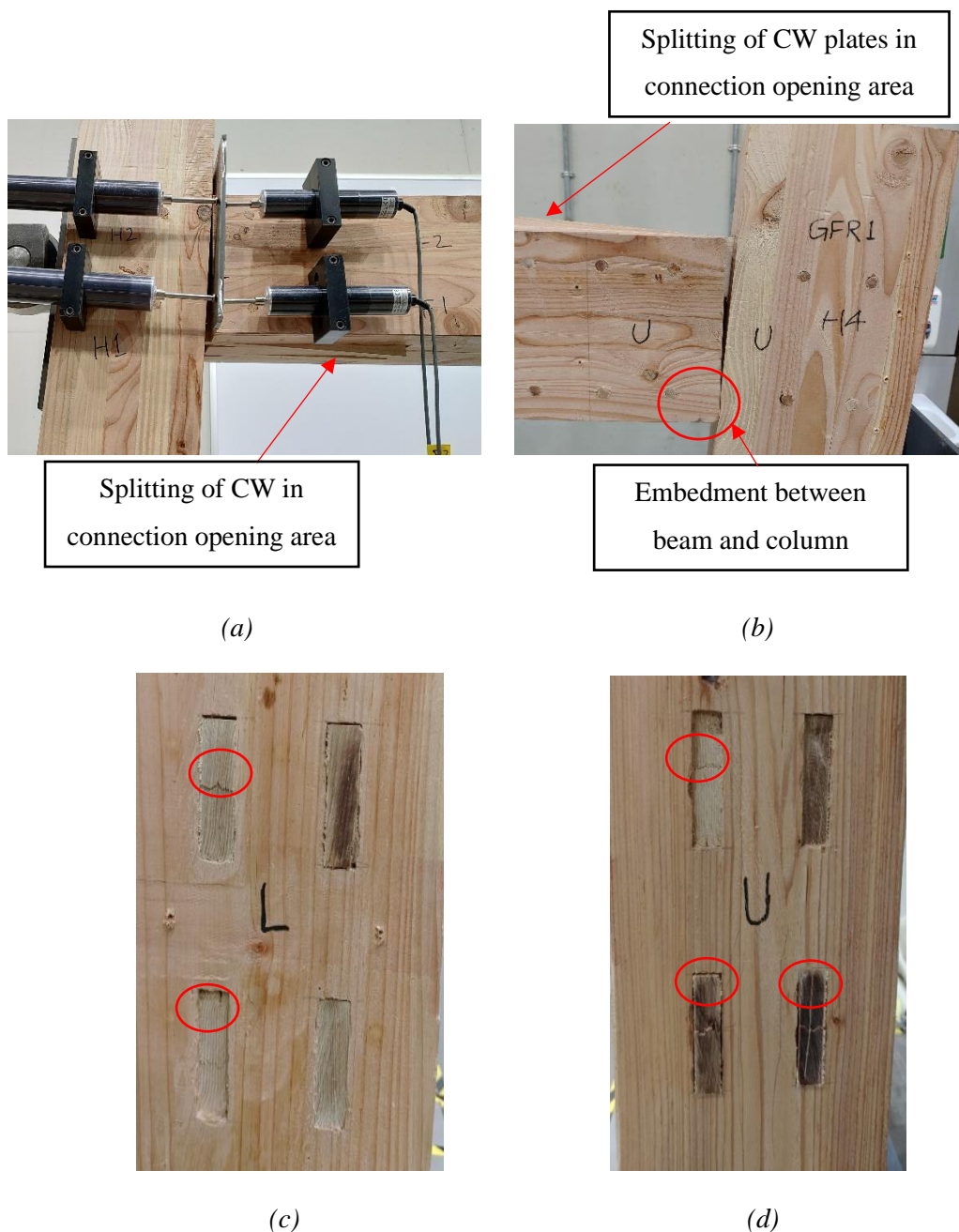


Figure 6.10- Typical failure mechanism in the connection area of the glued frame (a) loaded side, (b) unloaded side, (c) loaded end, (d) unloaded end

(b) Frames with CWDLT members (DFR1/2)

Figure 6.11 shows a typical failure mechanism within the connection area of frames with CWDLT members. When lateral displacement was applied, the frame started rotating. Similar to glued frames, initial splitting was observed within the CW plates of tension zone (connection opening area) at the loaded side (see Figure 6.11a). For DFR1, this was observed at approximately 14.9 kN load at a column base rotation of about 9.8°. This failure for DFR2 was observed at 15.8 kN load at 11.0° column base rotation. When compared with glued

frames, this splitting occurred in a similar load range of between 14.5-16 kN. This was expected as the connection configuration and geometry was the same for both frame types. The initial splitting led to a drop in the load-carrying capacity of approximately 0.2 kN and 0.9 kN for the DFR1 and DFR2 frames, respectively. After this point, DFR1 showed a “sawtooth or ratcheting” path in the load-base rotation graph between 9.8° to 10.8° . This is thought to be caused by the deformation and progressive failure of CW dowels. In the case of DFR2, this path was relatively shorter which can be seen between 11.0° to 11.2° column base rotation. Due to the negative bending moment on the unloaded side, splitting was observed within the CW plates in the connection opening area as shown in Figure 6.11b. This occurred at a load of 14.7 kN for DFR1, whereas this was 15.3 kN for DFR2. This failure led to a drop in the load-carrying capacity of approximately 1.9 kN for both frames. DFR1 and DFR2 recovered approximately 0.6 kN (at 13.4 kN) and 1.4 kN (14.8) load. This was probably embedment failure of CW plates and timber and also deformation of CW dowels. However, the load-carrying capacities of both frames were still lower than the corresponding maximum loads (DFR1 = 14.9 kN and DFR2 = 15.8), which were attained at initial failure. Splitting was observed in the remaining CW plates of DFR1 and DFR2 at approximately 10.9° and 11.2° column base rotation, respectively. This led to a continuous decrease in the load-carrying capacities of both frames. Figure 6.11c and Figure 6.11d show a typical splitting failure of CW plates loaded and unloaded end, respectively. The failure sequence was found to be similar for both glued and CWDLT frames. This was expected because the connection geometry was the same for both frame types. Failure occurred in the connection components and no failure was observed in the structural members. Overall, these frames also showed strong member and weak-connection failure modes.

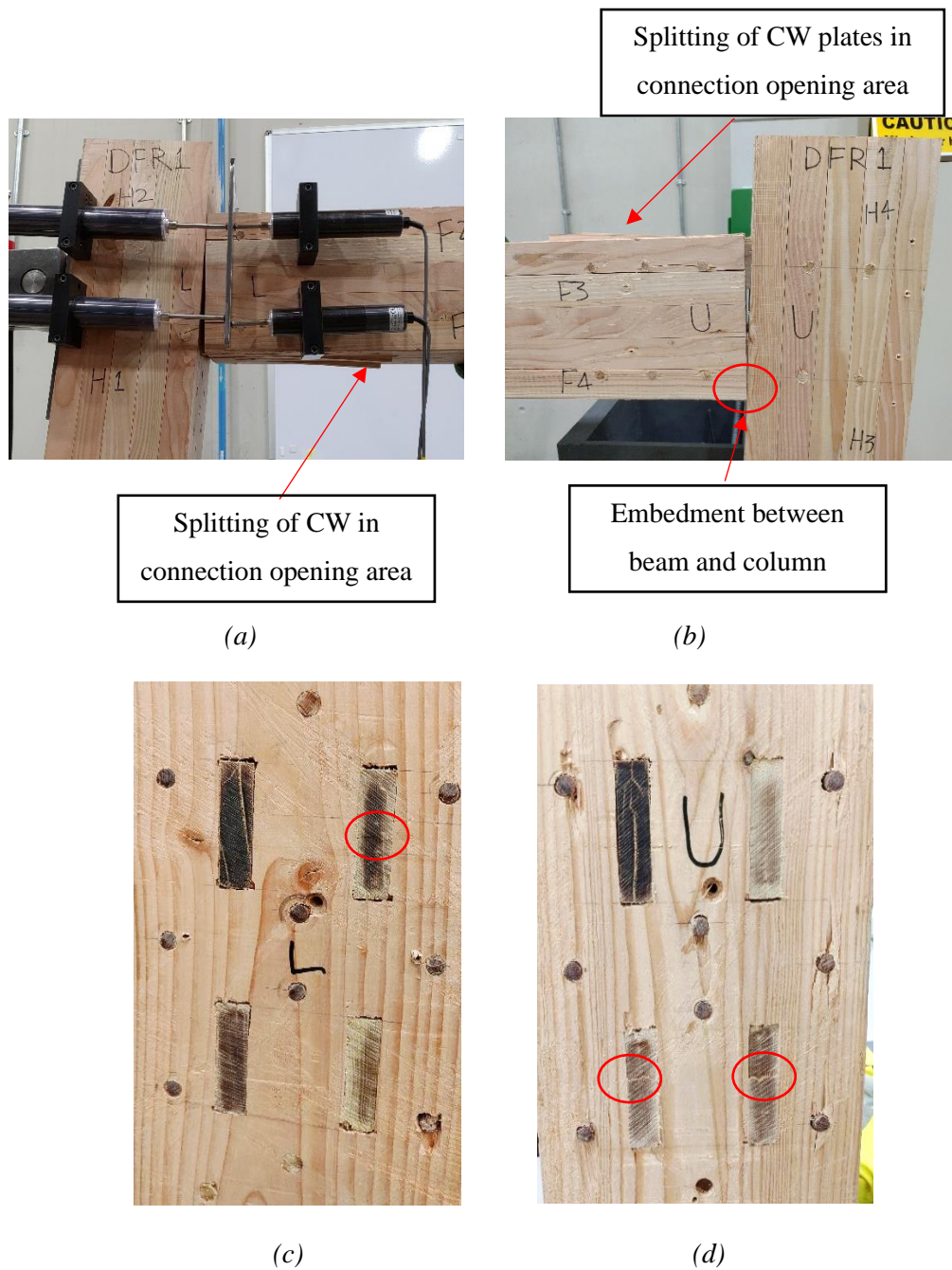


Figure 6.11- Typical failure mechanism in the connection area of frame with CWDLT members (a) loaded side, (b) unloaded side, (c) loaded end, (d) unloaded end

6.5 Summary and conclusions

This chapter discusses the structural applications of CW connectors in one bay portal frames. The chapter describes the manufacturing procedure, the configuration of localised connections between the beam and column, test procedures and results. Type-1 frames were manufactured using glued structural members and the Type-2 frames had CWDLT members. The design of localised connections remained constant for both frame types.

Both frames showed similar failure mechanisms, strong members and weak connection failure modes. Failure was observed in connection components and no failure was observed in the structural members. Test results showed that the mean load-carrying capacity of frames with CWDLT members was only 4.4% lower than that of the glued frames. The mean system stiffness (k_{sys}) of frames with glued members was approximately 53% higher than the frame with CWDLT members. This suggested that it would be beneficial to optimise the design of the CWDLT members in future studies to obtain greater system stiffness. For example, the optimisation process may involve larger diameter CW dowels for lamination, a greater number of dowel rows, varying dowel arrangements (line/staggered) and thickness of assembled timber boards, reducing dowel spacing and varying dowel insertion angles through experimental testing and computational modelling. The system ductility of the frames with glued members was 33% higher than the frames with CWDLT members. The analysis of localised connections showed that the moment capacity of the connections within CWDLT frames was only 4% less than that of the glued frames. This was expected as the connection design was the same for both frame types. The mean rotational stiffness of the connections in CWDLT frames was 22% lower than the glued frames. Variations were observed in the rotational stiffness values when compared between replications of similar frame types. These results are limited by the lower sample size in the current study. The rotational stiffness of connections in the frames with glued structural members showed a COV of 27%, whereas this was 30% for the frames with CWDLT structural members. Such differences in rotation stiffness values may not be completely prevented because it is mainly dependent on the localised connection parameters such as deformation of CW dowels and CW plates within the timber members. Also, rotational stiffness properties are affected by the bending stiffness of structural members [217]. Particularly, in the case of CWDLT members where the CW dowels are used for lamination, larger variations can be expected in the stiffness properties due to assembly tolerances and individual behaviour of the CW dowels within the members. As the research on CWDLT is a relatively new area compared to other engineered wood products, it requires further investigation on optimisation of the manufacturing and assembly process, material properties and structural behaviour of these products. Nevertheless, the developed connection systems can be used with glulam, DLT and CWDLT members in building applications.

Chapter 7 Design calculations for timber-CW connections

7.1 Introduction

The beam-beam and beam-column connections presented in Chapter 5 and Chapter-6 have slotted-in CW plates and CW dowels. In these connections, when the load is applied, the bending moment in the connection is resisted by the deformation of the CW plates, CW dowels and timber. The slots utilise the high cross-grain shear strength of CW dowels, whereas the CW plates reinforce the connection area by the virtue of its high embedment strength and greater bending strength and stiffness. The stress resultants within the connection are transferred between the structural members (beams/columns) by the CW plates and CW dowels. The rotation (θ) of the connection is a result of movement within the connection components due to assembly tolerances, shearing/bending of CW dowels and embedment of CW dowel within the structural members and CW plates. This chapter details the procedures to calculate the characteristic moment capacity and rotational stiffness of the experimentally tested timber-CW connection presented in Chapter-5.

7.2 Connection design moment capacity

EC 5 [55] does not provide guidelines for the design of moment-resisting dowel type connections. In this study, the moment capacity of timber-CW connections was calculated based on the guidelines given by Porteous and Kermani [54] and Blaß and Sandhaas [37]. The characteristic moment capacity of connections can be calculated from the minimum value of characteristic load-carrying capacity ($F_{v,rk}$) that is calculated from the strength equations.

EC 5 provides guidelines for the calculation of the load-carrying capacity of laterally loaded connections fastened using metal dowel type fasteners. The standard provides limits on dowel spacing and edge distances, which when followed ensure that brittle failure mechanisms such as row shear and plug shear do not occur. The considered failure modes are therefore limited to embedment failure of the connected members, yielding of the dowels and combinations thereof. Where steel plates are used no failure of the steel plate is considered.

The characteristic load-carrying capacity of laterally loaded double shear timber-timber connections fastened using metal dowels can be calculated based on the failure modes shown in Figure 7.1 and their corresponding strength equations.

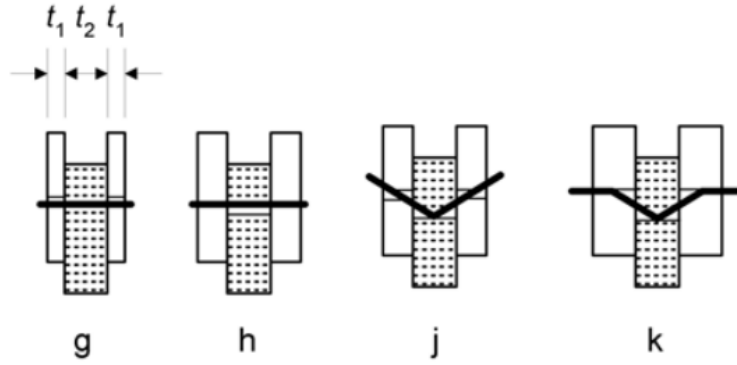


Figure 7.1- Possible failure modes of a double shear timber-timber connection [55]

Mode-g indicates the embedment failure of side members and mode-h indicates the embedment failure of a central member. Mode-j indicates the embedment failure of timber and yielding of dowel with one plastic hinge whereas Mode-k displays embedment failure of timber and dowel with three plastic hinges.

The characteristic load-carrying capacity per shear plane per fastener is the minimum value obtained from the following equations:

$$F_{v,RK} = \min \left\{ \begin{array}{l} f_{h,1,k} t_1 d \quad (g) \\ 0.5 f_{h,2,k} t_2 d \quad (h) \\ 1.05 \frac{f_{h,1,k} t_1 d}{2 + \beta} \left[\sqrt{2\beta(1 + \beta) + \frac{4\beta(2 + \beta) M_{y,Rk}}{f_{h,1,k} d t_1^2}} - \beta \right] + \frac{F_{ax,Rk}}{4} \quad (j) \\ 1.15 \sqrt{\frac{2\beta}{1 + \beta}} \sqrt{2M_{y,Rk} f_{h,1,k} d + \frac{F_{ax,Rk}}{4}} \quad (k) \end{array} \right. \quad Eq. 7.1$$

where

$F_{v,Rk}$ is the characteristic load-carrying capacity of per steel dowel per shear plane,

t_1 is the thickness of the side member,

t_2 is the thickness of the central member,

d is the diameter of the dowel,

$f_{h,1,k}$ is the characteristic embedment strength of the side member,

$f_{h,2,k}$ is the characteristic embedment strength of the central member,

$M_{y,Rk}$ is the characteristic yield moment of the fastener,

$F_{ax,Rk}$ is the characteristic axial withdrawal capacity of the fastener.

and

β is the ratio between the embedment strength of connected members.

Figure 7.2 shows possible failure modes for the laterally loaded double shear timber-steel (slotted-in steel plate) connection. Mode-f indicates the embedment failure of side members. Mode-g indicates the embedment failure of timber and yielding of dowel with one plastic hinge, whereas Mode-h displays the embedment failure of timber and dowel with three plastic hinges.

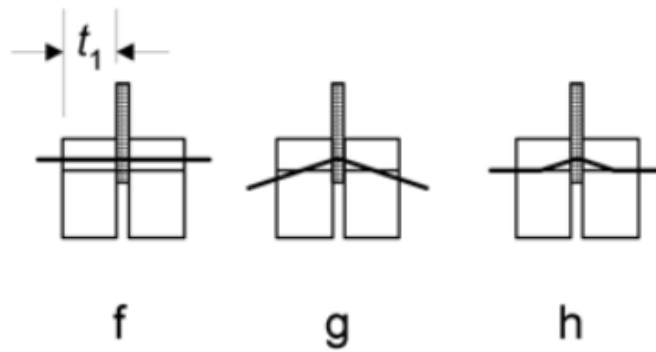


Figure 7.2- Possible failure modes for slotted-in steel plate timber connections [55]

Corresponding equations for each failure modes are as follows:

$$F_{v,Rk} = \min \begin{cases} f_{h,1,k} t_1 d & \text{(f)} \\ f_{h,1,k} \cdot t_1 \cdot d \left[\sqrt{2 + \frac{4M_{y,Rk}}{f_{h,1,k} \cdot t_1^2 \cdot d}} - 1 \right] + \frac{F_{ax,Rk}}{4} & \text{(g)} \\ 2.3 \sqrt{M_{y,Rk} \cdot f_{h,1,k} \cdot d + \frac{F_{ax,Rk}}{4}} & \text{(h)} \end{cases} \quad \text{Eq. 7.2}$$

where parameters are the same as defined for timber-timber connections.

Irrespective of connection types (beam-beam/beam-column), the characteristic moment capacity of the connection (M_{Rk}) can be calculated using Eq. 7.3.

$$M_{Rk} = F_{v,Rk} * r * n_{sp} \quad \text{Eq. 7.3}$$

where

$F_{v,rk}$ is the characteristic load-carrying capacity of the connection and should be determined by adding the contributions of the effective number of fasteners (n_{ef}),

r is the lever arm distance,

and n_{sp} is the number of shear planes.

7.2.1 Material properties used for design calculations

The timber structural members used for structural testing were manufactured using kiln-dried Irish grown Douglas Fir. The mean density of the glulam based on five clear specimens at 12% moisture content was 570 kg/m^3 . The embedment strength of the timber in parallel ($f_{h,1,0}$) and perpendicular ($f_{h,1,90}$) to the grain direction were determined experimentally in accordance with EN 383 [182] and as presented in Chapter-3. The characteristic values of the embedment strength were calculated as per EN 14358 [189]. Table 7.1 summarises the material properties of timber used throughout this chapter.

Table 7.1- Timber properties

Parameters	
Mean density of timber (ρ_m) in kg/m^3	570
Characteristic embedment strength of timber parallel to the grain ($f_{h,1,0,k}$) in MPa	37
Characteristic embedment strength of timber perpendicular to the grain ($f_{h,1,90,k}$) in MPa	22

The CW dowels of Scots Pine were used throughout this study. The nominal dowel diameter was 10 mm. For CW plates, Scots Pine and Western hemlock were used. However, Scots Pine CW plates were only used during initial testing of beam-beam connections developed using full-depth CW plates. For the remaining larger part of the study, only narrow-depth compressed Western hemlock plates were used. The design calculations presented in this chapter only consider the embedment strength properties of CW Western hemlock. The relevant material properties of CW connectors were extracted from Chapter-3. Table 7.2 summarises the material properties of the CW material used in this chapter. Two additional failure modes were identified for CW dowels that do not arise in the case of steel dowels. CW dowels exhibit interlaminar shear failure along the length of the dowel between the interphase of the latewood and earlywood, and cross-grain shear failure, which is not the case for the steel dowels. Therefore, in addition to bending failure of the dowels new design rules for dowel shear failure will need to be developed. This will require testing of a wide range of test diameters and compression ratios to establish appropriate design values. For calculation purposes, the characteristic yield moment capacity of the CW dowels ($M_{y,Rk,CW}$) is calculated based on the experimental results of all 15 specimens (including radial and tangential directions and at an angle of 45°) as presented in Chapter-3. Similarly, characteristic cross-grain shear strength of CW dowels ($f_{sp,k}$) is calculated based on the experimental results of all 10 specimens (including radial and tangential directions) as presented in Chapter-3.

Table 7.2- Material properties of CW material

Parameters	
Mean density of CW plates (ρ_{CW}) in kg/m ³	1300
Characteristic yield moment of CW dowel ($M_{y,Rk, CW}$) in N.mm	3972
Characteristic cross-grain shear strength of the CW dowel ($f_{sp,k}$) in MPa	50
Characteristic embedment strength of CW parallel to the grain ($f_{h,2,0,k}$) in MPa	189
Characteristic embedment strength of CW perpendicular to the grain ($f_{h,2,90,k}$) in MPa	142

To allow the comparison with timber-CW connections, design calculations were also carried out for the timber-steel beam-beam connections presented in the Chapter-5. The grade of steel used in this study for plates and dowels was S275. The ultimate tensile strength of the steel was extracted from the EN 10025 and characteristic yield moment capacity of the dowel was calculated based on the following expression of EC 5 [55] as given in Table 7.3.

$$M_{y,k} = 0.3f_{u,k}d^{2.6} \quad \text{Eq. 7.4}$$

where, $M_{y,k}$ is the characteristic yield moment capacity, $f_{u,k}$ is the characteristic ultimate tensile strength of the dowel (MPa), d is the diameter of the dowel in mm.

Table 7.3- Properties of steel connectors

Parameters		Basis/Standard
Characteristic ultimate tensile strength of the steel dowels ($f_{u,k}$) in MPa	410	EN 10025[194]
Characteristic yield moment capacity ($M_{yRk,steel}$) in N.mm	27412	Table 10.5 of EC 5 [55]

7.2.2 Beam-beam connections with full-depth steel plates

Figure 7.3 shows design configuration of these connections.

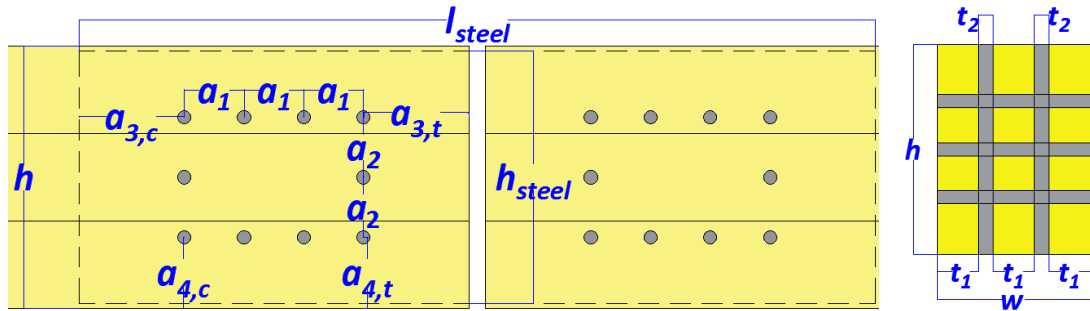


Figure 7.3- Connection configuration of beam-beam connections with full-depth steel plates

Geometric parameters of connection components

Depth of the beam (h) = 157.5 mm

Width of the beam (w) = 115 mm

Length of each beam = 1575 mm

Length of connected specimen = 3160 mm

Span of the connection = 2835 mm

Width of timber side members (t_1) = 31 mm

Thickness of steel plates (t_2) – middle member = 10 mm

Length of steel plates (l_{steel}) = 480 mm

Depth of steel plates (h_{steel}) = 152.5 mm

Connection parameters

Dowel Spacing parallel to grain (a_1) = 36 mm

Dowel Spacing perpendicular to the grain (a_2) = 36 mm

Loaded end distance ($a_{3,t}$) = 63.5 mm

Unloaded end distance ($a_{3,c}$) = 63.5 mm

Loaded edge distance ($a_{4,t}$) = 42.75 mm

Unloaded edge distance ($a_{4,c}$) = 42.75 mm

Dowel diameter (d) = 8 mm

Number of dowels per shear plane (n) = 10

Number of shear planes in connection (n_{sp}) = 4

Load angle on fastener (α) = 56° (see Figure 7.4)

Characteristic moment capacity

Characteristic embedment strength of timber at 56° to the grain from the following expression is 25 MPa.

$$F_{h,\alpha,k} = \frac{f_{h,1,0,k}}{K_{90} \sin^2 \alpha + \cos^2 \alpha} \quad \text{Eq. 7.5}$$

where $K_{90} = f_{h,1,0,k} / f_{h,2,0,k} = 1.7$

The characteristic load-carrying capacity of the connection was calculated using EC 5 strength equations of timber-steel connection design.

The characteristic load-carrying capacity per dowel per shear plane ($F_{v,Rk}$)

$$F_{v,Rk (f)} = 6397 \text{ N}$$

$$F_{v,Rk (g)} = 3801 \text{ N}$$

$$F_{v,Rk (h)} = 5412 \text{ N}$$

The characteristic load-carrying capacity of the connection per shear plane per steel dowel is limited by failure Mode-g with one plastic hinge. Thus,

$$F_{v,Rk} = \min (F_{v,Rk (f)}, F_{v,Rk (g)}, F_{v,Rk (h)}) = 3801 \text{ N}$$

The connection pattern is symmetrical, and all CW dowels are of the same type although at different lever arms to the centroid of the dowel group (see Figure 7.4). Table 7.4 shows the lever arm distances and distribution of the dowel in terms of x and y coordinates.

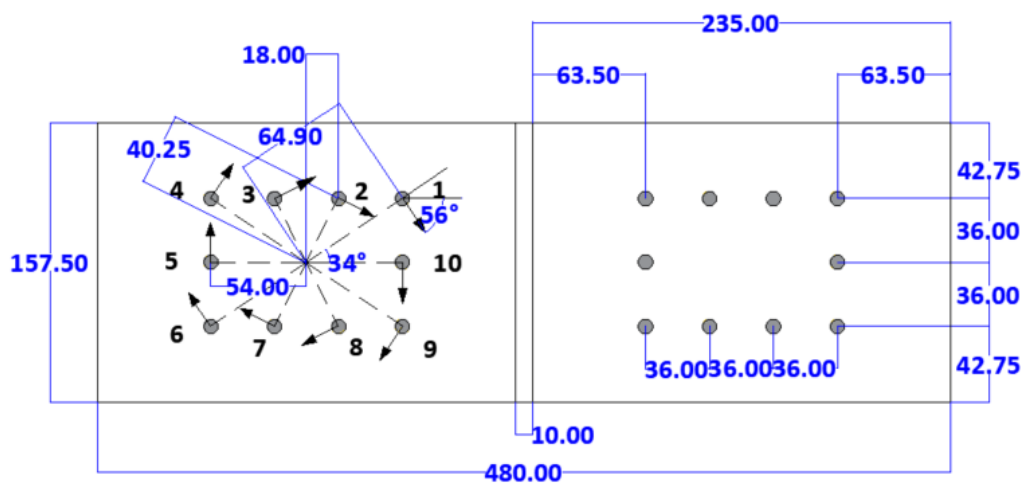


Figure 7.4- The rotation of steel dowels (all dimensions are in mm)

Table 7.4- Dowel distribution and lever arm distances (beam-beam connections with full-depth steel plates)

CW dowel label	Total Number CW dowels	$x^2 + y^2$ (mm)	Sum ($x^2 + y^2$) (mm)	Lever arm (r) (mm)
1,4,6,9	4	4212	16848	64.9
2,3,7,8	4	1620	6480	40.3
5,10	2	2916	5832	54.0
			Σ 29160	Maximum level arm (r_{max}) = 64.9

The calculated characteristic moment capacity of this connection design is calculated using Eq. 7.6. Table 7.5 gives the experimental mean moment capacity and characteristic moment capacity of these connections.

$$M_{Rk} = F_{v,Rk} \times \frac{\sum x^2 + y^2}{r_{max}} \times n_{sp} \quad \text{Eq. 7.6}$$

Table 7.5- Experimental mean moment capacity and characteristic moment capacity of the beam-beam connections with full-depth steel plates

	Experimental mean moment capacity (kN.m)	Characteristic moment capacity (kN.m)
Beam-beam connections with slotted-in full-depth steel plates	5.1	6.8

The calculated characteristic moment capacity of the connections cannot be compared with the experimental results because of the limited number of replicates tested in the current study. Comparison between characteristic moment capacity values from experiments using a larger sample size is assumed to be even lower than the mean experimental values. Thus, the difference will likely increase between the calculated characteristic moment capacity and the experimental characteristic moment capacity.

The experimental results showed premature splitting of the timber along the row of dowels in the tension zone. This means full capacity of the dowels was not achieved. The EC 5 strength equations to calculate the characteristic load-carrying of a single dowel per shear plane is based on the ductile failure mode of the timber (embedment) and steel dowels (bending). Thus,

the calculation of the characteristic moment capacity, based on the minimum value strength equation, will not be safe for the developed connection designs. Further, it should be noted that the dowel spacing, and distance used in this design were based on the EC 5 design rules which are essentially developed for connections loaded in tension. Thus, to avoid the premature splitting of timber and to maximise the use of dowel capacity, larger dowel spacing and end distances may be used as recommended by Porteous and Kermani [54].

7.2.3 Beam-beam connections with full-depth CW plates

These connections had similar design configuration as beam-beam connections with full-depth steel plates. The design calculations are as follow:

Geometric parameters of connection components

Depth of the beam (h) = 157.5 mm

Width of the beam (w) = 115 mm

Length of each beam = 1575 mm

Length of connected specimen = 3160 mm

Span of the connection = 2835 mm

Width of timber side members (t_1) = 31 mm

Thickness of CW plates (t_2) – middle member = 10 mm

Length of CW plates (l_{CW}) = 480 mm

Depth of CW plates (h_{CW}) = 157.5 mm

Connection parameters

Dowel Spacing parallel to grain (a_1) = 36 mm

Dowel Spacing perpendicular to the grain (a_2) = 36 mm

Loaded end distance ($a_{3,t}$) = 63.5 mm

Unloaded end distance ($a_{3,c}$) = 63.5 mm

Loaded edge distance ($a_{4,t}$) = 42.75 mm

Unloaded edge distance ($a_{4,c}$) = 42.75 mm

Dowel diameter (d) = 8 mm

Number of dowels per shear plane (n) = 10

Number of shear planes in connection (n_{sp}) = 4

Load angle on fastener (α) = 56° (see Figure 7.5)

Characteristic moment capacity

Characteristic embedment strength of timber ($f_{h,1,\alpha,k}$) at 56° to the grain from Eq. 7.5 is 25 MPa. Similarly, characteristic embedment strength of CW plates ($f_{h,2,\alpha,k}$) from Eq. 7.5 is 154 MPa. As specified in EC 5 for timber-timber connections, friction effect parameter (β) should be used. The friction effect (β) from the following expression is 6.1.

$$\beta = \frac{f_{h,2,\alpha,k}}{f_{h,1,\alpha,k}} \quad \text{Eq. 7.7}$$

The characteristic load-carrying capacity of the connection was calculated using EC 5 strength equations of timber-timber connection design. The characteristic load-carrying capacity per dowel per shear plane ($F_{v,Rk}$)

$$F_{v,Rk (g)} = 7830 \text{ N}$$

$$F_{v,Rk (h)} = 8455 \text{ N}$$

$$F_{v,Rk (j)} = 3429 \text{ N}$$

$$F_{v,Rk (k)} = 2135 \text{ N}$$

The characteristic load-carrying capacity of the connection per shear plane per steel dowel is limited by failure Mode-k with two plastic hinges. Thus,

$$F_{v,Rk} = \min (F_{v,Rk (g)}, F_{v,Rk (h)}, F_{v,Rk (j)}, F_{v,Rk (k)}) = 2135 \text{ N}$$

The connection pattern is symmetrical, and all CW dowels are of the same type although at different lever arms to the centroid of the dowel group (see Figure 7.5). Table 7.6 shows the lever arm distances and distribution of the dowel in terms of x and y coordinates.

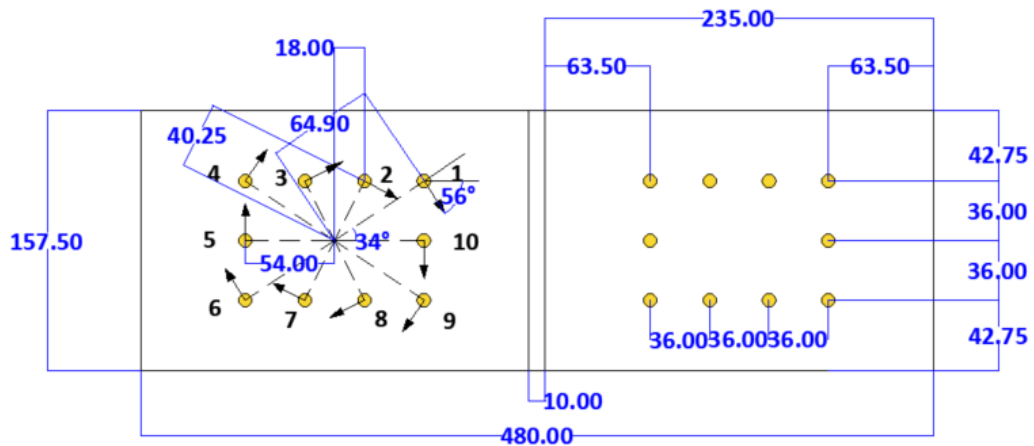


Figure 7.5- The rotation of CW dowels (all dimensions are in mm)

Table 7.6- Dowel distribution and lever arm distances (beam-beam connections with full-depth CW plates)

CW dowel label	Total Number CW dowels	$x^2 + y^2$ (mm)	Sum ($x^2 + y^2$) (mm)	Lever arm (r) (mm)
1,4,6,9	4	4212	16848	64.9
2,3,7,8	4	1620	6480	40.3
5,10	2	2916	5832	54.0
			Σ 29160	Maximum level arm (r_{max}) = 64.9

The characteristic moment capacity of this connection design can be calculated using from Eq. 7.6. The calculated characteristic moment capacity of this connection is 3.8 kN.m.

Additionally, in these connections, cross-grain shear failure was observed within CW dowels. To take into account this failure mode, the characteristic load carrying capacity of the connections was calculated using the following expression as recommended by Schmidt et al. [136] and Sandberg et al. [180].

$$F_{v,Rk,cross-grain\ shear} = \frac{\pi d^2}{4} f_{sp,k} \quad Eq. 7.8$$

where

$F_{v,Rk,cross-grain\ shear}$ is the characteristic load-carrying capacity per CW dowel per shear plane,

d is the diameter of the dowel,

$f_{sp,k}$ is the characteristic cross-grain shear strength of the CW dowels.

The characteristic load-carrying capacity per dowel per shear plane using characteristic cross-grain shear strength of CW dowel from Eq. 7.8 is

$$F_{v,Rk(cross-grain\ shear)} = 3925 \text{ N}$$

$F_{v,Rk(cross-grain\ shear)}$ is higher than the minimum value of $F_{v,Rk}$ calculated from the EC 5 strength equations. Thus, it was not considered for the calculation of characteristic moment capacities of connections. Table 7.7 shows the experimental moment capacity and characteristic moment capacities of these connections. Similar to beam-beam connections with full-depth steel plates, these connections also showed premature splitting of the timber along the row of dowels in the tension zone. Thus, calculation of characteristic moment capacity based on the $F_{v,Rk}$, calculated from the EC 5 strength equations, and from $F_{v,Rk(cross-grain\ shear)}$ will not be safe to predict the moment capacity of these connections. Further, design and spacing rules need to

be developed to ensure the ductile failure mode of these connections to utilise the full capacity of the CW dowels.

Table 7.7- Experimental mean moment capacity and characteristic moment capacity of the beam-beam connections with full-depth CW plates

	Experimental mean moment capacity (kN.m)	Characteristic moment capacity (kN.m) using minimum value $F_{v,Rk}$ chosen from EC 5 strength equations and $F_{v,Rk}$ (cross-grain shear) (kN.m)
Beam-beam connections with slotted-in full-depth CW plates	4.1	3.8

7.2.4 Beam-beam connections with narrow-depth CW plates

In these connection designs, the centre of rotation (bearing point) is located at the top of the beam (see Figure 7.6). Dowels which are located in the top row was assumed to have insignificant contribution in moment transfer mechanism due to relatively lower lever arm distance when compared to dowels those are located in the bottom row. Therefore, moment contribution from dowels which are located in the bottom was considered for calculations in this study. The lever arm distance (r) was calculated from the bottom row of CW dowels to the top of the beam, which was 130 mm. The CW dowels are loaded in a row parallel to the grain of the beam and CW plates. Therefore, an effective number of CW dowels (n_{ef}) was used to determine the characteristic load-carrying capacity ($F_{v,Rk}$) of the connection.

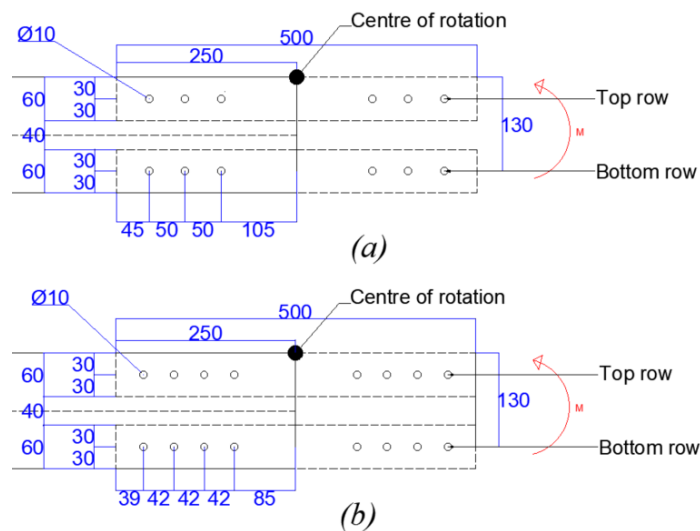


Figure 7.6- Transfer of the bending moment among the connection components, (a) connections with 6-dowel arrangement, and (b) connections with 8-dowel arrangement (all dimensions are in mm)

Geometric parameters of connection components

Depth of the beam (h) = 160 mm

Width of the beam (w) = 130 mm

Length of each beam = 1580 mm

Length of connected specimen = 3160 mm

Span of the connection = 2880 mm

Thickness of CW plates (t_2) – middle member = 10 mm

Width of timber side members (t_1) = 37 mm (with 10 mm CW plates) or 30 mm (with 20 mm CW plates)

Length of CW plates (l_{CW}) = 500 mm

Depth of CW plates (h_{CW}) = 60 mm

Dowel diameter (d) = 10 mm

Connection parameters

Connection parameters of both connection types are given in Table 7.8

Table 7.8- Connection parameters for specimens with 6-dowel arrangement and 8-dowel arrangement

Connection parameters		
	6-dowel arrangement	8-dowel arrangement
Dowel Spacing parallel to grain (a_1) in mm	50	42
Dowel Spacing perpendicular to the grain (a_2) in mm	100	100
Loaded end distance ($a_{3,t}$) in mm	105	85
Unloaded end distance ($a_{3,c}$) in mm	45	39
Loaded edge distance ($a_{4,t}$) in mm	30	30
Unloaded edge distance ($a_{4,c}$) in mm	30	30
Number of dowels per shear plane (n)	3	4
Number of shear planes in connection (n_{sp})	4	4
Load angle on fastener (α) in °	0	0
Effective number of connectors (n_{ef}) from EC 5	2.1	2.6
Friction effect (β) from Eq. 7.7	5.1	5.1

Characteristic moment capacity

The characteristic load-carrying capacity of the connection was calculated using EC 5 strength equations of timber-timber connections for each connection design (see Table 7.9).

Table 7.9- Characteristic load-carrying capacity per shear plane per CW dowel for beam-beam connections with narrow-depth CW plates for each failure modes

Characteristic load-carrying capacities per shear per dowel for each failure modes (N)				
	6-dowel arrangement using 10 mm thick CW plates	6-dowel arrangement using 20 mm thick CW plates	8-dowel arrangement using 10 mm thick CW plates	8-dowel arrangement using 20 mm thick CW plates
$F_{v,Rk (g)}$	13700	11209	13700	11209
$F_{v,Rk (h)}$	9456	18911	9456	18911
$F_{v,Rk (j)}$	5793	4798	5793	4798
$F_{v,Rk (k)}$	2560	2560	2560	2560

The characteristic load-carrying capacities of the connections per dowel per shear plane ($F_{v,Rk}$) were unaffected by the thickness of the CW plates. The load-carrying capacity of the connection per shear plane per CW dowel is limited by failure Mode-k with two plastic hinges. The design load-carrying capacities of the connections for all the shear plane were calculated using n_{ef} as given in Table 7.8. This is because the direction of load in the dowels is acting parallel to the grain direction of the timber and CW plates.

Further, taking into account the cross-grain shear failure of CW dowels, characteristic load-carrying capacities of the connections per CW dowel per shear plane for each connection type was calculated using Eq. 7.8. This was

$$F_{v,Rk (cross-grain shear)} = 3925 \text{ N}$$

The characteristic moment capacities of connections were calculated using Eq. 7.3. Table 7.10 shows the experimental mean moment capacity and calculated characteristic moment capacity based on the minimum value $F_{v,Rk}$ from EC 5 strength equations and $F_{v,Rk (cross-grain shear)}$ for each configuration of the narrow-depth beam-beam connections. In case of these connections, calculation of the characteristic moment capacity is safe. This is because the characteristic results are expected to be lower than the mean experimental results. EC 5 dowel spacing, and distance rules may be suitable for designing these connection designs because of their similarity with tension type dowelled timbers connections. These findings are based on the

limited number of specimens of each connection type tested in this study. This needs to be validated with a larger sample size.

Table 7.10- Experimental moment capacities and calculated characteristic moment capacities of beam-beam connections with narrow-depth CW plates

	Experimental mean moment capacity (kN.m)	Characteristic moment capacity (kN.m) using minimum value $F_{v,Rk}$ chosen from EC 5 strength equations and $F_{v,Rk}$ (cross-grain shear) (kN.m)
6-dowel using 10 mm thick CW plate	6.9	2.8
6-dowel using 20 mm thick CW plates	6.4	
8-dowel using 10 mm thick CW plates	6.5	3.5
8 dowel using 20 mm thick CW plates	8.9	

Further, it should be noted that in these connections the gap between connected beams was eliminated. This should be accounted for in the calculation of moment capacity as this may also affect the transfer of internal forces through the CW plates and loaded end faces of the beams in the compression zone as shown in Figure 7.7. The compression stresses parallel to the grain of both timber and CW plates contribute in the moment transfer mechanism. Thus, it requires further analytical models to reasonably approximate the moment capacity and rotational stiffness of these designs of timber-CW connections.



Figure 7.7- Transfer of internal forces through the contact surfaces of loaded ends of the beams in the compression zone

7.2.5 Beam-column connections with CWDLT members (Design-IV-2)

Figure 7.8 shows the connection configuration. Considering that the force component is perpendicular to the beam axis (F), the same loading pattern is generated inside the dowels

similar to beam-beam connections with narrow-depth CW plates. The plates located on the upper side of the connection are in tension, while the ones in the lower side are in compression. The beam transfers the bending moment to CW dowels, then from CW dowels on to CW plates and finally to the column through CW plates and embedment/contact between the beam and column. The moment capacity of the connection involves contributions from the shearing of the CW dowels and embedment between CW dowels and timber/CW plates and embedment between beam and column through the contact zone.

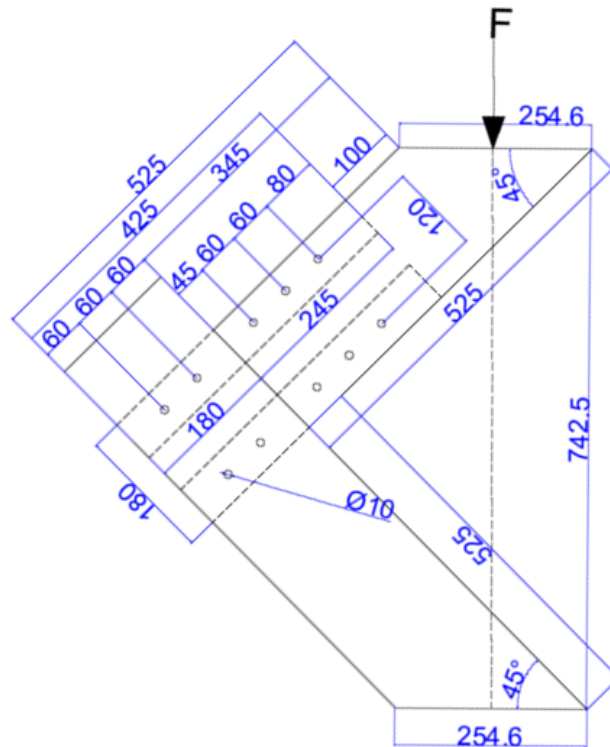


Figure 7.8- Beam-column connection configuration (Design-IV-2)

Geometric parameters of connection components

Depth of the beam/column (h) = 180 mm

Width of the beam/column (w) = 180 mm

Width of timber side members (t_1) = 49.6 mm

Thickness of CW plates (t_2) – middle member = 15 mm

Length of CW plates (l_{cw}) = 500 mm

Depth of CW plates (h_{cw}) = 60 mm

Nominal diameter of CW dowels (d) = 10 mm

Connection parameters

Dowel Spacing parallel to grain (a_1) = 60 mm

Dowel Spacing perpendicular to the grain (a_2) = 120 mm

Loaded end distance ($a_{3,t}$) = 45 mm

Unloaded end distance ($a_{3,c}$) = 80 mm

Loaded edge distance ($a_{4,t}$) = 30 mm

Unloaded edge distance ($a_{4,c}$) = 30 mm

Dowel diameter (d) = 10 mm

Number of dowels per shear plane (n) = 3

Number of shear planes in connection (n_{sp}) = 4

Load angle on fastener (α) = 0° (Figure 7.8)

Effective number of connectors (n_{ef}) from EC 5 = 2.6

Friction effect (β) from Eq. 7.7 = 5.1

Characteristic moment capacity

The characteristic load-carrying capacity of the connection was calculated using EC 5 strength equations of timber-timber connection design. The characteristic load-carrying capacity per dowel per shear plane ($F_{v,Rk}$)

$$F_{v,Rk(g)} = 18682 \text{ N}$$

$$F_{v,Rk(h)} = 14183 \text{ N}$$

$$F_{v,Rk(j)} = 7807 \text{ N}$$

$$F_{v,Rk(k)} = 2560 \text{ N}$$

The characteristic load-carrying capacity of the connection per shear plane per steel dowel is limited by failure Mode-k with two plastic hinges. Thus,

$$F_{v,Rk} = \min (F_{v,Rk(g)}, F_{v,Rk(h)}, F_{v,Rk(j)}, F_{v,Rk(k)}) = 2560 \text{ N}$$

Further, taking into account the cross-grain shear failure of CW dowels, characteristic load-carrying capacity of the connection per CW dowel per shear plane for each connection is

$$F_{v,Rk(\text{cross-grain shear})} = 3925 \text{ N}$$

The characteristic load-carrying capacities of the connections for all the shear plane were calculated using n_{ef} . The design moment capacities of connections were calculated using Eq. 7.3. The lever arm distance (r) of the dowels was 305.5 mm.

The characteristic moment capacity of the connection is calculated from Eq. 7.3 using minimum value $F_{v,Rk}$ calculated from the EC 5 strength equations and $F_{v,Rk(\text{cross-grain shear})}$. Table

7.11 shows the experimental mean moment capacity and calculated characteristic moment capacity based on the $F_{v,Rk}$ from EC 5 strength equations and $F_{v,Rk}$ (cross-grain shear).

Table 7.11- Experimental mean moment capacity and characteristic moment capacity of the beam-column connections with narrow-depth CW plates and CWDLT members

	Experimental mean moment capacity (kN.m)	Characteristic moment capacity (kN.m) using minimum value $F_{v,Rk}$ chosen from EC 5 strength equations and $F_{v,Rk}$ (cross-grain shear) (kN.m)
Beam-column connections with CWDLT members (Design-IV-2)	9.6	3.4

Similar to the beam-beam connections with narrow-depth CW plates, the characteristic moment capacity of the connection can be calculated using minimum value $F_{v,Rk}$ from the EC 5 strength equations and $F_{v,Rk}$ (cross-grain shear). Further, taking into account the embedment between the column and beam (see Figure 7.9) would give a closer approximation of the calculated characteristic moment capacity when compared to the characteristic experimental moment capacity.

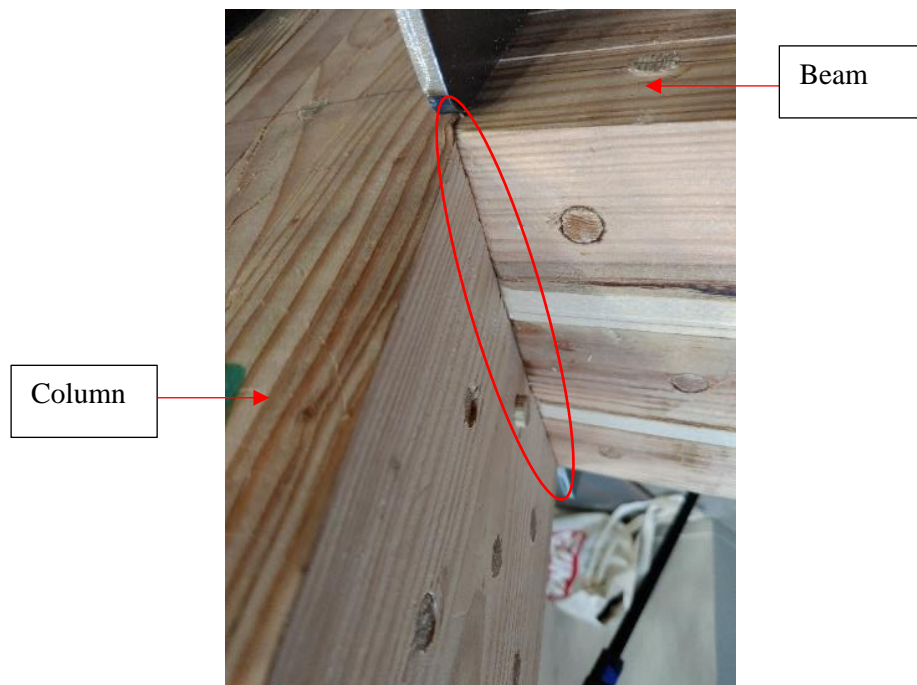


Figure 7.9- Embedment between beam-column around bearing point

7.2.6 Results summary

Table 7.12 summarises the experimental mean moment capacities and calculated characteristic moment capacities of the beam-beam and beam-column connections that are developed in the current study. Based on the analysis of the experimental results and calculated moment capacities, it can be said that the calculation of the characteristic moment capacities of beam-beam connections with full-depth steel/CW plates is not safe while using the minimum value $F_{v,Rk}$ calculated from EC 5 strength equations and $F_{v,Rk(cross-grain\ shear)}$. However, calculations of the characteristic moment capacities of the narrow-depth beam-beam and beam-column connections are safe. This is because CW dowels in these connections are acting in compression or tension which utilises the full capacity of the CW dowels. Therefore, EC 5 dowel spacing, and distances are valid for these connection designs.

Table 7.12- Results summary of the experimental mean moment capacities and calculated characteristic moment capacities

	Experimental mean moment capacity (kN.m)	Characteristic moment capacity (kN.m) using $F_{v,Rk}$ calculated from EC 5 strength equations (kN.m)
Beam-beam connections with full-depth steel plates	5.1	6.8
Beam-beam connections with full-depth CW plates	4.1	3.8
Beam-beam connections with 6-dowel arrangement using 10 mm thick CW plates	6.9	2.8
Beam-beam connections with 6-dowel arrangement using 20 mm thick CW plates	6.4	2.8
Beam-beam connections with 8-dowel arrangement using 10 mm thick CW plates	6.5	3.5
Beam-beam connections with 8-dowel arrangement using 20 mm thick CW plates	8.9	3.5
Beam-column connections (Design-IV-2)	9.6	3.4

7.3 Connection design rotational stiffness

EC 5 does not provide guidance to calculate the rotational stiffness of the semi-rigid type timber connections. Therefore, in this study, the rotational stiffness of the developed beam-beam and beam-column connections were calculated using guidelines proposed by Porteous and Kermani [54]. For timber-CW or timber-steel connections developed in the current study, CW/steel plates are connected in series to two members (beam or column) using CW/steel dowels. Thus, the rotational stiffness of the connection ($k_{ser,con}$) can be calculated using Eq. 7.9.

$$K_{ser,con} = \frac{1}{\left(\frac{1}{k_{ser,1}} + \frac{1}{k_{ser,2}}\right)} \quad Eq. 7.9$$

where $k_{ser,1}$ and $k_{ser,2}$ are rotational stiffnesses at the SLS for each side of connection within beam-beam connections.

For beam-column connections, $k_{ser,1}$ and $k_{ser,2}$ are denoted as $k_{beam-CW}$ and $k_{column-CW}$ respectively.

The k_{ser} can be calculated using the following expression:

$$k_{ser} = n_{sp} \left(\frac{K_{ser}}{(1 + k_{def})} \right) \sum_{i=1}^n r_i^2 \quad Eq. 7.10$$

where

K_{ser} is the slip modulus per shear plane per fastener,

k_{def} is the deformation factor. Here, this is not used for the calculation to allow for comparison with experimental results,

n is the number of fasteners on each side of the connection, and

r_i is the lever arm distance of fastener i .

The slip modulus, K_{ser} , for a single dowel-type connector per shear plane for timber-timber connections can be calculated using the following expression as given in Table 7.1 of EC 5:

$$K_{ser} = \frac{\rho_m^{1.5} d}{23} \quad Eq. 7.11$$

where ρ_m is the mean density of timber/ wood-based products (kg/m^3) in the connection and d is the diameter of the fastener (mm).

In the case of connections involves members of different densities, ρ_m is calculated using the following expression:

$$\rho_m = \sqrt{\rho_{m1} \cdot \rho_{m2}} \quad \text{Eq. 7.12}$$

where ρ_{m1} and ρ_{m2} are the densities of materials.

It should be noted that K_{ser} for timber-steel should be multiplied by a factor of 2 (see Eq. 7.13). This assumes that there is no clearance between the steel dowel and steel plates. Further, this assumption also ignores the bending of dowel in the steel plate and yielding of the steel plates around the dowel hole.

$$K_{ser} = 2 \times \frac{\rho_m^{1.5} d}{23} \quad \text{Eq. 7.13}$$

where ρ_m is the mean density of timber and d is the diameter of the steel dowel (mm).

It should be noted that while calculating the K_{ser} for the timber-CW connections, the mean density (ρ_m) of connected materials should not be calculated using the mean densities of CW and timber. This is because it is mainly the elastic deformation of timber members that affects the initial rotational stiffness of the connection. In timber-CW connections, CW dowels and CW plates have twice the density of timber. Thus, the elastic deformation of timber by embedment is more likely to occur compared to CW dowel and CW plates. This means deformation of timber in the elastic phase will be a critical factor for determining the rotational stiffness of timber-CW connections. Hence, only the mean density of timber should be used. Detailed information on this is given in Appendix-D.

7.3.1 Beam-beam connections with full-depth steel plates

To calculate the rotational stiffness of these connections, the slip modulus (K_{ser}) per steel dowel per shear plan was calculated using Eq. 7.13.

$$K_{ser} = 9446.8 \text{ N/mm}$$

The full connection comprises two similar connections in series (one in each beam). For each connection, the rotational stiffness from Eq. 7.10 is

$$k_{ser,1} = k_{ser,2} = 1104.2 \text{ kN.m/rad}$$

For the above calculations $r_i^2 = \sum_{i=1}^{n=10} (x_i^2 + y_i^2) = 29160 \text{ mm}^2$ (see Table 7.4)

The full connection rotational stiffness ($k_{ser,con}$) from Eq. 7.9 is then

$$k_{ser,con} = 552.1 \text{ kN.m/rad}$$

The design rotational stiffness of full connection ($k_{ser,con}$) is approximately 310% higher than that of the experimental results (134.8 kN.m/rad). This indicates that EC 5 rules may not be suitable for calculations of rotational stiffness of these connections. Previous studies [54,216,218] has also shown that the calculation of K_{ser} based on the EC 5 rules are not suitable for multiple shear plane multidowel connections. This because the empirical equation does not account for the direction of the load to the grain and the thickness of the side and central members. Further research is required to find a simple and efficient analytical model to predict the rotational stiffness of these connections.

Table 7.13- Comparison between experimental mean rotational stiffness and calculated rotational stiffness of beam-beam connections with full-depth steel plates

	Experimental mean rotational stiffness (kN.m/rad)	Calculated rotational stiffness (kN.m/rad)
Beam-beam connections with slotted-in full-depth steel plates	134.8	552.1

7.3.2 Beam-beam connections with full-depth CW plates

To calculate the rotational stiffness of these connections, the slip modulus (K_{ser}) per CW dowel per shear plan using the mean density of timber was calculated using Eq. 7.11.

$$K_{ser} = 5916.8 \text{ N/mm}$$

The full connection comprises two similar connections in series (one in each beam). For each connection, the rotational stiffness from Eq. 7.10 is

$$k_{ser,1} = k_{ser,2} = 690.1 \text{ kN.m/rad}$$

For the above calculations $r_i^2 = \sum_{i=1}^{n=10} (x_i^2 + y_i^2) = 29160 \text{ mm}^2$ (see Table 7.6)

The full connection rotational stiffness ($k_{ser,con}$) from Eq. 7.9 is then

$$k_{ser,con} = 345.1 \text{ kN.m/rad}$$

The design rotational stiffness of full connection ($k_{ser,con}$) is approximately 122% higher than that of the experimental results (155.2 kN.m/rad). Similar to timber-steel connections with full-depth steel plates, EC 5 rules may not be suitable for calculations of the rotational stiffness of timber-CW connections. However, it should be noted that these findings are based on only two connection specimens, further research is required to find a suitable method to calculate the rotational stiffness of these connections with larger experimental data.

Table 7.14- Comparison between experimental mean rotational stiffness and calculated rotational stiffness of beam-beam connections with full-depth CW plates

	Experimental mean rotational stiffness (kN.m/rad)	Calculated rotational stiffness (kN.m/rad)
Beam-beam connections with slotted-in full-depth CW plates	155.2	345.1

7.3.3 Beam-beam connections with narrow-depth CW plates

The slip modulus (K_{ser}) per CW dowel per shear plan using the mean density of timber was calculated using Eq. 7.11.

$$K_{ser} = 5916.8 \text{ N/mm}$$

The full connection comprises two similar connections in series (one in each beam). For each connection, the rotational stiffness from Eq. 7.10 is

$$k_{ser,1} = k_{ser,2} = 177.5 \text{ kN.m/rad}$$

For the above calculations $\sum_{i=1}^{n=6} r_i^2 = 15000 \text{ mm}^2$ (see Table 7.6). Here the lever arm distance of each dowel is 50 mm from the neutral axis.

The full connection rotational stiffness ($k_{ser,con}$) from Eq. 7.9 is then

$$k_{ser,con} = 345.1 \text{ kN.m/rad}$$

Similarly, the rotational stiffness of one side of connection with 8-dowel arrangement from using Eq. 7.11 is

$$k_{ser,1} = k_{ser,2} = 473.3 \text{ kN.m/rad}$$

For the above calculations $\sum_{i=1}^{n=8} r_i^2 = 20000 \text{ mm}^2$ (see Table 7.6). Here the lever arm distance of each dowel is 50 mm from the neutral axis.

Then, the rotational stiffness of full connection with 8-dowel arrangement from Eq. 7.9 is

$$k_{ser,con} = 236.7 \text{ kN.m/rad.}$$

For the 6-dowel arrangement using 10 mm thick CW plates, the comparison between design rotational stiffness and mean experimental rotational stiffness has shown that the design values are 24% higher than the experimental result. In the case of the 6-dowel arrangement using 20 mm, design values are 11% lower than the mean experimental results. Furthermore, in the case of connections with the 8-dowel arrangement using 10 mm and 20 mm thick CW plates, design values are 27% and 41% higher than the experimental results, respectively. However,

the comparison between design rotational stiffness values with the highest value obtained from the experimental results of an 8-dowel arrangement using 20 mm thick CW plates (BB-8-20-3) shows 23% overestimation. The calculated values of rotational stiffness from EC 5 were reasonably close to experimental results given that only a limited number of specimens were tested in this study.

Table 7.15- Comparison between experimental mean rotational stiffness and calculated rotational stiffness of beam-beam connections with narrow-depth CW plates

	Mean experimental rotational stiffness (kN.m/rad)	Calculated rotational stiffness (kN.m/rad)
Beam-beam connection with 6-dowel arrangement using 10 mm thick CW plate	142.9	177.5
Beam-beam connection with 6-dowel arrangement using 20 mm thick CW plates	196.5	
Beam-beam connection with 8-dowel arrangement using 10 mm thick CW plates	186.4	236.7
Beam-beam connection with 8-dowel arrangement using 20 mm thick CW plates	167.4	

7.3.4 Beam-column connections with CWDLT members (Design-IV-2)

The slip modulus (K_{ser}) per CW dowel per shear plan using the mean density of timber was calculated using Eq. 7.11.

$$K_{ser} = 5916.8 \text{ N/mm}$$

As the connection is comprised of two separate connections: beam-CW connectors and column-CW connectors, the rotational stiffness of both connections is calculated separately from Eq. 7.10 which is as follows:

$$k_{ser, beam-CW} = 511.2 \text{ kN.m/rad}$$

For the above calculations $\sum_{i=1}^{n=6} r_i^2 = 21600 \text{ mm}^2$ (see Figure 7.8). Here, lever arm distance (r) of each dowel is 60 mm from the neutral axis.

$$k_{ser, column-CW} = 340.8 \text{ kN.m/rad}$$

For the above calculations $\sum_{i=1}^{n=6} r_i^2 = 14400 \text{ mm}^2$ (see Figure 7.8). Here, lever arm distance (r) of each dowel is 60 mm from the neutral axis.

The rotational stiffness of the full connection ($k_{ser, con}$) from Eq. 7.9 is

$$k_{ser, con} = 204.5 \text{ kN.m/rad}$$

The calculated rotational stiffness is approximately 50% lower than the mean experimental rotational stiffness (305.6 kN.m/rad). However, this is only 9% lower than the least value of experimental rotational stiffness (223.4 kN.m/rad) observed for one of the specimens of this design. To confirm the suitability of the EC 5 design rules for calculations of rotational stiffness these connections need further investigation with larger sample size.

Table 7.16- Comparison between experimental mean rotational stiffness and calculated rotational stiffness of beam-column connections with CWDLT members

	Experimental mean rotational stiffness (kN.m/rad)	Calculated rotational stiffness (kN.m/rad)
Beam-column connections with CWDLT members (Design-IV-2)	305.6	204.5

7.3.5 Result summary

Table 7.17 summarises the experimental mean rotational stiffness and calculated rotational stiffness of the beam-beam and beam-column connections that are developed in the current study. Based on the analysis of the experimental results and calculated rotational stiffness, it can be said that the calculation of the rotational stiffness of beam-beam connections with full-depth steel plates/CW plates using K_{ser} calculated from EC 5 empirical expression is not safe and should not be used. However, the calculation of the rotational stiffness of beam-beam connections with narrow-depth CW plates can be calculated based on the K_{ser} calculated from EC 5 guidelines.

Table 7.17- Results summary of the experimental mean rotational stiffness and calculated rotational stiffness

	Experimental mean rotational stiffness (kN.m/rad)	Calculated rotational stiffness (kN.m/rad)
Beam-beam connections with full-depth steel plates	134.8	552.1
Beam-beam connections with full-depth CW plates	155.2	345.1
Beam-beam connections with 6-dowel arrangement using 10 mm thick CW plates	142.9	177.5
Beam-beam connections with 6-dowel arrangement using 20 mm thick CW plates	196.5	177.5
Beam-beam connections with 8-dowel arrangement using 10 mm thick CW plates	186.4	236.7
Beam-beam connections with 8-dowel arrangement using 20 mm thick CW plates	167.4	236.7
Beam-column connections (Design-IV-2)	305.6	204.5

7.4 Conclusions

EC 5 does not include design rules for timber moment connections and timber-timber connections using wooden connectors. Therefore, the moment capacity and rotational stiffness of timber-CW connections were calculated based on the guidelines presented by Porteous and Kermani [54], and Blaß and Sandhaas [37]. The moment capacity was calculated based on the characteristic load-carrying of single dowel per shear plane and rotational stiffness was calculated based on the slip modulus of single CW dowels. The conclusions are as follows:

-Moment capacity

The determination of characteristic moment capacity of the beam-beam connections with full-depth CW/steel plates using characteristic load-carrying capacity calculated based on the EC 5 strength equations or using cross-grain shear strength of CW dowels are not safe. This is because of premature tensile splitting of timber members due to reduced dowel spacing and end distances. This kind of splitting does not utilise the full capacity of steel/CW dowels. In case of timber-steel connections, higher dowel spacing and end distances should be used and this can be done by using guidelines proposed by Porteous and Kermani [54]. In the case of timber-CW connections, further experiments will be needed to establish new dowel spacing and distance rules.

However, when a similar principle is applied to calculate the characteristic moment capacities of the beam-beam and beam-column connections with narrow-depth CW plates, relatively lower values were obtained when compared to the mean experimental results. The calculation method used in this study is deemed suitable for the calculation of the characteristic moment capacity of narrow-depth CW plates connections. Further redistribution of internal forces through embedment/localised compression between the connected timber members should be considered to effectively calculate the moment capacity of these connections. The EC 5 strength equations are relatively basic and do not account for the contribution from the embedment/localised friction of connected members as observed in the case of beam-beam/beam-column connection with narrow-depth CW plates. To consider the effect of contact/friction on the moment capacity of these connections, further analytical or computational solutions are needed.

-Rotational stiffness

The design rotational stiffness values for the beam-beam connections with full-depth CW plates and with the full-depth steel plates were 310% and 122% higher than the mean experimental values, respectively. This may be attributed to the fact that the equation for the calculation of K_{ser} presented in EC 5 is a function of the mean density of the timber elements and the fastener diameter. It does not consider the direction of the load to the grain and the thickness of the side and central members [216,218]. This may be a possible reason for the overestimation of rotational stiffness. Therefore, this method is not recommended for calculating the rotational stiffness of connections with full-depth CW/Steel plates configuration as used in this study.

The calculated values of rotational stiffness from EC 5 principles for the beam-beam/beam-column with narrow-depth CW plates connections were reasonably closer to the experimental results. This may be the case due to the fact that in these connections, CW dowel essentially subjected to tension and compression loading similar to the load cases covered in EC 5. However, these findings are based on the limited number of specimens tested in this study. Further studies will be needed to verify these findings with a wide range of connection configurations as a function of geometry and mechanical properties of the connection elements.

Chapter 8 Conclusions and recommendations

8.1 Introduction

The main aim of this thesis was to develop a novel approach to produce non-metallic and adhesive-free timber moment connections using CW connectors. Previous research on thermo-mechanically CW material has been mainly limited to its manufacturing process and primary strength and stiffness properties with limited information on its suitability as a connector material. The current study has addressed this research gap through extensive research on CW connectors and their structural performance within glulam beam-beam and beam-column moment connections. Furthermore, this study has also yielded a novel timber-CW connection solution for CWDLT load-bearing elements for mass timber structures.

This thesis is equipped with detailed information and research data on mechanical properties of CW connectors, and timber-CW connections including their manufacturing, assembly, structural performance with additional design calculations. It is expected that the current study will provide an improved understanding of the structural behaviour of CW connectors and timber-CW connections that may widen the knowledge base and help structural engineers, researchers, and architects etc. to design timber-CW connections. The findings are important to develop safe, sustainable, recyclable, and energy-efficient timber connection systems and mass timber products using CW connectors. This research aims to set an example that all-wood solutions using modified wood could be a potential alternative to wood products and connections that are produced using energy-intensive synthetic adhesives and mechanical fasteners. It is anticipated that this research will serve as a basis and lead the way to a wide range of research possibilities for the use of thermo-mechanically CW in structural applications. The following sections discuss the main conclusions, research contributions and recommendations for future research.

8.2 Material characterisation tests conclusions

The objective of the material characterisation tests was to characterise the mechanical properties of CW connectors. This was successfully achieved through a range of laboratory experiments on thermo-mechanically modified high-density CW connectors. The obtained test results were compared with other relevant materials such as uncompressed softwood/hardwood, DVW and composite materials. The embedment strength of CW was shown to be four to five times higher than normal uncompressed wood. Thermo-mechanically CW was found to have a similar embedment strength to resin impregnated DVW and high-density bamboo composites and could be used as an alternative reinforcement material within connections. The yield moment capacity of CW dowels was shown to be greater than that of

hardwood dowels and is comparable to other materials such as FRP and bamboo composite dowels. It was shown to be directionally dependent with a yield moment capacity approximately 2 times higher when loaded in the tangential direction. However, while using the CW dowels on-site, insertion of dowels in a specific orientation to take advantage of this is not practical. Therefore, this study recommends that the characteristic value of yield moment capacity be based on the full set of test results from specimens that are tested in all directions.

Yield moment and cross-grain shear tests on CW dowels showed two additional failure modes to those in conventional steel dowel fasteners: interlaminar shear and cross-grain shear failure. These results highlight the need to consider the aforementioned failure modes in the design of timber-CW connections. The cross-grain shear strength of the CW is about 1.6 times higher than hardwood dowels.

Based on the material characterisations test results, it can be concluded that CW connectors can be considered as potential replacements for hardwood dowels, synthetic adhesives, and metallic connectors within timber connections and for lamination of mass timber products. The experimental results of this study and the literature also confirm that the strength and stiffness of the densified wood are affected by the species and density of the material. Therefore, careful consideration should be given to species selection and the final density of the CW material, which were shown to be key parameters affecting the mechanical performance of these connectors.

8.3 Swelling/shrinkage behaviour of CW and timber-CW connections tests conclusions

The objective of these tests was to quantify the long-term moisture dependent swelling/shrinkage behaviour of CW and determine the effect of ageing on the structural performance of timber-CW and timber hardwood connections. Long-term unconstrained swelling/shrinkage results have indicated that, after manufacture, CW expands rapidly in the first 45 days when exposed to standard conditioning of 65 ± 5 % RH and 20 ± 2 °C. Therefore, if CW dowels are used as a replacement for hardwood dowels in DLT manufacturing, laminated timber specimens should be conditioned for at least 45 days at standard conditioning to take advantage of the springback of CW. The accelerated ageing tests, presented in the current study, quantitatively proved that springback leads to continuous expansion of CW dowels and facilitates form and friction fit with the timber substrate and yields a higher pull-out strength of the dowel.

8.4 Development of novel semi-rigid timber connections using CW connectors

The objective of small-scale beam-beam and beam-column timber-CW moment connections tests was to characterise the structural performance of these connections. The literature review indicated that there is limited information available on timber-CW connections between load-bearing elements. Therefore, to fill this research gap, the structural feasibility of CW connectors within beam-beam and beam-column connections was evaluated using extensive experimental research on a range of connection configurations. The selected connection designs were developed based on an evaluation of carpentry and modern jointing techniques.

To date, the moment-rotation behaviour of timber-CW connections has not been investigated under pure bending. In this research, the bending performance of five different design configurations of timber-CW beam-beam connections has been investigated. Beam-beam connections with slotted-in full-depth CW plates were found to have comparable moment capacity and rotational stiffness to similar design of timber-steel connections with approximate capacity. Further, designs of beam-beam connections were improved, while respecting the limitations on laboratory-produced clear specimens of CW plates, to meet other relevant design criteria such as moment capacity, rotational stiffness, and ductility. Higher moment-capacity can be achieved by increasing the number of CW dowels and the thickness of the CW plates within the connections, but this ultimately leads to a brittle response at failure. A more ductile response with high rotational stiffness was shown to be achieved through larger dowel spacing and thicker CW plates. Designers may choose an appropriate design based on the end-use and strength/stiffness requirement.

Seven different designs of beam-column timber moment connections were also developed using glulam members and CW dowels with and without CW plates. Similar to beam-beam connections, the current study indicates that there is a trade-off between ductility and moment capacity of the proposed connections. Carpentry mortise and tenon connections with CW dowels and an exposed tenon have a higher ductile response but relatively lower moment capacity when compared to connections with CW dowels and CW plates. In contrary to this, similar connection designs with unexposed tenons offer a higher moment capacity and rotational stiffness than the carpentry connection designs with exposed tenons. Also, these connections have comparable performance to connections with CW dowels and CW plates. The carpentry connection designs are well suited to solid timber and glued timber members. In the context of the current research, connection designs with CW plates and a shouldered column were shown to be most suitable for CWDLT members, due to their good structural performance, ease of manufacture and assembly.

Two designs of novel all-wood beam-column connections were successfully developed using CW connectors and CWDLT members, and their structural performance was evaluated experimentally. The moment capacity, rotational stiffness and ductility of such connections are comparable to connections that are developed using glued structural members. To avoid brittle failure of the CWDLT column, a minimum distance 2.5 times the dowel diameter is recommended between the column edge and the dowel axis and the same minimum distance is recommended between the plate slots and dowels within the connection area. The proposed connections are suitable for engineering applications where the sustainability and bio-based nature of the structural systems of buildings are of prime importance.

8.5 Experimental investigation of laterally loaded laminated timber portal frames with CW connections

The objective of portal frames tests was to design, develop and structurally characterise the mechanical performance of timber-CW connections within frames produced using glued/CWDLT members. Four one bay portal frames were successfully developed and tested under a horizontal load. Two frames were manufactured using conventional glued members and two frames were manufactured using CWDLT members. This research has shown a novel application of timber-CW connections within portal frames composed of CWDLT beams and columns. The lateral load-carrying capacity of the frames with CWDLT members was relatively similar (4.4% less) to the frames with glued members. However, the lateral stiffness of frames with CWDLT frames was approximately 53% lower than the frames with glued members. This was attributed to the lower bending stiffness of the CWDLT members compared to the glued members. Thus, further investigation is required to improve the stiffness of the CWDLT members for mainstream applications. Nevertheless, the moment capacity and rotational stiffness of the connections are comparable with the small-scale connections and connections within glued structural frames. The results on the Timber-CW connection systems have demonstrated that an all-wood connection concept may be used in heavy timber structures with CWDLT members as well as with solid timber and glulam members.

8.6 Design of timber-CW connections

The objective of design calculations for timber-CW connections was to compare the experimental test results of beam-beam and beam-column with design rules of EC 5 and research studies. This was successfully carried out using EC 5 design rules and design guidelines for timber moment connections proposed by Porteous and Kermani [54] and Blaß and Sandhaas [37]. When using EC 5 strength equations for calculating the characteristic load-carrying capacity of the all timber-CW connection systems proposed in this thesis are found

to demonstrate mode-k (EYM) as the governing failure mode due to the lower yield moment capacities of the CW dowels compared to steel dowels. This study recommends the use of a modified yield moment capacity of CW dowels (presented-in Chapter 3) for the design calculations. Further, CW dowels also show cross-grain shear failure. The determination of characteristic moment capacities of the beam-beam connections with full-depth CW plates using characteristic load-carrying capacity calculated based on the EC 5 strength equations or using cross-grain shear strength of CW dowels are not safe and should not be used for designing of these connections. This is because of the premature tensile splitting of timber members due to reduced dowel spacing and end distances. This kind of splitting does not utilise the full capacity of CW dowels. However, using a similar principle for calculation of the characteristic moment capacities of narrow-depth CW plates beam-beam and beam-column connections was safe. Further, interactions/contact between timber-CW and timber-timber members were as observed during experimental tests, and this should be considered while designing the connections. This study also recommends that the mean density of timber should be used for the calculation of slip modulus to determine the rotational stiffness of timber-CW connections. Using the mean density of connected timber and CW overestimates the rotational stiffness. The rotational stiffness of connections with full-depth CW plates was found to be overestimated by a factor of 2 when calculated using EC 5 empirical expressions. Therefore, it is not recommended for such connection types. However, it is suitable for beam-beam and beam-column connections with narrow-depth CW plates. The calculated rotational stiffness of such connections using narrow-depth CW plates was found to be reasonably comparable to the experimental values. However, this conclusion is limited by the number of specimens tested in this study, thus a larger sample size is needed to validate these findings.

8.7 Overall conclusion

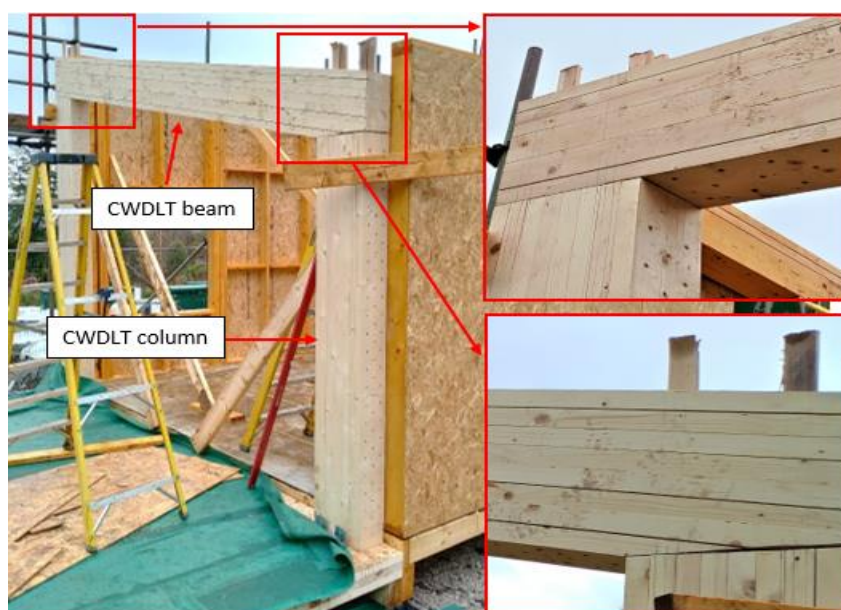
This research has demonstrated that CW offers superior mechanical properties than uncompressed softwoods and hardwoods and could be used as an ideal wood-based connector material in the form CW dowels and CW plates to connect glulam, DLT and CWDLT in mass timber structures. CW connectors have marked potential as an alternative to high embodied energy steel connectors and synthetic adhesives in the timber industry. Developed timber-CW connection systems can be disposed of/recycled at the end of the building's life cycle without posing any additional risk on the environment. Further, the idea of using wood-based connectors fits well with the ongoing transition towards a bio-based and circular economy.

8.8 Application of the proposed timber-CW connections for structural purposes

Based on the experimental research presented on timber-CW connections in this study, the designed connection systems were used in the development of a 35 m² field station at Ness Botanical Gardens, Liverpool, UK as part of the EU Interreg NWE project ‘Towards Adesive-free Timber Buildings’ (see Figure 8.1a). This structure is built up using CW laminated CLT wall and floor panels, CWDLT beams and columns, as well as timber-CW beam-column connections designed in the current study. This demonstrates that timber-CW connections can be used as an all-wood substitute for slotted-in steel plate connections in timber buildings. Figure 8.1b, Figure 8.1c and Figure 8.1d show the location and configurations of the designed timber-CW connections in the building.



(a)



(b)



(c)



(d)

Figure 8.1- Timber building using CWDLT members and designed timber-CW connection systems at Ness Botanical Garden, Liverpool, United Kingdom - Towards Adhesive Free Timber Building (a) demonstrator structure, (b) during construction, (c) internal space and location of timber-CW connections, (d) close up view of narrow-depth timber-CW connections

8.9 Recommendations for future work

The recommendations for future work are as follows:

- This study did not cover edge and spacing rules for the design of timber-CW connections. Further experiments are needed to optimise dowel spacing and distances criteria for timber-CW connections. This study looked at specific types of timber-CW connections while abiding by the geometrical constraints and shape of the laboratory-produced CW connectors. Also, unlike steel dowels, CW dowels show interlaminar and cross-grain shear failure. This should be accounted for while designing timber-CW connections. Additionally, the small and large-scale tests carried out on timber-CW connections highlighted significant scope for optimisation in the stiffness performance of CWDLT members. The optimisation could, for example, involve using larger diameter CW dowels for lamination, reducing dowel spacing and varying dowel insertion angles through experimental testing and computational modelling.
- Future studies should focus on creep, stress relaxation, durability, and the influence of environmental conditions on the structural performance of the timber-CW connections. Structural tests carried out in this study are based on the short-term static loading. Therefore, it will be important to validate the efficiency of the timber-CW connections under long-term load tests in variable climatic conditions. Based on these, safety/modification factors can be derived, and suitability of the proposed connection systems may be assessed for various code specified service classes. Apart from these, insect decay and fungal degradation of CW connectors can be investigated as these will negatively affect the strength and stiffness of the connections, and the overall stability of the structure.
- Future studies should investigate the combined effect of shear and bending moment on the capacity of the proposed connections. In timber structures, connections (particularly beam-column connections) are subjected to both shear forces and bending moment. Previous studies [157–159,168] showed that the interaction between the shear forces and bending moment affects the structural performance of the connections. However, the current study only considered the effect of bending moment on the capacity of timber-CW connections.
- A good quality control and density-based grading of CW connectors are required during the manufacturing and storage phase to avoid any inconsistency due to the variation in the material properties and geometrical parameters. CW connectors are prone to dimensional changes due to a change in the surrounding environmental conditions and springback. The variation in mechanical properties of CW connectors will have a negative effect on the moment capacity and rotational stiffness of the

connections. Also, variations in the diameter of the CW dowels along its circumference and the embedded length will affect the load-slip behaviour of the connections. Any slack or loose fit of the CW dowel will result in lower initial rotational stiffness. Further research is required to investigate the effect of tolerance allowances on the structural performance of timber-CW connections.

- Fire performance of proposed timber-CW connections should be evaluated and compared with the steel-connections. In the event of fire, connections are often the weakest link. Conventional steel connectors rapidly transfer the heat to the interior of timber members and accelerate the thermal decomposition (charring) of wood around the connection area. The resulted charred section has lower embedment strength which negatively affects the load carrying of the connection [219]. Previous studies [126,185,220–222] have shown non-metallic connectors may exhibit superior structural performance in the event of fire compared to steel connectors. However, such information is not available for timber-CW connections.
- Life Cycle Assessment (LCA) of the proposed connection systems and CWDLT products would be a vital area of research to assess the global warming potential of these products at each phase of their life cycle from raw material to end-of-life disposal. Although timber-CW connections and CWDLT are wood-based materials, there is a lack of quantitative information on energy usages and embodied carbon of these products during their manufacture, in-service use, maintenance requirements and end-of-life. Such information would serve as a basis to compare the sustainability credentials of these products against other conventional building materials and existing EWPs. Additionally, recycling and reusability possibilities may be evaluated.
- Finally, for wider uptake of timber-CW connections and CWDLT members in the timber industry, time and cost analysis should be done on the production, machining, and assembly processes.

References

- [1] International Energy Agency (IEA), 2019 Global Status Report for Buildings and Construction, 2019. doi:<https://doi.org/10.1038/s41370-017-0014-9>.
- [2] L.G.F. Tellnes, S. Eide, Assessment of carbon footprint of laminated veneer lumber elements in a six story housing – comparison to a steel and concrete solution, in: *LCA of Sustainable Materials and Technologies*, 2006: pp. 817–824.
- [3] C. Bataille, Low and zero emissions in the steel and cement industries, in: *Green Growth and Sustainable Development Forum*, OECD, Paris, 2019. doi:10.1787/5ccf8e33-en.
- [4] M. Herczeg, D. McKinnon, L. Milios, I. Bakas, E. Klaassens, K. Svatikova, O. Widerberg, Resource efficiency in the building sector. Final Report, Ecorys Netherlands BV and Copenhagen Resource Institute. (2014) 1–30.
- [5] J.L. Skullestad, R.A. Bohne, J. Lohne, High-rise Timber Buildings as a Climate Change Mitigation Measure - A Comparative LCA of Structural System Alternatives, *Energy Procedia*. 96 (2016) 112–123. doi:10.1016/j.egypro.2016.09.112.
- [6] J. Hart, F. Pomponi, More timber in construction: Unanswered questions and future challenges, *Sustainability (Switzerland)*. 12 (2020). doi:10.3390/SU12083473.
- [7] V. Masson-Delmotte, P. Zhai, H.-O. Pörtner, D. Roberts, J. Skea, P.R. Shukla, A. Pirani, W. Moufouma-Okia, C. Péan, R. Pidcock, S. Connors, J.B.R. Matthews, Y. Chen, X. Zhou, M.I. Gomis, E. Lonnoy, T. Maycock, M. Tignor, T. Waterfield, IPCC 2018: Summary for Policymakers. Global Warming of 1.5°C. An IPCC Special Report on the impacts of global warming of 1.5°C above pre-industrial levels and related global greenhouse gas emission pathways, in the context of strengthening the global resp, World Meteorological Organization, Geneva, Switzerland. (2018) 32. doi:10.1002/9783527809080.catatz09118.
- [8] Guidehouse Insights, Global Building Stock Database 2Q20, (2020). <https://guidehouseinsights.com/reports/global-building-stock-database-2q20> (accessed July 16, 2020).
- [9] OECD, Global Material Resources Outlook to 2060, Economic Drivers and Environmental Consequences, OECD Publishing, Paris. (2019). doi:10.1787/9789264307452-en.
- [10] R. Hough, Rethinking Timber Buildings. Report, Arup, London. (2019) 100. <https://www.arup.com/perspectives/publications/research/section/rethinking-timber->

buildings.

- [11] A.M. Harte, Mass timber – the emergence of a modern construction material, *Journal of Structural Integrity and Maintenance*. 2 (2017) 121–132. doi:10.1080/24705314.2017.1354156.
- [12] H.R. Milner, A.C. Woodard, Sustainability of engineered wood products, in: *Sustainability of Construction Materials (Second Edition)*, Woodhead Publishing, 2016: pp. 159–180. doi:10.1016/b978-0-08-100370-1.00008-1.
- [13] M.H. Ramage, H. Burrige, M. Busse-Wicher, G. Fereday, T. Reynolds, D.U. Shah, G. Wu, L. Yu, P. Fleming, D. Densley-Tingley, J. Allwood, P. Dupree, P.F. Linden, O. Scherman, The wood from the trees: The use of timber in construction, *Renewable and Sustainable Energy Reviews*. 68 (2017) 333–359. doi:10.1016/j.rser.2016.09.107.
- [14] A. Sotayo, D. Bradley, M. Bather, P. Sareh, M. Oudjene, I. El-Houjeiri, A.M. Harte, S. Mehra, C. O’Ceallaigh, P. Haller, S. Namari, A. Makradi, S. Belouettar, L. Bouhala, F. Deneufbourg, Z. Guan, Review of state of the art of dowel laminated timber members and densified wood materials as sustainable engineered wood products for construction and building applications, *Developments in the Built Environment*. 1 (2020) 100004. doi:10.1016/j.dibe.2019.100004.
- [15] R. Abrahamsen, Mjøstårnet - Construction of an 81 m tall timber building, in: *Proceedings of 23. Internationales Holzbau-Forum IHF*, Garmisch-Partenkirchen, Germany, 2017: p. 12.
- [16] The Skyscraper Center, Mjøstårnet, (n.d.). <https://www.skyscrapercenter.com/building/mjostarnet/26866> (accessed August 10, 2020).
- [17] StructureCraft, Dowel Laminated Timber (DLT) - Profile handbook, DLT Design Guide. (2017). <https://structurecraft.com/materials/mass-timber/dlt-dowel-laminated-timber>.
- [18] I. El-Houjeiri, V.D. Thi, M. Oudjene, M. Khelifa, Y. Rogaume, A. Sotayo, Z. Guan, Experimental investigations on adhesive free laminated oak timber beams and timber-to-timber joints assembled using thermo-mechanically compressed wood dowels, *Construction and Building Materials*. 222 (2019) 288–299. doi:https://doi.org/10.1016/j.conbuildmat.2019.05.163.
- [19] Z. Guan, A. Sotayo, M. Oudjene, I. El Houjeiri, A. Harte, S. Mehra, P. Haller, S. Namari, S. Belouettar, F. Deneufbourg, Development of adhesive free engineered wood products – Towards Adhesive Free Timber Buildings, in: *Proceedings of World*

- Conference on Timber Engineering, Seoul, Republic of Korea, 2018.
- [20] A. Sotayo, D.F. Bradley, M. Bather, M. Oudjene, I. El-houjeiri, Z. Guan, Development and structural behaviour of adhesive free laminated timber beams and cross laminated panels, *Construction and Building Materials*. 259 (2020) 119821.
- [21] R. Jockwer, P. Wiehle, P. Palma, M. Klippel, A. Frangi, D. Hebel, Structural Behaviour and Design of Timber Connections With Dowels and Slotted-in Plates Made of Bamboo Composites, in: *Proceedings of World Conference on Timber Engineering*, Seoul, Republic of Korea, 2018.
- [22] T. Mori, K. Umemura, M. Norimoto, Manufacture of drift pins and boards made from bamboo fiber for timber structures, in: *Proceedings of First International Conference on Modern Bamboo Structures (ICBS-2007)*, Changsha, China, 2007: p. 312/314.
- [23] W.S. Chang, N. Nearchou, Hot -pressed dowels in bonded-in rod timber connections, *Wood and Fiber Science*. 47 (2015) 199–208.
- [24] M. Riggio, J. Sandak, A. Sandak, Densified wooden nails for new timber assemblies and restoration works: A pilot research, *Construction and Building Materials*. 102 (2016) 1084–1092. doi:10.1016/j.conbuildmat.2015.06.045.
- [25] K. Jung, A. Kitamori, K. Komatsu, Evaluation on structural performance of compressed wood as shear dowel, *Holzforschung*. 62 (2008) 461–467.
- [26] Forest Products Laboratory, *Wood Handbook: Wood as an Engineering Material*. General Technical Report FPL-GTR-190, U.S. Department of Agriculture, Forest Service, Forest Products Laboratory, Madison, Wisconsin, 2010.
- [27] International Tropical Timber Organisation (ITTO), *Online Statistics Database - Biennial Review and Assessment of the World Timber Situation*, (2020). https://www.itto.int/biennial_review/ (accessed July 22, 2020).
- [28] Y. Li, Wood-Polymer Composites, in: P. Tesinova (Ed.), *Advances in Composite Materials - Analysis of Natural and Man-Made Materials*, 2011. doi:10.5772/17579.
- [29] Forest Products Laboratory, Difference between heartwood and sapwood. Technical note, U. S. Forest Service Research Note FPL-0147. (1966) 1–2.
- [30] A.M. Harte, Introduction to timber as an engineering material, in: Michael C. Forde (Ed.), *ICE Manual of Construction Materials*, London, UK, 2009: pp. 707–715. doi:10.1680/mocm.00000.0001.
- [31] M.S. Nascimento, A.L.B.D. Santana, C.A. Maranhão, L.S. Oliveira, L. Bieber, Phenolic Extractives and Natural Resistance of Wood, in: R. Chamy (Ed.),

- Biodegradation - Life of Science, 2013. doi:10.5772/56358.
- [32] Ü. Büyüksari, N. As, T. Dündar, Mechanical properties of earlywood and latewood sections of scots pine wood, *BioResources*. 12 (2017) 4004–4012. doi:10.15376/biores.12.2.4004-4012.
- [33] S. Cramer, D. Kretschmann, R. Lakes, T. Schmidt, Earlywood and latewood elastic properties in loblolly pine, *Holzforschung*. 59 (2005) 531–538. doi:10.1515/HF.2005.088.
- [34] G.Y. Jeong, A. Zink-Sharp, D.P. Hindman, Tensile properties of earlywood and latewood from loblolly pine (*Pinus taeda*) using digital image correlation, *Wood and Fiber Science*. 41 (2009) 51–63.
- [35] A. Kutnar, M. Šernek, Densification of wood, *Zbornik Gozdarstva in Lesarstva*. 82 (2007) 53–62.
- [36] P. Baas, N. Blokhina, T. Fujii, P.E. Gasson, D. Grosser, I. Heinz, J. Ilic, J. Xiaomei, R. Miller, L.A. Newsom, S. Noshiro, H.G. Richter, M. Suzuki, T. Terrazas, E. Wheeler, A. Wiedenhoef, IAWA List Of microscopic features for softwood identification, *IAWA Journal*. 25 (2004) 1–70. doi:10.1163/22941932-90000349.
- [37] H.J. Blaß, C. Sandhaas, *Timber Engineering-Principles for Design*, KIT Scientific Publishing, 2017. doi:10.5445 / KSP / 1000069616.
- [38] C. Chen, Y. Kuang, S. Zhu, I. Burgert, T. Keplinger, A. Gong, T. Li, L. Berglund, S.J. Eichhorn, L. Hu, Structure–property–function relationships of natural and engineered wood, *Nature Reviews Materials*. (2020) 19–21. doi:10.1038/s41578-020-0195-z.
- [39] S. Thelandersson, H.J. Larsen, *Timber Engineering*, John Willey & Sons Ltd, 2003. <https://www.wiley.com/en-us/Timber+Engineering-p-9780470844694>.
- [40] C. Plomion, G. Leprévost, A. Stokes, Wood Formation in Trees, *Plant Physiology*. 127 (2001) 1513–1523. doi:10.1104/pp.010816.1.
- [41] R. Rowell, R. Rowell, R. Pettersen, M. Tshabalala, Cell Wall Chemistry, in: *Handbook of Wood Chemistry and Wood Composites*, Second Edition, 2012: pp. 33–72. doi:10.1201/b12487-5.
- [42] M. Boonstra, Dimensional Stabilization of Wood and Wood Composites, in: M.N.B. and A. Pizzi (Ed.), *Lignocellulosic Fibers and Wood Handbook: Renewable Materials for Today’s Environment*, Scrivener Publishing, 2016: pp. 629–655.
- [43] H.A. Schroeder, Shrinking and swelling differences between hardwoods and softwoods, *Wood Fiber Sci*. 4 (1972) 20–25.

- [44] J.F. Siau, Wood Structure and Chemical Composition, in: *Transport Processes in Wood*, First, Springer-Verlag Berlin Heidelberg, 1984: pp. 35–72. doi:10.1007/978-3-642-69213-0.
- [45] J.C.F. Walker, *Primary wood processing - principles and practice*, Second, Springer Netherlands, 2006. doi:10.1007/1-4020-4393-7.
- [46] V. Angst, M. Augustin, K. Bell, A.S. Hansen, P. Kuklik, A. Lokaj, K.A. Malo, A. Marynowicz, A. Materna, M. Premrov, M. Tajnik, *Handbook 1- Timber Structures, Educational Materials for Designing and Testing of Timber Structures*, 2008. <https://in.b-ok.as/book/3220704/fb5c6c>.
- [47] J. Brauns, K. Rocens, *Modification of Wood: Mechanical Properties and Application*, *Encyclopedia of Materials: Science and Technology (Second Edition)*. (2007) 1–9.
- [48] M. Legg, S. Bradley, Measurement of stiffness of standing trees and felled logs using acoustics: A review, *The Journal of the Acoustical Society of America*. 139 (2016) 588–604. doi:10.1121/1.4940210.
- [49] S. Franke, B. Franke, A.M. Harte, Failure modes and reinforcement techniques for timber beams-State of the art, *Construction and Building Materials*. 97 (2015) 2–13. doi:10.1016/j.conbuildmat.2015.06.021.
- [50] CEN, EN 338:2016. *Structural timber - Strength Classes*, CEN, Comité Européen de Normalisation, Brussels, Belgium, 44 (2012) 7–10.
- [51] M.A. Ritter, Properties of wood and structural wood products, in: *Timber Bridges: Design, Construction, Inspection, and Maintenance*, U.S. Dept. of Agriculture, Forest Service, Washington DC, 1990: p. 944. <https://babel.hathitrust.org/cgi/pt?id=umn.31951d00276578k&view=1up&seq=4>.
- [52] A. Kutnar, D. Sandberg, P. Haller, Compressed and moulded wood from processing to products, *Holzforschung*. 69 (2015) 885–897. doi:10.1515/hf-2014-0187.
- [53] W.M. Bulleit, L.B. Sandberg, M.W. Drewek, T.L. O’Bryant, Behavior and modelling of wood-pegged timber frames, *Journal of Structural Engineering*. 125 (1999) 3–9. doi:10.1061/(ASCE)0733-9445(1999)125:1(3).
- [54] J. Porteous, A. Kermani, *Structural Timber Design to Eurocode 5*, Blackwell Publishing, 2007.
- [55] EN 1995-1-1:2004&A1:2008&A2:2014&AC:2006. *Eurocode 5: Design of timber structures- Part 1-1: General- Common rules and rules for buildings*, CEN, Comité Européen de Normalisation, Brussels, Belgium, (2014).

- [56] EN 13183-1, Moisture content of a piece of sawn timber - Part 1: Determination of oven dry method, CEN, Comité Européen de Normalisation, Brussels, Belgium, (2002).
- [57] EN 13183-2: 2002, Moisture content of a piece of sawn timber - Part 2: Estimation by Electrical Resistance Method, CEN, Comité Européen de Normalisation, Brussels, Belgium, 44 (2014).
- [58] EN 13183-3: 2005, Moisture content of a piece of sawn timber - Part 1: Estimation by capacitance method, CEN, Comité Européen de Normalisation, Brussels, Belgium, 44 (2014).
- [59] R. Sargent, Evaluating dimensional stability in solid wood: a review of current practice, *Journal of Wood Science*. 65 (2019) 1–11. doi:10.1186/s10086-019-1817-1.
- [60] K. Laine, T. Belt, L. Rautkari, J. Ramsay, C.A.S. Hill, M. Hughes, Measuring the thickness swelling and set-recovery of densified and thermally modified Scots pine solid wood, *Journal of Materials Science*. 48 (2013) 8530–8538. doi:10.1007/s10853-013-7671-4.
- [61] S. Holzer, J. Loferski, D. Dillard, A review of creep in wood: concepts relevant to develop long-term behavior predictions for wood structures, *Wood and Fiber Science*. 21 (1989) 376–392.
- [62] Z. Guan, K. Komatsu, K. Jung, A. Kitamori, Structural Characteristics of Beam - Column Connections Using Compressed Wood Dowels and Plates, in: *Proceedings of the World Conference on Timber Engineering (WCTE)*, Trentino, Italy, 2010.
- [63] J. Henderson, S. Foster, M. Bridgestock, Brettstapel Construction - massive timber without glues or nails, 2013. http://www.brettstapel.org/Brettstapel/What_is_it.html (accessed May 12, 2020).
- [64] D. Sandberg, A. Kutnar, G. Mantanis, Wood modification technologies - A review, *IForest*. 10 (2017) 895–908. doi:10.3832/ifor2380-010.
- [65] C.A.S. Hill, Wood modification: An update, *BioResources*. 6 (2011) 918–919. doi:10.15376/biores.6.2.918-919.
- [66] C.A.S. Hill, *Wood Modification: Chemical, Thermal and Other Processes*, John Wiley & Sons, 2006. doi:10.1002/0470021748.
- [67] D. Jones, D. Sandberg, G. Goli, L. Todaro, *Wood Modification in Europe : a state-of-the-art about processes , products and applications.*, Firenze University Press, 2019. doi:10.36253/978-88-6453-970-6.

- [68] G. Torgovnikov, P. Vinden, High-intensity microwave wood modification for increasing permeability, *Forest Products Journal*. 59 (2009) 84–92.
- [69] M. Wålinder, A. Omidvar, J. Seltman, K. Segerholm, Micromorphological studies of modified wood using a surface preparation technique based on ultraviolet laser ablation, *Wood Material Science and Engineering*. 4 (2009) 46–51. doi:10.1080/17480270903151233.
- [70] D. Sandberg, P. Navi, Introduction to Thermo-hydro-mechanical (THM) wood processing. Report No. 30, Växjö universitet, Växjö, 2007. <http://urn.kb.se/resolve?urn=urn:nbn:se:lnu:diva-18871>.
- [71] P. Navi, A. Pizzi, Property changes in thermo-hydro-mechanical processing, *Holzforschung*. 69 (2015) 863–873. doi:10.1515/hf-2014-0198.
- [72] R. Adlam, Thermomechanical Densification of Timber: Initial Investigations of the Potential of Softwood Timber, Forest and Wood Products Research and Development Corporation, 2005.
- [73] F.F.P. Kollmann, E.W. Kuenzi, A.J. Stamm, Principles of Wood Science and Technology, First, Springer-Verlag Berlin Heidelberg, 1975. doi:10.1007/978-3-642-87928-9.
- [74] J. Song, C. Chen, S. Zhu, M. Zhu, J. Dai, U. Ray, Y. Li, Y. Kuang, Y. Li, N. Quispe, Y. Yao, A. Gong, U.H. Leiste, H.A. Bruck, J.Y. Zhu, A. Vellore, H. Li, M.L. Minus, Z. Jia, A. Martini, T. Li, L. Hu, Processing bulk natural wood into a high-performance structural material, *Nature*. 554 (2018) 224–228. doi:10.1038/nature25476.
- [75] A.J. Stamm, S. R.M., Resin-treated, compressed wood, *Transaction of the American Institute of Chemical Engineers*. 37 (1941) 385–398.
- [76] R. Seborg, M. Millet, A. Stamm, Heat-stabilized compressed wood (Staypak), *Mechanical Engineering*. 67 (1945) 25–31.
- [77] L. Rautkari, Surface Modification of Solid Wood Using Different Techniques. PhD thesis, Aalto University, 2012. <http://urn.fi/URN:ISBN:978-952-60-4465-1>.
- [78] K. Jung, A. Kitamori, K. Komatsu, Development of a joint system using a compressed wooden fastener II: Evaluation of rotation performance for a column-beam joint, *Journal of Wood Science*. 56 (2010) 118–126.
- [79] A. Kitamori, K. Jung, K. Komatsu, Utilization of Compressed Wood As Mechanical Fasteners of Friction Joints in, in: Proceedings of 11th International Conference on Non-Conventional Materials and Technologies, NOCMAT, Bath, United Kingdom, 2009.

- [80] K. Jung, A. Kitamori, K. Komatsu, Development of a joint system using a compressed wooden fastener I: Evaluation of pull-out and rotation performance for a column-sill joint, *Journal of Wood Science*. 55 (2009) 273–282. doi:10.1007/s10086-009-1027-3.
- [81] D. Sandberg, P. Haller, P. Navi, Thermo-hydro and thermo-hydro-mechanical wood processing: An opportunity for future environmentally friendly wood products, *Wood Material Science and Engineering*. 8 (2013) 64–88. doi:10.1080/17480272.2012.751935.
- [82] J. Blomberg, Mechanical and Physical Properties of Semi-Isostatically Densified Wood. PhD Thesis, Luleå University of Technology, 2006.
- [83] C.R. Welzbacher, J. Wehsener, A.O. Rapp, P. Haller, Thermo-mechanical densification combined with thermal modification of Norway spruce (*Picea abies* Karst) in industrial scale – Dimensional stability and durability aspects, *Holz Roh Werkst*. 66 (2008) 39–49. doi:10.1007/s00107-007-0198-0.
- [84] P. Navi, F. Girardet, Effects of Thermo-Hydro-Mechanical Treatment on the Structure and Properties of Wood, *Holzforschung*. 54 (2000) 287–293. doi:10.1515/HF.2000.048.
- [85] F.A. Kamke, A. Kutnar, Transverse Compression Behavior of Wood in Saturated Steam at 150-170 Degrees C, *Wood and Fiber Science*. 42 (2010) 377–387.
- [86] A. Kutnar, F.A. Kamke, Compression of wood under saturated steam, superheated steam, and transient conditions at 150°C, 160°C, and 170°C, *Wood Science and Technology*. 46 (2012) 73–88. doi:10.1007/s00226-010-0380-0.
- [87] F.A. Kamke, A. Kutnar, Influence of stress level on compression deformation of wood in 170°C transient steam conditions, *Wood Material Science and Engineering*. 6 (2011) 105–111. doi:10.1080/17480272.2010.535907.
- [88] C.H. Fang, N. Mariotti, A. Cloutier, A. Koubaa, P. Blanchet, Densification of wood veneers by compression combined with heat and steam, *European Journal of Wood and Wood Products*. 70 (2012) 155–163. doi:10.1007/s00107-011-0524-4.
- [89] K. Laine, K. Segerholm, M. Wålinder, L. Rautkari, M. Hughes, Wood densification and thermal modification: hardness, set-recovery and micromorphology, *Wood Science and Technology*. 50 (2016) 883–894. doi:10.1007/s00226-016-0835-z.
- [90] N. Morsing, Densification of wood - the influence of hygrothermal treatment on compression of beech perpendicular to grain. PhD Thesis, Technical University of Denmark, 2000.

- [91] L. Salmen, On the Interaction between Moisture and Wood Fiber Materials, Symposium - Materials Interactions Relevant to the Pulp, Paper, and Wood Industries. 197 (1990) 193–201. doi:10.1557/PROC-197-193.
- [92] A. Reiterer, S.E. Stanzl-Tschegg, Compressive behaviour of softwood under uniaxial loading at different orientations to the grain, *Mechanics of Materials*. 33 (2001) 705–715. doi:10.1016/S0167-6636(01)00086-2.
- [93] J.A.A. Nairn, Numerical Simulations of Transverse Compression and Densification in Wood, *Wood and Fiber Science*. 38 (2006) 576–591.
- [94] B. Anshari, Z. Guan, Finite Element Modeling of the Pre- Camber of Glulam Beams Reinforced By Compressed Wood, in: *Proceedings of World Conference on Timber Engineering*, Trentino, Italy, 2010.
- [95] K. Jung, S. Murakami, A. Kitamori, W.S. Chang, K. Komatsu, Improvement of glued-in-rod joint system using compressed wooden dowel, *Holzforschung*. 64 (2010) 799–804.
- [96] T. Ohuchi, M. Kinjyo, Y. Murase, Withdrawal strength of new type connection with sugi compressed-dowel, in: *Proceedings of World Conference on Timber Engineering*, Miyazaki, Japan, 2010.
- [97] P. Navi, F. Heger, Combined Densification and Thermo-Hydro-Mechanical Processing of Wood, *MRS Bulletin*. 29 (2004) 332–336.
- [98] L. Rautkari, M. Hughes, Eliminating Set-recovery in Densified Wood using a Steam Heat-treatment Process, in: *Proceedings European Conference on Wood Modification*, Stockholm, Sweden, 2009: pp. 393–396.
- [99] D. Tu, X. Su, T. Zhang, W. Fan, Q. Zhou, Thermo-mechanical densification of populus tomentosa var. tomentosa with low moisture content, *BioResources*. 9 (2014) 3846–3856.
- [100] M. Inoue, M. Norimoto, M. Tanahashi, R.M. Rowell, Steam or heat fixation of compressed wood, *Wood and Fiber Science*. 25 (1993) 224–235.
- [101] M. Inoue, T. Morooka, M. Norimoto, R.M. Rowell, G. Egawa, Permanent Fixation of Compressive Deformation of Wood .2. Mechanisms of Permanent Fixation, in: *Chemical Modification of Lignocellulosics*, Rotorura, New Zealand, 1992: pp. 181-189.
- [102] B. Anshari, Z.W. Guan, A. Kitamori, K. Jung, I. Hassel, K. Komatsu, Mechanical and moisture-dependent swelling properties of compressed Japanese cedar, *Construction*

- and *Building Materials*. 25 (2011) 1718–1725. doi:10.1016/j.conbuildmat.2010.11.095.
- [103] P. Grönquist, T. Schnider, A. Thoma, F. Gramazio, M. Kohler, Investigations on densified beech wood for application as a swelling dowel in timber joints, *Holzforschung*. 76 (2019) 1–10. doi:https://doi.org/10.1515/hf-2018-0106.
- [104] A. Kutnar, F.A. Kamke, M. Sernek, Density profile and morphology of viscoelastic thermal compressed wood, *Wood Science and Technology*. 43 (2009) 57–68. doi:10.1007/s00226-008-0198-1.
- [105] A. Darwis, I. Wahyudi, W. Dwianto, T.D. Cahyono, Densified wood anatomical structure and the effect of heat treatment on the recovery of set, *Journal of the Indian Academy of Wood Science*. 14 (2017) 24–31.
- [106] C.H. Fang, N. Mariotti, A. Cloutier, A. Koubaa, P. Blanchet, Densification of wood veneers by compression combined with heat and steam, *European Journal of Wood and Wood Products*. 70 (2012) 155–163.
- [107] M. Gong, L. Li, Breakeven point in ultimate thickness between moisture-reduced shrinkage and thickness recovery of densified softwood species: part 1 : at room temperature, *Wood and Fiber Science*. 50 (2017) 1–8.
- [108] H. Pelit, A. Sönmez, M. Budakçı, Effects of ThermoWood® Process Combined with Thermo-Mechanical Densification on some Physical Properties of Scots Pine (*Pinus sylvestris* L.), *BioResources*. 9 (2014) 4552–4567.
- [109] H. Pelit, A. Sönmez, M. Budakçı, Effects of thermomechanical densification and heat treatment on density and Brinell hardness of scots pine (*Pinus sylvestris* L.) and Eastern beech (*Fagus orientalis* L.), *BioResources*. 10 (2015) 3097–3111.
- [110] J. Wehsener, C. Brischke, L. Meyer-Veltrup, J. Hartig, P. Haller, Physical, mechanical and biological properties of thermo- mechanically densified and thermally modified timber using the Vacu3-process, *European Journal of Wood and Wood Products*. 76 (2018) 809–821. doi:10.1007/s00107-017-1278-4.
- [111] P. Bekhta, S. Proszyk, T. Krystofiak, J. Sedliacik, I. Novak, M. Mamonova, Effects of short-term thermomechanical densification on the structure and properties of wood veneers, *Wood Material Science and Engineering*. 12 (2015) 40–54.
- [112] N. Cruz, C. Bustos, M.G. Aguayo, A. Cloutier, R. Castillo, Impact of the Chemical Composition of *Pinus radiata* Wood on its Physical and Mechanical Properties Following Thermo-Hygro-mechanical Densification, *BioResources*. 1226 (2018).

- [113] M. Schwarzkopf, Densified wood impregnated with phenol resin for improved set-recovery, *Wood Material Science and Engineering*. 16 (2020) 34–41. doi:10.1080/17480272.2020.1729236.
- [114] H. Yoshihara, S. Tsunematsu, Bending and shear properties of compressed Sitka spruce, *Wood Science and Technology*. 41 (2007) 117–131. doi:10.1007/s00226-006-0091-8.
- [115] F.A. Kamke, DENSIFIED RADIATA PINE FOR STRUCTURAL COMPOSITES, *Maderas. Ciencia y Tecnología*. 8 (2006) 83–92. doi:10.4067/S0718-221X2006000200002.
- [116] A. Kutnar, F.A. Kamke, M. Sernek, The mechanical properties of densified VTC wood relevant for structural composites, *Holz Roh Werkst*. 66 (2008) 439–446. doi:10.1007/s00107-008-0259-z.
- [117] F.A. Kamke, H. Sizemore, Viscoelastic thermal compression of wood. United States Patent Application Publication, US 2005/0006004 A1, 2005.
- [118] K. Tanaka, Y. Demoto, J. Ouchi, M. Inoue, Strength property of densified Sugi adopted as material of connector, in: *Proceedings of World Conference on Timber Engineering*, Trentino, Italy, 2010.
- [119] S. Shekhorkina, A. Kesariisky, M. Makhinko, T. Nikiforova, O. Savytskyi, Experimental Investigation and FEM Modeling of Glued Timber Connections with Slotted-In Steel Plates, *Slovak Journal of Civil Engineering*. 27 (2019) 18–23. doi:10.2478/sjce-2019-0027.
- [120] A.J.M. Leijten, D. Brandon, Advances in moment transferring dwv reinforced timber connections – Analysis and experimental verification, Part 1, *Construction and Building Materials*. 43 (2013) 614–622. doi:10.1016/j.conbuildmat.2013.03.020.
- [121] M. Snow, A. Asiz, Z. Chen, Y.H. Chui, North American practices for connections in wood construction, *Progress in Structural Engineering and Materials*. 8 (2006) 39–48. doi:10.1002/pse.212.
- [122] TRADA, Timber Connections, Learning Resources Modules. (2016). <https://www.trada.co.uk/academic/timber-connections/>.
- [123] D. Sandberg, Additives in wood products—today and future development, in: A. Kutnar, S.S. Muthu (Eds.), *Environmental Impacts of Traditional and Innovative Forest-Based Bioproducts*, Springer, Singapore, 2016: pp. 19–44.
- [124] J. Moradei, J. Brütting, C. Fivet, N. Sherrow-Groves, D. Wilson, A. Fischer, J. Ye, J.

- Cañada, Structural Characterization of Traditional Moment-Resisting Timber Joinery, in: Proceedings of the IASS Symposium 2018, Creativity in Structural Design, Boston, USA, 2018.
- [125] A. Bukauskas, P. Mayencourt, P. Shepherd, B. Sharma, C. Mueller, P. Walker, J. Bregulla, Whole timber construction: A state of the art review, *Construction and Building Materials*. 213 (2019) 748–769. doi:10.1016/j.conbuildmat.2019.03.043.
- [126] W.S. Chang, A. Thomson, R. Harris, P. Walker, J. Shanks, Development of all-wood connections with plywood flitch plate and oak pegs, *Advances in Structural Engineering*. 14 (2011) 123–131. doi:10.1260/1369-4332.14.2.123.
- [127] J. Jasieńko, T. Nowak, A. Karolak, Historical carpentry joints, *Journal of Heritage Conservation*. 40 (2014) 58–82.
- [128] E. Erman, Timber joint design: The geometric breakdown method, *Building Research and Information*. 30 (2002) 446–469. doi:10.1080/09613210210150991.
- [129] K. Šobra, C.F. Ferreira, M. Riggio, D.F.D. Ayala, J.-R. Aira, A new tool for the structural assessment of historic carpentry joints, in: Proceedings of 3rd International Conference on Structural Health Assessment of Timber Structures (SHATIS), Wrocław - Poland, 2015.
- [130] K. Bonham, Ken's Great Barns, (2020). http://greatbarns.org.uk/barn_intro/barn_intro14.html (accessed August 1, 2020).
- [131] E. Hirst, A. Brett, A. Thomson, P. Walker, R. Harris, The Structural Performance of Traditional Oak Tension & Scarf Joints, in: Proceedings of World Conference on Timber Engineering, Miyazaki, Japan, 2008.
- [132] A. Arciszewska-Kedzior, J. Kunecký, H. Hasníková, V. Sebera, Lapped scarf joint with inclined faces and wooden dowels: Experimental and numerical analysis, *Engineering Structures*. 94 (2015) 1–8. doi:10.1016/j.engstruct.2015.03.036.
- [133] A. Arciszewska-Kędzior, J. Kunecký, H. Hasníková, Mechanical response of a lap scarf joint with inclined faces and wooden dowels under combined loading, in: Proceedings of the International Structural Health Assessment of Timber Structures (SHATIS), Wrocław - Poland, 2015: pp. 849–858. doi:10.17425/WK46WOODEN.
- [134] P. Fajman, J. Máca, The effect of inclination of scarf joints with four pins, *International Journal of Architectural Heritage*. 12 (2018) 599–606. doi:10.1080/15583058.2018.1442520.
- [135] J. Shanks, P. Walker, Strength and Stiffness of All-Timber Pegged Connections,

Journal of Materials in Civil Engineering. 21 (2009) 10–18. doi:10.1061/(ASCE)0899-1561(2009)21:1(10).

- [136] R.J. Schmidt, C.E. Daniels, Design Considerations for Mortise and Tenon. Research Report. University of Wyoming, Laramie, Wyoming, 1999.
- [137] R.L. Brungraber, Traditional timber joinery: A modern analysis. PhD thesis, Stanford University, California, 1985.
- [138] R.J. Schmidt, R.B. Mackay, Timber Frame Tension Joinery. Research Report. University of Wyoming, Laramie, Wyoming, University of Wyoming, Laramie, Wyoming, 1997.
- [139] J.F. Miller, R.J. Schmidt, Capacity of pegged mortise and tenon joinery. Research Report. University of Wyoming, Laramie, Wyoming, 2004.
- [140] J. Shanks, P. Walker, Testing of traditional connections in green oak carpentry, in: 8th World Conference on Timber Engineering, Lahti, Finland, 2004: pp. 8–11. <http://opus.bath.ac.uk/681/>.
- [141] J. Shanks, Developing rational guidelines for traditional joints in oak frame construction. PhD Thesis, University of Bath, 2005.
- [142] J.D. Shanks, W.-S. Chang, K. Komatsu, Experimental study on mechanical performance of all-softwood pegged mortice and tenon connections, Biosystems Engineering. 100 (2008) 562–570. doi:10.1016/j.biosystemseng.2008.03.012.
- [143] S. Pang, J. Oh, J. Park, C. Park, J. Lee, Moment-Carrying Capacity of Dovetailed Mortise and Tenon Joints with or without Beam Shoulder, Journal of Structural Engineering. 137 (2011) 785–789. doi:10.1061/(ASCE)ST.1943-541X.0000323.
- [144] Z.W. Guan, A. Kitamori, K. Komatsu, Experimental study and finite element modelling of Japanese “Nuki” joints - Part two: Racking resistance subjected to different wedge configurations, Engineering Structures. 30 (2008) 2041–2049. doi:10.1016/j.engstruct.2008.01.004.
- [145] W.S. Chang, M.F. Hsu, K. Komatsu, Rotational performance of traditional Nuki joints with gap I: Theory and verification, Journal of Wood Science. 52 (2006) 58–62. doi:10.1007/s10086-005-0734-7.
- [146] W.S. Chang, M.F. Hsu, Rotational performance of traditional Nuki joints with gap II: The behavior of butted Nuki joint and its comparison with continuous Nuki joint, Journal of Wood Science. 53 (2007) 401–407. doi:10.1007/s10086-007-0880-1.
- [147] H. Suesada, K. Miyamoto, T. Shibusawa, K. Aoki, M. Inayama, Reinforcing effect of

- hardwoods on the moment resistance performance of traditional Japanese “nuki”-column joints, *Journal of Wood Science*. 65 (2019). doi:10.1186/s10086-019-1844-y.
- [148] R. Crocetti, Large-Span Timber Structures, in: *Proceedings of the World Congress on Civil, Structural, and Environmental Engineering*, Prague, Czech Republic, 2016. doi:10.11159/icsenm16.124.
- [149] J.-F. Bocquet, R. Lemaître, T.K. Bader, Design recommendations and example calculations for dowel-type connections with multiple shear planes, in: *Design of Connections in Timber Structures : A State-of-the-Art Report by COST Action FP1402/WG3*, 2018: pp. 241–295. <http://urn.kb.se/resolve?urn=urn:nbn:se:lnu:diva-78702>.
- [150] C. Zhang, Reinforcement of Timber Dowel-Type Connections Using Self-Tapping Screws. PhD Thesis, University of Bath, United Kingdom, 2018.
- [151] S. Rossi, R. Crocetti, D. Honfi, E.F. Hansson, Load-bearing capacity of ductile multiple shear steel-to-timber connections, in: *Proceedings of the World Conference on Timber Engineering (WCTE)*, Vienna, Austria, 2016.
- [152] Y. Ma, X. Song, T. Xu, L. Luo, Rotational Behavior of Bolted Glulam Beam-to-Column Connections Reinforced with Section Steel, *Applied Mechanics and Materials*. 858 (2016) 15–21. doi:10.4028/www.scientific.net/AMM.858.15.
- [153] X.H. Fan, S.D. Zhang, W.J. Qu, Load-Carrying Behaviour of Dowel-Type Timber Connections with Multiple Slotted-in Steel Plates, *Applied Mechanics and Materials*. 94–96 (2011) 43–47. doi:10.4028/www.scientific.net/AMM.94-96.43.
- [154] M. Yurrita, J.M. Cabrero, P. Quenneville, Brittle failure in the parallel-to-grain direction of multiple shear softwood timber connections with slotted-in steel plates and dowel-type fasteners, *Construction and Building Materials*. 216 (2019) 296–313. doi:10.1016/j.conbuildmat.2019.04.100.
- [155] T.H. Miller, Metal-Plate-Connected Wood Joints : A literature review, *Forest Research Laboratory*. (1996). doi:10.1016/j.profnurs.2010.10.006.
- [156] Z. Wang, K. Liu, H. Ren, Z. Huang, H. Li, G. Zhang, Connections design and its load carrying-capacity for post and beam joints of larch glulam, in: *Proceedings of the World Conference on Timber Engineering*, Auckland, New Zealand, 2012: pp. 1–5.
- [157] A. Awaludin, W. Smittakorn, T. Hayashikawa, T. Hirai, M- θ curve of timber connection with various bolt arrangements under monotonic loading, *Journal of Structural Engineering*. 53 (2007) 853–862. doi:10.11532/structcivil.53A.853.

- [158] M. Wang, X. Song, X. Gu, Y. Wu, Mechanical Behavior of Bolted Glulam Beam-To-Column Connections With Slotted-in Steel Plates Under Pure Bending, in: Proceedings of the World Conference on Timber Engineering (WCTE), Vienna Austria, 2016.
- [159] M. Wang, X. Song, X. Gu, J. Tang, Bolted glulam beam-column connections under different combinations of shear and bending, *Engineering Structures*. 181 (2019) 281–292. doi:10.1016/j.engstruct.2018.12.024.
- [160] A. Jorissen, M. Fragiaco, General notes on ductility in timber structures, *Engineering Structures*. 33 (2011) 2987–2997. doi:10.1016/j.engstruct.2011.07.024.
- [161] C. Zhang, H. Guo, K. Jung, R. Harris, W.-S. Chang, Using self-tapping screw to reinforce dowel-type connection in a timber portal frame, *Engineering Structures*. 178 (2019) 656–664. doi:10.1016/j.engstruct.2018.10.066.
- [162] H. Li, F. Lam, H. Qiu, Flexural performance of spliced beam connected and reinforced with self-tapping wood screws, *Engineering Structures*. 152 (2017) 523–534. doi:10.1016/j.engstruct.2017.08.032.
- [163] H.J. Blaß, P. Schädle, Ductility aspects of reinforced and non-reinforced timber joints, *Engineering Structures*. 33 (2011) 3018–3026. doi:10.1016/j.engstruct.2011.02.001.
- [164] T. Gečys, A. Daniunas, T.K. Bader, L. Wagner, J. Eberhardsteiner, 3D finite element analysis and experimental investigations of a new type of timber beam-to-beam connection, *Engineering Structures*. 86 (2015) 134–145. doi:10.1016/j.engstruct.2014.12.037.
- [165] T. Gečys, A. Daniunas, Experimental investigation of glued laminated timber beam to beam connections filled with cement based filler, *Procedia Engineering*. 57 (2013) 320–326. doi:10.1016/j.proeng.2013.04.043.
- [166] T. Gečys, A. Daniūnas, Rotational stiffness determination of the semi-rigid timber-steel connection, *Journal of Civil Engineering and Management*. 23 (2017) 1021–1028. doi:10.3846/13923730.2017.1374305.
- [167] D. Brandon, Moment transmitting dvw reinforced timber connection with internal steel plate and expanded tube fasteners influence of restrain effects on the behaviour. Master Thesis, Eindhoven University of Technology, 2011.
- [168] D. Brandon, A.J.M. Leijten, Advances in moment transferring dvw reinforced timber connections - Numerical analyses and verification, Part 2, *Construction and Building Materials*. 56 (2014) 32–43. doi:10.1016/j.conbuildmat.2014.01.026.
- [169] A.J.M. Leijten, *Densified Veneer: An Alternative to Steel Plate in Timber Joints*,

- Structural Engineering International. 3 (1993) 181–183.
doi:10.2749/101686693780607859.
- [170] P.D. Rodd, A.J.M. Leijten, High-performance dowel-type joints for timber structures, *Progress in Structural Engineering and Materials*. 5 (2003) 77–89.
doi:10.1002/pse.144.
- [171] M. He, J. Luo, D. Tao, Z. Li, Y. Sun, G. He, Rotational behavior of bolted glulam beam-to-column connections with knee brace, *Engineering Structures*. 207 (2020) 110251. doi:10.1016/j.engstruct.2020.110251.
- [172] F. Solarino, L. Giresini, W.-S. Chang, H. Huang, Experimental Tests on a Dowel-Type Timber Connection and Validation of Numerical Models, *Buildings*. 7 (2017) 116.
doi:10.3390/buildings7040116.
- [173] Y. Liu, H. Xiong, Lateral performance of a semi-rigid timber frame structure: theoretical analysis and experimental study, *Journal of Wood Science*. 64 (2018) 591–600. doi:10.1007/s10086-018-1727-7.
- [174] F. Lam, M. Gehloff, M. Closen, Moment-resisting bolted timber connections, in: *Proceedings of the Institution of Civil Engineers*, 2001: p. 30.
doi:10.1680/stbu.2010.163.4.267.
- [175] M. Gehloff, M. Closen, F. Lam, Reduced Edge Distances in Bolted Timber Moment Connections With Perpendicular To Grain Reinforcements, in: *Proceedings of the World Conference on Timber Engineering*, Trentino, Italy, 2010.
- [176] A. Awaludin, Y. Sasaki, A. Oikawa, T. Hirai, T. Hayashikawa, Moment Resisting Timber Joints with High-Strength Steel Dowels: Natural Fiber Reinforcements, in: *Proceedings of the World Conference on Timber Engineering*, Trentino, Italy, 2010.
http://www.ewpa.com/Archive/2010/june/Paper_275.pdf.
- [177] A.J.M. Leijten, *Densified veneer wood reinforced timber joints with expanded tube fasteners*. PhD Thesis, Delft University of Technology, 1998.
- [178] I. Hassel, P. Berard, K. Komatsu, Development of wooden block shear wall - Improvement of stiffness by utilizing elements of densified wood, *Holzforschung*. 62 (2008) 584–590. doi:10.1515/HF.2008.091.
- [179] K. Jung, A. Kitamori, M. Minami, K. Komatsu, Development of joint system using by compressed wooden fastener, in: *Proceedings of the World Conference on Timber Engineering*, Miyazaki, Japan, 2008.
- [180] L.B. Sandberg, W. Bulleit, E.H. Reid, Strength and stiffness of oak pegs in traditional

- timber-frame joints, *Journal of Structural Engineering*. 126 (2000) 717–723. doi:10.1061/(ASCE)0733-9445(2000)126:6(717).
- [181] EN 408:2010+A1:2012. Timber structures - Structural timber and glued laminated timber - Determination of some physical and mechanical properties, CEN, Comité Européen de Normalisation, Brussels, Belgium, (2012).
- [182] EN 383:2007. Timber structures - test methods - determination of embedment strength and foundation values for dowel type fasteners, CEN, Comité Européen de Normalisation, Brussels, Belgium, (2007).
- [183] EN 26891:1991. Timber structures - Joint made with mechanical fasteners - General principles for the determination of strength and deformation characteristics, CEN, Comité Européen de Normalisation, Brussels, Belgium, (1991).
- [184] EN 409:2009. Timber structures - Test methods - Determination of the yield moment of dowel type fasteners, CEN, Comité Européen de Normalisation, Brussels, Belgium, (2009).
- [185] A. Thomson, The structural performance of non-metallic timber connections. PhD Thesis, University of Bath, United Kingdom, 2010.
- [186] ASTM-D4475-02:2016. Standard Test Method for Apparent Horizontal Shear Strength of Pultruded Reinforced Plastic Rods By the Short-Beam Method 1, (2016).
- [187] EN 12512:2001/A1:2005. Timber Structures - Test methods - Cyclic testing of joints made with mechanical fasteners, CEN, Comité Européen de Normalisation, Brussels, Belgium, (2005).
- [188] BS 373: 1957. Methods of testing small Clear specimens of timber, British Standard Institution (BSI), (1957).
- [189] EN 14358:2016. Timber structures - Calculation and verification of characteristic values, CEN, Comité Européen de Normalisation, Brussels, Belgium, (2016).
- [190] P. Palma, P. Kobel, A. Minor, A. Frangi, Dowelled Timber Connections With Internal Members of Densified Veneer Wood and Fibre-Reinforced Polymer Dowels, in: World Conference on Timber Engineering, Vienna, Austria, 2016.
- [191] A. Minor, Non-metallic dowelled timber connections with internal panels of densified veneer wood. Master Thesis, ETH Zurich, 2014.
- [192] C. Sandhaas, G.J.P. Ravenshorst, H.J. Blass, J.W.G. van de Kuilen, Embedment tests parallel-to-grain and ductility aspects using various wood species, *European Journal of Wood and Wood Products*. 71 (2013) 599–608. doi:10.1007/s00107-013-0718-z.

- [193] R. Jockwer, G. Fink, J. Köhler, Assessment of the failure behaviour and reliability of timber connections with multiple dowel-type fasteners, *Engineering Structures*. 172 (2018) 76–84. doi:10.1016/j.engstruct.2018.05.081.
- [194] EN 10025-2:2004 . Hot rolled products of structural steels - Part 2: Technical delivery conditions for non-alloy structural steels, CEN, Comité Européen de Normalisation, Brussels, Belgium, 44 (2012) 7–10.
- [195] C. Ceraldi, V. Mormone, E. Russo Ermolli, Restoring of timber structures: Connections with timber pegs, in: *Proceedings of Structural Analysis of Historic Construction: Preserving Safety and Significance*, CRC Press, Bath, United Kingdom, 2008.
- [196] C. Fang, A. Cloutier, P. Blanchet, C. Barbuta, *Densified Engineered Wood Flooring for Heavy-Duty Use*. Technical report. Université Laval, 2011.
- [197] A. Kitamori, K.H. Jung, T. Mori, K. Komatsu, Mechanical Properties of Compressed Wood in Accordance with the Compression Ratio, *Mokuzai Gakkaishi*. 56 (2010) 67–78.
- [198] P.E. Humphrey, *Wood : Thermal Properties*, *Encyclopedia of Materials: Science and Technology* (Second Edition). (2001) 9748–9750.
- [199] D. Dauksta, Brettstapel. Technical Report. Wales Forest Business Partnership, 2014.
- [200] J.B. Plowas, W.; Bell, T.; Hairstans, R.; Williamson, *Understandig the compatibility of UK resource for dowel laminated timber construction*, *TH Building Construction*. (2015) 1–12. https://napier-surface.worktribe.com/169670/1/hairstans_v2.pdf.
- [201] J. Mayo, *Solid Wood: Case Studies in Mass Timber Architecture, Technology and Design*, First, Routledge, 2015. <https://www.archdaily.com/600021/solid-wood-the-rise-of-mass-timber-architecture%3E> ISSN 0719-8884.
- [202] ISO, ISO 12580. Timber structures — Glued laminated timber — Methods of test for glue-line delamination, 44 (2015).
- [203] EN 13182:2016. Timber Structures - Test methods - Withdrawal capacity of timber fasteners, CEN, Comité Européen de Normalisation, Brussels, Belgium, 44 (2015).
- [204] D. Sandberg, O. Sö Derström, Crack formation due to weathering of radial and tangential sections of pine and spruce, *Wood Material Science and Engineering*. 1 (2006) 12–20. doi:10.1080/17480270600644407.
- [205] K.U. Schober, A.M. Harte, R. Kliger, R. Jockwer, Q. Xu, J.F. Chen, FRP reinforcement of timber structures, *Construction and Building Materials*. 97 (2015) 106–118.

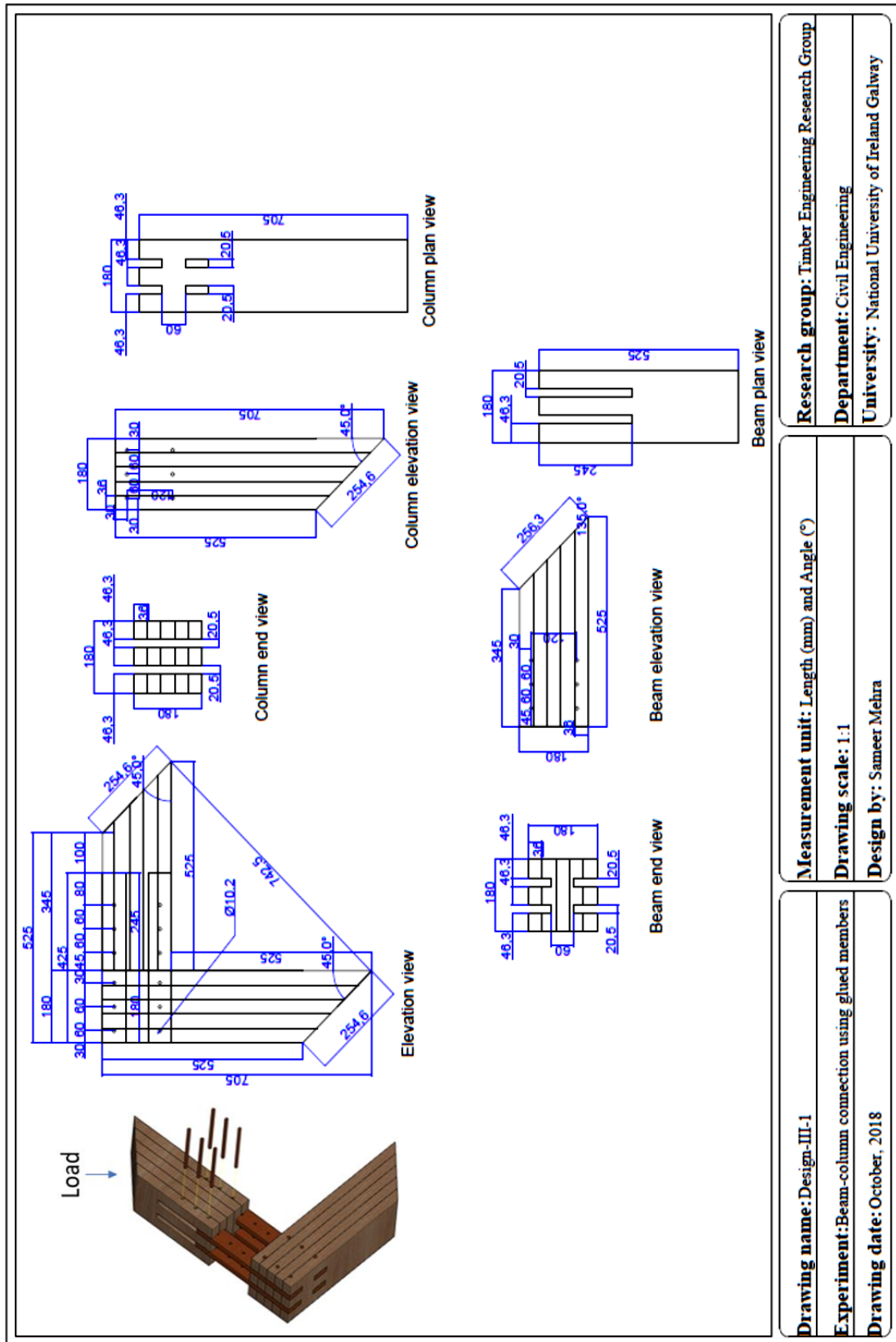
doi:10.1016/j.conbuildmat.2015.06.020.

- [206] H. Yang, W. Liu, W. Lu, S. Zhu, Q. Geng, Flexural behavior of FRP and steel reinforced glulam beams: Experimental and theoretical evaluation, *Construction and Building Materials*. 106 (2016) 550–563. doi:10.1016/j.conbuildmat.2015.12.135.
- [207] K.A. Malo, R.B. Abrahamsen, M.A. Bjertnæs, Some structural design issues of the 14-storey timber framed building “Treet” in Norway, *European Journal of Wood and Wood Products*. 74 (2016) 407–424. doi:10.1007/s00107-016-1022-5.
- [208] EN 14080. Timber structures - Glued laminated timber and glued solid timber - Requirements, (2013).
- [209] Hans Hundegger AG, Joinery Machine K2i. Product Manual, (2015). www.hundegger.de.
- [210] Micro-Epsilon, optoNCDT // Laser displacement sensors (triangulation), (2010). <https://www.micro-epsilon.com/download/products/cat--capaNCDT--en.pdf>.
- [211] Denison Mayes Group, Denison hydraulic testing machine - Model T42B, (2020). <https://www.denisonmayesgroup.com/Universal-default.htm> (accessed December 15, 2020).
- [212] R.G. Erikson, R.J. Schmidt, Behavior of Traditional Timber Frame Structures Subjected To Lateral Load. Research Report. University of Wyoming, Laramie, Wyoming, 2003.
- [213] A. Sotayo, S. Au, Z. Guan, Finite Element Modelling and Testing of Timber Laminated Beams Fastened With Compressed Wood Dowels, in: *Proceedings of the WCTE World Conference on Timber Engineering*, Seoul, Republic of Korea, 2018.
- [214] L. Bouhala, D. Fiorelli, A. Makradi, S. Belouettar, A. Sotayo, D.F. Bradley, Z. Guan, Advanced numerical investigation on adhesive free timber structures, *Composite Structures*. 246 (2020) 112389. doi:10.1016/j.compstruct.2020.112389.
- [215] Maschinenfabrik ALBERT GmbH, INKOMA - GROUP SGT screw jack. Product Manual, (2014).
- [216] R. Jockwer, A. Jorissen, Stiffness and deformation of connections with dowel-type fasteners. *Design of Connections in Timber Structures: A state-of-the-art report by COST Action FP1402 / WG3*, Shaker Verlag GmbH, 2018.
- [217] R.J. Leichti, R.A. Hyde, M.L. French, S.G. Camillos, The continuum of connection rigidity in timber structures, *Wood and Fiber Science*. 32 (2000) 11–19.
- [218] C. O’Ceallaigh, A.M. Harte, The elastic and ductile behaviour of CLT wall-floor

- connections and the influence of fastener length, *Engineering Structures*. 189 (2019) 319–331. doi:10.1016/j.engstruct.2019.03.100.
- [219] C. Maraveas, K. Miamis, C.E. Matthaiou, Performance of Timber Connections Exposed to Fire: A Review, *Fire Technology*. 51 (2015) 1401–1432. doi:10.1007/s10694-013-0369-y.
- [220] D. Brandon, Fire and structural performance of non-metallic timber connections. PhD Thesis, University of Bath, Bath, United Kindom, 2015.
- [221] L. Peng, G. Hadjisophocleous, J. Mehaffey, M. Mohammad, Fire resistance performance of unprotected woodwoodwood and woodsteelwood connections: A literature review and new data correlations, *Fire Safety Journal*. 45 (2010) 392–399. doi:10.1016/j.firesaf.2010.08.003.
- [222] M.U. Pedersen, Dowel Type Timber Connections. PhD Thesis, Technical University of Denmark, 2002.

Appendix-A

Design-III-1

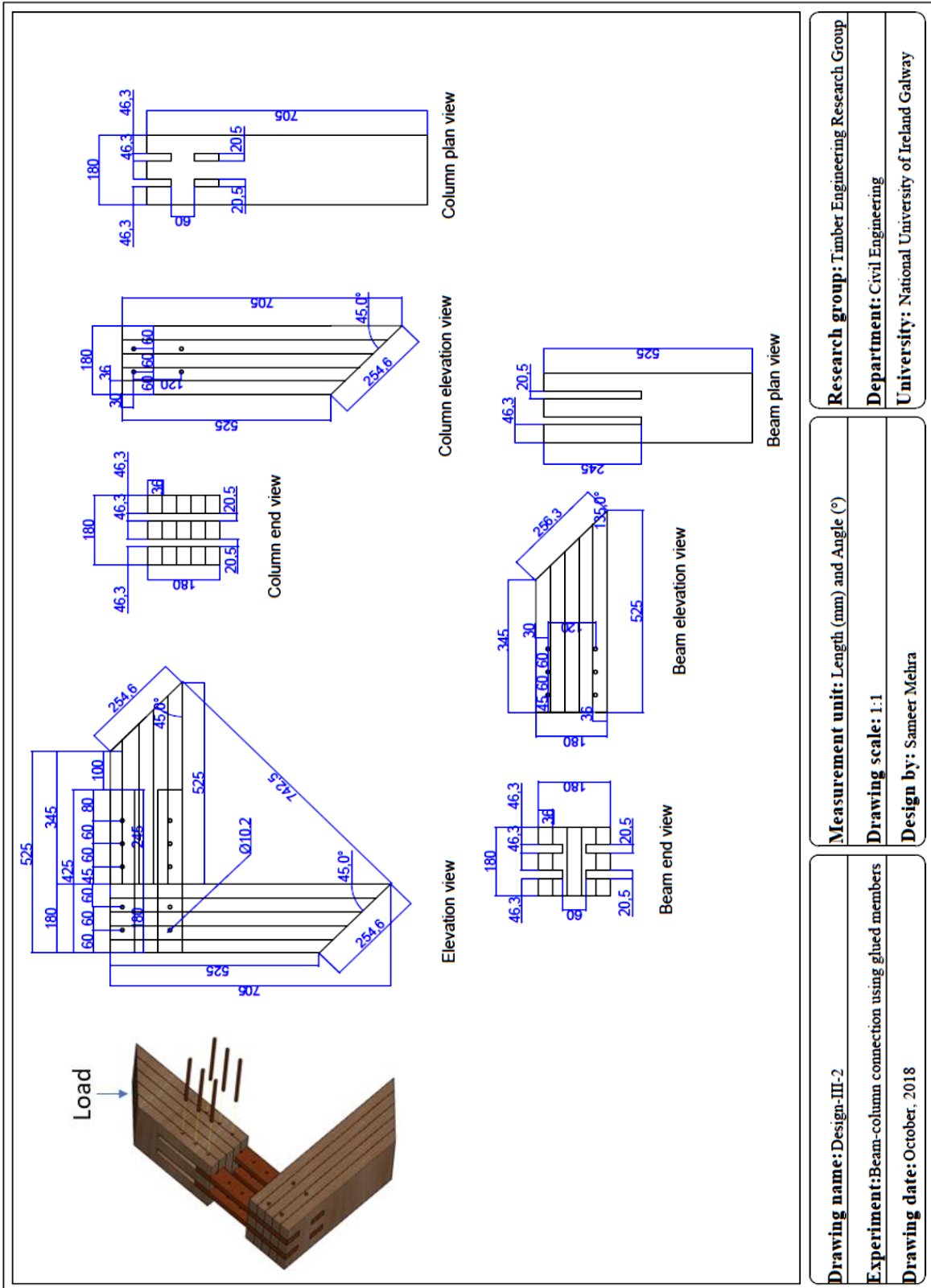


Research group: Timber Engineering Research Group
Department: Civil Engineering
University: National University of Ireland Galway

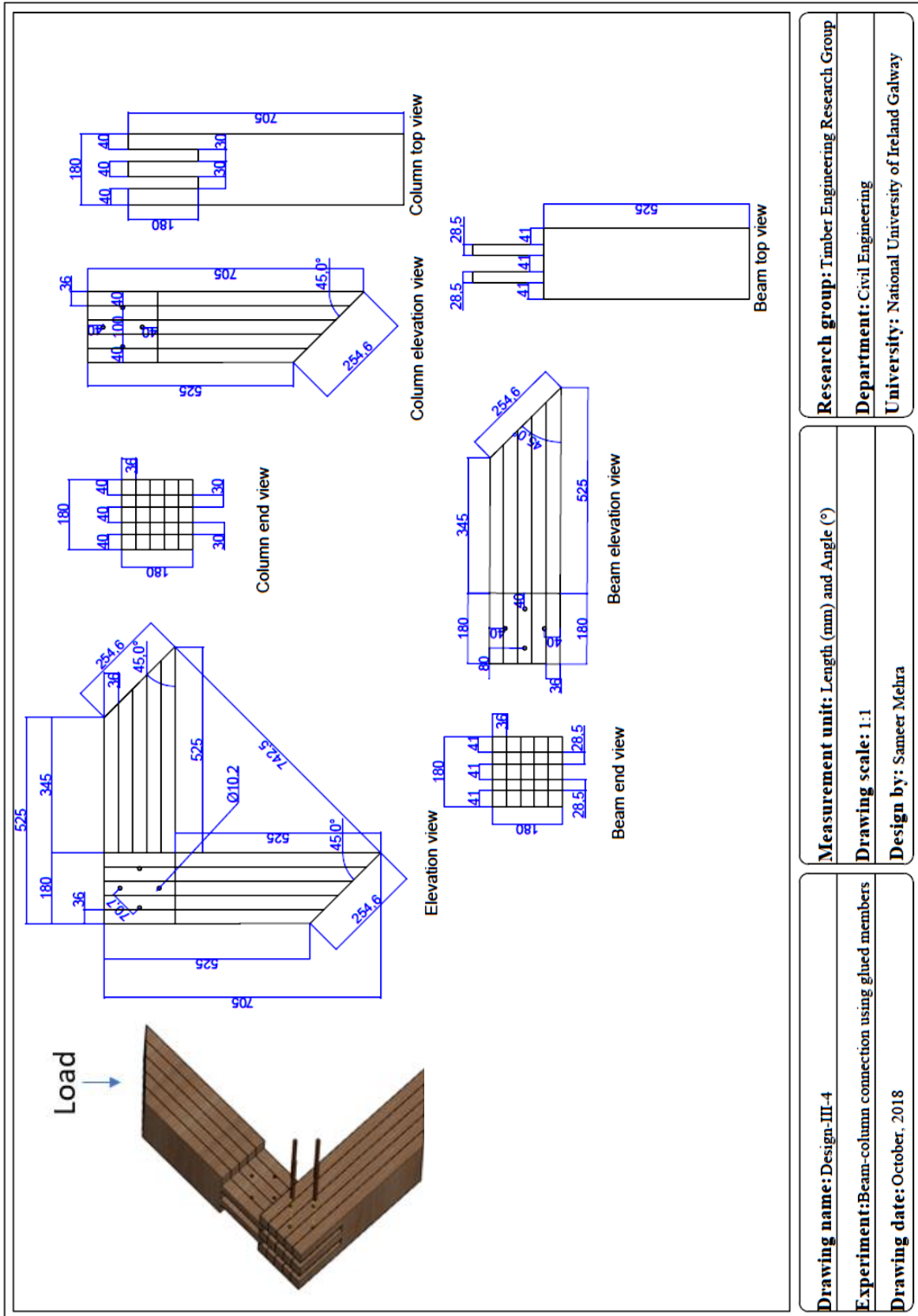
Measurement unit: Length (mm) and Angle (°)
Drawing scale: 1:1
Design by: Sameer Mehra

Drawing name: Design-III-1
Experiment: Beam-column connection using glued members
Drawing date: October, 2018

Design-III-2



Design-III-4

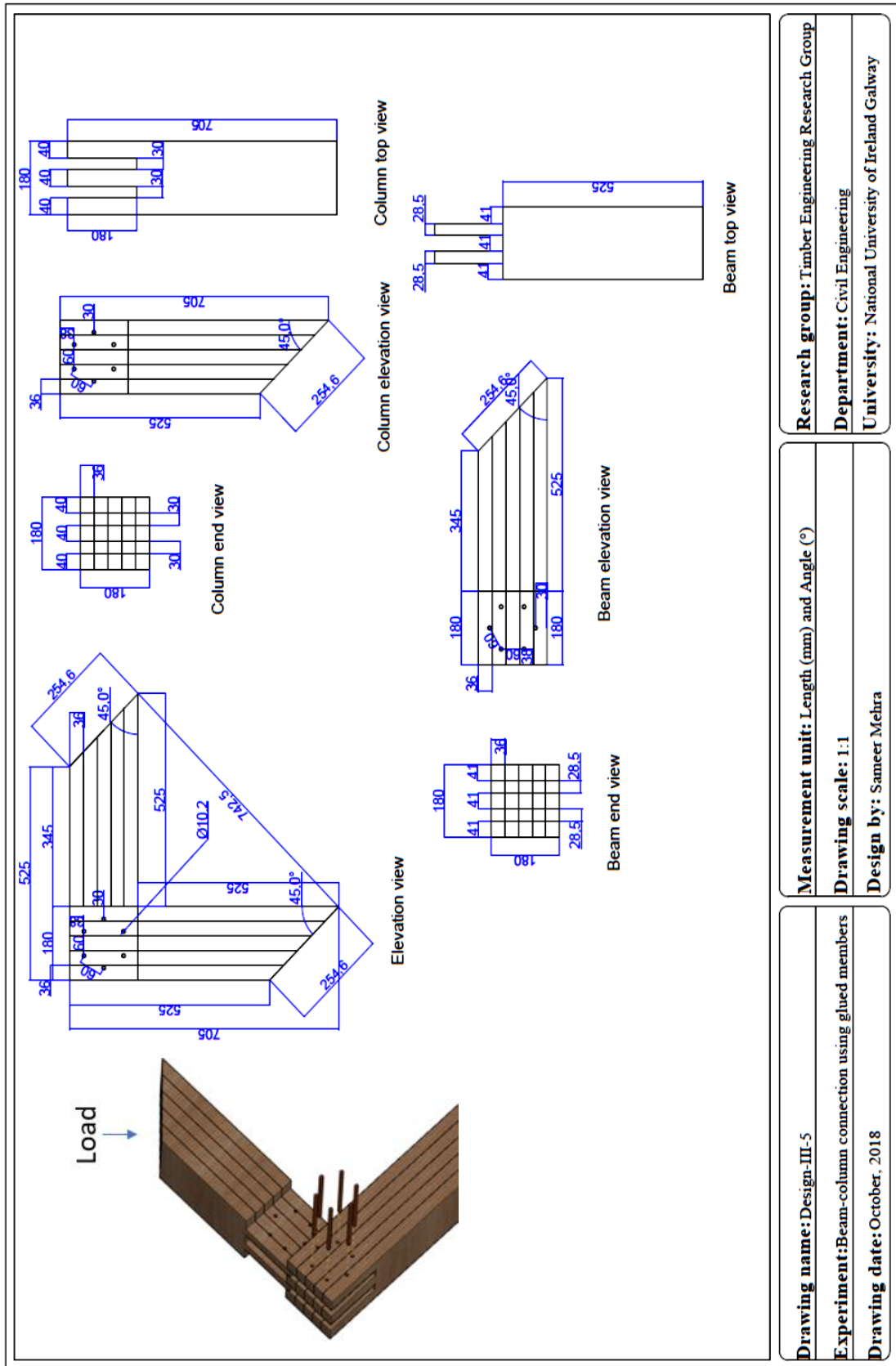


Research group: Timber Engineering Research Group
Department: Civil Engineering
University: National University of Ireland Galway

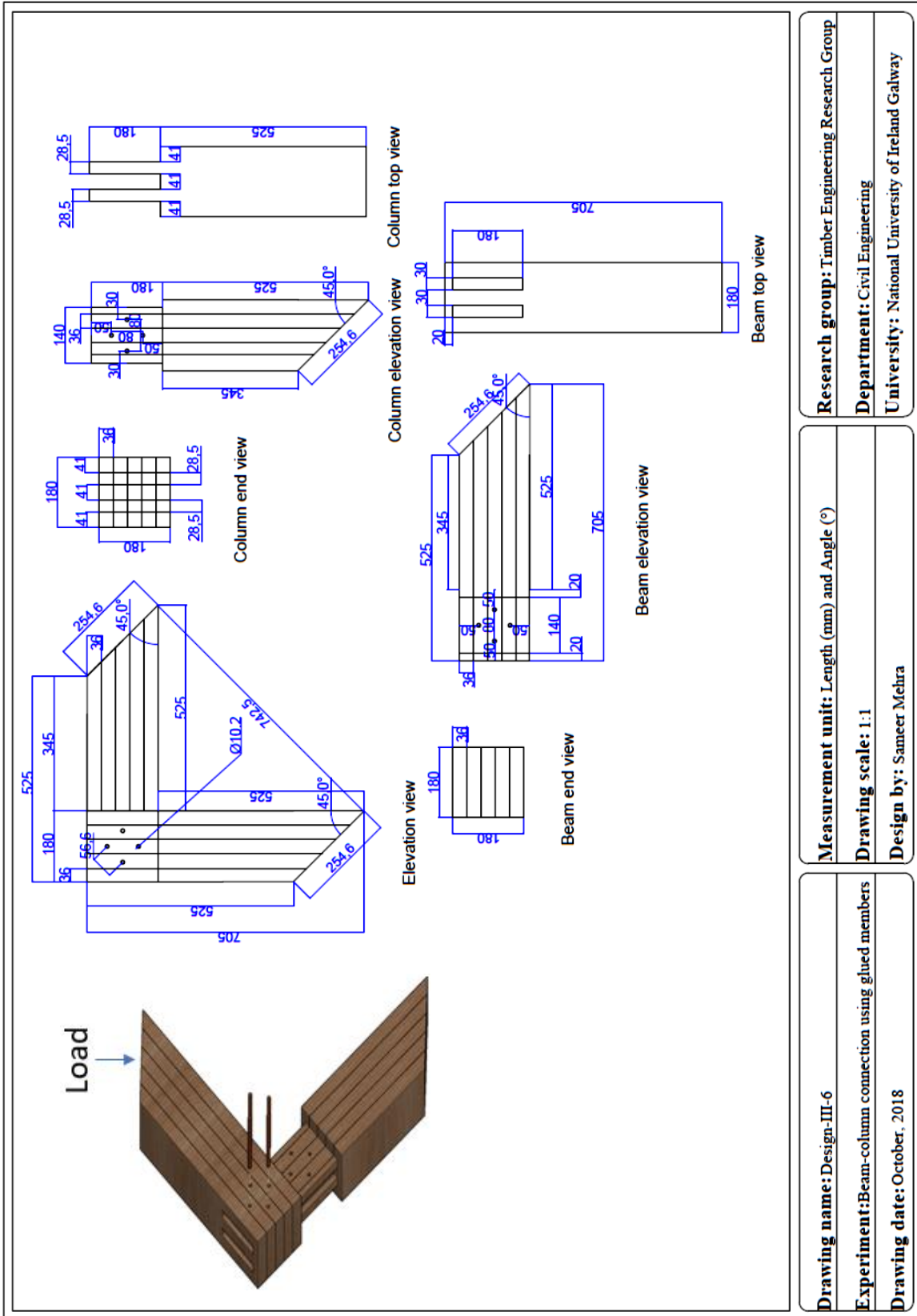
Measurement unit: Length (mm) and Angle (°)
Drawing scale: 1:1
Design by: Sameer Mehra

Drawing name: Design-III-4
Experiment: Beam-column connection using glued members
Drawing date: October, 2018

Design-III-5



Design-III-6



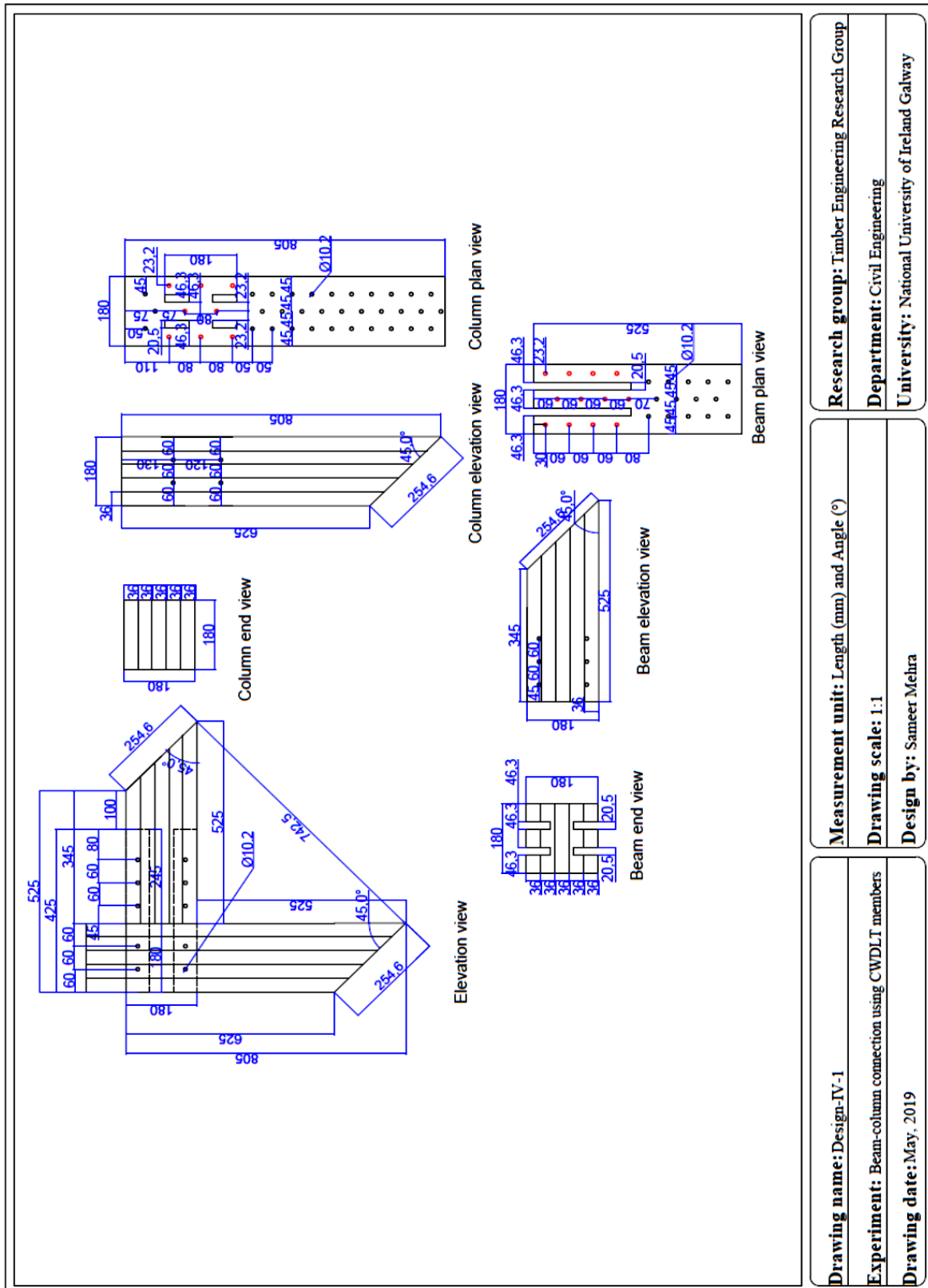
Research group: Timber Engineering Research Group
Department: Civil Engineering
University: National University of Ireland Galway

Measurement unit: Length (mm) and Angle ($^\circ$)
Drawing scale: 1:1
Design by: Sameer Mehra

Drawing name: Design-III-6
Experiment: Beam-column connection using glued members
Drawing date: October, 2018

Appendix-B

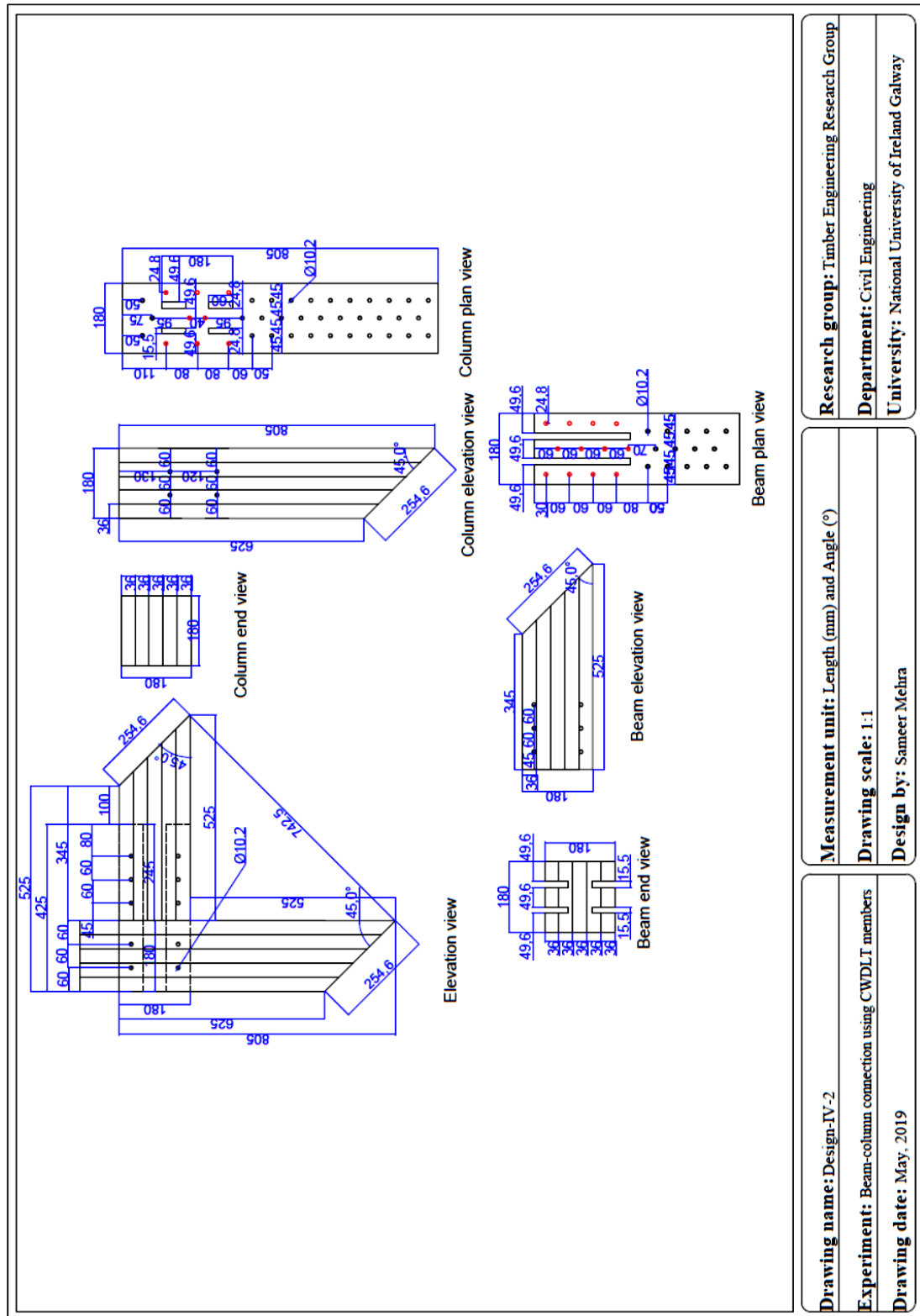
Design-IV-1



Red colour circles show the threaded beechwood dowels in the connection area.

Drawing name: Design-IV-1	Measurement unit: Length (mm) and Angle (°)	Research group: Timber Engineering Research Group
Experiment: Beam-column connection using CWDLT members	Drawing scale: 1:1	Department: Civil Engineering
Drawing date: May, 2019		University: National University of Ireland Galway
		Design by: Sameer Mehra

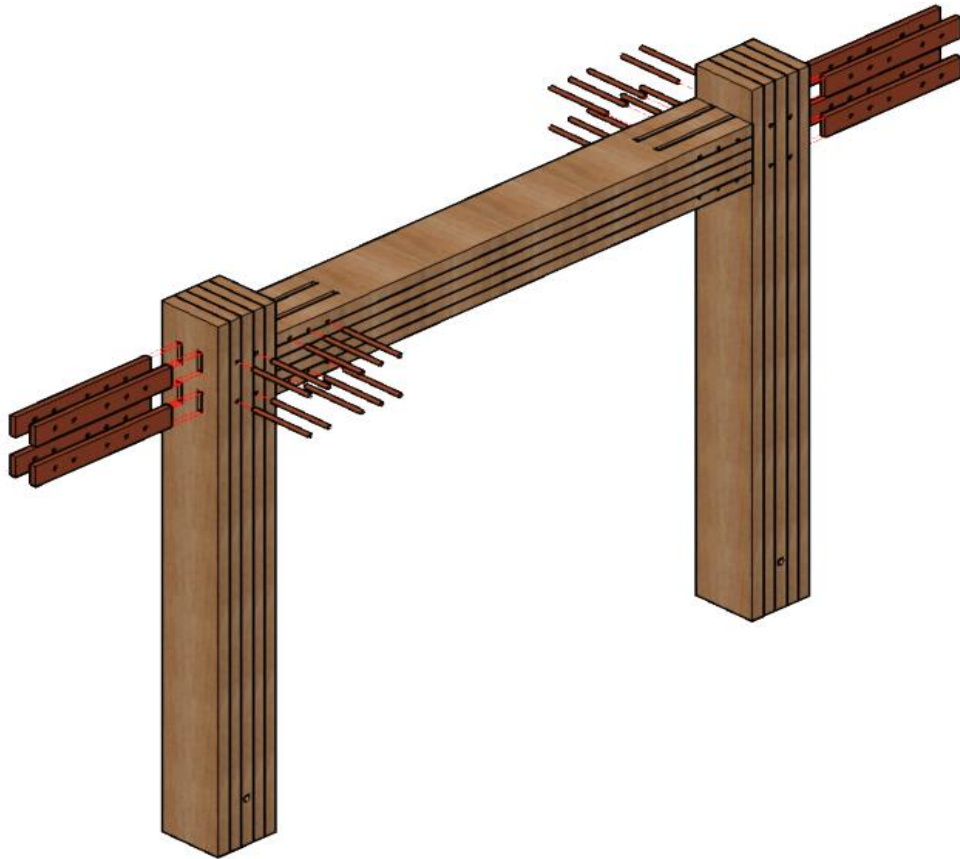
Design-IV-2



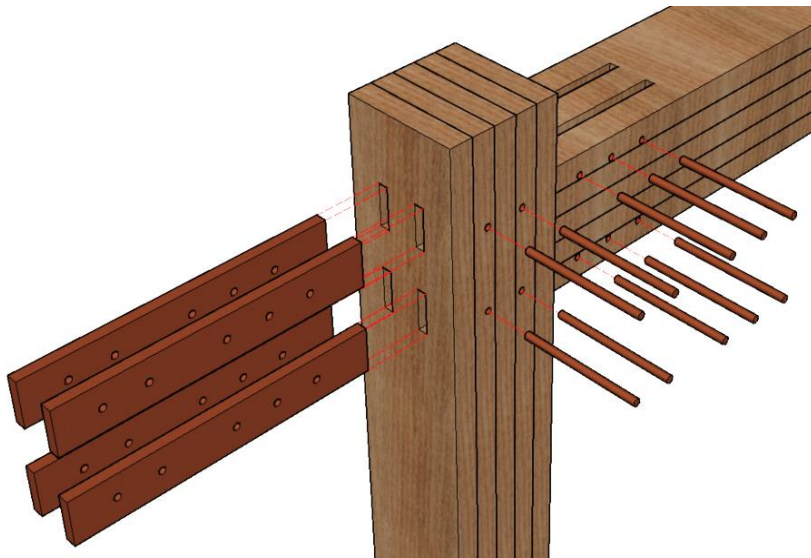
Red colour circles show the threaded beechwood dowels in the connection area.

Appendix-C

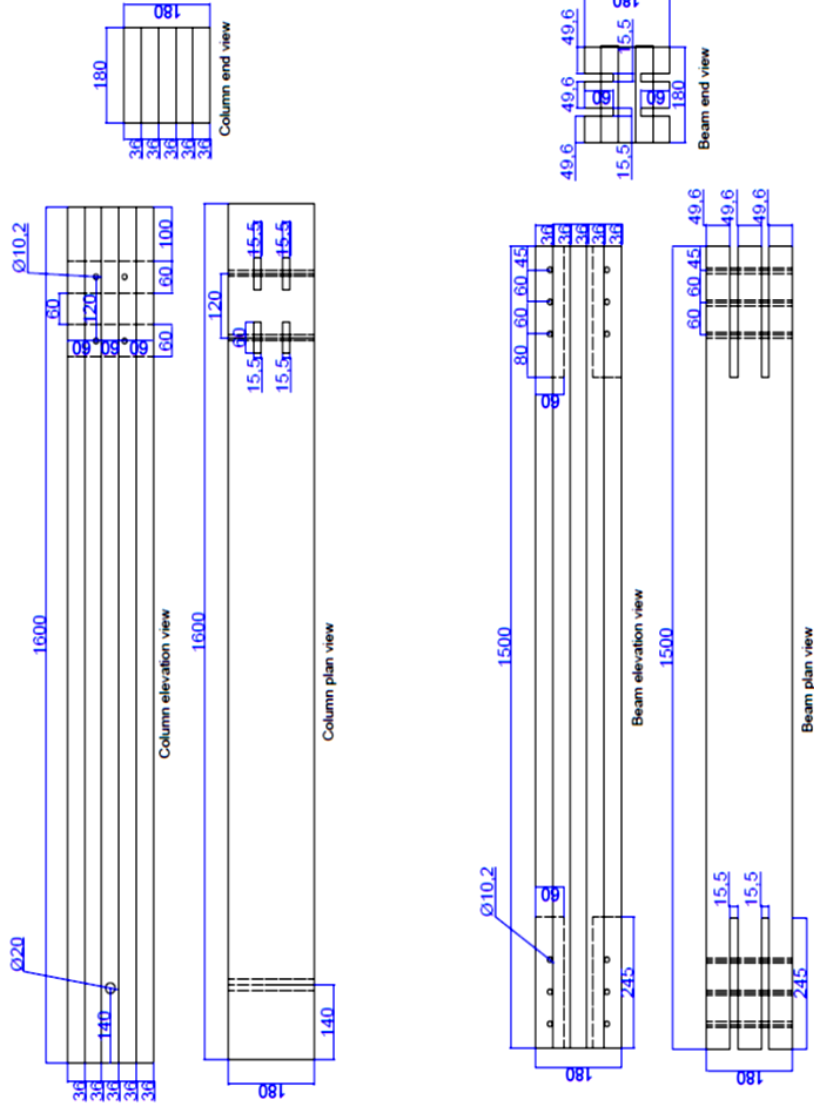
Portal frame using glued structural members



3D view of frame using glued structural members



3D view of localised connection between beam and column



Drawing name: Glued members for frame testing

Experiment: Portal frames: tests using glued members

Drawing date: May, 2019

Measurement unit: Length (mm) and Angle (°)

Drawing scale: 1:1

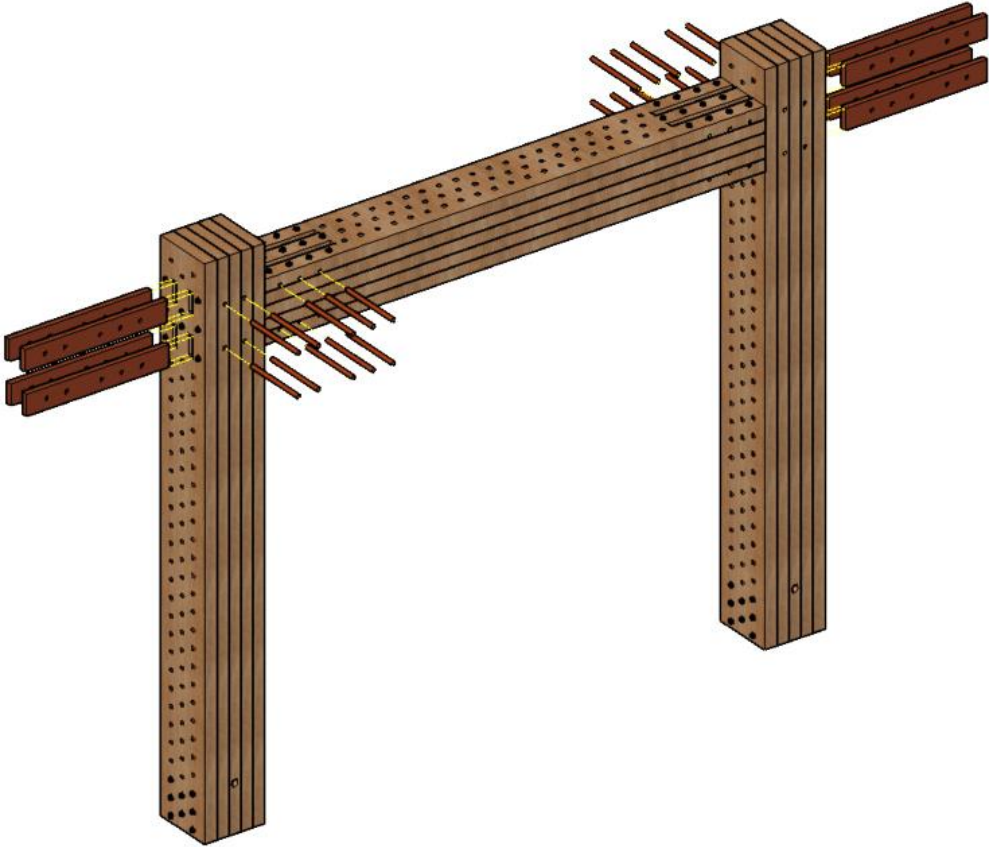
Design by: Sameer Mehra

Research group: Timber Engineering Research Group

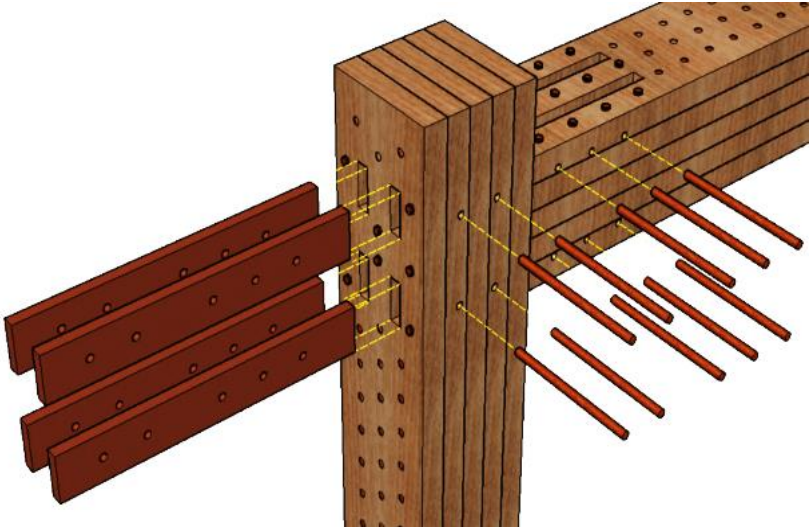
Department: Civil Engineering

University: National University of Ireland Galway

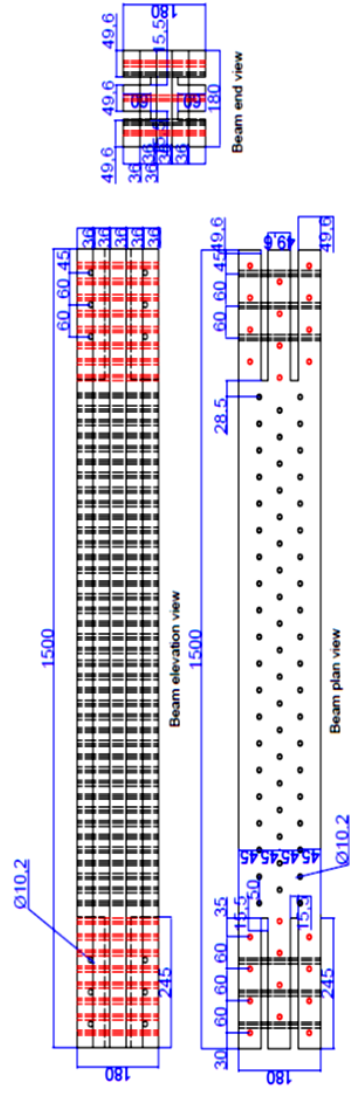
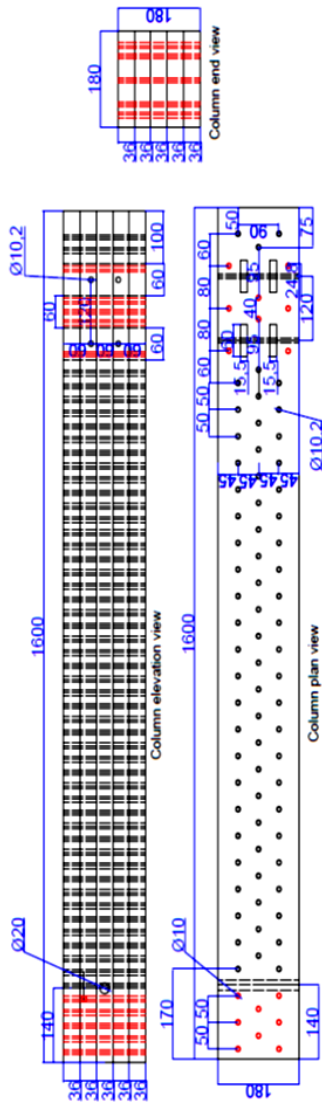
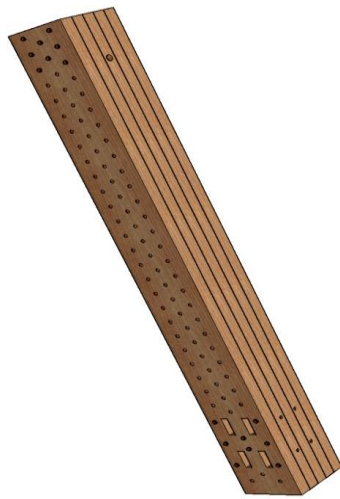
Portal frame using CWDLT members



3D view of frame using CWDLT structural members



3D view of localised connection between beam and column



Drawing name: CWDLT members for frame testing

Experiment: Portal frames tests using CWDLT members

Drawing date: May, 2019

Measurement unit: Length (mm) and Angle (°)

Drawing scale: 1:1

Design by: Sameer Mehra

Research group: Timber Engineering Research Group

Department: Civil Engineering

University: National University of Ireland Galway

Appendix-D

Suitability of EC 5 design rules and research studies to determine the rotational stiffness of the timber-CW connections

The calculation of the initial lateral stiffness/rotational stiffness is mainly dependent on the elastic deformation of the connected members attributed to the localised embedment or crushing of the wood fibres around the dowel hole. The rotational stiffness of the metal type dowel connections (timber-timber and timber-steel) can be calculated based on the slip modulus (K_{ser}) of a single fastener using following expression as recommended by Porteous and Kermani [54].

$$k_{ser,1} \text{ or } k_{ser,2} = n_{sp} \left(\frac{K_{ser}}{(1 + k_{def})} \right) \sum_{i=1}^n r_i^2 \quad 1$$

where

K_{ser} is the slip modulus per shear plane per fastener,

k_{def} is the deformation factor varying service classes. This is not used for the calculation to allow for comparison with experimental results,

n is the number of fasteners on each side of the beam-beam/beam-column connection,

and r_i is the lever arm distance of fastener i .

The calculation of K_{ser} for timber-timber connections and timber-steel connections differ due to following reasons:

1. Expression for calculation of mean density of connected members (ρ_m)
2. Use of multiplication factor for timber-steel connection

So, the question remains what should be an appropriate way to calculate the K_{ser} for timber-CW connections?

To find a solution, a parallel investigation was carried out using both timber-timber and timber-steel analogy (see Table 1). The obtained design values of rotational stiffness were then compared with the mean experimental rotational stiffness of one of the randomly chosen design configurations of beam-beam connections, 6-dowel arrangement using 20 mm thick narrow-depth CW plates (BB-6-20). In this design, lever arm distance (r) is 50 mm for each dowel from the neutral axis of beam.

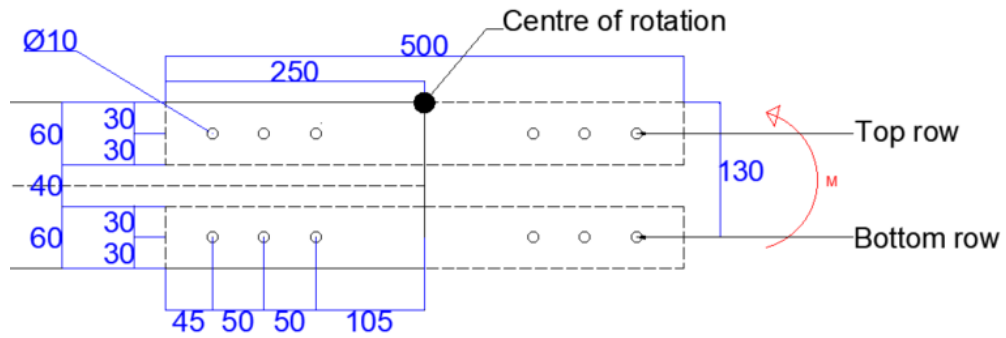


Figure 1- Rotation of CW dowels in the CW plates and deformation of CW plates around edges of the holes

Table-1- Comparison between experimental values and design values of rotational stiffness

	Timber-Timber Connection	Timber-Steel Connection
Calculation of K_{ser}	$(K_{ser}) = \frac{\rho_m^{1.5} d}{23}$	$(K_{ser}) = 2 \times \frac{\rho_m^{1.5} d}{23}$
Calculation of mean density (ρ_m)	<p>ρ_m is calculated based on the mean density of connected timber material using the following expression:</p> <p>Mean density of member (ρ_m)</p> $= \sqrt{\rho_{m1} \cdot \rho_{m2}}$ <p>where the connection involves timber members of different densities, ρ_{m1} and ρ_{m2}</p> <p>Mean density of timber $\rho_{m1} = \rho_{Timber} = 570 \text{ kg/m}^3$</p> <p>Mean density of compressed wood $\rho_{m2} = \rho_{CW} = 1300 \text{ kg/m}^3$</p> <p>Thus $\rho_m = 860 \text{ kg/m}^3$</p> <p>Dowel diameter ($d$) = 10 mm</p>	<p>ρ_m is the mean density of the timber</p> <p>$\rho_m = \rho_{Timber} = 570 \text{ kg/m}^3$</p> <p>Dowel diameter ($d$) = 10 mm</p>
Multiplication factor	-	2
Experimental mean rotational stiffness for BB-6-20 (kN.m/rad)	196.5	196.5
Design value of rotational	329.0 (Utilises mean density based on timber and CW = 860 kg/m ³)	355

stiffness from Eq. 1 (kN.m/rad)		(Utilises mean density of timber and multiplication factor)
------------------------------------	--	---

The design values of rotational stiffness calculated using timber-timber and timber-steel analogy overestimate when compared with the experimental values. Table 2 shows a comparison between design and experimental rotational stiffness.

Table 2 – Overestimation of design rotational stiffness from timber-timber and timber-steel analogy

	Rotational stiffness (kN.m/rad)	Overestimated by (in %)
Mean experimental rotational	196.5	
Using EC 5 timber-timber design equations	329.4	68
Using EC 5 timber-steel design equations	355.0	81

Possible reasons for overestimated results of the design rotational stiffness

1. If the timber-CW connection considered analogous to the timber-timber connection

Using ρ_m based on the mean density of timber and CW overestimates the rotational stiffness by 68% times than the experimental values. Although CW is a wood-based material, the mean density (ρ_m) of connected materials should not be calculated using the mean densities of CW and timber. Because it is mainly the elastic deformation of connected members that affects the initial rotational stiffness of the connection. In timber-CW connections, CW dowels and CW plates have twice the density of the normal timber. Thus, the elastic deformation of timber by embedment is more likely to occur compared to that of CW connectors. This means deformation of timber in the elastic phase will be a critical factor for determining the initial rotational stiffness of the timber-CW connection. Hence, the mean density of timber should be used only as ρ_m .

When only the mean density of timber was used for calculation of rotational stiffness of the timber-CW connection, the design value of 177.5 kN.m/rad was obtained which is only 10% lower than that of experimental values.

2. If the timber-CW connection considered analogous to the timber-steel connection

The EC 5 empirical expression for determination of K_{ser} uses a multiplication factor of 2. The multiplication factor is used because the instantaneous slip of timber-steel connection is half of the timber-timber connection. However, $2 \times K_{ser}$ formula is reported to overestimate the stiffness values[54]. This is because it ignores

1. Effect of clearance between steel dowel and the steel plates
2. Bending/rotation of steel dowel within the steel member
3. Yielding/deformation of steel plate where it is in contact with the steel dowel

When the rotational stiffness of timber-CW connections was calculated using a timber-steel analogy, it overestimated the rotational stiffness by 81% than the experimental values. Therefore, the question is whether to use a multiplication factor for timber-CW connection?

Through the analysis of dissected sections of one of the tested specimens of BB-6-20, as shown in Figure 2, it has been observed that

1. CW dowels rotate in the timber and CW plates.
2. CW plates deform where it is in contact with the CW dowels (however this should be considered conservative because the elastic deformation of CW was not measured during the experiment due to practical difficulties).

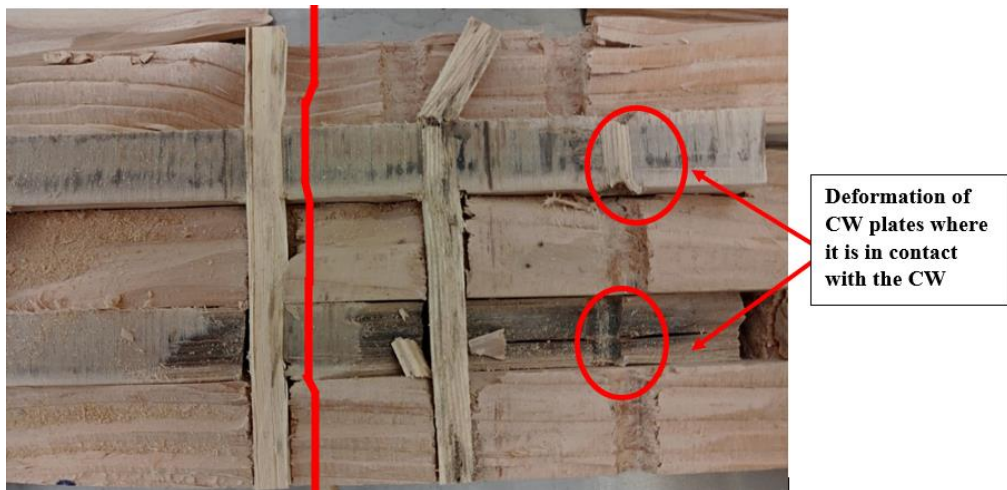


Figure 2- Rotation of CW dowels in the CW plates and deformation of CW plates around edges of the holes

Based on the above explanation, it can be said that the joint slip/deformation for timber-CW connections would be in between timber-timber and timber-steel connection as explained in Figure 3. Hence, using a multiplication factor of 2 would be an overestimation of K_{ser} value and ultimately the rotational stiffness. Thus, a smaller value or no multiplication factor should be used for the determination of K_{ser} value for the timber-CW connections.

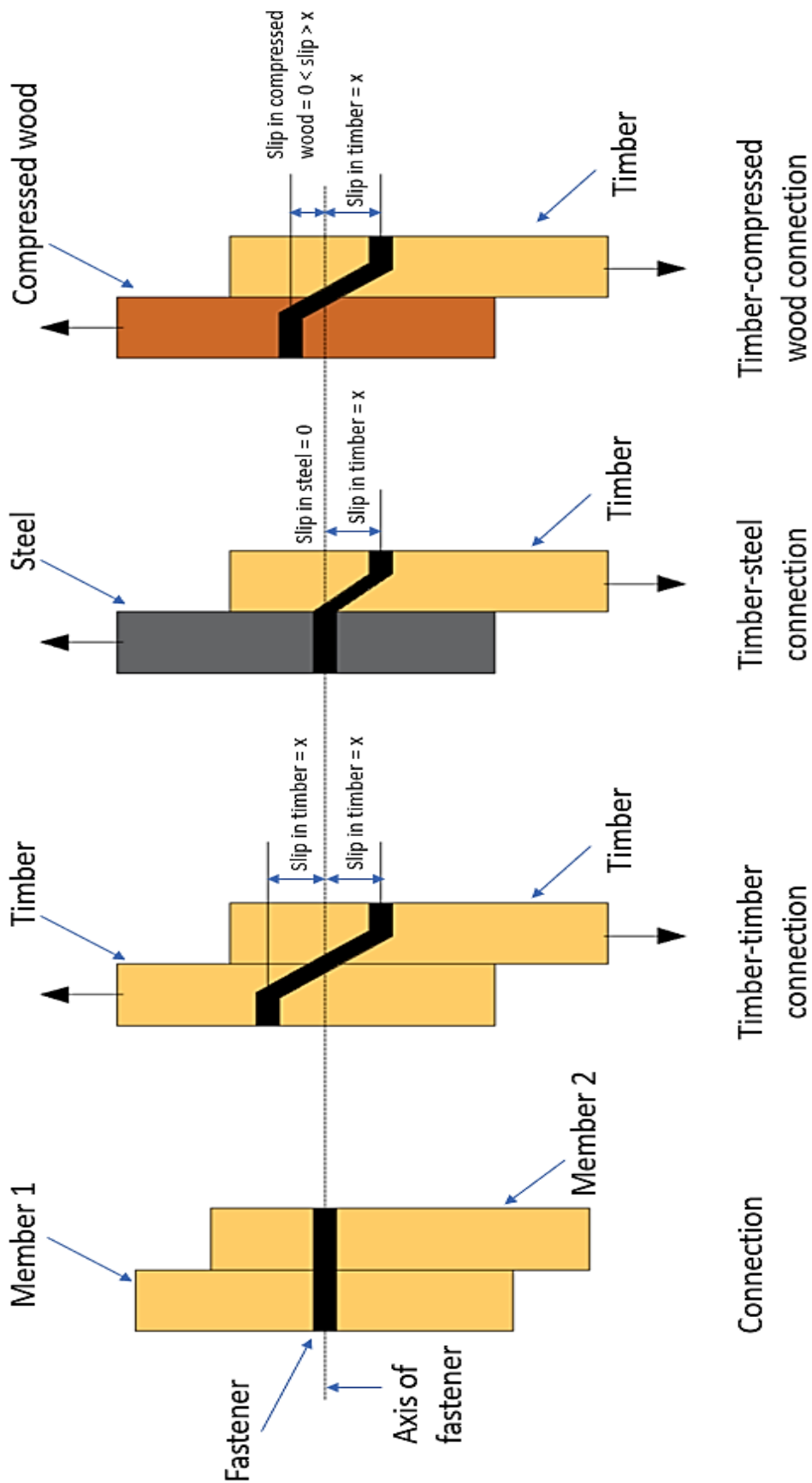


Figure 3- Possible slip behaviour of timber-timber, timber-steel and timber-CW connections

Since the density and stiffness of CW material are twice than the timber, it can be assumed that the joint slip of timber-CW connection would be half of the slip of timber-timber connection. Thus, K_{ser} for timber-CW connection would be 1.3 times higher than the timber-timber connection ($1.3 \times K_{ser}$). Figure 2 compares the slip of timber-timber, timber-CW and timber-steel connection.

Table 3- Slip modulus comparison

	Timber-timber (From EC 5)	Timber-CW connection (Approximation)	Timber-steel connection (From EC 5)
Slip modulus (K_{ser})	K_{ser}	$1.3 \times K_{ser}$	$2 \times K_{ser}$

When the rotational stiffness of timber-CW connection was calculated using the slip modulus values with a multiplication factor of 1.3, the design rotational stiffness was 231 kN.m/rad which is approximately 17% higher than that of experimental values. If the multiplication factor was not used, the design value of rotational stiffness was 177.5 kN.m/rad which is approximately 10% lower than the experimental values.

Concluding remark

The design rotational stiffness of timber-CW connections based on K_{ser} calculated from timber-timber and timber-steel analogies of EC 5 rules overestimates it by 68% and 81%, respectively, when compared to the mean experimental rotational stiffness. The design rotational stiffness of timber-CW connection can be approximated reasonably if the K_{ser} is calculated based on only the mean density of timber without using any multiplication factor. However, this is an approximation further research would be needed to calculate an appropriate multiplication factor to avoid overestimation.